ADVANCES IN PRECISION CALCULATIONS OF HIGGS BOSON AND SINGLE TOP QUARK PRODUCTION AT THE LARGE HADRON COLLIDER

Zur Erlangung des akademischen Grades eines
DOKTORS DER NATURWISSENSCHAFTEN (Dr. rer. nat)
von der KIT-Fakultät für Physik
des Karlsruher Instituts für Technologie (KIT)
genehmigte
DISSERTATION
von
M.SC. JÉRÉMIE JUVIN-QUARROZ

Tag der mündlichen Prüfung:	14.07.2023
Referent:	Prof. Dr. Kirill Melnikov
Korreferent:	Prof. Dr. Gudrun Heinrich

This document is licensed under a Creative Commons
Attribution-ShareAlike 4.0 International License (CC BY-SA 4.0):
https://creativecommons.org/licenses/by-sa/4.0/deed.en

L’absurde naît de cette confrontation entre l’appel humain
et le silence déraisonnable du monde.

— Albert Camus

ABSTRACT

Since the discovery of the Higgs boson in 2012 [1], particle physics has entered an era of precision. With the upcoming increase in luminosity of the Large Hadron Collider (LHC) [2], we will gain access to deep and detailed insights into the behaviour of fundamental particles. On the theoretical side, the description of partonic cross sections with next-to-next-to-leading order (NNLO) accuracy in Quantum Chromodynamics (QCD) is becoming a standard.

Despite the astonishing agreement between the experiments and theoretical predictions [3], it is clear that the Standard Model (SM) of particle physics is incomplete. One way to search for New Physics is to push the accuracy of the theoretical predictions and experimental measurements further. In this thesis, we study three problems related to precision description of Higgs boson and top quark production at the LHC.

In the first part, we investigate the interference contribution between two Higgs production mechanisms in the $pp \to H + \mathrm{jet}_c$ process. This process can be used to study the Yukawa coupling of the charm quark [4]. The interference studied in this thesis requires a helicity flip on the charm-quark line, forcing us to treat the charm quarks as massive. This requirement leads to unconventional QCD phenomena, such as the importance of soft quarks and unusual collinear factorisation.

In the second part, we calculate the so-called non-factorisable corrections to t-channel single top production. These corrections arise from the crosstalk between the two fermion lines present in this process. Until now, the non-factorisable contributions to single top production have been neglected because they do not appear at next-to-leading order (NLO) and they are colour-suppressed compared to the factorisable ones [5, 6]. However, recent studies indicate that the factorisable corrections are relatively small at NNLO and that the non-factorisable ones can be dynamically enhanced [7]. We compute the non-factorisable corrections and discuss their numerical impact on t-channel single top production at the LHC and the Future Circular Collider (FCC) [8, 9].

In the third part, we consider the same type of corrections to Higgs production in weak boson fusion (WBF). Contrary to the case of t-channel single top production, an exact computation of these corrections is currently impossible. Following Ref. [7], we construct an expansion of the double-virtual contribution around the forward limit of the tagging jets. It turns out that the expression of the double-virtual contribution at the next-to-leading order in the eikonal approximation can be expressed in a quite compact form.

PUBLICATIONS

Many figures and results presented in this thesis are based on the following peer-reviewed publications and proceedings written by the author of this thesis

[1] Wojciech Bizon, Kirill Melnikov, and Jérémie Quarroz. "On the interference of ggH and $\bar{c}c$H Higgs production mechanisms and the determination of charm Yukawa coupling at the LHC." In: *JHEP* 06 (2021), p. 107. DOI: 10.1007/JHEP06(2021)107. arXiv: 2102.04242 [hep-ph].

[2] Christian Brønnum-Hansen, Kirill Melnikov, Jérémie Quarroz, and Chen-Yu Wang. "On non-factorisable contributions to t-channel single-top production." In: *JHEP* 11 (2021), p. 130. DOI: 10.1007/JHEP11(2021)130. arXiv: 2108.09222 [hep-ph].

[3] Christian Brønnum-Hansen, Jeremie Quarroz, Chiara Signorile-Signorile, and Chen-Yu Wang. "Non-factorisable corrections to *t*- channel single-top production: comparing results for the LHC and FCC." In: *Strong interactions from QCD to new strong dynamics at LHC and Future Colliders*. 2022, pp. 67–72.

[4] Christian Brønnum-Hansen, Kirill Melnikov, Jérémie Quarroz, Chiara Signorile-Signorile, and Chen-Yu Wang. "Non-factorisable contribution to t-channel single-top production." In: *JHEP* 06 (2022), p. 061. DOI: 10.1007/JHEP06(2022)061. arXiv: 2204.05770 [hep-ph].

[5] Christian Brønnum-Hansen, Jérémie Quarroz, and Chen-Yu Wang. "Non-factorisable two-loop contribution to *t*-channel single-top production." In: *14th International Workshop on Top Quark Physics*. Jan. 2022. arXiv: 2201.03480 [hep-ph].

[6] Christian Brønnum-Hansen, Jérémie Quarroz, Chiara Signorile-Signorile, and Chen-Yu Wang. "Non-factorisable contributions to *t*-channel single-top production at the LHC and FCC." In: *PoS* LL2022 (2022), p. 035. DOI: 10.22323/1.416.0035. arXiv: 2207.10350 [hep-ph].

[7] Ming-Ming Long, Kirill Melnikov, and Jérémie Quarroz. "Non-factorizable virtual corrections to Higgs boson production in weak boson fusion beyond the eikonal approximation." In: *JHEP* 07 (2023), p. 035. DOI: 10.1007/JHEP07(2023)035. arXiv: 2305.12937 [hep-ph].

CONTENTS

1 INTRODUCTION 1

I HIGGS PRODUCTION IN ASSOCIATION WITH A CHARM-QUARK JET AND THE DETERMINATION OF CHARM YUKAWA COUPLING AT LHC

2 INTRODUCTION 7

3 MATCHING PARTON DISTRIBUTION FUNCTIONS 11
  3.1 Charm-quark pair annihilation to a Higgs boson 12
    3.1.1 NLO QCD corrections within $\overline{\text{MS}}$ scheme 12
    3.1.2 NLO QCD corrections with massive charm quarks 18
    3.1.3 PDF matching 22
  3.2 Off-diagonal coefficients 23
    3.2.1 Yukawa-like Higgs production 24
    3.2.2 Higgs production in gluon fusion 26

4 UNCONVENTIONAL COLLINEAR STRUCTURE AND QUASI-SOFT QUARK SINGULARITY 29
  4.1 Unconventional collinear structure 29
  4.2 Quasi-soft quark singularity 40

5 TREATMENT OF THE REAL-EMISSION CORRECTIONS 43
  5.1 Real-emission amplitudes 43
  5.2 Extraction of the logarithms of the charm-quark mass 44
    5.2.1 Quasi-soft quark subtraction term 45
    5.2.2 Integrated collinear subtraction terms 46
  5.3 Numerical check 50

6 INTEGRATED EIKONAL FUNCTIONS 53
  6.1 Integrated quasi-soft quark eikonal functions 53
    6.1.1 One massive and one massless emitters 57
    6.1.2 Two massive emitters 57

7 VIRTUAL AMPLITUDE AND RENORMALISATION 59

8 NUMERICAL SETUP AND RESULTS 65

9 CONCLUSION 69

II NON-FACTORISABLE CORRECTIONS TO T-CHANNEL SINGLE TOP PRODUCTION

10 INTRODUCTION 73

11 COLOUR STRUCTURE AND INFRARED POLE CANCELLATION 77
  11.1 Colour structure 77
    11.1.1 Elastic process 77

11.1.2 Single-real emission contributions 79
11.1.3 Double-real emission amplitudes 82
11.2 Construction of the subtraction terms 83
11.2.1 Double-real cross section 83
11.2.2 Real-virtual cross section 85
11.2.3 Double-virtual cross section 86
11.3 Pole cancellation 87
12 INTEGRATED EIKONAL FUNCTIONS 89
12.1 One massive emitter, one massless – arbitrary angle 89
12.1.1 Regulated integral 90
12.1.2 Results 91
12.2 Integrated soft function 92
13 THE DOUBLE-VIRTUAL CONTRIBUTION 93
13.1 Divergences of the loop amplitudes 93
13.2 Tensor decomposition 96
13.3 Form factors and master integrals 99
13.4 Numerical evaluation of the master integrals 100
13.5 Numerical results 105
14 CALCULATION OF THE REAL-EMISSION AMPLITUDES 109
14.1 Tree-level amplitudes 109
14.2 One-loop five-point amplitude 110
15 RESULTS 115
16 CONCLUSION 123

III NON-FACTORISABLE DOUBLE-VIRTUAL CONTRIBUTION TO HIGGS PRODUCTION IN WBF – BEYOND THE EIKONAL APPROXIMATION

17 INTRODUCTION 127
18 MASSLESS SINGLE TOP PRODUCTION – A TOY MODEL 129
18.1 One-loop amplitude in the forward limit 129
18.2 The eikonal contribution 132
18.3 Approximation of the master integrals using differential equations 136
18.3.1 Boundary conditions 140
18.4 Expansion by regions 142
18.4.1 Hard region 144
18.4.2 First collinear region 144
18.4.3 Next-to-leading order of the master integrals 146
19 SUB-EIKONAL CORRECTIONS TO THE HIGGS PRODUCTION IN WBF 149
19.1 Kinematics 149
19.2 One-loop amplitude 150
19.2.1 Glauber region 152
19.2.2 Glauber-soft region 155

19.2.3 Soft and collinear regions 156
19.2.4 Final result 157
19.3 Two-loop amplitude 158
19.4 IR pole cancellation and finite remainder 163
19.5 Numerical results 164
20 CONCLUSION 169
21 CONCLUSION 171

IV APPENDIX

A ON THEORETICAL PREDICTIONS IN PARTICLE PHYSICS 175
A.1 Feynman rules in QCD 175
A.2 UV divergences 177
A.3 Predictions for hadronic cross section 178
B DETAILED INTEGRATION OF THE SOFT-QUARK EIKONAL FUNCTIONS 181
B.1 Integral from the soft-collinear subtraction term in sector 41 - cg channel 181
B.2 Integrated quasi-soft quark eikonal functions 185
C BOUNDARY INTEGRALS 193
C.1 Loop-integral calculations using differential equations 193
C.2 Solution to the differential equation in canonical form 195
C.3 Two-loop triangle integrals at the boundary 196
C.3.1 Dispersion integrals – bubble with one massive propagator 196
C.3.2 Application to the two-loop triangle integrals I_{16} and I_{17} 198
D DETERMINATION OF THE BOUNDARY CONDITIONS FOR THE MASSLESS SINGLE-TOP MASTER INTEGRALS. 203
D.1 Fixing $c_5(\varepsilon)$ using Feynman parametrisation 203
D.2 Fixing $c_4(\varepsilon)$ using Mellin-Barnes representation 205

BIBLIOGRAPHY 207

LIST OF FIGURES

Figure 1.1 Production cross sections of different Standard Model particles at the LHC. Figure from the ATLAS Standard Model physics group [3]. 2
Figure 2.1 Experimental results related to the Yukawa couplings of the second and third generation of fermions and to the massive gauge bosons of the SM. 7
Figure 2.2 Higgs boson production mechanisms for the leading order partonic process $cg \to cH$. 8

Figure 3.1 NLO QCD contribution to charm-quark pair annihilation to a Higgs boson. 12

Figure 3.2 The two mechanisms behind the production of the Higgs boson in association with a charm-quark jet. These processes can be used to determine the off-diagonal coefficients G^{cg} and G^{gc}. 24

Figure 4.1 In the collinear limit $\rho_{14} \to 0$, the amplitude can be split into a quasi-singular part $\mathcal{M}^{-1}$ illustrated on the left pane and into a finite part $\mathcal{M}^0$ shown on the right pane. 30

Figure 4.2 The amplitude $\mathcal{M}$ is the sum of the Yukawa-like amplitude $\mathcal{M}_{y_c}$ and the effective ggH amplitude $\mathcal{M}_{ggh}$. 35

Figure 4.3 Quasi soft-quark contributions are also provided by emissions off initial state partons. Similar to Eq. (4.54), in the quasi soft-quark limit, these two amplitudes factorise into lower-order amplitudes and vector currents. 42

Figure 5.1 Examples of diagrams contributing to the NLO QCD corrections of the process $pp \to H + \text{jet}_c$. They are sorted by the pair of partons in the initial state. Both Higgs boson production type have to be included. 43

Figure 5.2 Numerical validation of the extraction of the $\ln(m_c)$ terms for the interference of $gg \to c\bar{c}H$ with $m_c \neq 0$. Denoted with green squares, the cross sections σ_{real} is obtained by keeping the mass of the charm finite. In blue dot, the reconstructed cross section σ_{rec} is build from the sum of the regulated term where the massless limit has been considered and the sum of the subtraction terms as defined in Eq. (5.2). 51

Figure 7.1 Examples of diagrams contributing to the virtual corrections to the interference between the two Higgs boson production mechanisms that occurs in cg collisions. 59

Figure 8.1 Relative size of the leading order (LO) cross sections σ^{LO}_{ggh}, $\sigma^{\text{LO}}_{\text{Yuk}}$ and $\sigma^{\text{LO}}_{\text{Int}}$. On the left panel, the dependence of the three cross sections on the charm-tagged jet transverse momentum cut is presented. We denote with blue square $\sigma^{\text{LO}}_{\text{Int}}$, with green triangle $\sigma^{\text{LO}}_{\text{Yuk}}$ and with orange circle σ^{LO}_{ggh}. On the right panel, we show the ratio in percent of the interference to the squared Yukawa contribution. 66

Figure 8.2 Distribution of the Higgs boson transverse momentum (left panel) and rapidity (right panel). In both plots, the LO interference is drawn with a blue dashed line and the NLO interference with a solid red line. 67

Figure 10.1 Single-top quark are produced through different channels. We sort them by importance at the LHC where on the left, the t-channel represents 70% of the total production and on the right, the s-channel represents only 5%. 73
Figure 10.2 Diagrams contributing to the t-channel single top production. On the left panel, a gluon emitted by a fermion line is absorbed by the same fermion line. On the right panel, we show a diagram contributing to non-factorisable corrections since the two fermion lines are strongly interacting. 75
Figure 11.1 Diagrams with triple-gluon vertex vanishes because of colour conservation once projected on the Born amplitude. 79
Figure 11.2 Example of diagram interference that contribute to non-factorisable, real-virtual corrections to the single-top t-channel production. 81
Figure 11.3 Example of diagram interference that contribute to non-factorisable, double real-emission corrections to the t-channel single top production. 82
Figure 13.1 The nine integral families that form the two-loop amplitude projections Q_i. Dashed lines stand for massless external legs or propagators. Massive legs or propagators are represented with solid line and the colour indicates to which particle it refers; blue corresponds to the top quark and pink to the W boson. 100
Figure 13.2 Illustration of the auxiliary mass flow method. We start at the irregular point in orange where $x = -i\infty$, move in the complex plane to regular points, denoted in blue. The step size is determined by how far is the closest singularity of the differential equation. 103
Figure 13.3 Example of integrals required at the boundary $m_W^2 \to -i\infty$ that are difficult to calculate analytically . Dashed lines stand for massless legs and propagators, whereas solid lines stand for massive legs or propagators. We denote in blue the lines that corresponds to m_t. 103
Figure 13.4 Integrals that are required as boundary conditions to evaluate the 428 master integrals. Dashed lines stand for massless legs or propagators, whereas solid line represents massive legs or propagators with mass m_t. 104
Figure 13.5 Description of the displacement in the parameter space. 105
Figure 14.1 Two of the one-loop five-point diagrams required to compute the real-virtual contribution to t-channel single top production. We split them into B_1^{sL} where the gluon is emitted from the light-fermion line and B_1^{sH} where the gluon is emitted from the heavy-fermion line. 111

Figure 15.1 Distribution of the top-quark transverse momentum. We report the LO distribution evaluated at $\mu_F = m_t$ with a blue solid line. Non-factorisable corrections are plotted with a red dashed line for $\mu = m_t$ and the scale variation is indicated by the lighter red bands. In green dotted line, we show the corrections at $\mu =$ 40 GeV. 116

Figure 15.2 Distribution of the top-quark rapidity. We report the LO distribution evaluated at $\mu_f = m_t$ with a blue solid line. Non-factorisable corrections are plotted with a red dashed line for $\mu = m_t$ and the scale variation is indicated by the lighter red bands. In green dotted line, we show the corrections at $\mu = 40$ GeV. 117

Figure 15.3 Distribution of the leading-jet transverse momentum. We report the LO distribution evaluated at $\mu_F = m_t$ with a blue solid line. Non-factorisable corrections are plotted with a red dashed line for $\mu = m_t$ and the scale variation is indicated by the lighter red bands. In green dotted line, we show the corrections at $\mu =$ 40 GeV. 118

Figure 15.4 Distribution of the sum of transverse momenta H. We report the LO distribution evaluated at $\mu_F = m_t$ with a blue solid line. Non-factorisable corrections are plotted with a red dashed line for $\mu = m_t$ and the scale variation is indicated by the lighter red bands. In green dotted line, we show the corrections at $\mu = 40$ GeV. 119

Figure 15.5 Distribution of the leading-jet rapidity. We report the LO distribution evaluated at $\mu_F = m_t$ with a blue solid line. The non-factorisable corrections are plotted with a red dashed line for $\mu = m_t$ and the scale variation is indicated by the lighter red bands. In green dotted line, we show the distribution at $\mu = 40$ GeV. 120

Figure 17.1 Cross sections of the main Higgs production channels at the LHC. The Higgs boson production channels are sorted by importance; the gluon fusion, shown on the first line, is the dominant one. The grey bands indicate the theoretical uncertainties, whereas the black intervals stand for the total experimental ones. Figure from Ref. [164]. 127

Figure 18.1 Example of planar (left) and crossed (right) diagrams contributing to the one-loop amplitude for the process described in Eq. (18.1). 130

Figure 18.2 Definition of the four diagrams. The external momenta are on-shell. The transverse momentum is defined as $r = p_1 - p_3$. The diagrams $\mathcal{M}_3^{(1)}$ and $\mathcal{M}_4^{(1)}$ are respectively related to $\mathcal{M}_1^{(1)}$ and $\mathcal{M}_2^{(1)}$) by the momentum mapping $p_1 \leftrightarrow -p_3$. 132

Figure 18.3 Master integrals of the first integral family. The double lines indicate massive W boson propagators. Dashed lines are related to massless propagators and on-shell legs. Solid lines are used to denote off-shell legs. 137
Figure 19.1 To compute the one-loop amplitude, shown on the left, we consider the two quark currents separately. The convention for momentum assignment is described for the upper current on the right. The lower current is defined in an analogous way. 151
Figure 19.2 Similar to the computation of the one-loop amplitude, we think of the two-loop amplitude, shown on the left, in terms of the two quark currents that make it up. The convention for momentum assignment are presented for the upper current on the right. The lower current is defined in an analogous way. 159
Figure 19.3 On the left, we show the distribution of the typical values of δ_3 and δ_4 for points passing the WBF cuts and $y_H < 1$ in the partonic centre-of-mass frame. On the right, we show the distribution of X_δ as defined in Eq. (19.72). 164
Figure 19.4 Double-virtual contribution to the absolute value of the transverse momentum distribution of the leading jet (left) and the sub-leading jet (right) in the forward limit. The leading-order contribution is plotted with a red dashed line and the sub-leading one with a green solid line. On the lower panes, we show the next-to-leading order corrections, normalised to the eikonal contribution. 165
Figure 19.5 Double-virtual contribution to the rapidity distributions of the transverse momentum distribution of the leading jet (left) and the sub-leading jet (right) in the forward limit. The leading-order contribution is plotted with a red dashed line and the sub-leading one with a green solid line. On the lower panes, we show the next-to-leading order corrections, normalised to the eikonal contribution. 166
Figure 19.6 Double-virtual contribution to the absolute value of the transverse momentum of the Higgs boson (left) and to its rapidity distribution (right) in the forward limit. The leading-order contribution is plotted with a red dashed line and the sub-leading one with a green solid line. On the lower panes, we show the next-to-leading order corrections, normalised to the eikonal contribution. 167
Figure A.1 Generic process where two incoming partons produce n outgoing particles. 178

Figure C.1 Two-loop triangle integrals required as boundary conditions by the auxiliary mass flow method to evaluate the two-loop amplitude. Double lines stand for massive propagators and legs with mass m^2. Massive leg with $p^2 = s$ is denoted by a thick line. Simple solid lines are massless. Dots indicate that the propagator is squared. 194

LIST OF TABLES

Table 8.1 Contributions of the single and quadratic charm-quark mass logarithm $L = \ln(m_H/m_c)$ in femtobarns (fb). The interference at NLO QCD is split into the different partonic channels as well as the contribution from the PDF matching. We observe a strong cancellation of the simple and the quadratic logarithms. 67

Table 13.1 Definitions of the integral families. The propagators are defined by the loop momenta k_1 and k_2 and the external momenta p_1, p_2, and p_3 as defined in Eq. (11.1). Three of them are planar and six are non-planar. The nine integral families that contribute to the Q_i but which are not defined here can be obtained by the crossing symmetry $p_1 \leftrightarrow -p_3$. 101

Table 13.2 Comparison of the two-loop amplitude evaluation and the pole prediction at a typical phase space point $s \approx 104337$ GeV^2 and $t \approx -5179.68$ GeV^2. 106

Table 13.3 Evaluations of the two-loop amplitude at three different phase-space points. 106

Table 15.1 Dependence of the non-factorisable corrections on a cut on the transverse momentum of the top quark for 13 TeV proton-proton collisions. The factorisation scale is set to $\mu_F = m_t$. Each row corresponds to a value of the cut given in the first column. In the second column, we report the LO cross section. In the third and fifth columns, we present the non-factorisable contributions in picobarn at $\mu_R = m_t$ and $\mu_R = 40$ GeV, respectively. We refer the reader to the main text for further information. 116

Table 15.2 Dependence of the non-factorisable corrections on a cut on the transverse momentum of the top quark for 100 TeV proton-proton collisions. The factorisation scale is set to $\mu_F = m_t$. Each lines corresponds to a value of the cut, given in the first column. The second column reports the LO cross section. In the third and fifth columns, we present non-factorisable contributions in picobarn at $\mu_R = m_t$ and $\mu_R = 40$ GeV, respectively. We refer the reader to the main text for additional informations. 117

Table 19.1 Relevant regions for the non-factorisable, one-loop amplitude. Each column is related to one component of the loop momentum $k_1 = (\alpha_1, \beta_1, \mathbf{k}_{1,\perp})$, as defined in Eq. (19.15). We do not list symmetric regions. 152

ACRONYMS

BSM	beyond the Standard Model
CKM	Cabibbo–Kobayashi–Maskawa
DIS	deep-inelastic scattering
EW	electroweak
HPL	harmonic polylogarithm
MPL	multiple polylogarithm
HEFT	Higgs effective field theory
HL-LHC	high-luminosity phase of the Large Hadron Collider
IBP	integration-by-parts
IR	infrared
LHC	Large Hadron Collider
LO	leading order
$\overline{\text{MS}}$	modified minimal subtraction
NLO	next-to-leading order
NNLO	next-to-next-to-leading order
N^{3}LO	next-to-next-to-next-to-leading order
PDF	parton distribution function
QCD	Quantum Chromodynamics

QED	Quantum Electrodynamics
RGE	renormalisation group equation
SM	Standard Model
UV	ultraviolet
VEV	vacuum expectation value of the Higgs field
WBF	weak boson fusion
vNV	van Neerven-Vermaseren
NLL	next-to-leading logarithmic order
FCC	Future Circular Collider

1

INTRODUCTION

Particle physics aims to describe the elementary building blocks of matter and their interactions. Everything in Nature, from stellar objects to living beings, is built out of a rather small set of elementary particles. These particles interact through fundamental forces, such as the strong force (which is responsible for binding quarks to form protons and neutrons), the weak force (which allows for the neutron decay), the electromagnetic force (which keeps electrons around nuclei), and the gravitational force. Except for gravity, the Standard Model (SM) of particle physics combines all these forces in a unified framework where fundamental matter is represented by fermion fields subject to local gauge symmetries.

In 1929, H. Weyl successfully described electrodynamics as a gauge theory. The conservation of the electric charge, described by a global $U(1)$ symmetry, was promoted to a local symmetry, giving rise to the photon as an electrically neutral gauge boson [10]. In 1954, the first formulation of a non-Abelian gauge theory by C. Yang and R. Mills, in the context of the isospin symmetry, was a crucial step towards developing the SM as it generalised Weyl's formalism to charged gauge boson [11]. However, gauging the isospin symmetry led to unacceptable phenomenology, and the idea was shelved for about 15 years.

In 1964, M. Gell-Mann and G. Zweig independently proposed the idea of quarks to explain the multitude of observed mesons and baryons [12, 13]. They suggested the existence of three quarks: the up, the down, and the strange. The observation of the baryon Δ^{++} later necessitated the introduction of a color charge [14], giving rise to the theory of strong interactions, Quantum Chromodynamics (QCD).

At the time, the quark model faced skepticism from the physics community. However, in 1969, R. Feynman developed the parton model to explain properties of protons observed in deep inelastic scattering experiments at SLAC [15]. In the early 1970s, S. Glashow, J. Iliopoulos, and L. Maiani postulated the existence of a fourth quark to construct a model of weak interactions [16]. In 1973, M. Kobayashi and T. Maskawa predicted the existence of an additional pair of quarks to explain CP violation [17]. The same year, H. Fritzsch, M. Gell-Mann, and H. Leutwyler understood that QCD can be described as a non-Abelian gauge theory [18].

This mathematical framework was used to formulate the SM of particle physics as a $SU(3)_c \otimes SU(2) \otimes U(1)$ non-Abelian gauge theory, supplemented with the idea of the spontaneous electroweak (EW) symmetry breaking [19–23]. The three Goldstone bosons produced by this mechanism provide the longitudinal polarisations of the weak gauge bosons Z and $W^{\pm}$. The single degree of freedom that remains out of a complex $SU(2)$ scalar doublet is the celebrated Higgs boson, which was discovered in 2012 at the Large Hadron Collider (LHC) [1]. The discovery of the Higgs boson validated the theoretical construction first introduced by P. W. Higgs, F. Englert, and R. Brout in 1964 [24, 25] and completed the verification of the SM of particle physics.

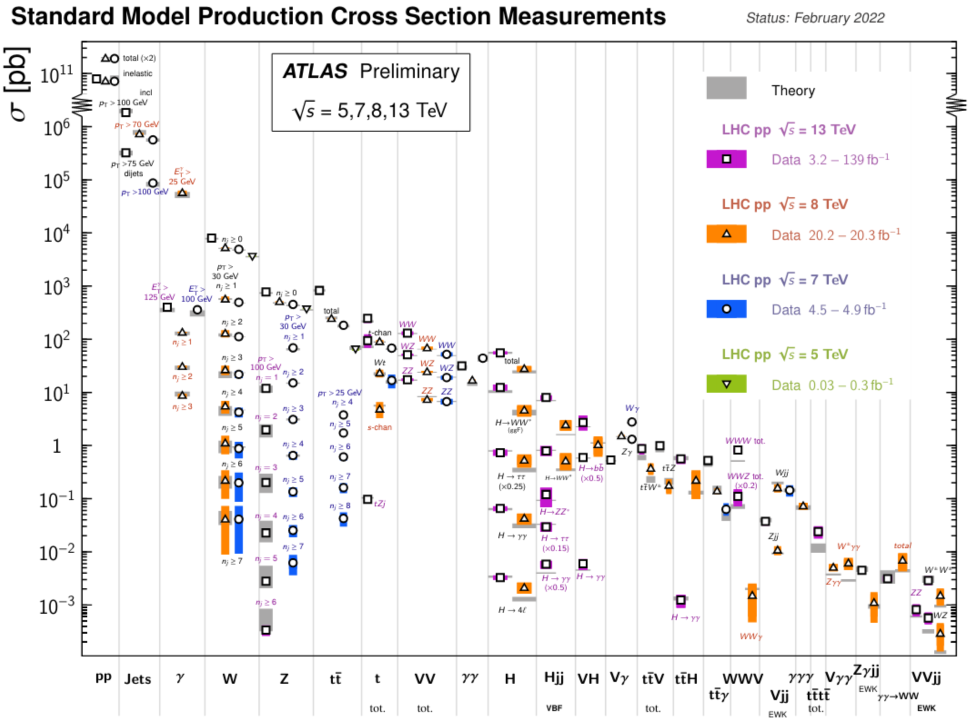

Figure 1.1: Production cross sections of different Standard Model particles at the LHC. Figure from the ATLAS Standard Model physics group [3].

Exploration of particle physics has now entered an era of precision. On the experimental side, the LHC luminosity will be increased in the coming years, leading to a high-luminosity phase [2]. On the theoretical side, description of partonic cross section with next-to-next-to-leading order (NNLO) accuracy is rapidly becoming a standard practice. For certain processes, predictions have been extended to include next-to-next-to-next-to-leading order ($\mathrm{N}^3\mathrm{LO}$) QCD corrections [26, 27]. Mixed QCD-EW corrections [28] are also known for some important processes. The current effort of the theory community is focused on the reduction of the theoretical uncertainties and on establishing perturbative

QCD and collinear factorisation as a trustworthy and reliable framework to describe hard hadron collisions.

Fig. 1.1 shows a comparison of various theoretical predictions and experimental measurements for cross sections of many different LHC processes. The overall agreement between theory and experiment is quite remarkable, proving that the SM of particle physics provides excellent description of Nature.

Despite this agreement, it has been long understood that the SM cannot be the complete theory of Nature. Indeed, the SM cannot account for the matter-anti-matter asymmetry and lacks a candidate for dark matter. Additionally, it does not provide a dynamic explanation of EW symmetry breaking. Therefore, it is crucial to search for physics beyond the Standard Model (BSM) in many different ways. Increasing the precision of LHC processes is one way to achieve this goal since the collision energy of the collider is fixed.

STRUCTURE OF THE THESIS In this thesis, we improve theoretical predictions for some LHC processes used to study propreties of the Higgs boson and the top quark. The thesis is divided into three parts.

In the first part, we investigate QCD radiative corrections to the interference between two mechanisms of Higgs boson production in association with a charm-quark jet. This process can be used to study the Yukawa coupling of the charm quark [4]. The interference that we study in this thesis requires a helicity flip on the charm-quark line, forcing us to consider charm quarks as massive. Since the charm quark appears as an initial state parton in the calculation, the need to account for its mass leads to unconventional phenomena from the point of view of perturbative calculations, such as the importance of soft quarks, unusual collinear factorisation and the need to redefine PDFs.

In the second part, we calculate the so-called non-factorisable contributions to the NNLO QCD corrections to the t-channel single top production. These corrections result from the crosstalk between the two fermion lines that appear in this process which are connected solely by a W boson at Born level. Until now, the non-factorisable corrections to single top production have been neglected because they are colour-suppressed compared to the factorisable ones [5, 6, 29–31]. However, recent studies indicate that the factorisable corrections are relatively small at NNLO [6] and that the non-factorisable corrections can be dynamically enhanced [7]. Therefore, it is interesting to explicitly compute them.

In the final part, we focus on the second most important Higgs boson production channel at the LHC: the weak boson fusion (WBF). Similar to the t-channel single top production, most of the existing studies of Higgs boson production in WBF systematically ignored non-factorisable corrections [32–34]. However, it has been shown that non-factorisable corrections are in fact enhanced for this process [7]. The main challenge lies in the accurate description of the double-virtual, non-factorisable contribution. Since an exact evaluation of the two-loop, non-factorisable amplitude is currently out of reach, we consider a different approach and extend the work of Ref. [7] by computing the sub-leading corrections to the double-virtual contribution in the forward limit.

Part I

HIGGS PRODUCTION IN ASSOCIATION WITH A CHARM-QUARK JET AND THE DETERMINATION OF CHARM YUKAWA COUPLING AT LHC

In the SM, the strength of the Higgs boson interaction with a SM particle grows with the particle's mass. For this reason, couplings of the Higgs boson to fermions of the second and the third generations and to EW gauge bosons have been accurately measured at the LHC. The results of such measurements are found to be consistent with the SM. However, measuring the Yukawa couplings of light fermions, such as the electron, up, down, and strange quarks, is considered unfeasible.

The charm quark is a borderline case between light and heavy fermions, and many suggestions of how to measure charm Yukawa coupling were put forward. Measuring the production rate of a Higgs boson in association with a charm-quark jet is a promising way to determine the charm Yukawa coupling [4]. Two mechanisms mediate Higgs production in this process: direct interaction of the Higgs boson with the charm quark and the gluon fusion. The interference of these two mechanisms vanishes for a massless charm quark. Nevertheless, since the charm quark is massive, it is important to estimate this interference reliably. We explain how to do this in what follows.

This part of the thesis is based on Ref. [35].

2 INTRODUCTION

It is expected that $\mathcal{O}(10^7)$ Higgs bosons per year will be produced during the high-luminosity phase of the Large Hadron Collider (HL-LHC), providing an opportunity to study in great detail the properties of the only elementary scalar particle known so far. One of these properties is the Higgs boson couplings to SM fermions through the Yukawa interactions. These couplings are proportional to masses of fermions that the Higgs boson interacts with. The Yukawa coupling of a fermion f reads

$$y_f = \sqrt{2}\frac{m_f}{v}, \tag{2.1}$$

where m_f is the fermion mass and $v = 246.22$ GeV is the vacuum expectation value of the Higgs field (VEV).

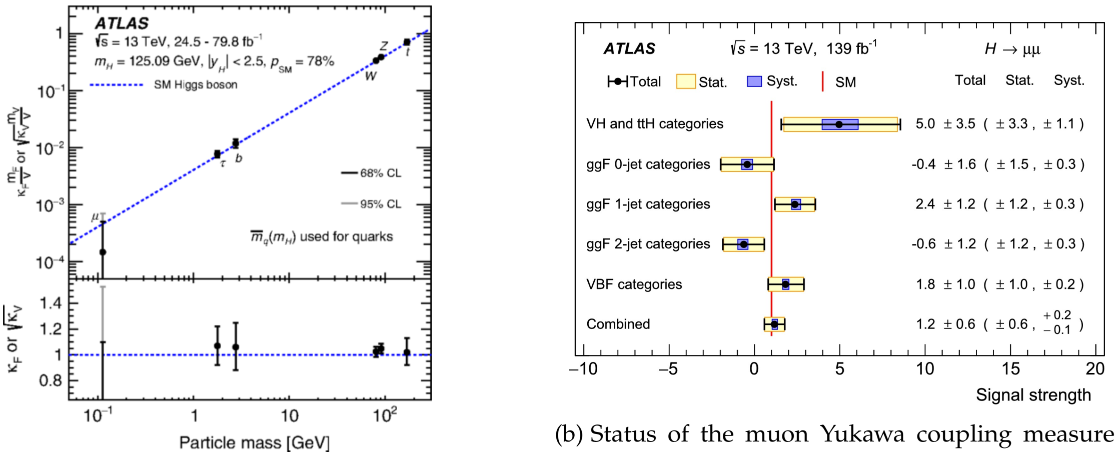

(a) Status of the measurements of different Yukawa couplings. Figure from Ref. [36]

(b) Status of the muon Yukawa coupling measurements. The measurement is split into different event categories. Figure from Ref. [37]

Figure 2.1: Experimental results related to the Yukawa couplings of the second and third generation of fermions and to the massive gauge bosons of the SM.

The couplings of the Higgs boson to fermions of the second and third generations and to EW gauge bosons of the SM have been measured at the LHC with relatively high precision [37–42]. Fig. 2.1a summarises these measurements; the linear dependence of the couplings' strengths on particles' masses is clearly visible. Interestingly, despite its relatively small mass, the muon Yukawa coupling can be measured at the LHC, as the decay $H \to \mu^+\mu^-$ provides a sufficiently clear signature. In Fig. 2.1b, various measurements of the muon Yukawa coupling are shown. The averaged value is compatible with the SM prediction at the level of 50%.

Because the Yukawa couplings of the lightest particles of the SM, such as the electron, up, down, and strange quarks, are very small, measuring them is probably impossible. However, the charm quark with the mass $m_c = 1.3$ GeV, is a borderline case, and its Yukawa coupling could potentially be measured at the HL-LHC if it is somewhat larger than what is expected in the SM [43]. Prospects for measuring the charm Yukawa coupling using the current and future HL-LHC data were recently reviewed in Ref. [44]. We note that, although the charm quark is 12 times heavier than the muon, the measurement of the charm Yukawa is made difficult because the charm quark is a strongly-interacting particle.

Different ways were suggested to measure the Yukawa coupling of the charm quark. One approach is to extract it from Higgs decays, either inclusive $H \to \bar{c}c$ or exclusive $H \to J/\psi + \gamma$, as described in Refs. [45–47]. The exclusive decay profits from clear Higgs decay signatures, such as the presence of an energetic photon, but it is expected to occur only about $\mathcal{O}(10)$ times over the lifetime of the HL-LHC. On the other hand, the inclusive decay of the Higgs $H \to c\bar{c}$ occurs much more often, but it suffers from a large QCD background.

The charm Yukawa coupling can also be measured by studying the production of a Higgs boson in association with a charm-quark jet, $p + p \to H + \text{jet}_c$ [4]. Focusing only on the clean $H \to \gamma\gamma$ decay channel, the authors of Ref. [4] estimate that this process could lead to $\mathcal{O}(1000)$ events during the lifetime of the HL-LHC, where the low efficiency of the charm-quark jet tagging has already been accounted for.

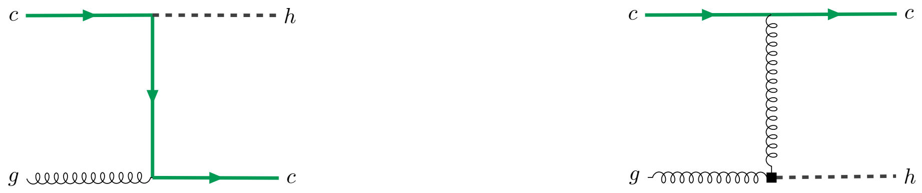

(a) Higgs production through Yukawa interaction with the charm-quark line.

(b) Higgs production through the Higgs effective field theory (HEFT) vertex ggH.

Figure 2.2: Higgs boson production mechanisms for the leading order partonic process $cg \to cH$.

At leading order (LO), the partonic process $cg \to cH$ provides the dominant contribution to $p + p \to H + \text{jet}_c$; the relevant diagrams are shown in Fig. 2.2. In Fig. 2.2a, the Higgs boson is produced through the Yukawa interaction with the charm quark. In

Fig. 2.2b, the Higgs boson directly couples to two gluons. The amplitude of the $cg \to cH$ process is the sum of two amplitudes which describe the two possible production mechanisms. We write

$$\mathcal{M} = \mathcal{M}_{\text{Yuk}} + \mathcal{M}_{ggH} \,. \tag{2.2}$$

The partonic cross section is obtained by integrating the amplitude squared over the phase-space of the final-state particles. We obtain

$$\hat{\sigma}_{Hc} = \hat{\sigma}_{\text{Yuk}} + \hat{\sigma}_{ggH} + \hat{\sigma}_{\text{Int}} \,, \tag{2.3}$$

where we display the cross sections due to ggH and Yukawa couplings, and the interference contribution.

To estimate these cross sections, we consider proton-proton collisions at 13 TeV. We choose the `NNPDF31_lo_as_0118` parton distribution functions and require the transverse momentum of the charm jet to exceed 20 GeV. We find that the LO cross sections evaluate to

$$\hat{\sigma}^{\text{LO}}_{ggh} = 176.6^{+47.6}_{-36.5}\ \text{fb}\,, \qquad \hat{\sigma}^{\text{LO}}_{\text{Yuk}} = 21.22^{+1.47}_{-1.67}\ \text{fb}\,, \tag{2.4}$$

where the uncertainties are provided by a variation of the factorisation scale μ_F by a factor two. It follows that the Higgs production through the Yukawa interaction is eight time smaller than through the ggH interaction. Naively, the interference contribution can be estimated as

$$\hat{\sigma}^{\text{LO}}_{\text{Int}} \sim \sqrt{\hat{\sigma}^{\text{LO}}_{ggh}\, \hat{\sigma}^{\text{LO}}_{\text{Yuk}}} = 61.2\ \text{fb}\,, \tag{2.5}$$

which is three times larger than $\hat{\sigma}^{\text{LO}}_{Yuk}$. However, the calculation of the interference contribution is subtle and, as we will discuss now, the interference is significantly smaller.

To compute the physical cross section σ_{Hc}, we consider the charm quark as an initial-state parton. Consequently, it has to be treated as massless in perturbative QCD calculations [48–51]. It is easy to see that for $m_c = 0$, the interference vanishes, as the Higgs production through Yukawa coupling flips the helicity of the charm quark, while the strong interaction conserves it. Since in reality the charm quark is fairly massive, it is essential to estimate the actual size of the interference contribution to the partonic cross section.

The simplest way to address this problem is to start with a massive charm quark, and then take the $m_c \to 0$ limit, keeping the leading non-vanishing term. This procedure is almost trivial at leading order. We account for the interference with a simple mass insertion on the charm-quark line, while taking $m_c \to 0$ limit everywhere else. Using the same numerical setup as before, we find that the LO interference evaluates to

$$\hat{\sigma}^{\text{LO}}_{\text{Int}} = -2.21^{+0.29}_{-0.31}\ \text{fb}\,. \tag{2.6}$$

Comparing Eqs. (2.5)-(2.6), we see that the interference is smaller than $\hat{\sigma}^{\rm LO}_{\rm Yuk}$, but it is clearly not negligible. The difference between Eq. (2.6) and the estimate in Eq. (2.5) can be understood because the mass insertion provides a suppression of the order $m_c/p_\perp$ which for $p_\perp \sim 20$ GeV is about $1/20$.

An interesting question is what happens to the interference if higher order QCD corrections are computed. One may argue that the charm-quark mass acts as a regulator of the collinear divergences and that the resulting large logarithms, $\ln(m_H/m_c) = 4.5$, should cancel out once virtual and real-emission contributions are considered. However, the presence of the helicity flip on the fermion line leads to unconventional infrared (IR) structure of the amplitude. Therefore, we expect that the perturbative expansion might be affected by single and even double logarithms whose resummation remains an open problem. As the result, we want to compute the next-to-leading order (NLO) QCD corrections to the interference, to extract terms that contain logarithms of the charm-quark mass, and to take $m_c \to 0$ limit everywhere else. As we explain below, doing this in practice is quite non-trivial.

It is possible to question the validity of this approach at higher orders in the perturbative expansion. Indeed, it is known that working with massive partons in the initial state can be problematic starting at NNLO as it leads to cross sections that are not infrared finite [52–63]. Fortunately, such offending factorisation-violating terms, described for instance in Ref. [64], are absent in the $pp \to H + \text{jet}_c$ process as it results from a collision of a massive quark with a massless gluon. Even if such factorisation-violating effects were present, they would be power-suppressed. Indeed, according to [64], such divergent contributions first affect terms that are suppressed by four powers of the initial state parton mass $\alpha_s^2 m_c^4/s^2 \; d\sigma^{\rm int}_{LO}$. In our approach, such terms are disregarded as we would only consider terms scaling like $\alpha_s^n \; d\sigma^{\rm int}_{LO}$, possibly accompanied by few logarithms of m_c.

In the upcoming chapter, we first explain how we deal with massive partons in the initial state. Then, we discuss in detail the origin of the unconventional collinear divergences in the presence of a helicity flip. We also explain how the $m_c \to 0$ divergences of the different contributing partonic channels are treated, and how the logarithms of the charm-quark mass are extracted. Next, we present the calculation of some unconventional subtraction terms. Finally, we discuss the computation of the virtual amplitude and provide numerical results for the interference at NLO QCD.

3

MATCHING PARTON DISTRIBUTION FUNCTIONS

In this chapter, we explain how to deal with massive partons in the initial state in perturbative QCD. We remind the reader that it is customary to consider initial state pratons as massless in standard applications of perturbative QCD and collinear factorisation [49–51]. Divergences related to collinear emissions off initial state partons are absorbed into parton distribution functions (PDFs), typically defined in the modified minimal subtraction ($\overline{\text{MS}}$) scheme. A short overview of the standard treatment of IR divergences can be found in Appendix A.

However, dimensional regularisation is not the only way to regulate the initial state collinear singularities. In principle, the PDFs could be defined in a scheme where a quark mass acts as a regulator. In this "mass-regulated" scheme for parton distribution function (PDF), poles in the dimensional regulator are replaced by logarithms of the charm-quark mass.

Since short-distance quantities, such as properly defined hadronic cross sections, cannot depend on the choice of a collinear regulator, a relation between PDFs defined in different schemes can be derived. For example, the physical cross section for a particular proton-proton collision can be written as

$$\begin{aligned} \sigma_{pp\to X} &= \sum_{ij} \int dx_1\, dx_2\, f^i_{\overline{\text{MS}}}(x_1,\mu) f^j_{\overline{\text{MS}}}(x_2,\mu)\, d\hat{\sigma}^{\overline{\text{MS}}}_{ij\to X}(x_1,x_2,\mu) \\ &= \sum_{ij} \int dx_1\, dx_2\, f^i_{m_c}(x_1) f^j_{m_c}(x_2)\, d\hat{\sigma}^{m_c}_{ij\to X}(x_1,x_2)\,. \end{aligned} \tag{3.1}$$

In Eq. (3.1), μ is the factorisation scale and we introduced the partonic cross sections and PDFs in both the $\overline{\text{MS}}$ and in the mass-regulated schemes. We assume that there exists a set of matching coefficients $\hat{\mathcal{O}}$ that relate the PDFs in the two schemes

$$f^i_{m_c}(x) = (\hat{\mathcal{O}}^{ij}(\mu,m_c) \otimes f^j_{\overline{MS}}(\mu))(x)\,. \tag{3.2}$$

In Eq. (3.2), the symbol $\otimes$ stands for the convolution

$$(f \otimes g)\,(z) = \int dx_1\, dx_2\, f(x_1)\, g(x_2)\, \delta(z - x_1\, x_2)\,. \tag{3.3}$$

We can expand the matching coefficients $\hat{\mathcal{O}}^{ij}$ in the strong coupling constant

$$\hat{\mathcal{O}}^{ij}(z) = \delta(1-z)\delta^{ij} + \left(\frac{\alpha_s(\mu)}{2\pi}\right) G^{ij}(z) + \mathcal{O}(\alpha_s^2)\,, \tag{3.4}$$

where the leading order (LO) coefficients have been set to $\delta(1-z)\delta_{ij}$.

Since the matching coefficients $\hat{\mathcal{O}}^{ij}$ are process-independent, we will consider various simple processes to determine them. First, we will determine $\hat{\mathcal{O}}^{cc}$ and $\hat{\mathcal{O}}^{\bar{c}\bar{c}}$ by considering the annihilation of a charm-quark pair into an on-shell Higgs boson at NLO QCD. Next, we will determine the off-diagonal coefficients $\hat{\mathcal{O}}^{cg}$ and $\hat{\mathcal{O}}^{gc}$ by considering the partonic process $c+g \to c+H$.

3.1 CHARM-QUARK PAIR ANNIHILATION TO A HIGGS BOSON

In this section, we compute the matching coefficients $\hat{\mathcal{O}}^{cc}$ and $\hat{\mathcal{O}}^{\bar{c}\bar{c}}$ by considering the annihilation of a charm quark and an charm antiquark to an on-shell Higgs boson. We compare the partonic cross section obtained by considering massless charm-quarks with the one obtained by considering massive charm quarks at NLO QCD. The matching coefficients are then determined using Eq. (3.1).

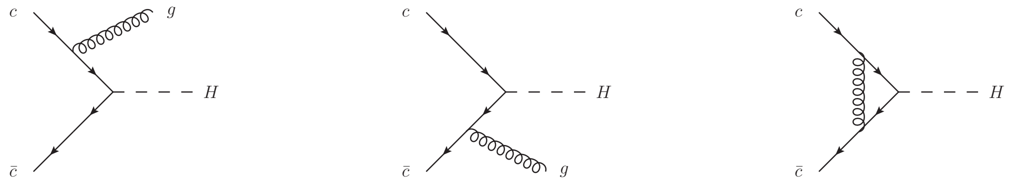

(a) Real emission from c (b) Real emission from $\bar{c}$ (c) Virtual correction

Figure 3.1: NLO QCD contribution to charm-quark pair annihilation to a Higgs boson.

3.1.1 *NLO QCD corrections within* $\overline{\text{MS}}$ *scheme*

Calculations with massless incoming partons are well documented in the literature. Nevertheless, to introduce notations, it is instructive to derive the NLO QCD cross section for the annihilation of a $c\bar{c}$ pair into a Higgs boson in the nested soft-collinear subtraction scheme. In our discussion, we follow Ref. [65].

The partonic cross section for the process $c+\bar{c} \to H$ can be expanded in the strong coupling

$$d\hat{\sigma}_{c\bar{c}} = d\hat{\sigma}^{LO}_{c\bar{c}} + d\hat{\sigma}^{NLO}_{c\bar{c}} + \mathcal{O}(\alpha_s^2)\,. \tag{3.5}$$

As mentioned earlier, the NLO partonic cross section is split into the real-emission and the virtual cross sections (see Fig. 3.1), and the term related to collinear renormalisation of PDFs. We write

$$d\hat{\sigma}_{c\bar{c}}^{NLO} = d\hat{\sigma}^{V} + d\hat{\sigma}^{R} + \delta\hat{\sigma}_{PDF}\,, \tag{3.6}$$

where

$$\delta\hat{\sigma}_{PDF} = \frac{\alpha_s(\mu)}{2\pi}\frac{1}{\varepsilon}\left(\hat{P}_{qq}^{(0)} \otimes d\hat{\sigma}^{LO} + d\hat{\sigma}^{LO} \otimes \hat{P}_{qq}^{(0)}\right)\,, \tag{3.7}$$

and $\hat{P}_{qq}^{(0)}$ stands for the Altarelli-Parisi splitting function

$$\hat{P}_{qq}^{(0)} = C_F\left[\frac{1+z^2}{1-z}\right]_+\,. \tag{3.8}$$

Each individual piece in Eq. (3.6) is divergent, but their sum is finite. We would like to extract these divergences such that the cancellation of the $1/\varepsilon$ poles is manifest. We start by calculating the real corrections.

The real-emission contribution corresponds to the emission of a gluon off the initial state quarks, see Fig. 3.1a and Fig. 3.1b. The partonic process reads

$$c(p_1) + \bar{c}(p_2) \to H + g(p_3)\,. \tag{3.9}$$

The real-emission cross section can be obtained from the following integral

$$2s \cdot d\hat{\sigma}^{R} = \frac{1}{4N_c^2}\int [dg_3] F_{\rm LM}\left(1_c, 2_c, 3_g\right)\,, \tag{3.10}$$

where s is the partonic centre-of-mass energy squared and $N_c = 3$ is the number of colours. The phase-space measure reads

$$[dg_3] = \frac{d^{d-1}p_3}{(2\pi)^{d-1}2E_3}\theta(E_{\rm max} - E_3)\,, \tag{3.11}$$

where we constrain the maximal energy of the gluon to be $E_{\rm max}$ for reasons that will be explained later. The parameter $E_{\rm max}$ is arbitrary but it should be larger than the largest energy that the gluon can have in the process $c + \bar{c} \to H + g$.

The last object introduced in Eq. (3.10) is

$$F_{\rm LM}\left(1_c, 2_c, 3_g\right) = d\text{Lips}_H\, |\mathcal{M}(1_c, 2_{\bar{c}}, 3_g, H)|^2\,, \tag{3.12}$$

where $d\text{Lips}_H$ is the phase space defined in Appendix A and $\mathcal{M}(1_c, 2_{\bar{c}}, 3_g, H)$ is the amplitude of the partonic process defined in Eq. (3.9).

If the emitted gluon energy vanishes or the emitted gluon is collinear to one of the emitters, the real-emission cross section diverges. To isolate such singularities, we introduce two operators. The first one is the soft operator defined as

$$S_3\mathcal{X} \equiv \frac{1}{E_3^2}\lim_{E_3\to 0} E_3^2\mathcal{X}\,. \tag{3.13}$$

where $\mathcal{X}$ stands for any object that depends on the kinematic of the process, and the limit extracts the leading singularity of $\mathcal{X}$. When this operator acts on $F_{\mathrm{LM}}(1_c, 2_{\bar{c}}, 3_g)$, it forces the energy of the emitted gluon to be zero not only in the amplitude, but also in the phase space which contains the energy-momentum conserving delta function. The introduction of $E_{\max}$ constrains the integral over the gluon energy in the soft limit. Similarly, the collinear operators are defined as

$$C_{ij}\mathcal{X} \equiv \frac{1}{\rho_{ij}}\lim_{\rho_{ij}\to 0}\rho_{ij}\mathcal{X}\,, \tag{3.14}$$

where

$$\rho_{ij} = 1 - \vec{n}_i\cdot\vec{n}_j\,. \tag{3.15}$$

In Eq. (3.15), $\vec{n}_{i,j}$ are the unit vectors in the directions of the momenta of the particles i and j.

We can use the two operators to extract the $1/\varepsilon$ pole from the real-emission cross section. We write

$$\begin{aligned} 2s\cdot d\hat{\sigma}^R_{c\bar{c}} &\equiv \langle F_{\mathrm{LM}}\left(1_c, 2_{\bar{c}}, 3_g\right)\rangle \\ &= \langle (1-S_3)F_{\mathrm{LM}}\left(1_c, 2_{\bar{c}}, 3_g\right)\rangle + \langle S_3 F_{\mathrm{LM}}\left(1_c, 2_{\bar{c}}, 3_g\right)\rangle\,, \end{aligned} \tag{3.16}$$

where we use the notation $\langle\ldots\rangle$ to denote the integration over the momenta of the final state particles. In Eq. (3.16), the first term remains regular as $E_3\to 0$ and the second term can be integrated over E_3 for arbitrary F_{LM}. We also need to subtract the collinear divergences. We write

$$\begin{aligned} 2s\cdot d\hat{\sigma}^R_{c\bar{c}} = {}& \langle \hat{O}_{\mathrm{NLO}}F_{\mathrm{LM}}(1_c, 2_{\bar{c}}, 3_g)\rangle + \langle (C_{31}+C_{32})(1-S_3)F_{\mathrm{LM}}\left(1_c, 2_{\bar{c}}, 3_g\right)\rangle \\ &+ \langle S_3 F_{\mathrm{LM}}\left(1_c, 2_c, 3_g\right)\rangle\,, \end{aligned} \tag{3.17}$$

where we have defined the fully regulated NLO cross section

$$\langle \hat{O}_{\mathrm{NLO}}F_{\mathrm{LM}}(1_c, 2_{\bar{c}}, 3_g)\rangle = \langle (1-C_{31}-C_{32})(1-S_3)F_{\mathrm{LM}}(1_c, 2_{\bar{c}}, 3_g)\rangle\,. \tag{3.18}$$

This term is free of divergences and can be computed in four dimensions. The subtraction terms in Eq. (3.17) are analytically integrated in $d = 4-2\varepsilon$ dimensions and provide soft and collinear $1/\varepsilon$ poles.

We consider the sum of the two subtraction terms in Eq. (3.17), and rewrite them as follows

$$\langle (1 - C_{31} - C_{32}) S_3 F_{\rm LM}\left(1_c, 2_{\bar{c}}, 3_g\right)\rangle + \langle (C_{31} + C_{32}) F_{\rm LM}\left(1_c, 2_{\bar{c}}, 3_g\right)\rangle\,. \tag{3.19}$$

In the soft limit, the real-emission amplitude factorises into an eikonal function and the Born amplitude. We find

$$S_3 F_{\rm LM}\left(1_c, 2_{\bar{c}}, 3_g\right) = \bar{g}_s^2 \frac{2C_F}{E_3^2} \frac{\rho_{12}}{\rho_{13}\rho_{23}} F_{\rm LM}(1_c, 2_{\bar{c}})\,, \tag{3.20}$$

where $\bar{g}_s$ is the bare strong coupling constant and

$$F_{\rm LM}(1_c, 2_{\bar{c}}) = 2s \cdot d\hat{\sigma}^{LO} = \frac{1}{4N_c^2} \int d{\rm Lips}_H |\mathcal{M}(1_c, 2_{\bar{c}}, H)|^2 \mathcal{F}_{kin}(1_c, 2_{\bar{c}}, H)\,. \tag{3.21}$$

The dependence on the momentum p_3 only appears in the eikonal factor. We use the fact that, in the partonic centre-of-mass frame, the c and $\bar{c}$ momenta are back-to-back. Then, $\rho_{12} = 2$ and $\rho_{13} = 2 - \rho_{23}$. The eikonal function in Eq. (3.20) simplifies to

$$\frac{\rho_{12}}{\rho_{13}\rho_{23}} = \frac{1}{\rho_{13}} + \frac{1}{\rho_{23}}\,. \tag{3.22}$$

In the collinear limits, the same eikonal function becomes

$$C_{13} \frac{\rho_{12}}{\rho_{13}\rho_{23}} = \frac{1}{\rho_{13}}, \qquad C_{23} \frac{\rho_{12}}{\rho_{13}\rho_{23}} = \frac{1}{\rho_{23}}\,. \tag{3.23}$$

The consequence of Eqs. (3.22)-(3.23) is that the first term in Eq. (3.19) vanishes. We focus now on the second term which provides the integrated subtraction terms.

In the collinear limit $\rho_{13} \to 0$, we define $E_3 = (1-z)E_1$ where $(1-z)$ parametrises the fraction of energy taken by the gluon from the incoming charm quark with energy E_1. In this limit, the real-emission amplitude factorises and the real-emission cross section becomes

$$C_{13} F_{\rm LM}(1_c, 2_{\bar{c}}, 3_g) = \bar{g}_s^2 \frac{(1-z)P_{qq}(z)}{E_3^2 \rho_{31}} \frac{F_{\rm LM}(z \cdot 1_c, 2_{\bar{c}})}{z}\,, \tag{3.24}$$

where the splitting function reads

$$P_{qq}(z) = C_F \left[\frac{1+z^2}{1-z} - \varepsilon(1-z)\right] = P_{qq}^{(0)}(z) + \varepsilon P_{qq}^{(\varepsilon)}(z)\,. \tag{3.25}$$

We emphasise that $P_{qq}(z)$ is divergent in the limit $z \to 1$. This is expected as this limit corresponds to the emission of a soft gluon. We note that we need to consider the $\mathcal{O}(\varepsilon)$

part of the splitting function since the integration of $1/\rho_{13}$ over the gluon emission angle produces a pole in ε. Specifically, we find[1]

$$\begin{aligned}\langle C_{13} F_{\rm LM}(1_c, 2_{\bar{c}}, 3_g)\rangle = &-\frac{[\alpha_s]}{\varepsilon}\frac{\Gamma(1-\varepsilon)^2}{\Gamma(1-2\varepsilon)}(2E_1)^{-2\varepsilon} \\ &\times \int_0^1 \frac{dz}{(1-z)^{2\varepsilon}} P_{qq}(z) \langle \frac{F_{\rm LM}(z\cdot 1_c, 2_{\bar{c}})}{z}\rangle\,.\end{aligned} \tag{3.26}$$

Note that we have renormalised the strong coupling constant $\bar{g}_s^2 = (4\pi)\mu^{2\varepsilon} S_\varepsilon\, \alpha_s(\mu)$, where $S_\varepsilon = e^{\varepsilon\gamma_E}/(4\pi)^\varepsilon$, and defined

$$[\alpha_s] = \frac{\alpha_s(\mu)}{2\pi}\frac{\mu^{2\varepsilon}e^{\gamma_E}}{\Gamma(1-\varepsilon)}\,. \tag{3.27}$$

The integral in Eq. (3.26) still diverges in the soft $z \to 1$ limit. To extract this divergence, we isolate the singular part of the splitting function and write

$$P_{qq}(z) = \frac{2C_F}{1-z} + P_{qq}^{\rm reg}(z)\,, \tag{3.28}$$

where $P_{qq}^{\rm reg}(z)$ is regular at $z = 1$. Then, for an arbitrary function $G(z)$ which is regular at $z = 1$, we can write

$$\begin{aligned}\int_0^1 \frac{dz}{(1-z)^{2\varepsilon}} P_{qq}(z) G(z) &= \int_0^1 dz \left[\frac{2C_F}{(1-z)^{1+2\varepsilon}} + (1-z)^{-2\varepsilon} P_{qq}^{\rm reg}(z)\right] G(z) \\ &= -\frac{C_F}{\varepsilon}G(1) + \int_0^1 dz \left[\frac{2C_F}{(1-z)^{1+2\varepsilon}}(G(z)-G(1)) + \frac{P_{qq}^{\rm reg}(z)}{(1-z)^{2\varepsilon}}G(z)\right]\,,\end{aligned} \tag{3.29}$$

In Eq. (3.29), the soft divergence has been extracted and the integral over z has been regulated. After some manipulations, we find that the integrated collinear subtraction term in Eq. (3.26) becomes

$$\begin{aligned}\langle C_{13} F_{\rm LM}(1_c, 2_{\bar{c}}, 3_g)\rangle = [\alpha_s] s^{-\varepsilon}\frac{\Gamma(1-\varepsilon)^2}{\Gamma(1-2\varepsilon)}\Bigg[&\left(\frac{C_F}{\varepsilon^2} + \frac{3C_F}{2\varepsilon} + \frac{7}{2}\right)\langle F_{\rm LM}(1_c, 2_c)\rangle \\ &- \int_0^1 dz\, \left(\hat{P}_{qq}^{(0)}(z) + \varepsilon P_{qq,R}^{(\varepsilon)}(z)\right)\langle \frac{F_{\rm LM}(z\cdot 1_c, 2_{\bar{c}})}{z}\rangle\Bigg]\,.\end{aligned} \tag{3.30}$$

In Eq. (3.30), we have introduced

$$\hat{P}_{qq,R}^{(\varepsilon)}(z) = -C_F\left[\frac{\ln(1-z)}{1-z}2(1+z^2)\right]_+ - (1-z)C_F\,. \tag{3.31}$$

---

[1] We have set the lower integration boundary to 0 in Eq. (3.26) since otherwise the incoming partons would not have enough energy to produce the Higgs boson.

It is easy to obtain the result for the second collinear region, defined by $\vec{n}_3 \cdot \vec{n}_2 \to 1$, by exchanging $p_1 \leftrightarrow p_2$. We define $F_{\rm LM}(1_c, 2_{\bar{c}}; z) = F_{\rm LM}(1_c \cdot z, 2_{\bar{c}})/z + F_{\rm LM}(1_c, 2_{\bar{c}} \cdot z)/z$ and find that the real-emission contribution to the partonic cross section reads

$$\begin{aligned}
2s \cdot d\hat{\sigma}^R_{c\bar{c}} = {} & [\alpha_s] s^{-\epsilon} C_F \frac{\Gamma(1-\epsilon)^2}{\Gamma(1-2\epsilon)} \left(\frac{2}{\epsilon^2} + \frac{3}{\epsilon} + 7 \right) \langle F_{\rm LM}(1_c, 2_c) \rangle \\
& - \frac{[\alpha_s] s^{-\epsilon}}{\epsilon} \frac{\Gamma(1-\epsilon)^2}{\Gamma(1-2\epsilon)} \int_0^1 dz \, \left(\hat{P}^{(0)}_{qq}(z) + \epsilon \hat{P}^{(\epsilon)}_{qq,R}(z) \right) \langle F_{\rm LM}(1_c, 2_{\bar{c}}; z) \rangle \\
& + \hat{O}_{\rm NLO} F_{\rm LM}(1_c, 2_{\bar{c}}, 3_g) \,.
\end{aligned} \tag{3.32}$$

It is clear that the ϵ-pole in the second line of Eq. (3.32) and the one from the PDF renormalisation in Eq. (3.7) cancel each other. The double and the single ϵ-poles in the first line in Eq. (3.32) will cancel with the ones from the virtual contribution, which we calculate now.

The virtual correction to the cross section is given by

$$2s \cdot d\hat{\sigma}_V = \frac{1}{4N_c^2} \int d{\rm Lips}\, 2{\rm Re} \left\{ M^{(0)*}(1_c, 2_{\bar{c}}) M^{(1)}(1_c, 2_{\bar{c}}) \right\}, \tag{3.33}$$

where $M^{(0)}$ is the Born amplitude and $M^{(1)}$ is the one-loop amplitude shown in Fig. 3.1c. The IR structure of the renormalised one-loop amplitude is universal and follows from kinematics and colour charges of the external partons in a given process. Using Catani's operator [66], we split the cross section into two terms

$$2s \cdot d\hat{\sigma}_V = -2[\alpha_s] \cos(\epsilon\pi) C_F \left(\frac{1}{\epsilon^2} + \frac{3}{2\epsilon} \right) s^{-\epsilon} \langle F_{\rm LM}(1_c, 2_{\bar{c}}) \rangle + \langle F^{\rm fin}_{LV}(1_c, 2_{\bar{c}}) \rangle \,, \tag{3.34}$$

where $\langle F^{\rm fin}_{LV}(1, 2_{\bar{c}}) \rangle$ is finite as $\epsilon \to 0$ and is the only process-dependent part of the virtual cross section. Since $\cos(\epsilon\pi) = 1 + \mathcal{O}(\epsilon^2)$, it is clear that the poles in Eq. (3.34) cancel with the ones in the first line of Eq. (3.32). To finalise this calculation, we need to determine the finite part $\langle F^{\rm fin}_{LV}(1_c, 2_{\bar{c}}) \rangle$.

To obtain the one-loop correction to $c\bar{c} \to H$ amplitude, we need to compute the diagram in Fig. 3.1c. After a standard calculation, we find

$$\mathcal{M}^{(1)} = -[\alpha_s] C_F \, (-s - i\epsilon)^{-\epsilon} \left\{ \frac{1}{\epsilon^2} + \frac{3}{2\epsilon} + 1 - \frac{3}{2} \ln \left(\frac{\mu^2}{-s} \right) + \mathcal{O}(\epsilon) \right\} \mathcal{M}^{(0)} \,, \tag{3.35}$$

where the Born amplitude $\mathcal{M}^{(0)}$ reads $\mathcal{M}^{(0)} = y_c/\sqrt{2} \delta_{ij} \bar{v}(p_2) u(p_1)$. Both the strong and the Yukawa coupling have been renormalised in $\overline{\rm MS}$ scheme. We use Eq. (3.35) to determine the virtual contributions in Eq. (3.33). By comparing Eqs. (3.33)-(3.34), for the partonic process $c + \bar{c} \to H$, the process-dependent part of the virtual amplitude reads

$$\langle F^{\rm fin}_{LV}(1, 2_{\bar{c}}) \rangle = - \left(\frac{\alpha_s}{2\pi} \right) C_F \left[2 - 3 \ln \left(\frac{\mu^2}{s} \right) \right] \,. \tag{3.36}$$

Finally, by combining the results in Eq. (3.7), Eq. (3.32), and Eq. (3.34), the NLO QCD correction to the Higgs boson production cross section in the collision of two massless charm quarks reads

$$\boxed{\begin{aligned} 2s \cdot d\hat{\sigma}^{NLO}_{c\bar{c}} =& C_F \frac{\alpha_s(\mu)}{2\pi}\left[5 + \frac{2\pi^2}{3} + 3\ln\left(\frac{\mu^2}{m_H^2}\right)\right]\langle F_{\mathrm{LM}}(1_c, 2_{\bar{c}})\rangle \\ &+ \langle \hat{O}_{\mathrm{NLO}} F_{\mathrm{LM}}(1_c, 2_{\bar{c}}, 3_g)\rangle \\ &+ C_F \frac{\alpha_s(\mu)}{2\pi}\int_0^1 dz\, P_{qq}^{(\varepsilon)}(z) F_{\mathrm{LM}}(1_c, 2_{\bar{c}}, z)\,, \end{aligned}} \tag{3.37}$$

where we set $s = m_H^2$ in the elastic part.

3.1.2 *NLO QCD corrections with massive charm quarks*

We continue with the case of the massive incoming charm quarks. As mentioned at the beginning of this chapter, the charm-quark mass regulates the initial state collinear singularities. Poles in the dimensional regulator will only come from virtual corrections and soft gluon emissions.

Our goal is to extract all terms that become singular as $m_c \to 0$, and set $m_c \to 0$ in the remaining ones. As a consequence, we need to keep the collinear operator in the subtraction since logarithms of m_c will be generated in this kinematical limit. The real-emission contribution to the partonic cross section is given by the formula already derived for the massless quarks

$$\begin{aligned} 2s \cdot d\sigma_R &= \int [dg_3] F_{\mathrm{LM}}\left(1_c, 2_{\bar{c}}, 3_g\right) = \langle F_{\mathrm{LM}}\left(1_c, 2_{\bar{c}}, 3_g\right)\rangle \\ &= \langle S_3 F_{\mathrm{LM}}\left(1_c, 2_{\bar{c}}, 3_g\right)\rangle + \langle (C_{31} + C_{32})(1 - S_3) F_{\mathrm{LM}}\left(1_c, 2_{\bar{c}}, 3_g\right)\rangle \\ &\quad + \langle (1 - C_{31} - C_{32})(1 - S_3) F_{\mathrm{LM}}\left(1_c, 2_{\bar{c}}, 3_g\right)\rangle\,. \end{aligned} \tag{3.38}$$

The last term in Eq. (3.38) corresponds to $\langle \hat{O}_{\mathrm{NLO}} F_{\mathrm{LM}}(1_c, 2_{\bar{c}}, 3_g)\rangle$ in Eq. (3.37). It is free of soft and collinear singularities and, therefore, does not depend on the choice of the regulator.

We need to determine the two integrated subtraction terms in Eq. (3.38). The real-emission amplitude $1_c + 2_{\bar{c}} \to 3_g + H$ factorises in the soft and collinear limits. In the soft limit, where the energy of the emitted gluon goes to zero, the real-emission amplitude can be written as the product of eikonal functions and the Born amplitude [49]

$$\begin{aligned} S_3 F_{\text{LM}}(1_c, 2_{\bar{c}}, 3_g) = C_F \bar{g}_s^2 &\left\{ \frac{2 p_1 \cdot p_2}{(p_1 \cdot p_3)(p_2 \cdot p_3)} - \frac{m_c^2}{(p_1 \cdot p_3)^2} - \frac{m_c^2}{(p_2 \cdot p_3)^2} \right\} \\ &\times F_{\text{LM}}(1_c, 2_{\bar{c}}) \,. \end{aligned} \tag{3.39}$$

The dependence on the gluon momentum p_3 only appears in the soft function. To obtain the soft integrated subtraction term $\langle S_3 F_{\text{LM}}(1_c, 2_{\bar{c}}, 3_g) \rangle$, we integrate the soft function over the gluon phase space

$$\begin{aligned} \langle S_3 F_{\text{LM}}(1_c, 2_{\bar{c}}, 3_g) \rangle = C_F\, \bar{g}_s^2 \langle F_{\text{LM}}(1_c, 2_{\bar{c}}) \rangle \int [dg_3] \\ \times \left\{ \frac{2 p_1 \cdot p_2}{(p_1 \cdot p_3)(p_2 \cdot p_3)} - \frac{m_c^2}{(p_1 \cdot p_3)^2} - \frac{m_c^2}{(p_2 \cdot p_3)(p_2 \cdot p_3)} \right\} . \end{aligned} \tag{3.40}$$

The phase space measure of the emitted gluon is given in Eq. (3.11). We use the fact that we work in the partonic centre-of-mass frame to define $E \equiv E_1 = E_2$. We write the phase space measure explicitly

$$\begin{aligned} &\langle S_3 F_{\text{LM}}(1_c, 2_{\bar{c}}, 3_g) \rangle \\ &= C_F \frac{\alpha_s(\mu)}{2\pi} \langle F_{\text{LM}}(1_c, 2_{\bar{c}}) \rangle \int_{-1}^{1} d(\cos\theta) (\sin^2\theta)^{-\varepsilon} \int_0^{E_{\max}} \frac{dE_3}{E_3^{1+2\varepsilon}} \\ &\times \left\{ \frac{m_H^2}{E^2 (1 - \beta\cos\theta)(1 + \beta\cos\theta)} - \frac{m_c^2}{E^2 (1 - \beta\cos\theta)^2} - \frac{m_c^2}{E^2 (1 + \beta\cos\theta)^2} \right\} , \end{aligned} \tag{3.41}$$

where the integration over the solid angle in $(d-2)$-dimensions has been performed and the strong coupling constant has been renormalised. The factor $\beta = \sqrt{1 - m_c^2/E^2}$ is the velocity of the incoming quarks. The integration over the energy of the emitted gluon is straightforward and provides a pole in the dimensional regulator. To simplify Eq. (3.41), we define $\cos\theta = x$ and rewrite it as

$$\begin{aligned} \langle S_3 F_{\text{LM}}(1_c, 2_{\bar{c}}, 3_g) \rangle = C_F \frac{\alpha_s(\mu)}{2\pi} \langle F_{\text{LM}}(1_c, 2_{\bar{c}}) \rangle \frac{E_{\max}^{-2\varepsilon}}{(-2\varepsilon)} \int_{-1}^{1} dx\, (1 - x^2)^{-\varepsilon} \\ \times \left\{ \frac{4}{(1 - \beta x)(1 + \beta x)} - \frac{m_c^2}{E_1^2 (1 - \beta x)^2} - \frac{m_c^2}{E_2^2 (1 + \beta x)^2} \right\} . \end{aligned} \tag{3.42}$$

The integration over the polar angle remains to be done. One can use partial fractioning to rewrite the first term as the sum of two simple denominator

$$\frac{1}{1 - \beta x} \frac{1}{1 + \beta x} = \frac{1}{2} \left(\frac{1}{1 - \beta x} + \frac{1}{1 + \beta x} \right) . \tag{3.43}$$

The soft limit can therefore be expressed as

$$\langle S_3 F_{\text{LM}}(1_c, 2_{\bar{c}}, 3_g) \rangle = C_F \frac{\alpha_s(\mu)}{2\pi} \frac{E_{\max}^{-2\varepsilon}}{-2\varepsilon} \langle F_{\text{LM}}(1_c, 2_{\bar{c}}) \rangle \left[4 I_{1m} - 2 I_{2m} \right] , \tag{3.44}$$

where

$$I_{1m} = \int_{-1}^{1} dx\, \frac{(1-x^2)^{-\varepsilon}}{1-\beta x}\,, \tag{3.45}$$

$$I_{2m} = \frac{m_c^2}{E_1^2} \int_{-1}^{1} dx\, \frac{(1-x^2)^{-\varepsilon}}{(1-\beta x)^2}\,. \tag{3.46}$$

These integrals need to be computed in the limit $m_c/\sqrt{s} \ll 1$. We find

$$I_{1m} = \frac{2^{-2\varepsilon}\Gamma\left(1-\varepsilon\right)^2}{(-\varepsilon)\Gamma\left(1-2\varepsilon\right)} \left\{1 - \frac{\Gamma\left(1+\varepsilon\right)\Gamma\left(1-2\varepsilon\right)}{\Gamma\left(1-\varepsilon\right)} \left(\frac{m^2}{4E_1^2}\right)^{-\varepsilon}\right\} + \mathcal{O}\left(\frac{m_c^2}{s}\right), \tag{3.47}$$

$$I_{2m} = 2\left(\frac{m_c^2}{E^2}\right)^{-\varepsilon} \Gamma\left(1-\varepsilon\right)\Gamma\left(1+\varepsilon\right) + \mathcal{O}\left(\frac{m_c^2}{s}\right). \tag{3.48}$$

The integrated soft subtraction term in Eq. (3.44) simplifies to

$$\langle S_3 F_{LM}(1_c, 2_{\bar{c}}, 3_g)\rangle = C_F \frac{\alpha_s(\mu)}{2\pi} \frac{2E_{\max}^{-2\varepsilon}}{\varepsilon}\left[1 - \ln\left(\frac{s}{m_c^2}\right)\right] \langle F_{LM}(1_c, 2_{\bar{c}})\rangle\,. \tag{3.49}$$

The last term in Eq. (3.38) is obtained by considering the collinear limits where ρ_{13} and ρ_{23} goes to zero. Since the scalar product $p_1 \cdot p_3$ scales as m_c^2 in these limits, the divergent terms in the limit $m_c \to 0$ can be obtained by a series expansion around $m_c = 0$ of the real-emission amplitude. The integrated collinear subtraction term reads

$$\begin{aligned}\langle C_{31} F_{LM}(1_c, 2_{\bar{c}}, 3_g)\rangle = C_F \bar{g}_s^2 \int [dg_3] \Bigg\{ &\frac{1}{p_1 \cdot p_3}\left(\frac{s^2 + m_H^4}{m_H^2(s - m_H^2)} - \varepsilon \frac{s - m_H^2}{m_H^2}\right) \\ &- \frac{m_c^2}{(p_1 \cdot p_3)^2}\Bigg\} \langle F_{LM}(z \cdot \tilde{1}_c, 2_{\bar{c}})\rangle + \mathcal{O}(m_c^0)\,,\end{aligned} \tag{3.50}$$

where we took the massless limit in the Born amplitude which implies that $\tilde{p}_1^2 = 0$. To write Eq. (3.50), we introduced the standard parametrisation in the collinear limit $p_3 = (1-z)\,\tilde{p}_1$ with $z \in [0,1]$. It leads to $E_3 = (1-z)E_1$ and $s = m_H^2/z$. The integral reads

$$\begin{aligned}\langle C_{31} F_{LM}(1_c, 2_{\bar{c}}, 3_g)\rangle &= C_F \bar{g}_s^2 \int \frac{d\Omega_4^{(d-2)}}{2(2\pi)^{d-1}} \int_{-1}^{1} d(\cos)\sin^{-2\varepsilon}\theta\, E_1^{-4\varepsilon} \\ &\times \int_0^1 dz\,(1-z)^{1-2\varepsilon}\Bigg[\frac{1}{E_1^2(1-z)(1-\beta\cos\theta)}\left(\frac{1+z^2}{1-z} - \varepsilon(1-z)\right) \\ &\qquad - \frac{z\,m_c^2}{E_1^2(1-z)^2}\frac{1}{(1-\beta\cos\theta)^2}\Bigg]\langle\frac{F_{LM}(z\cdot\tilde{1}_c, 2_{\bar{c}})}{z}\rangle\,.\end{aligned} \tag{3.51}$$

The angular integrals have already been calculated when computing the integrated soft subtraction term. Therefore, we find

$$\begin{aligned}\langle C_{31}F_{LM}(1_c,2_{\bar{c}},3_g)\rangle &= \frac{\alpha_s(\mu)}{2\pi}C_F E_1^{-2\varepsilon}\int_0^1 dz\,(1-z)^{-2\varepsilon}\\ &\times\left[\left(\frac{1+z^2}{1-z}-\varepsilon(1-z)\right)I_{1m}-\frac{z}{1-z}I_{2m}\right]\langle\frac{F_{\rm LM}(z\cdot\tilde{1}_c,2_{\bar{c}})}{z}\rangle\,.\end{aligned} \tag{3.52}$$

This integral is singular at $z=1$, corresponding to the limit where the emitted gluon is soft. We must regulate this integral by subtracting the integrated soft-collinear term $\langle C_{31}S_3F_{\rm LM}(1_c,2_{\bar{c}},3_g)\rangle$. It is important to emphasise again that, in this limit, the integration over the gluon phase space decouples. The integrated soft-collinear subtraction term reads

$$\begin{aligned}&\langle C_{31}S_3F_{\rm LM}(1_c,2_{\bar{c}},3_g)\rangle\\ &=\frac{\alpha_s(\mu)}{2\pi}C_F E_1^{-2\varepsilon}\langle F_{\rm LM}(1_c,2_{\bar{c}})\rangle\int_{z_{min}}^1 dz\,\frac{2I_{1m}-I_{2m}}{(1-z)^{1+2\varepsilon}}\\ &=\frac{\alpha_s(\mu)}{2\pi}C_F E_1^{-2\varepsilon}\langle F_{\rm LM}(1_c,2_{\bar{c}})\rangle\,(2I_{1m}-I_{2m})\left\{-\frac{1}{2\varepsilon}\left(\frac{E_{max}}{E_1}\right)^{-2\varepsilon}\right\},\end{aligned} \tag{3.53}$$

where in the second line we use $z_{min}=1-\frac{E_{max}}{E}$. Combining collinear and soft-collinear limits in Eqs. (3.52)-(3.53), we obtain

$$\begin{aligned}&\langle C_{31}(1-S_3)F_{\rm LM}(1_c,2_{\bar{c}},3_g)\rangle=\frac{\alpha_s(\mu)}{2\pi}C_F E_1^{-2\varepsilon}\\ &\times\left\{I_{1m}\int_0^1 dz\,\overline{P}_{qq}^{NLO}(z)\langle F_{\rm LM}(z\cdot\tilde{1}_c,\tilde{2}_{\bar{c}})\rangle-I_{2m}\int_0^1 dz\,\overline{P}_{qq}^{(m)}\langle F_{\rm LM}(z\cdot\tilde{1}_c,2_{\bar{c}})\rangle\right\}.\end{aligned} \tag{3.54}$$

In Eq. (3.54), two splitting functions are defined

$$\overline{P}_{qq}^{NLO}(z)=(1-z)^{-2\varepsilon}\left(\frac{1+z^2}{1-z}-\varepsilon(1-z)\right)+\frac{1}{\varepsilon}\delta(1-z)\left(\frac{E_{max}}{E_1}\right)^{-2\varepsilon} \tag{3.55}$$

$$\overline{P}_{qq}^{(m)}(z)=(1-z)^{-2\varepsilon}\frac{z}{1-z}+\frac{1}{2\varepsilon}\delta(1-z)\left(\frac{E_{max}}{E_1}\right)^{-2\varepsilon}. \tag{3.56}$$

The expression for the second collinear subtraction term $\langle C_{32}(1-S_3)F_{\rm LM}(1_c,2_{\bar{c}},3_g)\rangle$ is analogous. We find

$$\begin{aligned}&\langle C_{31}(1-S_3)F_{\rm LM}(1_c,2_{\bar{c}},3_g)\rangle=\frac{\alpha_s(\mu)}{2\pi}C_F E_1^{-2\varepsilon}\\ &\times\left\{I_{1m}\int_0^1 dz\,\overline{P}_{qq}^{NLO}(z)\langle F_{\rm LM}(\tilde{1}_c,z\cdot\tilde{2}_{\bar{c}})\rangle-I_{2m}\int_0^1 dz\,\overline{P}_{qq}^{(m)}\langle F_{\rm LM}(1_c,z\cdot 2_{\bar{c}})\rangle\right\}.\end{aligned} \tag{3.57}$$

We have calculated all the integrated subtraction terms needed in Eq. (3.38) for the computation of $c+\bar{c} \to H+g$ cross section at NLO QCD. The final results for the real-emission contribution to the cross section reads

$$\begin{aligned} 2s\cdot d\hat{\sigma}_R^{\text{NLO}} &= \frac{\alpha_s(\mu)}{2\pi}\,C_F\int_0^1 dz\left\{P_{qq}^{(0)}(z)\ln\left(\frac{\mu^2}{m_c^2}\right)+P_{qq}^{\text{fin}}(z)\right\}\langle F_{\text{LM}}(1_c,2_{\bar{c}};z)\rangle \\ &+\frac{\alpha_s(\mu)}{2\pi}\,C_F\Big\{-\frac{2L_c}{\varepsilon}-L_c^2+1-\frac{2\pi^2}{3}-3L_c+2L_c\ln\left(\frac{m_H^2}{\mu^2}\right)\Big\}\langle F_{\text{LM}}\left(1_c,2_{\bar{c}}\right)\rangle\,, \end{aligned} \tag{3.58}$$

where $F_{\text{LM}}(1_c,2_{\bar{c}};z) \equiv \frac{1}{z}\left[F_{\text{LM}}(z\cdot 1_c,2_{\bar{c}})+F_{\text{LM}}(1_c,z\cdot 2_{\bar{c}})\right]$. For convenience, we defined $L_c = \ln(m_H^2/m_c^2)-1$. In writing Eq. (3.58), we also used

$$\hat{P}_{qq}^{(0)}(z) = C_F\left[\frac{1+z^2}{1-z}\right]_+\,, \tag{3.59}$$

$$P_{qq}^{\text{fin}}(z) = \hat{P}_{qq}^{(0)}(z)\left(\ln\left(\frac{m_H^2}{\mu^2}\right)-1\right)+C_F(1-z)\,. \tag{3.60}$$

The remaining ε-pole in Eq. (3.58) cancels with the one from the virtual contribution. The calculation is analogous to the one performed for the massless charm quark in the previous section. After renormalisation of the strong coupling and the charm Yukawa coupling, we find in the $m_c \to 0$ limit

$$\begin{aligned} 2s\cdot d\hat{\sigma}_V^{\text{NLO}} = \frac{\alpha_s(\mu)}{2\pi}\,C_F\Bigg\{&\frac{2L_c}{\varepsilon}+4{+}8\frac{\pi^2}{6}+L_c^2+2L_c\ln\left(\frac{\mu^2}{m_H^2}\right) \\ &+3L_c+3\ln\left(\frac{\mu^2}{m_H^2}\right)\Bigg\}\langle F_{\text{LM}}\left(1_c,2_{\bar{c}}\right)\rangle\,. \end{aligned} \tag{3.61}$$

Combining Eq. (3.58) and Eq. (3.61), we obtain the formula for the NLO QCD corrections to the annihilation cross section of two massive charm quarks into a Higgs boson in the limit $m_c/\sqrt{s} \ll 1$. It reads

$$\boxed{\begin{aligned} &2s\cdot d\hat{\sigma}_{c\bar{c}}^{\text{NLO}} = \langle \hat{O}_{\text{NLO}}F_{\text{LM}}\left(1_c,2_{\bar{c}},3_g\right)\rangle \\ &+\frac{\alpha_s(\mu)}{2\pi}\,C_F\left\{5+\frac{2\pi^2}{3}+3\ln\left(\frac{\mu^2}{m_H^2}\right)\right\}\langle F_{\text{LM}}\left(1_c,2_{\bar{c}}\right)\rangle \\ &+\frac{\alpha_s(\mu)}{2\pi}\int_0^1 dz\left(\hat{P}_{qq}^{(0)}(z)\ln\left(\frac{\mu^2}{m_c^2}\right)+P_{qq}^{\text{fin}}(z)\right)\langle F_{\text{LM}}\left(1_c,2_{\bar{c}};z\right)\rangle\,. \end{aligned}} \tag{3.62}$$

3.1.3 *PDF matching*

We have obtained the partonic cross sections for the Higgs production in $c\bar{c}$ annihilation in the $\overline{\text{MS}}$ scheme and in the massive charm-quark scheme. We use Eq. (3.1) to find a relation between them. Since there is no difference between c and $\bar{c}$, we can set $G^{\bar{c}\bar{c}} = G^{cc}$ At order $\mathcal{O}(\alpha_s)$, we find

$$\begin{aligned}
&\int dx_1\, dx_2\, f^{c}_{\overline{\mathrm{MS}}}(x_1,\mu)\, f^{\bar{c}}_{\overline{\mathrm{MS}}}(x_2,\mu)\, d\hat{\sigma}^{\overline{\mathrm{MS}},NLO}_{c\bar{c}\to H} \\
&= \int dx_1\, dx_2 \left(G^{cc}\otimes f^{c}_{\overline{\mathrm{MS}}}\right)(x_1,\mu)\, f^{\bar{c}}_{\overline{\mathrm{MS}}}(x_2,\mu)\, d\hat{\sigma}^{\overline{\mathrm{MS}},NLO}_{c\bar{c}\to H} \\
&\qquad + \int dx_1\, dx_2\, f^{c}_{\overline{\mathrm{MS}}}(x_1,\mu) \left(G^{cc}\otimes f^{\bar{c}}_{\overline{\mathrm{MS}}}\right)(x_2,\mu)\, d\hat{\sigma}^{\overline{\mathrm{MS}},NLO}_{c\bar{c}\to H}\,.
\end{aligned} \tag{3.63}$$

The differences between the two partonic cross sections in Eq. (3.37) and in Eq. (3.62) is absorbed by the coefficient G^{cc}. We find

$$\boxed{G^{cc}(\mu,z) = -\ln\left(\frac{\mu^2}{m_c^2}\right)\hat{P}^{(0)}_{qq}(z) + C_F\left[\frac{1+z^2}{1-z}(1+2\ln(1-z))\right]_+ .} \tag{3.64}$$

Note that any other process with charm quarks in the initial state can also be considered to determine the matching coefficient since PDFs are universal, process-independent objects.

To check our calculations, we studied the charm-quark pair annihilation to the weak boson Z. The singular structure of this process is similar to $c\bar{c}\to H$. The real-emission contribution for a massive and a massless charm quark is given by the result from Eq. (3.32) and Eq. (3.58). The virtual contribution are different from $c\bar{c}\to H$ and need to be calculated. For a massless charm quark, we compute $F^{\mathrm{fin}}_{LV}(1_c, 2_{\bar{c}})$ and, for a massive charm quark, we can use the expression of the form factor from Ref. [67]. Combining everything, we find the same matching coefficient $G^{c\bar{c}}$ in Eq. (3.64), confirming its universality.

3.2 OFF-DIAGONAL COEFFICIENTS

Collinear emissions can change the identity of a hard parton. This leads to the fact that matching coefficients have off-diagonal elements that we now determine. For our purpose, we need to calculate the off-diagonal coefficients G^{cg} and G^{gc}.

We consider the process

$$c(p_1) + g(p_2) \to c(p_3) + H(p_H)\,, \tag{3.65}$$

and compute its cross section in the $\overline{\mathrm{MS}}$ scheme and in the mass-regulated scheme for each of the Higgs boson production mechanisms, see Fig. 3.2.

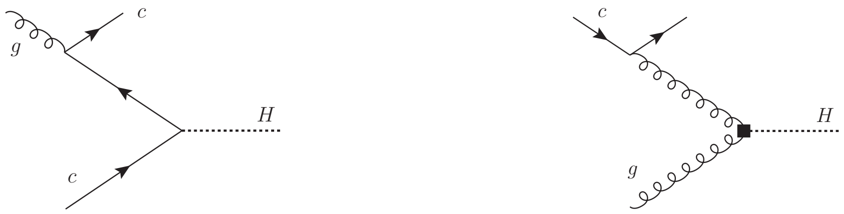

(a) Charm quark + Higgs production through Yukawa coupling.

(b) Charm quark + Higgs production through HEFT vertex.

Figure 3.2: The two mechanisms behind the production of the Higgs boson in association with a charm-quark jet. These processes can be used to determine the off-diagonal coefficients G^{cg} and G^{gc}.

3.2.1 *Yukawa-like Higgs production*

To compute the first off-diagonal coefficient $G^{gc}(z)$, we study the process $cg \to cH$ shown in Fig. 3.2a.

MASSLESS CHARM QUARK For a massless charm quark, there is a collinear singularity as $\rho_{23} \to 0$, where ρ_{ij} is defined in Eq. (3.15). This singularity is regularised dimensionally. It leads to a $1/\varepsilon$ pole which is canceled against the PDF renormalisation term $\delta\hat{\sigma}_{PDF}$ in Eq. (3.7).

We write the cross section as

$$\begin{aligned} 2s \cdot d\hat{\sigma}_{gc} &= \langle F_{\text{LM}}(1_c, 2_g, 3_c) \rangle \\ &= \langle (1 - C_{32}) F_{\text{LM}}(1_c, 2_g, 3_c, H) \rangle + \langle C_{32} F_{\text{LM}}(1_c, 2_g, 3_c, H) \rangle \,. \end{aligned} \tag{3.66}$$

The collinear limit $\rho_{32} \to 0$ of the $H + c$ production cross section (see Fig. 3.2a) is written using the Altarelli-Parisi splitting functions. It reads

$$C_{32} F_{\text{LM}}(1_c, 2_g, 3_c) = \bar{g}_s^2 \frac{P_{qg}^{(0)}(z) + \varepsilon P_{qg}^{(\varepsilon)}(z)}{p_2 \cdot p_3} \frac{F_{\text{LM}}(1_c, z \cdot 2_{\bar{c}})}{z} \,, \tag{3.67}$$

where

$$P_{qg}^{(0)} = T_F[1 - 2z(1-z)] \,, \qquad P_{qg}^{(\varepsilon)} = T_F[-2z(1-z)] \,. \tag{3.68}$$

In Eq. (3.67), we introduced a parameter z defined through an equation $E_3 = E_2(1-z)$. Rewriting the phase space and integrating over ρ_{32}, we find

$$\begin{aligned} \langle C_{32} F_{\text{LM}}(1_c, 2_g, 3_c) \rangle = &-\frac{\alpha_s(\mu)}{2\pi} \left(\frac{\mu^2}{E_2^2} \right)^{\varepsilon} \int_0^1 \frac{dz}{(1-z)^{2\varepsilon}} \\ &\times \left[P_{qg}^{(0)}(z) + \varepsilon P_{qg}^{(\varepsilon)}(z) \right] \left(\frac{1}{\varepsilon} - 2\ln(2) \right) \langle \frac{F_{\text{LM}}(1_c, z \cdot 2_{\bar{c}})}{z} \rangle \,. \end{aligned} \tag{3.69}$$

It is evident that the $1/\varepsilon$ pole cancels against the collinear renormalisation term shown in Eq. (3.7). Finally, the real-emission contribution to the $gc \to Hc$ process through the Yukawa interaction for a massless charm quark reads

$$\begin{aligned} d\hat{\sigma}_{cH} + \delta\hat{\sigma}_{PDF} = -\frac{\alpha_s(\mu)}{2\pi}\frac{1}{2s}\int_0^1 \frac{dz}{(1-z)^{2\varepsilon}}\Bigg[& P_{qg}^{(\varepsilon)}(z) \\ + P_{qg}^{(0)}(z)\left(\ln\left(\frac{\mu^2}{E_2^2}\right) - 2\ln(1-z) - 2\ln(2)\right)\Bigg] & \langle\frac{F_{LM}(1_c, z\cdot 2_{\bar{c}})}{z}\rangle\,. \end{aligned} \tag{3.70}$$

MASSIVE CHARM QUARK The cross section for a massive charm quark is written as a sum of a regularised part and a subtraction term in the same way as in Eq. (3.66). We focus on the integrated collinear term. The collinear limit of F_{LM} reads

$$C_{32}F_{LM}(1_c, 2_g; 3_c) = g_s^2\left[\frac{P_{qg}^{(0)}(z)}{p_2\cdot p_3} + T_F\frac{m_c^2\, z}{(p_2\cdot p_3)^2}\right]\frac{F_{LM}(1_c, z\cdot 2_{\bar{c}})}{z}\,, \tag{3.71}$$

where we do not need to consider $P_{qg}^{(\varepsilon)}$ as in Eq. (3.67) since the m_c regulates the collinear limit and the integration over z is not divergent.

The $m_c \to 0$ limit can be taken everywhere except in the two propagators in Eq. (3.71). This is justified by the absence of soft divergence. We can use the results from Eqs. (3.47)-(3.48) to perform the angular integration of the propagators in Eq. (3.71). We find that the integrated subtraction term, in the limit $m_c \ll \sqrt{s}$, reads

$$\begin{aligned} \langle C_{32}F_{LM}(1_c, 2_g, 3_c, H)\rangle = \frac{\alpha_s(\mu)}{2\pi}\int_0^1 dz\, \Big\{ & 2P_{qg}^{(0)}(z)\left[L_c + \ln(1-z)\right] \\ & + 2T_F\, z(1-z)\Big\}\langle\frac{F_{LM}(1_c, z\cdot 2_{\bar{c}})}{z}\rangle\,, \end{aligned} \tag{3.72}$$

where we have defined $L_c = \ln\left(\frac{2E_2}{m_c}\right)$.

PDF MATCHING We compare the results from Eq. (3.70) and Eq. (3.72) and use Eq. (3.1) to determine the off-diagonal matching coefficient. We find

$$\boxed{G^{cg}(z,\mu) = P_{qg}^{(0)}(z)\ln\left(\frac{m_c^2}{\mu^2}\right)\,.} \tag{3.73}$$

We note that this result agrees with the one recently derived in the context of the electron structure function in Quantum Electrodynamics (QED) in Ref. [68].

3.2.2 *Higgs production in gluon fusion*

To compute the second off-diagonal coefficient $G^{gc}(z)$, we study the $cg \to Hc$ process shown in Fig. 3.2b.

MASSLESS CHARM QUARK In the massless case, the collinear limit $\rho_{13} \to 0$, where ρ_{ij} is defined in Eq. (3.15), is singular. We write

$$\begin{aligned} d\hat{\sigma}_{cg} &= \langle F_{\mathrm{LM}}(1_c, 2_g, 3_c) \rangle \\ &= \langle (1 - C_{31}) F_{\mathrm{LM}}(1_c, 2_g, 3_c, H) \rangle + \langle C_{31} F_{\mathrm{LM}}(1_c, 2_g, 3_c, H) \rangle \,. \end{aligned} \tag{3.74}$$

The collinear subtraction term reads

$$\langle C_{31} F_{\mathrm{LM}}(1_c, 2_g, 3_c) \rangle = \bar{g}_s^2 \left[\frac{P_{gq}^{(0)}(z) + \varepsilon P_{gq}^{(\varepsilon)}}{p_1 \cdot p_3} \right] \langle \frac{F_{\mathrm{LM}}(z \cdot 1_g, 2_g)}{z} \rangle \,. \tag{3.75}$$

We keep the $\mathcal{O}(\varepsilon)$ part of the splitting function as the integral over charm emission angle will lead to a $\frac{1}{\varepsilon}$ pole. In Eq. (3.75), we introduced the splitting functions

$$P_{gq}^{(0)}(z) = C_F \left[\frac{1 + (1-z)^2}{z} \right] \,, \qquad P_{gq}^{(\varepsilon)}(z) = -C_F z \,. \tag{3.76}$$

We perform the integration over the angle of the emitted particle, renormalise the strong coupling constant, and find that the integrated collinear subtraction term in Eq. (3.75) becomes

$$\begin{aligned} \langle C_{31} F_{\mathrm{LM}}(1_c, 2_g, 3_c) \rangle = \frac{\alpha_s(\mu)}{2\pi} \left(\frac{\mu^2}{E_1^2} \right)^{\varepsilon} \int_0^1 dz \, \left(P_{gq}^{(0)}(z) + \varepsilon P_{gq}^{(\varepsilon)}(z) \right) \frac{1}{(1-z)^{2\varepsilon}} \\ \times \left(-\frac{1}{\varepsilon} + 2 \ln(2) \right) \langle \frac{F_{\mathrm{LM}}(z \cdot 1_g, 2_g)}{z} \rangle \,. \end{aligned} \tag{3.77}$$

Comparing this result with the one from the PDF renormalisation term in Eq. (3.7), we observe that in their sum the $1/\varepsilon$ cancels. We find

$$\begin{aligned} d\hat{\sigma}_{cg} + \delta\hat{\sigma}_{PDF} = & \frac{\alpha_s(\mu)}{2\pi} \frac{1}{2s} \int_0^1 dz \, \Bigg\{ P_{gq}^{(\varepsilon)}(z) \\ & - 2 P_{gq}^{(0)}(z) \left(\ln\left(\frac{\mu}{2E_1} \right) - \ln(1-z) \right) \Bigg\} \langle \frac{F_{\mathrm{LM}}(z \cdot 1_g, 2_g)}{z} \rangle \,. \end{aligned} \tag{3.78}$$

MASSIVE CHARM QUARK We consider the subtraction as in the massless case, see Eq. (3.74), and focus on the collinear subtraction term. The collinear limit reads

$$C_{31} F_{\mathrm{LM}}(1_c, 2_g, 3_c) = \bar{g}_s^2 \left[\frac{P_{gq}^{(0)}}{p_1 \cdot p_3 - m_c^2} - C_F \frac{m_c^2 z}{(p_1 \cdot p_3 - m_c^2)^2} \right] \frac{F_{\mathrm{LM}}(z \cdot 1_g, 2_g)}{z} \,. \tag{3.79}$$

We can safely consider the $m_c \to 0$ limit everywhere except in the two propagators in Eq. (3.79) since there is no soft singularity as $E_3 \to 0$. We compute the two integrals over the solid angle of the emitted particle in the limit $m_c \ll \sqrt{s}$. We find that the integrated collinear subtraction term with a massive charm quark reads

$$\begin{aligned}\langle C_{31} F_{\mathrm{LM}}(1_c, 2_g, 3_c) \rangle = \frac{\alpha_s(\mu)}{2\pi} \int_0^1 dz \Bigg\{ &- 2C_F \left(\frac{1-z}{z} \right) \\ &+ 2P_{gq}^{(0)}(z) \left(\ln\left(\frac{2E_1}{m_c} \right) + \ln(1-z) - \ln(z) \right) \Bigg\} \langle \frac{F_{\mathrm{LM}}(z \cdot 1_g, 2_g)}{z} \rangle \,.\end{aligned} \tag{3.80}$$

PDF MATCHING We compare Eq. (3.78) and Eq. (3.80) and use Eq. (3.1) to determine the second off-diagonal coefficient. We find

$$\boxed{G^{gc}(z,\mu) = P_{gq}^{(0)}(z) \left(1 + \ln\left(\frac{m_c^2}{\mu^2} \right) + 2\ln(z) \right) \,.} \tag{3.81}$$

We note that this results agrees with the one derived for the $\Gamma^{[1]}_{\gamma/e}$ matching coefficient in the context of electron structure function, see Eq.(4.189) of Ref. [68].

In the next chapter, we discuss the collinear limit of the interference in the presence of a helicity flip and the importance of *quasi-soft* quark singularities.

4 UNCONVENTIONAL COLLINEAR STRUCTURE AND QUASI-SOFT QUARK SINGULARITY

As already mentioned in the Introduction, the structure of the $cg \to cHg$ amplitude in the soft and collinear limits is affected by requiring the helicity flip of the charm quark. In this chapter, we investigate this issue in detail. We first elucidate the origin of unconventional terms in the collinear limits and then discuss the logarithmic sensitivity of the amplitude to the emission of *quasi-soft* quarks.

4.1 UNCONVENTIONAL COLLINEAR STRUCTURE

Collinear singularities occur when an incoming or an outgoing massless parton emits a gluon or a quark. If the emission angle is so small that the emitted particles cannot be distinguished from the emitters, the amplitude becomes singular. In this limit, the amplitude factorises into a lower-order amplitude and the Altarelli-Parisi splitting functions [69–71]. If the emitter is massive, the collinear singularities are naturally regulated by the emitter's mass and, once integrated over the emission angle, turn into logarithms of the emitter's mass. In the rest of this chapter, we will refer to such terms as *quasi-singular*.

The helicity flip on the fermion line affects the conventional factorisation and leads to *additional* quasi-singular terms. To understand this phenomenon, we start by calculating the squared matrix elements for the case of a collinear gluon emission, without requiring a helicity flip. By doing so, we expect to recover a familiar structure predicted by the collinear factorisation of the amplitude. To understand the effect of the helicity flip, we consider the collinear limit of the interference between the two production mechanisms of the Higgs boson in cg collisions and identify new quasi-singular terms.

We consider the process

$$c(p_1) + g(p_2) \to c(p_3) + g(p_4) + H\,, \tag{4.1}$$

where the Higgs boson is produced either through Yukawa interaction with the charm quark or in the gluon fusion. We are considering the matrix element squared of both production mechanisms. Since the squared matrix element either conserves the helicity of the charm quark or requires to flip it twice in $H\bar{c}c$ vertex, there is no need for an additional helicity flip in this case. We consider the squared matrix element in the collinear limit $p_1 \cdot p_4 \sim m_c^2$. In this limit, the amplitude can be decomposed into two parts

$$\mathcal{M} = \mathcal{M}^{-1} + \mathcal{M}^{0}\,, \tag{4.2}$$

where $\mathcal{M}^{-1}$ is quasi-singular and $\mathcal{M}^{0}$ is *non-singular* or *integrable* in the collinear limit.

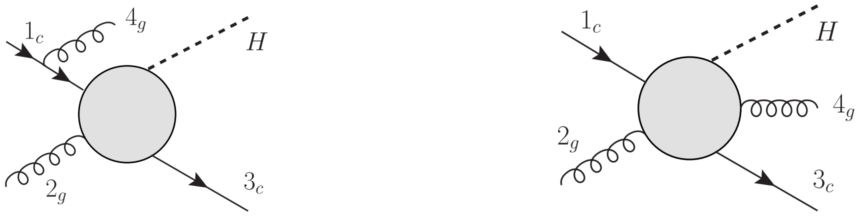

(a) Quasi-singular part of the amplitude.

(b) Finite part of the amplitude.

Figure 4.1: In the collinear limit $\rho_{14} \to 0$, the amplitude can be split into a quasi-singular part $\mathcal{M}^{-1}$ illustrated on the left pane and into a finite part $\mathcal{M}^{0}$ shown on the right pane.

The quasi-singular part of the amplitude reads

$$\mathcal{M}^{-1} \equiv g_s \hat{\mathcal{M}}_{\otimes\, i_q} \frac{\not{p}_1 - \not{p}_4 + m_c}{-2 p_1 \cdot p_4} t^{a_4}_{i_q i_1} \not{\epsilon}_4 u_1\,, \tag{4.3}$$

where $\hat{\mathcal{M}}_{\otimes}$ describes the part of the diagram in Fig. 4.1a without the charm-quark propagator and the spinor of the incoming charm quark u_1. We note that in Eq. (4.3) the sum over repeated colour index i_q is assumed.

We decompose the massive charm-quark momentum p_1 into two light-like momenta

$$p_1 = \alpha \tilde{p}_1 + \beta p_2\,, \tag{4.4}$$

where $\tilde{p}_1^2 = p_2^2 = 0$. We also choose $2\tilde{p}_1 \cdot p_2 = s = (p_1 + p_2)^2$. These conditions fix α and β. We find

$$p_1^2 = m_c^2 = \alpha\beta s\,, \qquad s = (\alpha\tilde{p}_1 + (1+\beta)p_2)^2 = s\alpha(1+\beta)\,, \tag{4.5}$$

so that

$$\alpha = 1 - \frac{m_c^2}{s}\,, \qquad \beta = \frac{m_c^2}{s - m_c^2}\,. \tag{4.6}$$

The Sudakov decomposition of the final state gluon momentum reads

$$p_4 = (1-z)\tilde{p}_1 + y p_2 + p_{4,\perp}\,. \tag{4.7}$$

Using $p_4^2 = 0$, we obtain

$$y = -\frac{p_{4,\perp}^2}{(1-z)s} \,. \tag{4.8}$$

The quasi-singular propagator in Eq. (4.3) can be written as

$$2p_1 \cdot p_4 = \frac{s - m_c^2}{s(1-z)} \left[\frac{(1-z)^2 m_c^2 s}{s - m_c^2} - p_{4,\perp}^2 \right] \approx \frac{1}{1-z} \left[(1-z)^2 m_c^2 - p_{4,\perp}^2 \right] , \tag{4.9}$$

where we kept only the leading terms in m_c^2/s. Using this result, the quasi-singular part of the amplitude becomes

$$\begin{aligned} \mathcal{M}^{-1} &= g_s \hat{\mathcal{M}}_{\otimes\, i_q} \frac{\not{p}_1 - \not{p}_4 + m_c}{-2p_1 \cdot p_4} t^{a_4}_{i_q i_1} \not{\varepsilon}_4 u_1 \\ &= g_s \hat{\mathcal{M}}_{\otimes\, i_q} \left(\not{p}_1 - \not{p}_4 + m_c \right) t^{a_4}_{i_q i_1} \not{\varepsilon}_4 u_1 \frac{1-z}{p_{4,\perp}^2 - (1-z)^2 m_c^2} \,. \end{aligned} \tag{4.10}$$

The logarithmic dependence of $|\mathcal{M}^{-1}|^2$ on m_c appears after the integration of the quasi-singular propagator over the gluon phase space

$$\int \frac{[dp_4]}{p_1 \cdot p_4} \sim \int \frac{d^2 \vec{p}_{4,\perp}}{\vec{p}_{4,\perp}^{\,2} + m_c^2 (1-z)^2} \sim \ln\left(m_c^2\right) , \tag{4.11}$$

where $\vec{p}_{4,\perp}^{\,2} = -p_{4,\perp}^2$. We note that the $z = 1$ limit corresponds to the case where the emitted gluon is soft, leading to a singularity that needs to be studied separately. Apart from this phase-space region, it follows from Eq. (4.11) that m_c protects the singular point $p_{4,\perp} = 0$ and that for the purpose of extracting the quasi-singular $\ln(m_c)$ terms, $p_{4,\perp} \sim m_c$.

For the rest of this calculation, we keep in mind that only those terms in the amplitude squared that scale as $p_{4,\perp}^{-2} \sim m_c^{-2}$ will generate logarithms of m_c once integrated over the gluon phase space. Less singular terms are integrable in the $m_c \to 0$ limit and can, therefore, be discarded when discussing the quasi-collinear limit.

We will now show that the amplitude $\mathcal{M}^{-1}$ scales as m_c^{-1} so that $|\mathcal{M}^{-1}|^2 \sim p_{4,\perp}^{-2} \sim m_c^{-2}$. To this end, we note that the spinor chain in Eq. (4.10) can be simplified using the Dirac algebra

$$\left(\not{p}_1 - \not{p}_4 + m_c \right) \not{\varepsilon}_4 u_1 = 2p_1 \cdot \varepsilon_4 u_1 - \not{p}_4 \not{\varepsilon}_4 u_1 = \left(2p_1 \cdot \varepsilon_4 - \not{p}_4 \not{\varepsilon}_4 \right) u_1 \,, \tag{4.12}$$

where we used the Dirac equation $\not{p}_1 u_1 = m_c u_1$. We need to further rewrite Eq. (4.12) to make its m_c and $p_{4,\perp} \sim m_c$ scaling manifest. To do that, we use the proximity of p_1

and p_4 in the collinear limit and compare the two scalar products $p_1 \cdot \varepsilon_4$ and $p_4 \cdot \varepsilon_4$. They read

$$p_1 \cdot \varepsilon_4 = \alpha \tilde{p}_1 \cdot \varepsilon_4 (1-z) + \beta p_2 \cdot \varepsilon_4 \,, \tag{4.13}$$

$$p_4 \cdot \varepsilon_4 = \tilde{p}_1 \cdot \varepsilon_4 (1-z) + y p_2 \cdot \varepsilon_4 + p_{4,\perp} \cdot \varepsilon_4 = 0 \,, \tag{4.14}$$

where the second scalar product vanishes for physical gluon polarisations. These two equations can be simplified by choosing p_2 as the reference vector for ε_4. [1] We find

$$p_1 \cdot \varepsilon_4 = -\alpha \frac{p_{4,\perp} \cdot \varepsilon_4}{1-z} \,. \tag{4.15}$$

It follows that

$$\begin{aligned} \not{p}_4 \not{\varepsilon}_4 u_1 &= -\not{\varepsilon}_4 \not{p}_4 u_1 = -\not{\varepsilon}_4 \left[\tilde{\not{p}}_1 (1-z) + y \not{p}_2 + \not{p}_{4,\perp} \right] u_1 \\ &= -\not{\varepsilon}_4 \left[\frac{(1-z)}{\alpha} \left[\not{p}_1 - \beta \not{p}_2 \right] + y \not{p}_2 + \not{p}_{4,\perp} \right] u_1 \,. \end{aligned} \tag{4.16}$$

From Eqs. (4.6)-(4.8), we find that $y \sim \vec{p}^{\,2}_{4,\perp}/s \sim m_c^2/s$ and $\beta \sim m_c^2/s$. These two terms lead to an overall scaling $p^0_{4,\perp} \sim m^0_c$ of the quasi-singular amplitude and therefore do not affect the quasi-collinear limit. For the same reason, we can replace α with 1 in Eq. (4.16). Finally, we use the Dirac equation $\not{p}_1 = m_c u_1$ and write Eq. (4.16) as

$$\not{p}_4 \not{\varepsilon}_4 u_1 = -\not{\varepsilon}_4 \left[(1-z) m_c + \not{p}_{4,\perp} \right] u_1 \,. \tag{4.17}$$

We use the results from Eqs. (4.12)-(4.17) and find the following quasi-singular part of the amplitude

$$\begin{aligned} \mathcal{M}^{-1} = g_s^2 \hat{\mathcal{M}}_{\otimes\, i_q} t^{a_4}_{i_q i_1} \frac{1-z}{p^2_{4,\perp} - m_c^2 (1-z)^2} \Bigg[&- \frac{2 p_{4,\perp} \cdot \varepsilon_4}{1-z} \\ &+ \not{\varepsilon}_4 \left((1-z) m_c + \not{p}_{4,\perp} \right) \Bigg] u_1 \,. \end{aligned} \tag{4.18}$$

It follows that $\mathcal{M}^{-1} \sim p^{-1}_{4,\perp} \sim m_c^{-1}$ since both terms in the square brackets in Eq. (4.18) scale as $p_{4,\perp} \sim m_c$.

We would like to find the expression for the quasi-singular contribution of the squared matrix element. Since the finite part of the amplitude scales as $p^0_{4,\perp} \sim m^0_c$, the interference between $\mathcal{M}^0$ and $\mathcal{M}^{-1}$ can be discarded since it scales as $p^{-1}_{4,\perp}$ and, therefore, is integrable in the $m_c \to 0$ limit. The only relevant contribution comes from the squared quasi-singular part

---

[1] We remind the reader that a reference vector r^μ can be arbitrary chosen such that $r \cdot \varepsilon_4 = 0$ as a gauge fixing condition. Together with $\varepsilon_4 \cdot p_4 = 0$ which forces that the longitudinal component to be zero, these conditions ensure that the gluon has only two physical polarisations.

$$\left|\mathcal{M}^{-1}\right|^2 = g_s^2 C_F \frac{(1-z)^2}{\left[p_{4,\perp}^2 - m_c^2(1-z)^2\right]^2} \mathrm{Tr}\Big\{ \hat{\mathcal{O}}\, \hat{\mathcal{M}}^\dagger_{\otimes i_q}\, \hat{\mathcal{M}}_{\otimes i_q} \Big\}, \tag{4.19}$$

where the sum over gluon's polarisations is implicit. In Eq. (4.19), we have defined the operator

$$\begin{aligned} \hat{\mathcal{O}} = & \left[\frac{-2p_{4,\perp}\cdot\varepsilon_4}{1-z} + \not{\varepsilon}_4\left((1-z)m_c + \not{p}_{4,\perp}\right)\right](\not{p}_1 + m_c) \\ & \times\left[\frac{-2p_{4,\perp}\cdot\varepsilon_4^*}{1-z} + \left((1-z)m_c + \not{p}_{4,\perp}\right)\not{\varepsilon}_4^*\right]. \end{aligned} \tag{4.20}$$

We already pointed out that both square brackets in Eq. (4.20) scale as $p_{4,\perp} \sim m_c$. It leads to $\hat{\mathcal{O}} \sim m_c^2$, resulting in an overall scaling $|\mathcal{M}^{-1}|^2 \sim m_c^{-2}$ in Eq. (4.19). The mass in the polarisation sum $\not{p}_1 + m_c$ can be dropped, as it leads to $|\mathcal{M}^{-1}|^2 \sim m_c^{-1}$ and, hence, is not relevant for the quasi-singular limit. We note that $\not{p}_1\not{p}_{4,\perp}\not{\varepsilon}_4 = \not{p}_{4,\perp}\not{\varepsilon}_4\not{p}_1 + \mathcal{O}(m_c^2)$ and write

$$\begin{aligned} \hat{\mathcal{O}} = & \left[\frac{-2p_{4,\perp}\cdot\varepsilon_4}{1-z} + \not{\varepsilon}_4\left((1-z)m_c + \not{p}_{4,\perp}\right)\right] \\ & \times\left[\frac{-2p_{4,\perp}\cdot\varepsilon_4^*}{1-z} + \left(-(1-z)m_c + \not{p}_{4,\perp}\right)\not{\varepsilon}_4^*\right]\not{p}_1 + \mathcal{O}\left(m_c^{-1}\right). \end{aligned} \tag{4.21}$$

To proceed further, it is convenient to define the operator $\hat{\mathcal{O}} = \hat{\mathcal{O}}_1^{\mu\nu}\varepsilon_{4,\mu}\varepsilon_{4,\nu}^*\,\not{p}_1$. It reads

$$\begin{aligned} \hat{\mathcal{O}}_1^{\mu\nu} &= \frac{p_{4,\perp}^\mu p_{4,\perp}^\nu}{(1-z)^2} + \eta^{\mu\nu}\left[-(1-z)^2 m_c^2 + p_{4,\perp}^2\right] - \frac{2p_{4,\perp}\cdot\varepsilon_4}{1-z}\left[2p_{4,\perp}\cdot\varepsilon_4^*\right] \\ &= \left(\frac{1}{(1-z)^2} - \frac{1}{1-z}\right)4p_{4,\perp}^\mu p_{4,\perp}^\nu + \eta_{\mu,\nu}\left[-(1-z)^2 m_c^2 + p_{4,\perp}^2\right]. \end{aligned} \tag{4.22}$$

Until now, we did not account for the sum over gluon's polarisations. In the axial gauge, the sum reads

$$\sum_{\text{pol.}} \varepsilon_{4,\mu}\varepsilon_{4,\nu}^* = -\eta_{\mu,\nu} + \frac{p_{2\mu}p_{4\nu} + p_{2\nu}p_{4\mu}}{p_2\cdot p_4}, \tag{4.23}$$

where we remind the reader that we have chosen p_2^μ as the reference vector for ε_4. We use this result and the fact that $p_2 \cdot p_{4,\perp} = 0$ to simplify $\hat{\mathcal{O}}_1^{\mu\nu}$. We find

$$\sum_{\text{pol.}} \hat{\mathcal{O}}_1^{\mu\nu}\varepsilon_{4,\mu}\varepsilon_{4,\nu}^* = -2p_{4,\perp}^2\frac{1+z^2}{(1-z)^2} + 2m_c^2(1-z)^2. \tag{4.24}$$

The matrix element squared in Eq. (4.19) becomes

$$\begin{aligned}\left|\mathcal{M}^{-1}\right|^2 =& g_s^2\, C_F \frac{(1-z)^2}{\left[p_{4,\perp}^2 - m_c^2(1-z)^2\right]^2} \left\{-2p_{4,\perp}^2 \frac{1+z^2}{(1-z)^2} + 2m_c^2(1-z)^2\right\} \\ & \times \mathrm{Tr}\left\{\, \not{p}_1\, \hat{\mathcal{M}}^\dagger_{\otimes i_q}\, \hat{\mathcal{M}}_{\otimes i_q} \right\} .\end{aligned} \tag{4.25}$$

To recover a familiar structure, we restore the scalar product $p_1 \cdot p_4$ using Eq. (4.9). To do this, we start by rewriting the term in curly brackets in Eq. (4.25) as follows

$$\begin{aligned}&\left\{-2p_{4,\perp}^2 \frac{1+z^2}{(1-z)^2} + 2m_c^2(1-z)^2\right\} \\ &\qquad = -2\left\{\left[p_{4,\perp}^2 - m_c^2(1-z)^2\right] \frac{1+z^2}{(1-z)^2} + 2z\, m_c^2\right\} .\end{aligned} \tag{4.26}$$

The quasi-singular contribution becomes

$$\begin{aligned}\left|\mathcal{M}^{-1}\right|^2 =& -2\, g_s^2\, C_F \left[\frac{(1-z)^2}{p_{4,\perp}^2 - m_c^2(1-z)^2} \frac{1+z^2}{(1-z)^2} + \frac{2z\, m_c^2 (1-z)^2}{\left[p_{4,\perp}^2 - m_c^2(1-z)^2\right]^2}\right] \\ & \times \mathrm{Tr}\left\{\, \not{p}_1\, \hat{\mathcal{M}}^\dagger_{\otimes i_q}\, \hat{\mathcal{M}}_{\otimes i_q} \right\} .\end{aligned} \tag{4.27}$$

It is now easy to use Eq. (4.9) to write

$$\left|\mathcal{M}^{-1}\right|^2 = g_s^2 C_F \left[\frac{1}{p_1 \cdot p_4} \frac{1+z^2}{1-z} - \frac{m_c^2 z}{(p_1 \cdot p_4)^2}\right] \left(\frac{\mathrm{Tr}\left\{\, z\, \not{p}_1\, \hat{\mathcal{M}}^\dagger_{\otimes i_q}\, \hat{\mathcal{M}}_{\otimes i_q} \right\}}{z}\right) , \tag{4.28}$$

This equation can be written in term of the Born amplitude $\mathcal{M}_0$ summed over polarisation of the external particles. It reads

$$\boxed{\left|\mathcal{M}^{-1}\right|^2 = g_s^2\, C_F \left[\frac{1}{p_1 \cdot p_4} \frac{1+z^2}{1-z} - \frac{m_c^2\, z}{(p_1 \cdot p_4)^2}\right] \left(\frac{|\mathcal{M}_0(z \cdot 1_c, 2_g, 3_c)|^2}{z}\right) .} \tag{4.29}$$

This result corresponds to the familiar collinear factorisation formula for a massive quark emitter [69].

As the next step, we would like to study the collinear limit of the interference where helicity flip must occur. We again consider the process in Eq. (4.1). The amplitude is constructed from the sum of diagrams where the Higgs boson directly couples to the charm-quark line, $\mathcal{M}_{y_c}$, and from the sum of diagrams where the Higgs boson interacts with two gluons, $\mathcal{M}_{ggh}$. We are interested in the interference

$$\mathrm{Int}\left\{|\mathcal{M}|^2\right\} \equiv \mathcal{M}_{y_c} \mathcal{M}^\dagger_{ggh} + \mathcal{M}^\dagger_{y_c} \mathcal{M}_{ggh} . \tag{4.30}$$

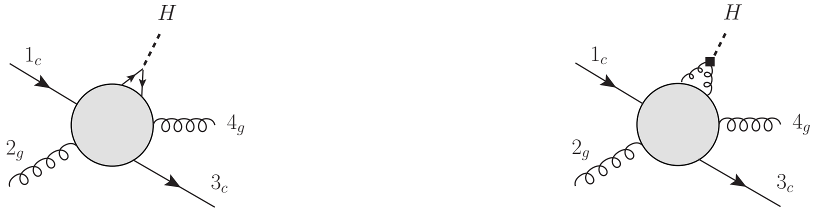

(a) Amplitude $\mathcal{M}_{y_c}$ with Yukawa interaction.

(b) Amplitude $\mathcal{M}_{ggh}$ with effective vertex.

Figure 4.2: The amplitude $\mathcal{M}$ is the sum of the Yukawa-like amplitude $\mathcal{M}_{y_c}$ and the effective ggH amplitude $\mathcal{M}_{ggh}$.

Proceeding as before, we consider the collinear limit of the emission of the gluon with momentum p_4 off the incoming charm-quark with momentum p_1. We split the amplitudes into the quasi-singular and integrable parts

$$\mathcal{M}_{y_c} = \mathcal{M}_{y_c}^{-1} + \mathcal{M}_{y_c}^{0}\,, \qquad\qquad \mathcal{M}_{ggh} = \mathcal{M}_{ggh}^{-1} + \mathcal{M}_{ggh}^{0}\,. \tag{4.31}$$

At the amplitude level, the treatment of $\mathcal{M}_{y_c}$ and $\mathcal{M}_{ggh}$ is the same. Following earlier discussion, we isolate the charm-quark propagator in the quasi-singular part of both amplitudes and find

$$\mathcal{M}_a^{-1} = g_s \hat{\mathcal{M}}_{a,\otimes,i_q} t^{a_4}_{i_q i_1} \left(2p_1 \cdot \varepsilon_4 - \not{p}_4 \cdot \not{\varepsilon}_4\right) \frac{1-z}{p_{4,\perp}^2 - (1-z)^2 m_c^2} u_1\,. \tag{4.32}$$

The index a distinguishes the two mechanisms of Higgs boson production. We use Eq. (4.15) to express the quasi-singular part of the amplitudes as

$$\begin{aligned}\mathcal{M}_a^{-1} = g_s \hat{\mathcal{M}}_{a,\otimes\, i_q} t^{a_4}_{i_q i_1} \Bigg[& \frac{-2p_{4,\perp} \cdot \varepsilon_4}{1-z} \\ & + \hat{\varepsilon}_4 \left(m(1-z) + \hat{p}_{4,\perp} + \kappa \hat{p}_2 \right) \Bigg] u_1 \frac{1-z}{p_{4,\perp}^2 - (1-z)^2 m_c^2}\,,\end{aligned} \tag{4.33}$$

where we used a quantity κ defined as

$$\kappa = \frac{-m_c^2(1-z)}{s} - \frac{p_{4,\perp}^2}{(1-z)s}\,. \tag{4.34}$$

The interference between the two Higgs boson production mechanisms in cg collisions reads

$$\begin{aligned}\mathrm{Int}\left\{|\mathcal{M}|^2\right\} = & \left(\mathcal{M}_{ggh}^{-1,\dagger} \mathcal{M}_{y_c}^{-1} + \mathrm{h.c.}\right) + \left(\mathcal{M}_{ggh}^{0,\dagger} \mathcal{M}_{y_c}^{-1} + \mathcal{M}_{y_c}^{0,\dagger} \mathcal{M}_{ggh}^{-1} + \mathrm{h.c.}\right) \\ & + \left(\mathcal{M}_{y_c}^{0,\dagger} \mathcal{M}_{ggh}^{0} + \mathrm{h.c.}\right)\,.\end{aligned} \tag{4.35}$$

The finite terms in the second line of Eq. (4.35) can de discarded. For the discussion of the quasi-collinear limit, first, we will calculate the mixed contributions in the second term in Eq. (4.35) and, then, the interference of the quasi-singular parts.

The power-counting argument that we used in the first part of this section has to be adapted. We remind the reader that the interference in Eq. (4.35) requires a helicity flip. In this case, logarithms of m_c are provided by terms in the amplitude squared which scales as $m_c\, p_\perp^{-2}$ before phase-space integration, where it has to be understood that m_c stands for the mass insertion and the helicity flip, and $p_\perp^{-2}$ stands for the required scaling as discussed earlier.

We begin the analysis of Eq. (4.35) with the mixed terms. One of them reads

$$\begin{aligned}\mathcal{M}^{0,\dagger}_{ggh}\mathcal{M}^{-1}_{y_c} ={}& g_s\, C_F \mathrm{Tr}\Bigg\{(\not{p}_1 + m_c)\mathcal{M}^{0,\dagger}_{ggh}\hat{\mathcal{M}}^{-1}_{y_c,\otimes\, i_q}\Bigg[\frac{-2p_{4,\perp}\cdot\varepsilon_4}{1-z}\\ &+ \not{\varepsilon}_4\big(m_c(1-z) + \not{p}_{4,\perp} + \kappa\not{p}_2\big)\Bigg]\Bigg\}\frac{1-z}{p^2_{4,\perp}-(1-z)^2 m_c^2}\,.\end{aligned} \tag{4.36}$$

Going back to Eq. (4.10), we note that terms in square brackets in Eq. (4.36) were originally two Dirac matrices, $(\not{p}_1 - \not{p}_4 + m_c)\not{\varepsilon}_4$. Then, to produce a helicity flip, we either have to consider terms with a single Dirac matrix in the square brackets or we will need a helicity flip to come from another part of $(\not{p}_1 + m_c)\mathcal{M}^{0,\dagger}_{ggh}\hat{\mathcal{M}}^{-1}_{y_c,\otimes}$. However, the latter cannot happen since the expression in the square brackets scales as m_c, resulting in a overall scaling $m_c p_\perp^{-1}$ of the mixed terms. Thus, the only relevant contribution for the quasi-collinear limit in Eq. (4.36) arises if we take $\not{p}_1$ from $(\not{p}_1 + m_c)$ and $\not{\varepsilon}_4 m_c(1-z)$ from the square brackets. We find

$$\begin{aligned}\mathcal{M}^{0,\dagger}_{ggh}\mathcal{M}^{-1}_{y_c} ={}& g_s\, C_F \frac{(1-z)^2 m_c}{p^2_{4,\perp}-(1-z)^2 m_c^2}\mathrm{Tr}\left\{\not{p}_1\mathcal{M}^{0,\dagger}_{ggh}\hat{\mathcal{M}}^{-1}_{y_c,\otimes\, i_q}\not{\varepsilon}_4\right\}\Big|_{m_c=0}\\ &+\mathcal{O}\left(m_c p_\perp^{-1}\right)\,.\end{aligned} \tag{4.37}$$

Analogously,

$$\begin{aligned}\mathcal{M}^{0,\dagger}_{y_c}\mathcal{M}^{-1}_{ggh} ={}& g_s\, C_F \frac{(1-z)^2 m_c}{p^2_{4,\perp}-(1-z)^2 m_c^2}\mathrm{Tr}\left\{\not{p}_1\mathcal{M}^{0,\dagger}_{y_c}\hat{\mathcal{M}}^{-1}_{ggh,\otimes\, i_q}\not{\varepsilon}_4\right\}\Big|_{m_c=0}\\ &+\mathcal{O}(m_c p_\perp^{-1})\,.\end{aligned} \tag{4.38}$$

We use Eq. (4.9) to rewrite the sum of Eqs. (4.37)-(4.38) and we find

$$\begin{aligned}\mathcal{M}^{0,\dagger}_{ggh}\mathcal{M}^{-1}_{y_c} + \mathcal{M}^{0,\dagger}_{y_c}\mathcal{M}^{-1}_{ggh} ={}& g_s\, C_F \frac{(1-z)m_c}{2p_1\cdot p_4}\mathrm{Tr}\Big\{\not{p}_1\mathcal{A}^{0,\dagger,i_1}(\tilde{1}_c,2_g,\tilde{3}_c,(1-z)\tilde{1}_c)\\ &\times\mathcal{A}^{-1,i_q}(z\cdot\tilde{1}_c,2_g,\tilde{3}_c)\not{\varepsilon}_4\Big\}+\mathcal{O}\left(m_c p_\perp^{-1}\right)\,,\end{aligned} \tag{4.39}$$

where both amplitudes $\mathcal{A}^{-1,i_q}$ and $\mathcal{A}^{0,\dagger,i_1}$ are computed in the $m_c \to 0$ limit. To emphasise this point, we mark the arguments of the amplitudes with tilde which means that the corresponding momenta are light-like, i. e. $\tilde{p}_i^2 = 0$, for $i = 1,3$. To understand the meaning of the amplitudes $\mathcal{A}^{-1}$ and $\mathcal{A}^0$, we note that they can be used to write down the Born amplitude and the finite part of the real-emission amplitude as

$$\mathcal{M}_0(\tilde{1}_c, 2_g, \tilde{3}_c) = \mathcal{A}_{i_q}(\tilde{1}_c, 2_c, \tilde{3}_c) u(\tilde{p}_1)\,, \tag{4.40}$$

$$\mathcal{M}^0(\tilde{1}_c, 2_g, \tilde{3}_c, 4_g) = \mathcal{A}^0_{i_q}(\tilde{1}_c, 2_c, \tilde{3}_c, 4_g) u(\tilde{p}_1)\,, \tag{4.41}$$

where i_q stands for the colour index of the incoming charm quark.

The next term to consider in Eq. (4.35) is the product of the two quasi-singular parts

$$\begin{aligned} I_{\text{sing}} \equiv \mathcal{M}^{-1,\dagger}_{ggh} \mathcal{M}^{-1}_{y_c} = g_s^2\, C_F \frac{(1-z)^2}{\left[p_{4,\perp}^2 - m_c^2(1-z)^2\right]^2} \mathrm{Tr}\Bigg\{ \Bigg[&\frac{-2p_{4,\perp}\cdot\varepsilon_4}{1-z} \\ &+ \not{\varepsilon}_4 \Big(m_c(1-z) + \not{p}_{4,\perp} + \kappa \not{p}_2 \Big) \Bigg] (\not{p}_1 + m_c) \Bigg[\frac{-2p_{4,\perp}\cdot\varepsilon_4^*}{1-z} \\ &+ \Big(m_c(1-z) + \not{p}_{4,\perp} + \kappa \not{p}_2 \Big) \not{\varepsilon}_4^* \Bigg] \hat{\mathcal{M}}^{-1,\dagger}_{ggh,\otimes\, i_q} \hat{\mathcal{M}}^{-1}_{y_c,\otimes\, i_q} \Bigg\}\,. \end{aligned} \tag{4.42}$$

To compute I_{sing}, we split it into three terms. We define these three terms by the power of $m_c(1-z)$ that appears once the square brackets are multiplied. We collect $\mathcal{O}\left((m_c(1-z))^2 \right)$ contributions in the first term

$$I^{(2)}_{\text{sing}} = g_s^2\, C_F \frac{(1-z)^4 m_c^2}{\left[p_{4,\perp}^2 - m_c^2(1-z)^2\right]^2} \mathrm{Tr}\left\{ \left(\not{\varepsilon}_4 (\not{p}_1 + m_c) \not{\varepsilon}_4^* \right) \hat{\mathcal{M}}^{-1,\dagger\, i_q}_{ggh,\otimes} \hat{\mathcal{M}}^{-1}_{y_c,\otimes\, i_q} \right\}\,. \tag{4.43}$$

We need an even number of Dirac matrices to have a non-vanishing trace. If we consider term with $\not{\varepsilon}_4 \not{p}_1 \not{\varepsilon}_4$, the mass insertion should come from the product $\hat{\mathcal{M}}^{-1,\dagger\, i_q}_{ggh,\otimes} \hat{\mathcal{M}}^{-1}_{y_c,\otimes\, i_q}$, whereas if we consider the term with $m_c \not{\varepsilon}_4 \not{\varepsilon}_4$, the product of the amplitudes can be computed in $m_c \to 0$ limit. Both cases need to be considered as they lead to an overall scaling $I^{(2)}_{\text{sing}} \sim m_c p_\perp^{-2}$. Then, accounting for the sum over the gluon's polarisations and using Eqs. (4.24)-(4.43), $I^{(2)}_{\text{sing}}$ becomes

$$I^{(2)}_{\text{sing}} = g_s^2\, C_F \frac{2(1-z)^4 m_c^2}{\left[p_{4,\perp}^2 - m_c^2(1-z)^2\right]^2} \mathrm{Tr}\left\{ (\not{p}_1 - m_c)\, \hat{\mathcal{M}}^{-1,\dagger}_{ggh,\otimes\, i_q} \hat{\mathcal{M}}^{-1}_{y_c,\otimes\, i_q} \right\}\,. \tag{4.44}$$

The second part in Eq. (4.42) is made of terms accompanied by one power of $m_c(1-z)$. We collect them and find

$$
\begin{aligned}
I^{(1)}_{\text{sing}} = g_s^2\, C_F \frac{(1-z)^3 m_c}{\left[p_{4,\perp}^2 - m_c^2(1-z)^2\right]^2} \mathrm{Tr}\Bigg\{ \Big[\frac{-2p_{4,\perp}\cdot\varepsilon_4}{1-z}\left(2m_c \slashed{\varepsilon}_4^* + 2\varepsilon_4^*\cdot p_1\right) \\
+ 2p_1\cdot(p_{4,\perp}+\kappa p_2)\slashed{\varepsilon}_4\slashed{\varepsilon}_4^* + 2m_c\slashed{\varepsilon}_4(\slashed{p}_{4,\perp}+\kappa\slashed{p}_2)\slashed{\varepsilon}_4^*\Big] \hat{\mathcal{M}}^{-1,\dagger}_{ggh,\otimes i_q} \hat{\mathcal{M}}^{-1}_{y_c,\otimes i_q} \Bigg\}.
\end{aligned}
\tag{4.45}
$$

In Eq. (4.45), we only need to consider terms in the square brackets that scale as m_c^2 since the factor in front of the trace scales as $m_c p_\perp^{-4}$. In addition, similar to the computation of $I^{(2)}_{\text{sing}}$, we need an even number of Dirac matrices in the trace. We find that the relevant terms in Eq. (4.45) can be written as

$$
\begin{aligned}
I^{(1)}_{\text{sing}} = g_s^2\, C_F \frac{-(1-z)^3 m_c}{\left[p_{4,\perp}^2 - m_c^2(1-z)^2\right]^2} \left[\frac{4p_{4,\perp}^2}{(1-z)^2} + 2\kappa s\right] \mathrm{Tr}\left\{ \hat{\mathcal{M}}^{-1,\dagger}_{ggh,\otimes i_q} \hat{\mathcal{M}}^{-1}_{y_c,\otimes i_q} \right\} \\
+ \mathcal{O}\left(m_c p_\perp^{-1}\right).
\end{aligned}
\tag{4.46}
$$

The last term in Eq. (4.42) is the one without $m_c(1-z)$ terms in the square brackets. It reads

$$
\begin{aligned}
I^{(0)}_{\text{sing}} = & g_s^2\, C_F \frac{(1-z)^2}{\left[p_{4,\perp}^2 - m_c^2(1-z)^2\right]^2} \mathrm{Tr}\Bigg\{ \left[\frac{-2p_{4,\perp}\cdot\varepsilon_4}{1-z} + \slashed{\varepsilon}_4\left(\slashed{p}_{4,\perp}+\kappa\slashed{p}_2\right) \right] \\
& \times (\slashed{p}_1 + m_c)\left[\frac{-2p_{4,\perp}\cdot\varepsilon_4}{1-z} + \left(\slashed{p}_{4,\perp}+\kappa\slashed{p}_2\right)\slashed{\varepsilon}_4\right] \hat{\mathcal{M}}^{-1,\dagger}_{ggh,\otimes i_q} \hat{\mathcal{M}}^{-1}_{y_c,\otimes i_q} \Bigg\}.
\end{aligned}
\tag{4.47}
$$

In this case, either we take m_c from $(\slashed{p}_1 + m_c)$ and consider the rest in the $m_c \to 0$ limit, or we keep the momentum $\slashed{p}_1$ in $(\slashed{p}_1 + m_c)$ and, then, the helicity flip has to be provided by the interference of the quasi-singular parts of the amplitudes $\hat{\mathcal{M}}^{-1,\dagger}_{ggh,\otimes i_q} \hat{\mathcal{M}}^{-1}_{y_c,\otimes i_q}$. In both cases, κ terms can be discarded. We use the fact that the commutator $[\slashed{p}_1, \slashed{\varepsilon}_4] = \mathcal{O}(m_c)$ and the polarisation sum in Eq. (4.23) to write Eq. (4.47) as

$$
\begin{aligned}
I^{(0)}_{\text{sing}} = g_s^2\, C_F \frac{(1-z)^2}{\left[p_{4,\perp}^2 - m^2(1-z)^2\right]^2} \left[-2p_{4,\perp}^2 \frac{1+z^2}{(1-z)^2}\right] \\
\times \mathrm{Tr}\left\{ (\slashed{p}_1 + m_c)\hat{\mathcal{M}}^{-1,\dagger}_{ggh,\otimes i_q} \hat{\mathcal{M}}^{-1}_{y_c,\otimes i_q} \right\}.
\end{aligned}
\tag{4.48}
$$

The three terms $I^{(i)}_{\text{sing}}$, $i = 1, 2, 3$, in Eq. (4.48), Eq. (4.46) and Eq. (4.44) can be combined. We use Eq. (4.9) to restore the scalar product $p_1 \cdot p_4$ and find

$$\begin{aligned} I_{\text{sing}} =& g_s^2 C_F \left(\frac{1}{p_1 \cdot p_4} \frac{1+z^2}{1-z} - \frac{C_F m_c^2 z}{(p_1 \cdot p_4)^2} \right) \text{Tr} \left\{ \frac{z \not{p}_1 \mathcal{M}^{-1,\dagger}_{ggh,\otimes} \hat{\mathcal{M}}^{-1}_{y_c,\otimes}}{z} \right\} \\ & - g_s^2 C_F \frac{m_c(1-z)}{z(p_1 \cdot p_4)} \text{Tr} \left\{ \mathcal{M}^{-1,\dagger}_{ggh,\otimes\, i_q} \hat{\mathcal{M}}^{-1}_{y_c,\otimes\, i_q} \right\} . \end{aligned} \tag{4.49}$$

Together, the mixed term in Eq. (4.39), its hermitian conjugate, and the double-singular term in Eq. (4.49) provide the complete quasi-singular structure of the interference in the quasi-collinear limit $\rho_{14} \to 0$. We find

$$\boxed{\begin{aligned} & \lim_{p_1 \cdot p_4 \to 0} \text{Int} \left\{ \mathcal{M}^2(1_c, 2_g; 3_c, 4_g) \right\} \\ & = g_s^2 \Bigg[\left(\frac{P_{qq}(z)}{(p_1 \cdot p_4)} - \frac{C_F m_c^2 z}{(p_1 \cdot p_4)^2} \right) \text{Int} \left\{ \frac{|\mathcal{M}_0(z \cdot 1_c, 2_g; 3_c)|^2}{z} \right\} \\ & \quad - \frac{C_F m_c (1-z)}{z(p_1 \cdot p_4)} \text{Int} \left\{ \text{Tr} \left[\hat{\mathcal{A}}^{i_c}(z \cdot \tilde{1}_c, 2_g; \tilde{3}_c) \hat{\mathcal{A}}^{i_c,\dagger}(z \cdot \tilde{1}_c, 2_g; \tilde{3}_c) \right] \right\} \Bigg] \\ & \quad + g_s C_F \, \frac{(1-z) m_c}{2(p_1 \cdot p_4)} \text{Int} \Big\{ \text{Tr} \Big[\hat{p}_1 \mathcal{A}^{i_c}(z \cdot \tilde{1}_c, 2_g; \tilde{3}_c) \\ & \qquad\qquad \times \hat{\mathcal{A}}^{i_c,\dagger}_0(\tilde{1}_c, 2_g; \tilde{3}_c, (1-z)\tilde{1}_g) \hat{\epsilon}_4 + \text{h.c.} \Big] \Big\} . \end{aligned}} \tag{4.50}$$

The different terms that appear in Eq. (4.50) can be understood as follows. The first term is the result of the standard collinear factorisation identical to the case where no helicity flip is required, cf. Eq. (4.29). In this case, the helicity flip occurs in the hard matrix element squared $|\mathcal{M}_0(z \cdot 1_c, 2_g; 3_c)|^2$. The second and the third terms are new contributions. The second term in Eq. (4.50) has an explicit factor of m_c as this terms originates from the helicity flip on the external charm-quark line. The massless limit is taken in the amputated Born amplitude $\hat{\mathcal{A}}^{i_c}(z \cdot \tilde{1}_c, 2_g; \tilde{3}_c)$. The third term originates from the interference between the finite part and the quasi-singular part of the amplitude. Such terms are not singular in the case of conventional collinear limits. We note that this term is proportional to the strong coupling constant g_s in the first power since another g_s is implicit in the finite part of the real-emission amplitude $\hat{\mathcal{A}}^{i_c}_0(\tilde{1}_c, 2_g; \tilde{3}_c, (1-z)\tilde{1}_g)$.

The determination of the NLO QCD corrections to the interference of the two production mechanisms of the Higgs boson in association with a charm-quark jet will require the analysis of several quasi-collinear limits. We proceed in the following way. From the exact amplitude, we extract the different quasi-collinear limits using the scaling arguments that allow us to derive the results presented in this chapter. After the scaling of each term of the interference in the considered quasi-collinear limit has been identified, we expand the expression in m_c. The quasi-collinear limit of the interference, accounting for the mass insertion, corresponds to the terms that scales as $m_c p_\perp^{-2} \sim m_c m_c^{-2}$.

4.2 QUASI-SOFT QUARK SINGULARITY

Collinear emission is not the only mechanism to produce $m_c \ln(m_c)$ terms. Indeed, we observe that *quasi-soft* quark limit contributes. It means that the real-emission amplitude displays a logarithmic sensitivity on m_c as the energy of the emitted quark goes to zero. The origin of this quasi-singularity can be understood in the following way. We consider the emission of a gluon from an outgoing massive charm quark

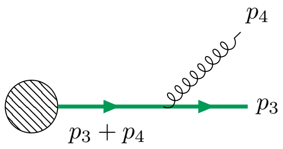

$$\sim \bar{u}(p_3)\frac{\hat{\epsilon}_4^*(\hat{p}_3+\hat{p}_4+m_c)}{2p_3\cdot p_4}\mathcal{A}(1_c,2_g;4_c)\,, \tag{4.51}$$

where the spinor of the outgoing charm quark and its propagator are written explicitly. In the case where the energy of the charm quark tends to $m_c \to 0$, the propagator scales as E_3^{-1}. For massless charm quarks, we have that

$$\bar{u}(p_3) \sim \sqrt{E_3}\,, \tag{4.52}$$

which, as the result, does not lead to any divergences once integrated over the emitted-quark phase space. However, if the helicity flip occurs on the external charm-quark line, the interference term will scale as

$$\mathrm{Int}|\mathcal{A}|^2 \sim \mathrm{Tr}\left[(\hat{p}_3+m_c)\mathcal{A}_{ggh}\mathcal{A}_{yuk}^*\right] \sim \frac{m_c}{E_3^2}\,, \tag{4.53}$$

which leads to $\ln(m_c)$ once integrated over the phase space. Similar to the quasi-collinear limit, the structure of quasi-soft quark singularities in the different contributing channels is found by the direct inspection of the interference, by keeping only terms that scale as $m_c p_\perp^{-2} \sim m_c m_c^{-2}$. We note that quasi-soft quark singularities have been studied at the level of the helicity amplitudes in Ref. [72]. We report here only main results related to the quasi-soft quark singularity obtained in that reference. Analogously to soft gluon factorisation in the soft quark limit, the amplitude factorises into a lower order amplitude and a vector current. It can be illustrated for cg collisions as

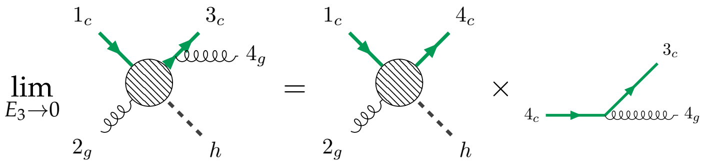

(4.54)

$$\lim_{E_3 \to 0} \mathcal{M}(1_c, 2_g; 3_c, 4_g) = \mathcal{A}^{i_c i_1}(\tilde{1}_c, 2_g; 4_c^{\lambda_q}) \times i g_s t^{a_4}_{i_3 i_c} \frac{\bar{u}_3 \hat{\epsilon}_4 u_4^{\lambda_q}}{2 p_3 \cdot p_4} \,.$$

We recall that the summation over repeated indices is assumed. For the same process, a quasi-soft quark can be emitted from both incoming legs, as shown in Fig. 4.3. Once the three contributions are combined, the real-emission amplitude, $\mathcal{M} = \mathcal{M}_{\mathrm{Y}uk} + \mathcal{M}_{ggh}$, in the quasi-soft quark limit is found to be

$$\begin{aligned} S_3 \mathcal{M}(1_c^{\lambda_1}, 2_g^{\lambda_2}; 3_c^{\lambda_3}, 4_g^{\lambda_4}) = {} & i g_s t^{a_5}_{i_3 i_c} \frac{f_{34}(\lambda_3, \lambda_4, \lambda_q)}{2 p_3 \cdot p_4} \mathcal{M}^{i_c i_1}(1_c^{\lambda_1}, 2_g^{\lambda_2}; 4_c^{\lambda_q}) \,, \\ & + i g_s t^{a_2}_{i_3 i_{\bar{c}}} \frac{f_{32}(\lambda_3, \lambda_2, \lambda_{\bar{q}})}{2 p_2 \cdot p_3} \mathcal{M}^{i_{\bar{c}} i_1}(1_c^{\lambda_1}, 2_{\bar{c}}^{-\lambda_{\bar{q}}}; 4_g^{\lambda_4}) \,, \\ & + i g_s t^{a_g}_{i_3 i_1} \frac{f_{31}(\lambda_3, \lambda_g, \lambda_1)}{2 m_c^2 - 2 p_1 \cdot p_3} \mathcal{M}_{ggh}(1_g^{-\lambda_g}, 2_g^{\lambda_2}; 4_g^{\lambda_4}) \,, \end{aligned} \tag{4.55}$$

where we define the currents

$$\begin{aligned} f_{34}(\lambda_3, \lambda_4, \lambda_q) &= \bar{u}(p_3, \lambda_3) \gamma_\mu u(p_4, \lambda_q) \varepsilon^{\mu *}(p_4, \lambda_4) \,, \\ f_{32}(\lambda_3, \lambda_4, \lambda_{\bar{q}}) &= \bar{u}(p_3, \lambda_3) \gamma_\mu v(p_2, -\lambda_{\bar{q}}) \varepsilon^{\mu}(p_2, \lambda_2) \,, \\ f_{31}(\lambda_3, \lambda_g, \lambda_1) &= \bar{u}(p_3, \lambda_3) \gamma_\mu u(p_1, \lambda_1) \varepsilon^{\mu}(p_1, \lambda_g) \,. \end{aligned} \tag{4.56}$$

The result in Eq. (4.55) is interesting. It assumes a form which is similar to the standard soft-gluon factorisation. Each possible emission comes with a quasi-singular propagator and an eikonal current denoted in this case by the functions f_{3i} , $i = 1, 2, 3$. The main difference is that the real-emission amplitude does not only factorises into the Born amplitude of the $cg \to cH$ process, but also in amplitudes of different processes, such as $c\bar{c} \to gH$, for the second line of Eq. (4.55), and $gg \to gH$, for the third line. We emphasise that in the third line of Eq. (4.55), only the direct coupling of the Higgs boson to two gluons contributes at this order.

We square the amplitude in Eq. (4.55) and keep only terms that provide interference contributions between the two Higgs boson production mechanisms. A detailed

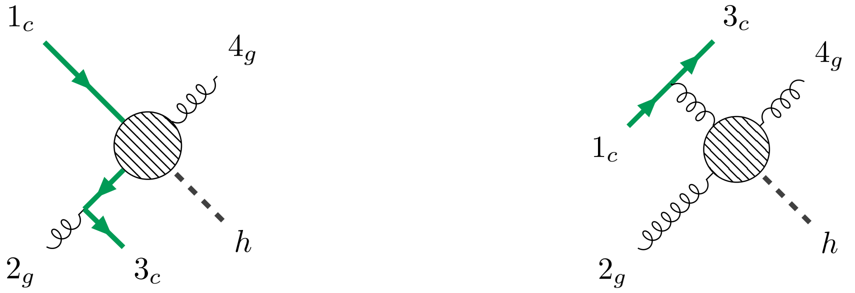

Figure 4.3: Quasi soft-quark contributions are also provided by emissions off initial state partons. Similar to Eq. (4.54), in the quasi soft-quark limit, these two amplitudes factorise into lower-order amplitudes and vector currents.

derivation can be found in Ref. [72]. We report the final form of the interference in the quasi-soft quark limit in the cg partonic channel

$$\begin{aligned}
S_3 \,\mathrm{Int} \sum_{\mathrm{hel}} |\mathcal{M}(1_c, 2_g; 3_c, 4_g)|^2 &= 2 m_c\, g_s^4\, g_{\mathrm{Yuk}}\, g_{ggh}\, N_c\, C_F \\
\times \Bigg[\frac{(2C_F - C_A) p_2 \cdot p_4}{p_2 \cdot p_3\, p_3 \cdot p_4} \left(\frac{s^3 + u^3}{s + u} \right) &+ \frac{C_A\, p_1 \cdot p_4}{(p_1 \cdot p_3 - m_c^2)\, p_3 \cdot p_4} \left(\frac{u^3 + m_h^6}{s\, t\, u} \right) \\
&+ \frac{C_A\, p_1 \cdot p_2}{(p_1 \cdot p_3 - m_c^2)\, p_3 \cdot p_2} \left(\frac{s^3 + m_h^6}{s\, t\, u} \right) \Bigg] .
\end{aligned} \tag{4.57}$$

The limit is similar to the soft function that one would have obtained in the case of a soft gluon emission. We observe the colour factors and the eikonal functions that clearly indicate where the soft quark has been emitted and absorbed. We emphasise that, in this case, the charm-quark mass is present in the propagators that appear in these new eikonal functions, which will require special attention when we will compute the integrated subtraction term. We note that this result has been compared to the one obtained by direct expansion of the exact $cg \to cgH$ amplitude and the agreement has been found.

In the next chapter, we present the different contributing partonic channels, and explain how one can extract the leading logarithms of the real-emission amplitude using the nested soft-collinear subtraction scheme.

5 TREATMENT OF THE REAL-EMISSION CORRECTIONS

In this chapter, we compute the real-emission, interference contributions to the process $pp \to H + \text{jet}_c$. The chapter is organised as follows. First, we present an overview of the different partonic channels contributing to $H + \text{jet}_c$ production. Then, we consider one of these partonic channels in detail to understand how the logarithms of the charm-quark mass can be extracted from the real-emission corrections. Finally, we provide numerical checks that show the correctness of our approach.

5.1 REAL-EMISSION AMPLITUDES

The real-emission contribution to the interference of both Higgs boson production mechanisms which contribute to the process $pp \to H + \text{jet}_c$ is described by several diagrams. We show some of them in Fig. 5.1. Each diagram corresponds to one of the relevant partonic channels. We note that we explicitly calculate the interference in the cg-channel and we obtain results for all the other channels by crossing symmetry. There are eight diagrams where the Higgs boson is emitted off the charm-quark line and eight where the Higgs boson couples to two gluons. We compute the interference between the two

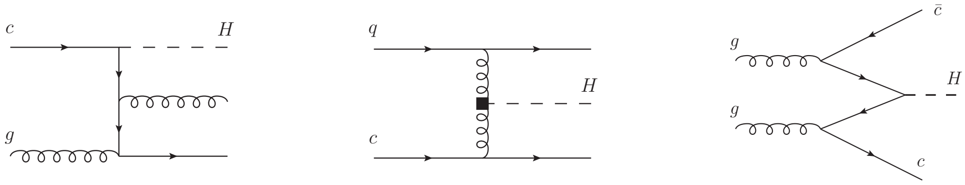

(a) cg channel (b) cq channel (c) gg channel

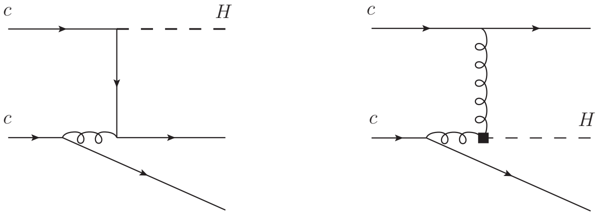

(d) cc channel (e) $c\bar{c}$ channel

Figure 5.1: Examples of diagrams contributing to the NLO QCD corrections of the process $pp \to H + \text{jet}_c$. They are sorted by the pair of partons in the initial state. Both Higgs boson production type have to be included.

production mechanisms using `FORM` [73–76]. To check the calculation, the interference in the cg channel is compared to the interference obtained with `MadGraph5_aMC@NLO` [77] for resolved kinematics.

As mentioned in the Introduction, it is not straightforward to take the limit of the massless charm quark once helicity flip is required. We have seen in Chapter 4 that the presence of the helicity flip affects the conventional collinear factorisation of the amplitude and generates quasi-soft quark singularity. For a numerical implementation, we would like to subtract all quasi-singular terms from the cross section and take the $m_c \to 0$ limit where possible. We explain how this can be done by considering a specific example in the next section.

5.2 EXTRACTION OF THE LOGARITHMS OF THE CHARM-QUARK MASS

To extract logarithms of the charm-quark mass from the real-emission contribution, we use the nested soft-collinear subtraction scheme [65]. This scheme has already been introduced in Chapter 3 in the context of the PDF matching. In this section, we focus on the gg partonic channel. We identify the quasi-singular regions, determine the subtraction terms, and extract the logarithms of m_c.

We consider the following partonic channel

$$g(p_1) + g(p_2) \longrightarrow H(p_H) + c(p_3) + \bar{c}(p_4)\,. \tag{5.1}$$

The process in Eq. (5.1) is symmetric under the exchange of p_3 and p_4. For this reason, we only need to consider the case where the anti-quark $4_{\bar{c}}$ becomes unresolved. The emitted quark can be quasi-soft and can develop mass singularities in the collinear limit. We isolate them by writing

$$\begin{aligned}\langle F_{\mathrm{LM}}(1_g, 2_g; 3_c, 4_{\bar{c}})\rangle = \sum_{i=1}^{3} &\langle (1 - C_{4i})(1 - S_4)\omega^{(i)} F_{\mathrm{LM}}(1_g, 2_g; 3_c, 4_{\bar{c}})\rangle \\ &+ \langle C_{4i}(1 - S_4)\omega^{(i)} F_{\mathrm{LM}}(1_g, 2_g; 3_c, 4_{\bar{c}})\rangle \\ &+ \langle S_4 F_{\mathrm{LM}}(1_g, 2_g; 3_c, 4_{\bar{c}})\rangle\,.\end{aligned} \tag{5.2}$$

In Eq. (5.2), we have introduced the partition of unity

$$\mathbb{1} = \sum_{i=1}^{3} \omega_{123}^{(i)}\,, \tag{5.3}$$

where

$$\omega^{(i)} = \frac{1}{\rho_{4i}} \cdot \left[\frac{1}{\rho_{41}} + \frac{1}{\rho_{42}} + \frac{1}{\rho_{43}}\right]^{-1}\,. \tag{5.4}$$

Partitions localise collinear singularities. Indeed, it is easy to see that the product of $\omega^{(i)}$ and the matrix element squared only develop mass singularities if $\rho_{4i} \to 0$. For instance, if the emitted anti-quark $4_{\bar{c}}$ is quasi-collinear to the incoming gluon 1_g, then $\rho_{14} \to 0$ and the partitions become $\omega^{(1)} = 1$ and $\omega^{(j)} = 0$ for $j = 2, 3$.

The first term on the right-hand side of Eq. (5.2) represents the fully-regulated term, which can be safely integrated with Vegas [78] in the $m_c \to 0$ limit. The second and the third terms are sources of large logarithms that need to be extracted. We begin with the soft subtraction term and, then, we compute the soft-regulated collinear subtraction term.

5.2.1 *Quasi-soft quark subtraction term*

The third term on the right-hand side of Eq. (5.2) is the soft subtraction term

$$\langle S_4 F_{LM}(1_g, 2_g; 3_c, 4_{\bar{c}}) \rangle \,. \tag{5.5}$$

From the discussion in Chapter 4, we know the form of the interference in the soft limit

$$\begin{aligned} S_4 \mathrm{Int}\left\{ |\mathcal{M}(1_g, 2_g; 3_c, 4_{\bar{c}})|^2 \right\} = {} & \frac{(2C_f - C_A)(p_1 \cdot p_2)}{(p_1 \cdot p_4)(p_2 \cdot p_4)} F_{12}(p_1, p_2, p_3) \\ & + \frac{C_A (p_1 \cdot p_3)}{(p_1 \cdot p_4)(m_c^2 + p_3 \cdot p_4)} F_{13}(p_1, p_2, p_3) \\ & + \frac{C_A (p_2 \cdot p_3)}{(p_2 \cdot p_4)(m_c^2 + p_3 \cdot p_4)} F_{23}(p_1, p_2, p_3) \,, \end{aligned} \tag{5.6}$$

where the functions of the Born momentum F_{12}, F_{13} and F_{23} are determined by direct inspection of the real-emission amplitude of the process in Eq. (5.1). Similar to the case of a soft-gluon emission, the integration over the phase space of the soft particle decouples. We obtain

$$\begin{aligned} \langle S_4 F_{LM}(1_g, 2_g; 3_c, 4_{\bar{c}}) \rangle = {} & (2C_f - C_A) \langle F_{12}(p_1, p_2, p_3) \int \frac{[dp_4](p_1 \cdot p_2)}{(p_1 \cdot p_4)(p_2 \cdot p_4)} \rangle \\ & + C_A \langle F_{13}(p_1, p_2, p_3) \int \frac{[dp_4](p_1 \cdot p_3)}{(p_1 \cdot p_4)(m_c^2 + p_3 \cdot p_4)} \rangle \\ & + C_A \langle F_{23}(p_1, p_2, p_3) \int \frac{[dp_4](p_2 \cdot p_3)}{(p_2 \cdot p_4)(m_c^2 + p_3 \cdot p_4)} \rangle \,. \end{aligned} \tag{5.7}$$

The soft-quark eikonal functions need to be integrated over the quark phase space. The fact that the emitted particle is massive makes such integrals unconventional and their calculation is presented in Chapter 6.

5.2.2 *Integrated collinear subtraction terms*

The second term in Eq. (5.2) corresponds to soft-regulated, quasi-collinear subtraction terms. We focus on the limit where the two outgoing quarks become quasi-collinear. It reads

$$\langle C_{43}(1-S_4)F_{\mathrm{LM}}(1_g,2_g;3_c,4_{\bar{c}})\rangle\,. \tag{5.8}$$

We split the calculation into the collinear and the soft-collinear subtraction terms

$$\begin{aligned}\langle C_{43}(1-S_4)F_{\mathrm{LM}}(1_g,2_g;3_c,4_{\bar{c}})\rangle =&\langle C_{43}F_{\mathrm{LM}}(1_g,2_g;3_c,4_{\bar{c}})\rangle\\ &-\langle C_{43}S_4F_{\mathrm{LM}}(1_g,2_g;3_c,4_{\bar{c}})\rangle\,.\end{aligned} \tag{5.9}$$

We start with the collinear subtraction term. We write explicitly the Lorentz-invariant phase space and find

$$\begin{aligned}\langle C_{43}F_{\mathrm{LM}}(1_g,2_g;3_c,4_{\bar{c}})\rangle = \sum_{i=1}^{2}\int &[dp_H][dp_3][dp_4](2\pi)^4\delta\left(p_{12}-p_H-p_3-\bar{p}_4\right)\\ &\times\frac{1}{(p_3+p_4)^2}\frac{p_i\cdot p_3}{p_i\cdot\bar{p}_4}C_i(1_g,2_g,3_c,\bar{4}_{\bar{c}})\,,\end{aligned} \tag{5.10}$$

where the functions C_1 and C_2 are determined by the direct inspection of the interference. In the energy-momentum conserving delta function, the momentum of the parton $\bar{4}_{\bar{c}}$ is $\bar{p}_4$ which corresponds to the quasi-collinear limit of the momentum of the emitted collinear anti-quark

$$C_{43}p_4 = (E_4,\beta_4\vec{n}_3)\equiv\bar{p}_4\,, \tag{5.11}$$

where we defined the velocity of the outgoing anti-quark $\beta_4=\sqrt{1-m_c^2/E_4^2}$. As expected, we see that the collinear subtraction term is quasi-singular in the limit where the outgoing charm-quark is quasi-soft. Therefore, we regulate the functions C_1 and C_2 by their expressions at $E_4\to 0$

$$C_i(1_g,2_g,3_c,\bar{4}_{\bar{c}}) = \left[C_i(1_g,2_g,3_c,\bar{4}_{\bar{c}})-C_{i,\mathrm{soft}}(1_c,2_g,3_c)\right]+C_{i,\mathrm{soft}}(1_c,2_g,3_c)\,, \tag{5.12}$$

where $C_{i,\mathrm{soft}}(1_c,2_g,3_c) = S_4C_i(1_g,2_g,3_c,\bar{4}_{\bar{c}})$. We refer to terms in square brackets in Eq. (5.12) as *regulated* and to the last term in Eq. (5.12) as *soft*. The regulated term is now, by construction, free of soft divergences and can be safely computed in the $m_c\to 0$ limit; the mass dependence should only be retained in the propagator $(p_3+p_4)^{-2}$. We would like to modify the phase-space integral to account for the fact that the two outgoing charm quarks are quasi-collinear. In what follows, we emphasise that the $m_c\to 0$ limit has been considered by introducing the light-like counterparts of the charm outgoing momenta $\tilde{p}_{3,4}$. We define

$$p_{34}=\tilde{p}_3+\tilde{p}_4\,, \tag{5.13}$$

such that

$$\tilde{p}_3 = z p_{34}\,, \qquad \tilde{p}_4 = (1-z) p_{34}\,. \tag{5.14}$$

where $p_{34} = E_{34}(1, \vec{n}_3)$ and, thus, $p_{34}^2 = 0$. The Jacobian is given by

$$J(z, p_{34}) = \frac{\partial(E_3, E_4)}{\partial(E_{34}, z)} = \begin{vmatrix} z & 1-z \\ E_{34} & -E_{34} \end{vmatrix} = E_{34}\,. \tag{5.15}$$

Therefore, the Lorentz-invariant phase space becomes

$$[d\tilde{p}_3][d\tilde{p}_4] = \frac{1}{2}[dp_{34}] E_{34}^2 z(1-z)\, dz\, \frac{d\Omega_4^{(3)}}{(2\pi)^3}\,. \tag{5.16}$$

Note that the phase space is considered in four dimensions since all the singularities are regulated by the charm quark mass. We can perform the integral over the solid angle of $4_{\bar{c}}$ in the regulated term to make the logarithm of the charm-quark mass explicit

$$\begin{aligned} \int \frac{d\Omega_4^{(3)}}{(2\pi)} \frac{1}{p_3 \cdot p_4 + m_c^2} &= \int_{-1}^{1} \frac{d(\cos\theta)}{m_c^2 + E_3 E_4 (1 - \beta_3 \beta_4 \cos\theta)} \\ &= \frac{2}{z(1-z)E_{34}^2} \left[\ln\left(\frac{2E_{34}}{m_c}\right) + \ln(1-z) + \ln(z) \right] + \mathcal{O}(m_c)\,. \end{aligned} \tag{5.17}$$

Inserting this result into the regulated term, we find

$$\begin{aligned} \langle C_{43} F_{\rm LM}(1_g, 2_g; 3_c, 4_{\bar{c}}) \rangle_{\rm reg} &= \frac{1}{(2\pi)^2} \sum_{i=1}^{2} \int [dp_H][dp_{34}](2\pi)^4 \delta\left(p_{12} - p_H - p_{34}\right) \\ &\times \int_0^1 \frac{z\, dz}{1-z} \Big[C_i(1_g, 2_g, z p_{34}, (1-z) p_{34}) - C_{i,\rm soft}(1_c, 2_g, z p_{34}) \Big] \\ &\times \Big[\ln(2E_{34}/m_c) + \ln(1-z) + \ln(z) \Big]\,. \end{aligned} \tag{5.18}$$

where we emphasise again that all four momenta in this subtraction term are light-like.

We are left with the soft term that we defined earlier in Eq. (5.12). It displays logarithmic sensitivity to m_c in the limit $E_4 \to 0$ and, for this reason, the massless limit cannot be taken there. We write

$$\begin{aligned} \langle C_{43} F_{\rm LM}(1_g, 2_g; 3_c, 4_{\bar{c}}) \rangle_{\rm soft} &= \sum_{i=1}^{2} \int [dp_H][dp_3][dp_4] \\ &\times (2\pi)^4 \delta\left(p_{12} - p_H - p_3 - \bar{p}_4\right) \frac{1}{(p_3 + p_4)^2} \frac{p_i \cdot p_3}{p_i \cdot \bar{p}_4} C_{i,\rm soft}(1_c, 2_g, 3_c)\,. \end{aligned} \tag{5.19}$$

This term can be regulated by a soft-collinear subtraction term. It is obtained from Eq. (5.6) by applying the collinear limit $\rho_{34} \to 0$. In this limit, only the last two eikonal functions survive. We find

$$\begin{aligned}\langle C_{43} S_4 F_{LM}(1_g, 2_g; 3_c, 4_{\bar{c}})\rangle = \sum_{i=1}^{2} \int [dp_H][dp_3][dp_4](2\pi)^4 \delta\,(p_{12} - p_H - p_3) \\ \times \frac{2C_A F_{i3}(p_1, p_2, p_3)}{(p_3+p_4)^2} \frac{p_i \cdot p_3}{p_i \cdot \bar{p}_4}\,. \end{aligned} \tag{5.20}$$

We emphasise that in the quasi-soft limit, the momentum p_4 is removed from the energy-momentum conserving delta function. It is interesting to note that the function $C_{i,\text{soft}}$ is proportional to the soft limit of the function F_i

$$C_{i,\text{soft}} = 2C_A F_{i3}(1_c, 2_g, 3_c)\,. \tag{5.21}$$

Therefore, the integrals in Eq. (5.19) and Eq. (5.20) can naturally be combined

$$\begin{aligned}&\langle C_{43} F_{LM}(1_g, 2_g; 3_c, 4_{\bar{c}})\rangle_{\text{soft}} - \langle C_{43} S_4 F_{LM}(1_g, 2_g; 3_c, 4_{\bar{c}})\rangle \\ &= \sum_{i=1}^{2} \int [dp_H][dp_3][dp_4](2\pi)^4 \Big[\delta\,(p_{12} - p_H - p_3 - \bar{p}_4) - \delta\,(p_{12} - p_H - p_3)\Big] \\ &\quad \times \frac{2C_A F_{i3}(p_1, p_2, p_3)}{(p_3+p_4)^2} \frac{p_i \cdot p_3}{p_i \cdot \bar{p}_4}\,. \end{aligned} \tag{5.22}$$

This term is regulated since, in the soft limit, where the energy of the emitted anti-quark $4_{\bar{c}}$ becomes very small $(E_4 \to 0)$, the difference between the two Dirac delta functions cancels out. However, to further understand how to treat the difference of two delta functions, we need to investigate integration over the energy.

Integrating over the solid angle of the quark $4_{\bar{c}}$ in Eq. (5.22) is straightforward as it only appears in the unexpanded propagator $(p_3 + p_4)^{-2}$. We use Eq. (5.17) to compute that integral. On the other hand, integration over energy fraction is non-trivial. To perform it, we split the energy of the soft contribution to the collinear subtraction term into two parts and write

$$\langle C_{43} F_{LM}(1_g, 2_g; 3_c, 4_{\bar{c}})\rangle_{\text{soft}} \equiv \langle C_{43}^{\text{low}}\rangle_{\text{soft}} + \langle C_{43}^{\text{high}}\rangle_{\text{soft}}\,, \tag{5.23}$$

where

$$\begin{aligned}\langle C_{43}^{\text{low}}\rangle_{\text{soft}} = \sum_{i=1}^{2} \int [dp_H][dp_3][dp_4] \frac{2C_A F_{i3}(p_1, p_2, p_3)}{(p_3+p_4)^2} \frac{p_i \cdot p_3}{p_i \cdot \bar{p}_4} \\ \times (2\pi)^4 \delta\,(p_{12} - p_H - p_3 - \bar{p}_4)\,\theta(E_4 - \sigma)\,, \end{aligned} \tag{5.24}$$

$$\begin{aligned}\langle C_{43}^{\text{high}}\rangle_{\text{soft}} = \sum_{i=1}^{2} \int [dp_H][dp_3][dp_4] \frac{2C_A F_{i3}(p_1, p_2, p_3)}{(p_3+p_4)^2} \frac{p_i \cdot p_3}{p_i \cdot \bar{p}_4} \\ \times (2\pi)^4 \delta\,(p_{12} - p_H - p_3 - \bar{p}_4)\,\theta(\sigma - E_4)\,. \end{aligned} \tag{5.25}$$

In Eqs. (5.24)-(5.25), we introduced a parameter σ such that $m_c \ll \sigma \ll E_3$. In the high energy region, the charm-quark mass can be neglected since $E_4 > \sigma$. We use the parametrisation introduced in Eq. (5.14) and find

$$\langle C_{43}^{\text{high}} \rangle_{\text{soft}} = \sum_{i=1}^{2} \int [dp_H][dp_{34}] \delta(p_{12} - p_H - p_{34}) \\ \times I^{c_{34}}(E_{34}, \sigma)\, 2C_A\, F_{i3}(p_1, p_2, z p_{34}) \,, \tag{5.26}$$

where we defined

$$I^{c_{34}}(E_{34}, \sigma) = \frac{1}{(2\pi)^2} \int_0^{1-\sigma/E_{34}} \frac{dz\, z}{1-z} \left[\ln\left(\frac{2E_{34}}{m_c}\right) + \ln(z) + \ln(1-z) \right] . \tag{5.27}$$

On the other hand, in the low energy region, we can use the fact that $E_4 \ll E_3$ and remove p_4 from the energy-momentum conserving delta function. The integral in this region reads

$$\langle C_{43}^{\text{low}} \rangle_{\text{soft}} = \sum_{i=1}^{2} \int [dp_H][dp_3][dp_4] \delta(p_{12} - p_H - p_3) \theta(\sigma - E_4) \\ \times \frac{2C_A F_{i3}(p_1, p_2, p_3)}{(p_3 + p_4)^2} \frac{p_i \cdot p_3}{p_i \cdot \bar{p}_4} \,. \tag{5.28}$$

This piece is identical to the soft-collinear subtraction term shown in Eq. (5.20) in the region $E_4 < \sigma$, and, therefore, they cancel out. We still need to compute the soft-collinear subtraction term at high energies, i. e.

$$\langle C_{43}^{\text{high}} \rangle_{\text{soft}} = \sum_{i=1}^{2} \int [dp_H][dp_3][dp_4] (2\pi)^4 \delta\left(p_{12} - p_H - p_3\right) \\ \times \frac{2C_A F_{i3}(p_1, p_2, p_3)}{(p_3 + p_4)^2} \frac{p_i \cdot p_3}{p_i \cdot \bar{p}_4} \theta(E_4 - \sigma) \,. \tag{5.29}$$

Writing explicitly the phase space of the parton $4_{\bar{c}}$ and introducing the variable $1 - z = E_4/E_3$, we find

$$\langle C_{43}^{\text{high}} \rangle_{\text{soft}} = \sum_{i=1}^{2} \int [dp_H][dp_3] \delta(p_{12} - p_H - p_3) I^{s_4}(E_3, E_{\max}, \sigma) \\ \times 2C_A F_{i3}(p_1, p_2, p_3) \,, \tag{5.30}$$

where, by analogy to Eq. (5.26), we defined

$$I^{s_4}(E_3, E_{\max}, \sigma) = \frac{1}{(2\pi)^2} \int_{\sigma/E_3}^{E_{\max}/E_3} \frac{dz}{1-z} \left[\ln\left(\frac{2E_3}{m_c}\right) + \ln\left(\frac{1-z}{2-z}\right) \right] . \tag{5.31}$$

We rename $p_3 \to p_{34}$ in Eq. (5.30) and use it to write Eq. (5.22) as

$$\begin{aligned}\langle C_{43} F_{\rm LM}(1_g,2_g;3_c,4_{\bar{c}})\rangle_{\rm soft} - \langle C_{43} S_4 F_{\rm LM}(1_g,2_g;3_c,4_{\bar{c}})\rangle &= \sum_{i=1}^{2}\int [dp_H][dp_{34}] \\ \times (2\pi)^4 \delta\left(p_{12}-p_H-p_{34}\right) 2 C_A F_{i3}(p_1,p_2,p_3) &\left[I^{c_{34}}(E_{34},\sigma) - I^{s_4}(E_{34},E_{\rm max},\sigma)\right].\end{aligned} \tag{5.32}$$

The difference between the two integrals in Eq. (5.32) can be explicitly calculated. We find

$$\begin{aligned}I^{c_{34}}(E_{34},\sigma) - I^{s_4}(E_{34},E_{\rm max},\sigma) &= \frac{1}{(2\pi)^2}\left[2 - \frac{\pi^2}{6} - \frac{1}{2}\ln^2\left(\frac{E_{\rm max}}{E_{34}}\right)\right. \\ &\left. - \ln\left(\frac{2E_{34}}{m_c}\right) - \ln\left(\frac{2E_{34}}{m_c}\right)\ln\left(\frac{E_{\rm max}}{E_{34}}\right) - {\rm Li}_2\left(-\frac{E_{\rm max}}{E_{34}}\right)\right].\end{aligned} \tag{5.33}$$

This concludes the study of the collinear sector with $\theta_{34} = 0$ for the gg partonic channel. The collinear subtraction term is composed of the regulated collinear subtraction term given in Eq. (5.18) and the difference between the high-energy region of the soft-collinear subtraction term and the collinear one, see Eq. (5.32). We have successfully extracted the logarithms of the charm-quark mass and took $m_c \to 0$ limit after that.

The $gg \to c\bar{c}H$ partonic channel also requires the study of the collinear region C_{41} and C_{42}. The extraction of the logarithms of m_c is done in full analogy to the above discussion. The only difference comes from the parametrisation of the quasi-collinear singularity, which is similar to what has been done in Chapter 3. We note that if one chooses $E_{\rm max} = E_{1,2}$, the term analogous to the one in Eq. (5.32) vanishes.

5.3 NUMERICAL CHECK

The validity of the results derived in the previous section can be proved numerically. As we already mentioned, the cross section of $gg \to c\bar{c}H$ process is finite in four dimensions if m_c is finite. On the other hand, we have just computed the same cross section by extracting all $\ln(m_c)$ enhanced terms and taking the $m_c \to 0$ limit where possible. Therefore, we can compare the interference computed for a small mass m_c and the results in Eqs. (5.18)-(5.32). If m_c is sufficiently small, the two results should agree.

The result of such a comparison is presented in Fig. 5.2. We use $\sigma_{\rm real}$ to denote the interference obtained from the interference for finite m_c and $\sigma_{\rm rec}$ to denote the one resulting from the application of the subtraction scheme. In the upper pane, we show the value of the cross section in femtobarn. In the lower pane, we display the relative difference of $\sigma_{\rm rec}$ and $\sigma_{\rm real}$. It is clear that the two results converge to each other as the

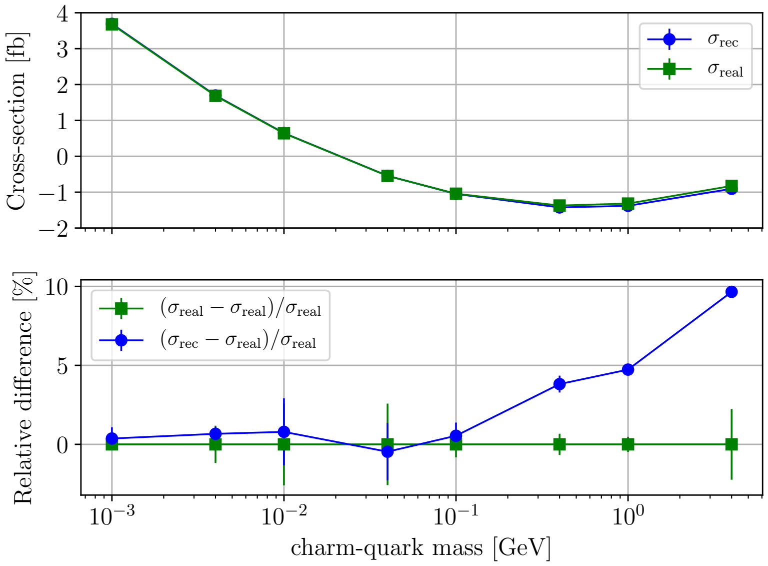

Figure 5.2: Numerical validation of the extraction of the $\ln(m_c)$ terms for the interference of $gg \to c\bar{c}H$ with $m_c \neq 0$. Denoted with green squares, the cross sections σ_{real} is obtained by keeping the mass of the charm finite. In blue dot, the reconstructed cross section σ_{rec} is build from the sum of the regulated term where the massless limit has been considered and the sum of the subtraction terms as defined in Eq. (5.2).

charm-quark mass m_c approaches zero.

The calculation of the real-emission amplitude and the extraction of the logarithms of m_c using the nested soft-collinear subtraction scheme has been demonstrated for one partonic channel. An important ingredient of this and related calculations in other channels is the integration of the soft-quark eikonal functions over the soft-quark momentum, cf.Eq. (5.7). In the next chapter, we explain how such eikonal functions can be computed.

6 INTEGRATED EIKONAL FUNCTIONS

In this chapter, we explain how to compute the eikonal functions that we encountered in the calculation of the real-emission contribution. These functions originate from soft-quark singularities. They are somewhat unconventional since the emitters and the emitted unresolved particle can be massive. We present in detail the calculation of two of the integrated eikonal functions, required to compute the subtraction terms, and provide analytical results for all other integrated eikonal functions.

6.1 INTEGRATED QUASI-SOFT QUARK EIKONAL FUNCTIONS

We have seen in Chapter 4 that the quasi-soft quark limit of the interference resembles the soft limit of gluon-emission amplitudes. Nevertheless, the eikonal functions required to describe the quasi-soft quark limit are different since, in addition to the emitters, the soft particle is massive. In this section, we explain how to compute the following integrated eikonal function

$$I_{AB}^{(m_A,m_B)} = \int \frac{d^3\vec{p}}{(2\pi)^3 E_{\vec{p}}} \theta(E_{\max} - E_{\vec{p}}) \frac{p_A \cdot p_B}{(p_A \cdot p)(p_B \cdot p)}\,, \tag{6.1}$$

where $p^2 = m^2$, $p_A^2 = m_A^2$ and $p_B^2 = m_B^2$. We consider this integral in the limit where $E_{\max} \gg m$ and $m \sim m_A \sim m_B$. We note that this integral appeared in the discussion of the real-emission contribution in gg-channel, cf. Eq. (5.7). For this channel, we will need both $I_{AB}^{(0,0)}$ and $I_{AB}^{(m,0)}$. The latter is slightly more difficult to compute because, in addition to the massive emitted particle, one of the emitters is massive as well. We provide here a short overview of the calculation. A detailed derivation is given in Appendix B. We start by calculating $I_{AB}^{(0,0)}$ and use this result to compute $I_{AB}^{(m,0)}$.

We start the calculation of $I_{AB}^{(0,0)}$ by combining the denominators in Eq. (6.1) using Feynman parameterisation and integrating over the emission angle of the unresolved particle. After the integration over the Feynman parameter is performed, we are left with the integral over the energy of the emitted quark. The integral $I_{AB}^{(0,0)}$ defined in Eq. (6.1) can be written as

$$I_{AB}^{(0,0)} = \frac{1}{16\pi^2} \int_0^{\beta_{\max}} d\beta\, \beta \frac{\partial}{\partial \beta} \left[\ln^2 \left(\frac{\sqrt{1-\beta^2\mathfrak{c}^2} + \beta\mathfrak{s}}{\sqrt{1-\beta^2\mathfrak{c}^2} - \beta\mathfrak{s}} \right) \right]\,, \tag{6.2}$$

where $\beta = \sqrt{1 - m^2/E^2}$ is the velocity of the emitted quark, $\mathfrak{s} = \sin(\theta_{AB}/2)$, θ_{AB} is the angle between the three momenta of the emitters A and B, and $\mathfrak{c} = \cos(\theta_{AB}/2)$.

We integrate by parts in Eq. (6.2) and expand the logarithm in the integrand in $m/E_{\max}$. The integral in Eq. (6.2) becomes

$$I_{AB}^{(0,0)} = \frac{1}{16\pi^2} \left\{ \ln^2\left(\frac{4\mathfrak{s}^2 E_{\max}^2}{m^2}\right) - I_\beta \right\}, \tag{6.3}$$

where

$$I_\beta = \int_0^1 d\beta \ln^2\left(\frac{\sqrt{1-\beta^2\mathfrak{c}^2} + \beta\mathfrak{s}}{\sqrt{1-\beta^2\mathfrak{c}^2} - \beta\mathfrak{s}}\right) . \tag{6.4}$$

This integral is calculated in the following way. We differentiate I_β with respect to $\mathfrak{s}$ and write the result as

$$\frac{\partial I_\beta}{\partial \mathfrak{s}} = -\frac{4}{\mathfrak{c}^2} \int_0^{1-\delta} d\beta \frac{\partial}{\partial \beta}\left[\sqrt{1-\beta^2\mathfrak{c}^2}\right] \ln\left(\frac{\sqrt{1-\beta^2\mathfrak{c}^2} + \beta\mathfrak{s}}{\sqrt{1-\beta^2\mathfrak{c}^2} - \beta\mathfrak{s}}\right) , \tag{6.5}$$

where, for technical reasons, we introduced the small parameter δ. We integrate by parts in Eq. (6.5) and find

$$\frac{\partial I_\beta}{\partial \mathfrak{s}} \approx -\frac{4}{\mathfrak{c}^2} \left\{ \mathfrak{s} \ln\left(\frac{2\mathfrak{s}^2}{\delta}\right) - 2\mathfrak{s} \int_0^{1-\delta} \frac{d\beta}{1-\beta^2} \right\} = -\frac{4\mathfrak{s}}{\mathfrak{c}^2} \ln\left(\mathfrak{s}^2\right) , \tag{6.6}$$

where, in the first step, we approximated the argument of the logarithm in the limit $\delta \ll 1$. It is now possible to calculate the integral in Eq. (6.4) by solving the differential equation in Eq. (6.6). We choose $\mathfrak{s} = 0$ as the boundary condition since it follows from Eq. (6.4) that $I_\beta(\mathfrak{s} = 0) = 0$. We find that the integral in Eq. (6.3) takes the following simple form

$$\boxed{I_{AB}^{(0,0)} = \frac{1}{16\pi^2} \left\{ \ln^2\left(\frac{4\mathfrak{s}^2 E_{\max}^2}{m^2}\right) - \frac{\pi^2}{3} + 2\mathrm{Li}_2\left(\mathfrak{c}^2\right) \right\} .} \tag{6.7}$$

We switch now to the computation of the integral $I_{AB}^{(m,0)}$. As before, we introduce a Feynman parameter and integrate over the azimuthal angle. The difference is that this time we integrate over β first. We find

$$I_{AB}^{(m,0)} = \frac{\mathfrak{s}^2}{4\pi^2} \int_0^1 \frac{dy}{1-\eta_y^2} \left\{ \ln\left(\frac{1+\beta_{\max}}{1-\beta_{\max}}\right) - \frac{1}{\eta_y} \ln\left(\frac{1+\beta_{\max}\eta_y}{1-\beta_{\max}\eta_y}\right) \right\} , \tag{6.8}$$

where $\beta_{\max} = \sqrt{1 - m^2/E_{\max}^2}$ and η_y reads

$$\eta_y^2 = 1 - 4y(1-y)\mathfrak{s}^2 - \xi_A^2 y(y + (1-y)\cos\theta_{AB}) , \tag{6.9}$$

and $\xi_A = \frac{m}{E_A}$. In Eq. (6.8), the massless limit $\beta_{\text{max}} \to 1$ cannot be taken because $\ln(1-\beta_{\text{max}})$ diverges in this limit. We isolate this singularity by rewriting Eq. (6.8) as follows

$$I_{AB}^{(m,0)} = I^{(0)} + I_y^{(m)}\,, \tag{6.10}$$

where

$$I^{(0)} = -\frac{\mathfrak{s}^2}{4\pi^2}\int_0^1 dy \left[\frac{1}{(1+\eta_y)\eta_y}\ln\left(\frac{1+\eta_y}{1-\eta_y}\right) + \frac{2}{1-\eta_y^2}\ln\left(\frac{1+\eta_y}{2}\right)\right] \tag{6.11}$$

$$I_y^{(m)} = \frac{\mathfrak{s}^2}{4\pi^2}\int_0^1 dy\, \frac{1}{1-\eta_y^2}\ln\left(\frac{1-\beta_{\text{max}}^2\eta_y^2}{1-\beta_{\text{max}}^2}\right)\,. \tag{6.12}$$

The integral $I_y^{(m)}$ in Eq. (6.10) is the only contribution to $I_{AB}^{(m,0)}$ where β_{max} cannot be set to 1. On the other hand, to calculate the integral $I^{(0)}$ in Eq. (6.10), we can safely consider the massless limit. As the result, we can use the result we have derived for $I_{AB}^{(0,0)}$ in Eq. (6.7) to deduce $I^{(0)}$. Indeed, in the case of $I_{AB}^{(0,0)}$, we could have performed the same manipulations up to Eq. (6.10) and would have found

$$I_{AB}^{(0,0)} = I^{(0)} + I_y^{(0)}\,, \tag{6.13}$$

where the only difference with Eq. (6.10) is the expression of η_y in $I_y^{(0)}$ since $m = 0$. It reads

$$I_y^{(0)} = \frac{\mathfrak{s}^2}{4\pi^2}\int_0^1 dy\, \frac{1}{1-\eta_y^2}\ln\left(\frac{1-\beta_{\text{max}}^2\bar{\eta}_y^2}{1-\beta_{\text{max}}^2}\right)\,, \tag{6.14}$$

where

$$\bar{\eta}_y^2 = \eta_y^2\Big|_{m=0} = 1 - 4y(1-y)\mathfrak{s}^2\,. \tag{6.15}$$

If we compute $I_y^{(0)}$, we can easily deduce an expression for $I^{(0)}$ by comparing Eqs. (6.7)-(6.13).

We focus on $I_y^{(0)}$ and restore the mass dependence of the argument of the logarithm

$$I_y^{(0)} = \frac{1}{16\pi^2}\int_0^1 dy\, \frac{1}{y(1-y)}\ln\left(\frac{\xi^2 + 4y(1-y)\mathfrak{s}^2}{\xi^2}\right)\,. \tag{6.16}$$

In Eq. (6.16), we introduced $\xi^2 = m^2/E_{\text{max}}^2$. To compute $I_y^{(0)}$, we use the fact that ξ is a small parameter that can be neglected except when $y \sim 0$ or $y \sim 1$. We introduce a small parameter $\xi \ll \Lambda \ll 1$ to split the integration intervals into three parts. We write

$$I_y^{(0)} = \sum_{j=1}^{3} I_j\,, \tag{6.17}$$

where

$$I_1 = \frac{1}{16\pi^2}\int_0^{\Lambda} dy\, \frac{1}{y(1-y)} \ln\left(\frac{\xi^2 + 4y(1-y)\mathfrak{s}^2}{\xi^2}\right) , \tag{6.18}$$

$$I_2 = \frac{1}{16\pi^2}\int_{\Lambda}^{1-\Lambda} dy\, \frac{1}{y(1-y)} \ln\left(\frac{\xi^2 + 4y(1-y)\mathfrak{s}^2}{\xi^2}\right) , \tag{6.19}$$

$$I_3 = \frac{1}{16\pi^2}\int_{1-\Lambda}^{1} dy\, \frac{1}{y(1-y)} \ln\left(\frac{\xi^2 + 4y(1-y)\mathfrak{s}^2}{\xi^2}\right) . \tag{6.20}$$

For each of these three integrals, we can simplify the integrands using the relations between Λ, y, and 1. For instance, in Eq. (6.18), we use the fact that $y \sim \Lambda \ll 1$ and construct the expansion of the integrand at small y. The sum of the integrals in Eq. (6.18), Eq. (6.19), and Eq. (6.20) does not depend on the auxiliary parameter Λ. We find

$$I_y^{(0)} = \frac{1}{16\pi^2} \ln^2\left(\frac{4\mathfrak{s}^2 E_{\text{max}}^2}{m^2}\right) . \tag{6.21}$$

Using this result of $I_y^{(0)}$ in Eq. (6.21) and by comparing Eqs. (6.7)-(6.13), we can deduce the expression for $I^{(0)}$. We find

$$I^{(0)} = \frac{1}{16\pi^2}\left[2\text{Li}_2\left(\mathfrak{c}^2\right) - \frac{\pi^2}{3}\right] . \tag{6.22}$$

To finish the computation of $I_{AB}^{(m,0)}$ in Eq. (6.10), we simply have to compute $I_y^{(m)}$ in Eq. (6.12). After expansion of the argument of the logarithm in the integrand of $I_y^{(m)}$, we find that $I_{AB}^{(m,0)}$ in Eq. (6.10) becomes

$$I_{AB}^{(m,0)} = I^{(0)} + \frac{\mathfrak{s}^2}{4\pi^2}\int_0^1 \frac{dy}{y}\, \frac{\ln\left(\frac{\xi^2 + 4y(1-y)\mathfrak{s}^2 + \xi_A^2 y(1-y)\cos\theta_{AB}}{\xi^2}\right)}{4\mathfrak{s}^2(1-y) + \xi_A^2\left(y + (1-y)\cos\theta_{AB}\right)} . \tag{6.23}$$

Similar to Eq. (6.17), $I_y^{(m)}$ is calculated by introducing an auxiliary parameter $\xi \ll \Lambda \ll 1$ which split the integration intervals into three parts, $[0,1] = [0,\Lambda] \cup [\Lambda, 1-\Lambda] \cup [1-\Lambda, 1]$. Once the three parts are combined, the dependence on Λ cancels as expected and we find the desired result

$$\boxed{I_{AB}^{(m,0)} = \frac{1}{16\pi^2}\left[2\text{Li}_2\left(\mathfrak{c}^2\right) - \frac{\pi^2}{3} + \text{Li}_2\left(-\frac{E_{\text{max}}^2}{E_A^2}\right) + \ln^2\left(\frac{4\mathfrak{s}^2 E_{\text{max}}^2}{m^2}\right)\right] .} \tag{6.24}$$

In the next subsection, we provide results for all other integrated eikonal functions required to study the interference of $pp \to \text{jet}_c + H$ at NLO QCD.

6.1.1 *One massive and one massless emitters*

In gg channel, we need the following eikonal function

$$\int \frac{[dp_4](p_a \cdot p_3)}{(p_a \cdot p_4)(m_c^2 + p_3 \cdot p_4)} = \frac{1}{(2\pi)^2} \bigg[\ln^2\left(\frac{2\mathfrak{s}E}{m_c}\right) - \frac{\pi^2}{12} + \mathrm{Li}_2\left(-\frac{E}{E_3}\right) + \frac{1}{2}\mathrm{Li}_2\left(\mathfrak{c}^2\right) \bigg], \tag{6.25}$$

where we defined $\mathfrak{s} = \sin(\theta_a/2)$ and $\mathfrak{c} = \cos(\theta_a/2)$ and θ_a is the angle between the momenta p_a and p_3, $a = 1, 2$. To simplify our expressions, we recall that we set $E_{\max} = E_1 = E_2$ and that $E_1 = E_2 = E$ because we work in the partonic centre-of-mass frame.

6.1.2 *Two massive emitters*

The partonic channels cc and $c\bar{c}$ lead to eikonal functions where both emitters as well as the emitted particle are massive. In cc channel, the charm-quark can be emitted by one of the two incoming partons with momenta $p_1 = E_1(1, \beta\vec{n}_1)$ and $p_2 = E_2(1, \beta\vec{n}_2)$. Since we work in the partonic centre-of-mass frame, we have $E_1 = E_2 \equiv E$ and $\vec{n}_1 = -\vec{n}_2$, i. e.the emitters are back-to-back. To simplify the result further, we set $E_{\max} = E$. The integrated eikonal function in this case is given by

$$\int \frac{[dp_4](p_1 \cdot p_2)}{(m_c^2 - p_1 \cdot p_4)(m_c^2 - p_2 \cdot p_4)} = \frac{1}{(2\pi)^2} \left[\ln^2\left(\frac{2E}{m_c}\right) + \frac{\pi^2}{4} \right]. \tag{6.26}$$

In $c\bar{c}$ channel, the quasi-soft anti-quark can be emitted either by the incoming charm anti-quark $2_{\bar{c}}$ or by the outgoing charm quark 3_c. The outgoing momentum is defined as $p_3 = E_3(1, \beta\vec{n}_3)$, and the angle between the two emitters can be expressed as $\cos(\theta_{23}) = \vec{n}_2 \cdot \vec{n}_3$. With $E_{\max} = E$, we find the following result for the eikonal function

$$\int \frac{[dp_4](p_2 \cdot p_3)}{(m_c^2 - p_2 \cdot p_4)(m_c^2 + p_3 \cdot p_4)} = \frac{1}{(2\pi)^2} \bigg[-\ln^2\left(\frac{2\mathfrak{s}E}{m_c}\right) - \frac{\pi^2}{12} - \frac{1}{2}\mathrm{Li}_2\left(\mathfrak{c}^2\right) - \mathrm{Li}_2\left(-\frac{E}{E_3}\right) \bigg], \tag{6.27}$$

where we defined $\mathfrak{s} = \sin(\theta_{23}/2)$ and $\mathfrak{c} = \cos(\theta_{23}/2)$.

7 VIRTUAL AMPLITUDE AND RENORMALISATION

In this chapter, we provide an overview of the computation of the one-loop corrections to the interference of $pp \to \text{jet}_c + H$ in the $m_c \to 0$ limit. Then, we discuss the ultraviolet (UV) renormalisation, as well as the definition of the finite part of the one-loop amplitude.

The one-loop contribution to any cross section is provided by the interference of the Born and the one-loop amplitudes. For our purpose, we need to select amplitudes that descibes different production mechanisms. We write

$$\text{Int}\left\{\mathcal{A}^{(0)\dagger}\mathcal{A}^{(1)} + \text{h.c}\right\} = \mathcal{A}^{(0)\dagger}_{ggH}\mathcal{A}^{(1)}_{\text{Yuk}} + \mathcal{A}^{(0)\dagger}_{\text{Yuk}}\mathcal{A}^{(1)}_{ggH} + \text{h.c.}\,, \tag{7.1}$$

where we denote Born amplitudes for each production mechanism with the superscript (0) and one-loop amplitudes with the superscript (1).

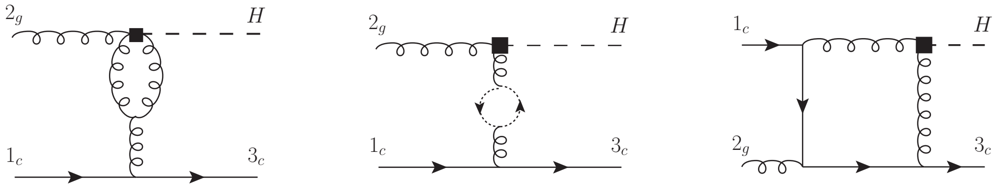

(a) gggH effective vertex (b) Ghost loop (c) Box diagram

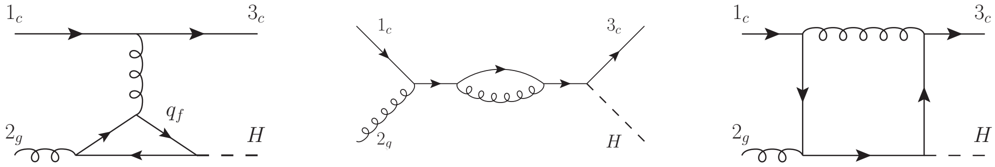

(d) Light-quark loop (e) s channel (f) Box diagram

Figure 7.1: Examples of diagrams contributing to the virtual corrections to the interference between the two Higgs boson production mechanisms that occurs in cg collisions.

We generate the one-loop diagrams using `QGRAF` [79]. Some examples are shown in Fig. 7.1. We perform the Dirac algebra with `FORM` [74]. We keep the mass of the charm-quark finite. The tensor integrals are reduced to scalar integrals using the Passarino-Veltman reduction [80]. We use `PackageX` [81] to express every scalar tadpole, bubble, triangle and box integral through logarithms and dilogarithms. The $m_c \to 0$ limit is considered in each integral separately. We keep the leading order term in m_c and identify the logarithms of m_c. We use these integral expansions to determine the one-loop amplitudes. We build their interference, keep one charm-quark mass insertion, and take the $m_c \to 0$ limit whenever possible.

The one-loop amplitude is divergent in four dimensions. As explained in Appendix A, one-loop amplitudes display UV poles that can be removed through renormalisation. We closely follow the renormalisation procedure described in Ref. [82], where the strong coupling constant and the charm-Yukawa coupling are renormalised in the $\overline{\text{MS}}$ scheme, while the charm-quark mass and the wave functions of the charm-quark, the light-quark, and the gluon are renormalised in the on-shell scheme.

In addition, the effective coupling C_1^{ggH} is expanded to $\mathcal{O}(\alpha_s)$. It reads [83]

$$C_1^{ggH} = C_{1,\text{LO}}^{ggH} \left[1 + \frac{\alpha_s(\mu)}{2\pi} \left(\frac{11}{2} - \frac{1}{3} \ln\left(\frac{\mu^2}{m_t^2} \right) \right) + \mathcal{O}(\alpha_s^2) \right] . \tag{7.2}$$

where $C_{1,\text{LO}}^{ggH}$ is the leading-order coupling. The result of Eq. (7.2) is the finite result for the matching coefficient of the ggH effective vertex, obtained from a two-loop calculation.

In contrast to UV poles, the IR poles of the amplitude cannot be removed. They cancel out with the ones of the real-emission contribution, as discussed in Chapter 5. As we mentioned in Chapter 3, the structure of the IR poles of renormalised one-loop amplitude with massive partons is known [66, 84]. Below we describe this result using the notations from Ref. [85].

Amplitudes can be conveniently expressed as vectors in colour space. IR poles of any amplitudes are described using the following equation

$$|\mathcal{A}\rangle = \mathbf{Z}|\mathcal{F}\rangle \,, \tag{7.3}$$

where $\mathbf{Z}$ is an operator in colour space and $\mathcal{F}$ is finite in four dimensions. These three objects are expanded in the strong coupling constant. For instance, the $\mathbf{Z}$-operator reads

$$\mathbf{Z} = 1 + \sum_{n=1}^{\infty} \left(\frac{\alpha_s}{4\pi} \right)^n \mathbf{Z}^{(n)} \,. \tag{7.4}$$

Using this result, we can write Eq. (7.3) as

$$\begin{aligned} |\mathcal{A}\rangle &= |\mathcal{A}^{(0)}\rangle + \frac{\alpha_s}{4\pi} |\mathcal{A}^{(1)}\rangle + \mathcal{O}(\alpha_s^2) \\ &= |\mathcal{A}^{(0)}\rangle + \frac{\alpha_s}{4\pi} \left(\mathbf{Z}^{(1)} |\mathcal{A}^{(0)}\rangle + |\mathcal{F}^{(1)}\rangle \right) + \mathcal{O}(\alpha_s^2) \,. \end{aligned} \tag{7.5}$$

In Eq. (7.5), $|\mathcal{A}^{(0)}\rangle$ is the Born amplitude. The second term corresponds to the one-loop amplitude $|\mathcal{A}^{(1)}\rangle$ and $|\mathcal{F}^{(1)}\rangle$ denotes its finite part

$$|\mathcal{F}^{(1)}\rangle = |\mathcal{A}^{(1)}\rangle - \mathbf{Z}^{(1)} |\mathcal{A}^{(0)}\rangle \,. \tag{7.6}$$

In Eq. (7.6), $1/\varepsilon$ poles present in the one-loop amplitude $\mathcal{A}^{(1)}$ and in the operator $\boldsymbol{Z}$ cancel out, resulting in the finite part $\mathcal{F}^{(1)}$.

The operator $\boldsymbol{Z}$ follows the renormalisation group equation (RGE). It reads

$$\mu\frac{d}{d\mu}\boldsymbol{Z} = -\boldsymbol{\Gamma}\boldsymbol{Z}\,, \tag{7.7}$$

where $\boldsymbol{\Gamma}$ is the anomalous dimension operator. Using the colour-charge operator $\boldsymbol{T}$, it can be expressed as [86–90]

$$\begin{aligned}\boldsymbol{\Gamma}(\{p_i\}, m_c, \mu) = &\sum_{(i,j)}\frac{\boldsymbol{T}_i\cdot\boldsymbol{T}_j}{2}\gamma_{\text{cusp}}(\alpha_s)L_{ij} + \sum_{(I,j)}\boldsymbol{T}_I\cdot\boldsymbol{T}_j\gamma_{\text{cusp}}(\alpha_s)L^{(m)}_{Ij}\\ &-\sum_{(I,J)}\frac{\boldsymbol{T}_I\cdot\boldsymbol{T}_J}{2}\gamma_{\text{cusp}}(\nu_{IJ},\alpha_s) + \sum_i\gamma^i(\alpha_s) + \sum_I\gamma^I(\alpha_s)\\ &+\sum_{(I,J,K)} if^{abc}T^a_I T^b_J T^c_K F_I(\nu_{IJ},\nu_{JK},\nu_{KI})\\ &+\sum_{(I,J)}\sum_k if^{abc}T^a_I T^b_J T^c_k f_2\left(\nu_{IJ}, \ln\left(\frac{-\sigma_{Jk}v_J\cdot p_k}{-\sigma_{Ik}v_I\cdot p_k}\right)\right)\,,\end{aligned} \tag{7.8}$$

where indices $i, j, \ldots$ label the massless partons, indices $I, J, \ldots$ label the massive ones, and pairs of index (i, j) refer to $i \neq j$. In Eq. (7.8), we used

$$L_{ij} = \ln\left(\frac{\mu^2}{-s_{ij}}\right)\,,\qquad L^{(m)}_{Ij} = \ln\left(\frac{m_c\mu}{-s_{Ij}}\right)\,. \tag{7.9}$$

The variable s_{ij} stands for the scalar product of four momenta p_i and p_j

$$s_{ij} = 2\sigma_{ij}p_i\cdot p_j + i0\,, \tag{7.10}$$

where $\sigma_{ij} = 1$ if the both partons are incoming or outgoing and $\sigma_{ij} = -1$ otherwise. The renormalisation group equation (RGE) in Eq. (7.7) is solved to write the $\boldsymbol{Z}$-operator as [87, 91]

$$\boldsymbol{Z} = 1 + \frac{\alpha_s}{4\pi}\left(\frac{\boldsymbol{\Gamma}^{(0)\prime}}{4\varepsilon^2} + \frac{\boldsymbol{\Gamma}^{(0)}}{2\varepsilon}\right) + \mathcal{O}(\alpha_s^2)\,, \tag{7.11}$$

where the prime denotes the derivative with respect to the logarithm of the renormalisation scale

$$\boldsymbol{\Gamma}'(\alpha_s,\mu) = \mu\frac{\partial}{\partial\mu}\boldsymbol{\Gamma}(\alpha_s,\mu)\,. \tag{7.12}$$

Next, we provide explicit expressions for all quantities that are relevant for computing the one-loop corrections to the process $cg \to cH$. The cusp anomalous dimension for the massless partons γ_{cusp} reads [87, 91]

$$\gamma_{\text{cusp}} = 4\left(\frac{\alpha_s}{4\pi}\right) + \mathcal{O}(\alpha_s^2)\,. \tag{7.13}$$

The anomalous dimensions in Eq. (7.8) are given by

$$\begin{aligned}\gamma^{g,i} &= \frac{\alpha_s}{4\pi}\left(-\beta^0\right) + \mathcal{O}(\alpha_s^2)\,,\\ \gamma^{q,i} &= \frac{\alpha_s}{4\pi}\left(-3C_f\right) + \mathcal{O}(\alpha_s^2)\,,\\ \gamma^{q,I} &= \frac{\alpha_s}{4\pi}\left(-2C_f\right) + \mathcal{O}(\alpha_s^2)\,.\end{aligned} \tag{7.14}$$

The cusp anomalous dimension for massive partons reads

$$\gamma_{\text{cusp}}(v_{IJ},\alpha_s) = \gamma_{\text{cusp}}\frac{1}{v_{IJ}}\left[\frac{1}{2}\ln\left(\frac{1+v_{IJ}}{1-v_{IJ}}\right) - i\pi\right] + \mathcal{O}(\alpha_s^2)\,, \tag{7.15}$$

where the relative velocity of two massive partons is given by

$$v_{IJ} = \sqrt{1 - \frac{m_I^2 m_J^2}{p_I\cdot p_J}}\,. \tag{7.16}$$

For the process $cg \to cH$, we have two incoming partons, 1_c and 2_g, and an outgoing one, 3_c. We consider the charm quark to be massive. We expand the cusp anomalous dimension related to two massive charm quarks in the final state in small m_c and find

$$\gamma_{\text{cusp}}(v_{IJ},\alpha_s) = 4\left[-\ln\left(\frac{m_c^2}{2p_1\cdot p_3}\right) - i\pi\right]\,. \tag{7.17}$$

Finally, the products of colour-charge operators that appear in Eq. (7.8) are expressed in terms of Casimir invariants. They read

$$2\boldsymbol{T}_1\cdot\boldsymbol{T}_2 = -C_A\,,\quad 2\boldsymbol{T}_2\cdot\boldsymbol{T}_3 = -C_A\,,\quad 2\boldsymbol{T}_1\cdot\boldsymbol{T}_3 = C_A - 2C_f\,. \tag{7.18}$$

The pole of the renormalised one-loop interference contribution is given by

$$\text{Int}\left\{\mathcal{A}^{(0)\dagger}\mathcal{A}^{(1)} + \text{h.c.}\right\} = 2\text{Re}\left\{Z^{(1)}(\varepsilon,\mu,1_c,2_g,3_c)\right\}\text{Int}\left\{\mathcal{A}^{(0)\dagger}\mathcal{A}^{(0)}\right\} + \mathcal{F}^{\text{ren}}_{\text{Int,V}}\,, \tag{7.19}$$

where $\mathcal{F}^{\text{ren}}_{\text{Int,V}}$ is the finite part of the one-loop contribution to the interference. The pole structure is given by the factor $Z^{(1)}$. In the $m_c \to 0$ limit, it reads

$$\boxed{\begin{aligned}Z^{(1)}(\varepsilon,\mu,1_c,2_g,3_c) = \frac{\alpha_s(\mu)}{2\pi}\Bigg\{&-\frac{C_A}{2\varepsilon^2} + \frac{1}{4\varepsilon}\Bigg[-\beta_0 - 2C_A\ln\left(\frac{\mu\, m_c}{2p_2\cdot p_3}\right)\\ &-4C_f + (C_A - 2C_f)\left(\ln\left(\frac{m_c^2}{2p_1\cdot p_3}\right) + i\pi\right) - 2C_A\ln\left(\frac{\mu\, m_c}{2p_1\cdot p_2}\right)\Bigg]\Bigg\}\,.\end{aligned}} \tag{7.20}$$

Using the crossing symmetry, this result can be compared to the one in Ref. [82] where the $\boldsymbol{Z}$-operator corresponding to the $H \to b + \bar{b} + g$ one-loop amplitude have been computed.

After subtraction of the Catani's operator calculated for Higgs boson production in association with a charm-quark jet in Eq. (7.20), we can compute the finite remainder of the one-loop contribution to the interference defined in Eq. (7.19). We find that

$$\mathcal{F}^{\text{ren}}_{\text{Int,V}} = -C_1^{ggH} \frac{g_s^3}{16\pi^2} C_F N_c m_c y_c \sqrt{2} \frac{s^2}{t\,u} \left\{ A \ln^2\left(\frac{\mu^2}{m_c^2}\right) + B \ln\left(\frac{\mu^2}{m_c^2}\right) + C \right\}, \tag{7.21}$$

where the coefficient of the leading logarithm reads

$$\begin{aligned} A = 3C_A \left(1 - \frac{m_H^2}{s}\right)\left(1 + \frac{t}{s}\right)\left(1 + \frac{u}{s}\right) \\ + 2C_F \left[1 - \frac{2t^3}{s^3} + \frac{u^3}{s^3} + \frac{8tu}{s^2} + \frac{6u^2}{s^2} + \frac{6u}{s}\right]. \end{aligned} \tag{7.22}$$

The coefficients B and C are complicated and we do not report them.

The origin of single- and double-logarithmic functions in Eq. (7.21) are not explained by Sudakov enhancement [92]. Non-Sudakov logarithms have, for instance, been studied in the case of Higgs boson production in gluon fusion in Ref. [93]. Nevertheless, the necessity of a helicity flip in $cg \to cH$ interference provides additional sources of logarithms. A better understanding of the origin of these logarithms is important as they can give large numerical contributions. We note that $\ln^2(m_c)$ terms in the interference at NLO QCD have been computed in Ref. [72] using diagrammatic analysis.

Calculations of one-loop corrections to the interference contribution to Higgs boson production in association with a charm-quark jet has been presented. Once these corrections are combined with the real contributions, a finite partonic cross section is obtained. It can be integrated in four dimensions using a Vegas integrator [78]. In the next chapter, the result of such calculations are presented.

8

NUMERICAL SETUP AND RESULTS

In this chapter, we discuss the numerical setup that we use to evaluate the $pp \to H + \text{jet}_c$ cross section. Then, we present results for the NLO QCD corrections to the interference contribution.

We consider proton-proton collisions with a centre-of-mass energy of 13 TeV. The mass of the Higgs boson is set to $m_H = 125$ GeV, and the on-shell mass of the charm quark to $m_c = 1.3$ GeV. The Yukawa coupling, which, as discussed in Chapter 7, is renormalised in the $\overline{\text{MS}}$ scheme, is determined using the $\overline{\text{MS}}$ charm-quark mass evaluated at the mass of the Higgs, $m_c^{\overline{\text{MS}}}(m_H) = 0.81$ GeV . We use `RunDec` [94] to determine the running of the charm-quark mass. The `NNPDF31_lo_as_0118` and `NNPDF31_nlo_as_0118` PDFs [95, 96] are used to evaluate LO and NLO cross sections, respectively. Values of the strong coupling constant are obtained from `NNPDF` routines.

To select events with at least one charm-quark jet in the final state, we use the anti-$k_\perp$ algorithm with $\Delta R = 0.4$ [97]. We require that the charm jet satisfies the following constrains on the transverse momentum $p_{t,j}$ and the pseudorapidity η_j

$$p_{t,j} > 20 \text{ GeV}\,, \qquad |\eta_j| < 2.5\,. \tag{8.1}$$

We remind the reader that the interference displays quasi-soft quark singularities. As the result, the jet algorithm shows a logarithmic sensitivity to m_c as the charm quark becomes quasi-soft. For a detailed explanation of this phenomenon, we refer the reader to Chapter 4. To circumvent this problem, we require that at least 75% of the momentum of the charm-tagged jet is carried by a charm quark or anti-quark.

We set the renormalisation scale μ_R and the factorisation scale μ_F to the same value $\mu = \mu_R = \mu_F = m_H$. The resulting uncertainty is obtained by varying the scale μ by a factor two. The LO cross sections evaluate to

$$\sigma_{ggh}^{\text{LO}} = 176.6^{+47.6}_{-36.5}\ \text{fb}\,, \quad \sigma_{\text{Yuk}}^{\text{LO}} = 21.22^{+1.47}_{-1.67}\ \text{fb}\,, \quad \sigma_{\text{Int}}^{\text{LO}} = -2.21^{+0.29}_{-0.31}\ \text{fb}\,. \tag{8.2}$$

It appears that, at LO, the interference is about $\mathcal{O}(10\%)$ of the squared Yukawa cross section. In Fig. 8.1, we show the dependence of σ_{ggh}^{LO}, $\sigma_{\text{Yuk}}^{\text{LO}}$ and $\sigma_{\text{Int}}^{\text{LO}}$ on the minimal value of the charm-tagged jet transverse momentum. We observe that σ_{ggh}^{LO} is large compared to $\sigma_{\text{Yuk}}^{\text{LO}}$ and $\sigma_{\text{Int}}^{\text{LO}}$ for any value of p_{t,jet_c}. However, the ratio $\sigma_{\text{LO}}^{\text{Int}}/\sigma_{\text{LO}}^{\text{Yuk}}$ remains constant

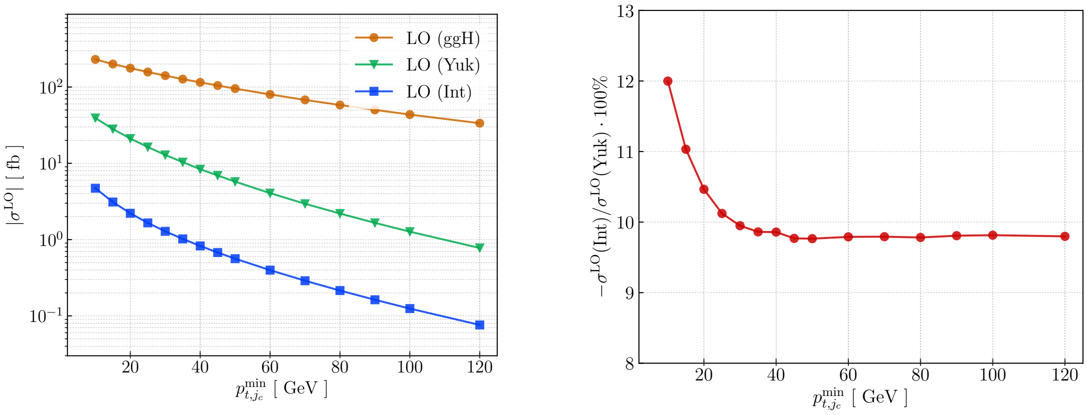

(a) LO cross sections dependences on p_{t,jet_c} cut.

(b) Ratio of $\sigma^{\mathrm{LO}}_{\mathrm{Int}}$ to $\sigma^{\mathrm{LO}}_{\mathrm{Yuk}}$.

Figure 8.1: Relative size of the LO cross sections $\sigma^{\mathrm{LO}}_{ggh}$, $\sigma^{\mathrm{LO}}_{\mathrm{Yuk}}$ and $\sigma^{\mathrm{LO}}_{\mathrm{Int}}$. On the left panel, the dependence of the three cross sections on the charm-tagged jet transverse momentum cut is presented. We denote with blue square $\sigma^{\mathrm{LO}}_{\mathrm{Int}}$, with green triangle $\sigma^{\mathrm{LO}}_{\mathrm{Yuk}}$ and with orange circle $\sigma^{\mathrm{LO}}_{ggh}$. On the right panel, we show the ratio in percent of the interference to the squared Yukawa contribution.

around $\mathcal{O}(10\%)$ for all values of p_{t,j_c}, see Fig. 8.1b.

The interference between the two Higgs production mechanisms in $pp \to cH$ at NLO QCD is found to be

$$\boxed{\sigma^{\mathrm{NLO}}_{\mathrm{Int}} = -1.024(5)^{+0.224}_{-0.144}\ \mathrm{fb}\,.} \tag{8.3}$$

We observe that the LO interference receives a large NLO QCD correction of -50%, which pushes $\sigma^{\mathrm{LO}}_{\mathrm{Int}}$ outside of the LO uncertainty obtained using the scale variation by a factor two. This emphasises the role of the logarithms of the charm-quark mass in the higher-order corrections, since those cannot be probed by the scale variation. To understand their role better, we split the NLO QCD corrections into the contribution of the five partonic channels and the one of the PDF matching described in Chapter 3. For each of these channels, we separate log-enhanced contributions from constant terms. We write the interference as

$$\sigma^{\mathrm{NLO}}_{\mathrm{Int}} = A\ln^2\left(\frac{m_H}{m_c}\right) + B\ln\left(\frac{m_H}{m_c}\right) + C \tag{8.4}$$

The individual contributions are collected in Table 8.1.

The cq partonic channel is free of logarithmic terms as there is no singular limit that involves the charm quark. We note that, in the cg and gg partonic channels, the

$\Delta\sigma^{\text{NLO}}$ [fb]	cg	cq	gg	cc	$c\bar{c}$	PDF	sum
const	-1.63	0.13	2.33	0.01	-0.01	0.11	0.94
L	2.23	–	-6.33	-0.04	0.01	1.66	-2.47
L^2	-0.06	–	2.66	0.01	-0.08	–	2.52
total	0.54	0.13	-1.34	-0.02	-0.08	1.76	1.00

Table 8.1: Contributions of the single and quadratic charm-quark mass logarithm $L = \ln(m_H/m_c)$ in femtobarns (fb). The interference at NLO QCD is split into the different partonic channels as well as the contribution from the PDF matching. We observe a strong cancellation of the simple and the quadratic logarithms.

contributions of single and quadratic logarithms does not have a clear pattern. In the cg channel, the single logarithms cancel the constant contribution, resulting in a small contribution to the total corrections. In gg channel, large corrections due to single logarithms are cancelled by quadratic logarithms and constant contributions. Overall, we observe a strong cancellation between single- and double-logarithmic terms.

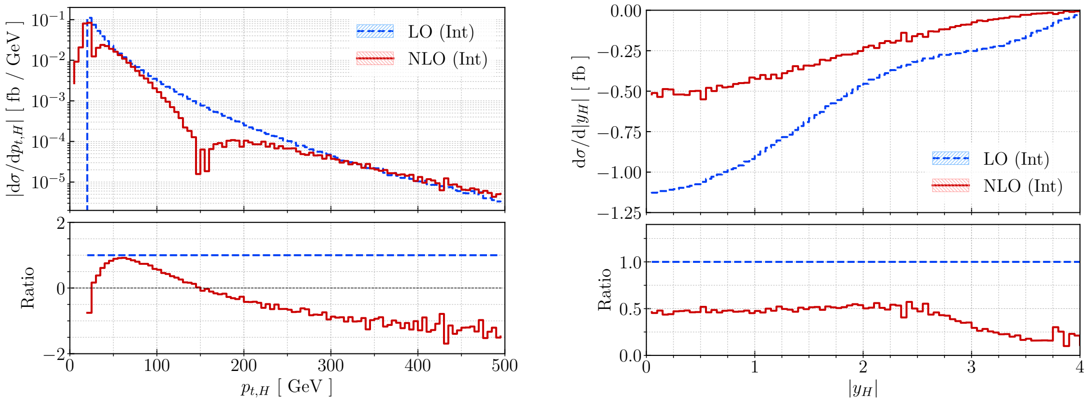

(a) Transverse momentum of the Higgs

(b) Rapidity of the Higgs boson.

Figure 8.2: Distribution of the Higgs boson transverse momentum (left panel) and rapidity (right panel). In both plots, the LO interference is drawn with a blue dashed line and the NLO interference with a solid red line.

In Fig. 8.2, we present the interference contributions to the transverse momentum and rapidity distributions of the Higgs boson at LO and NLO QCD. On the left pane of Fig. 8.2a, the Higgs boson transverse momentum distribution is significantly impacted by the NLO QCD corrections. The peak of the distribution around 25 GeV is smeared at NLO. We emphasise that the absolute value of the distributions is plotted in Eq. (8.2), which leads to discontinuities at 20 GeV and around 150 GeV. In lower panel of Fig. 8.2a, the ratio of the NLO to the LO distribution is shown.

In Fig. 8.2b, we show Higgs boson rapidity distribution. We observed that for $|y_H| < 2.5$, the leading order distribution is decreased by 50%. For larger rapidities, the NLO distribution decreases faster than the LO one.

Overall, the NLO QCD corrections appear to be large but still reasonable because of a significant cancellation of the simple and the quadratic logarithms of the charm-quark mass. Nevertheless, since corrections are large, it is interesting to understand how to systematically resum them.

9 CONCLUSION

Measurement of the Yukawa couplings of quarks and leptons is essential for testing properties of the Higgs boson. While couplings of fermions of the third and the second generations of the SM have been measured with reasonable accuracy, those of the lightest particles remain out of reach. In this part of the thesis, we studied one of the most promising ways for measuring the charm Yukawa coupling Ref. [4], namely, the Higgs production in association with a charm jet.

The interference between production of the Higgs boson caused by its interaction with the charm quark and its production in the gluon fusion requires an additional helicity flip to provide non-vanishing contribution. We decided to work with a finite charm-quark mass, to keep one mass insertion on the fermion line, and to carefully consider the massless limit. Although this procedure is simple at LO, it becomes non-trivial at NLO since it requires a delicate treatment of the infrared singularities. First, the presence of massive partons in the initial states requires a redefinition of the parton distribution function (PDF) that was presented in Chapter 3. Then, we showed in Chapter 4 that the necessity of a helicity flip on the fermion line leads to unconventional infrared soft and collinear limits of the interference. In Chapter 5, we extracted the logarithms of the charm-quark mass in the real-emission corrections using the nested soft-collinear subtraction scheme Ref. [65]. In Chapter 6, we provided detailed calculations of some eikonal functions resulting from quasi-soft quark singularity. The virtual contribution was discussed in Chapter 7. Finally, numerical results were presented in Chapter 8.

We find that the NLO QCD corrections to the interference are large as they reduce its value by 50%. However, they probably do not impact prospects for the extraction of the charm Yukawa coupling from $pp \to H + \text{jet}_c$ because the interference is still only about 10% of the Yukawa-dependent contribution to the cross section.

Part II

NON-FACTORISABLE CORRECTIONS TO T-CHANNEL SINGLE TOP PRODUCTION

We calculate the non-factorisable contribution to the t-channel single top production. This peculiar contribution, which first appears at NNLO QCD, describes QCD interactions between fermion lines connected at leading order by an exchange of an electroweak boson. Our calculation formally completes the NNLO QCD description of this process.

This part of the thesis follows the discussion in Refs. [98–102].

10 INTRODUCTION

Physics of top quarks provides many opportunities to extend our understanding of fundamental interactions. Being the heaviest particle of the SM, top quarks have the largest coupling to the Higgs boson. Therefore, studying top quarks may help to explore the mechanism of EW spontaneous symmetry breaking.

Top quarks have an exceptionally short lifetime. In fact, they decay almost instantly after they are produced in hadron collisions, before hadronisation takes place. As the result, top quarks, in many instances, behave as free quarks. Therefore, the possibility to study top quarks is highly appreciated in high-energy physics, as it provides a unique opportunity to test current theory of hadron collisions in a relatively simple and controlled environment.

At the LHC, top quarks are mainly produced in pairs via strong interactions, and theoretical predictions for this process are quite advanced. The NLO QCD [103] and NLO EW corrections [104] to top quark pair production were first calculated in 1987 and 2005, respectively. Recent calculations have included several improvements such as NNLO QCD corrections that account for top-quark decay in the narrow width approximation [105], threshold resummation [106], and soft-gluon resummation through the next-to-leading logarithmic order (NLL) [107].

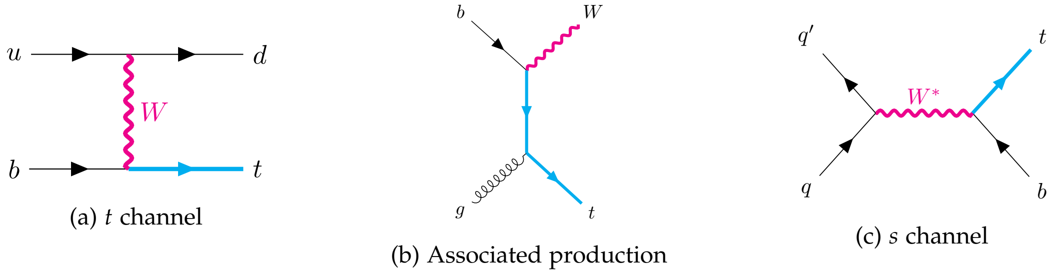

(a) t channel

(b) Associated production

(c) s channel

Figure 10.1: Single-top quark are produced through different channels. We sort them by importance at the LHC where on the left, the t-channel represents 70% of the total production and on the right, the s-channel represents only 5%.

Although the cross section for the single top production is smaller than the cross section for top-quark pair production, it is still significant at the LHC. Unlike top-quark pair production, single top production occurs through electroweak interactions, which provide a direct sensitivity to the CKM matrix element V_{tb} [108–111] and allow us to probe the tWb anomalous coupling [112, 113]. Additionally, single top production is an important process for studying the top quark width [114] and, probably, its mass [115].

At the LHC, single top quarks can be produced in several ways, see Fig. 10.1. The least frequent, which only contributes about 5% to the total production cross section, is the s-channel, see Fig. 10.1c. More frequently, single top quarks are produced in association with W bosons, see Fig. 10.1b. The t-channel process shown in Fig. 10.1a is the dominant one as it accounts for 70% of the single top production at the LHC.

The QCD corrections to the t-channel single top production have been calculated with an impressive precision. The NLO QCD corrections [116–120] and the NNLO QCD corrections that include top-quarks decay in the narrow width approximation [5, 6, 29–31] are known. However, the NNLO QCD corrections are incomplete since these computations were performed in the factorisation approximation, which systematically neglects diagrams where the two fermion lines interact with each other by gluon exchanges. The difference between factorisable and non-factorisable contributions is illustrated in Fig. 10.2. The non-factorisable contributions were neglected in early calculations as they vanish at NLO and are colour suppressed at NNLO by a factor $N_c^2 - 1 \sim \mathcal{O}(10)$ compared to their factorisable counterparts.

Since non-factorisable corrections first appear at NNLO, it is challenging to estimate their importance. However, one can argue that, because NNLO QCD corrections in the factorisable approximation are relatively small, non-factorisable corrections may be relevant. In addition, non-factorisable corrections might be enhanced by a factor π^2 originating from the Glauber phase [121]. This effect has been recently discussed in the case of non-factorisable corrections to Higgs production in WBF [7]. If such an enhancement exists also in the case of the single top production, it would largely compensate for the colour suppression.

Determining the non-factorisable corrections is a major challenge, especially when it comes to evaluating the two-loop, non-factorisable contributions. Partial reduction of the two-loop, non-factorisable amplitude to master integrals has been performed [122], as well as complete reduction with a fixed numerical relation between m_t and m_W [123]. Moreover, the master integrals are not known analytically, although some progress has been made recently in this direction [124, 125].

In this part of the thesis, we calculate the non-factorisable corrections to the t-channel single top production. We organise the discussion as follows. First, we demonstrate that non-Abelian contributions do not contribute to non-factorisable corrections, and

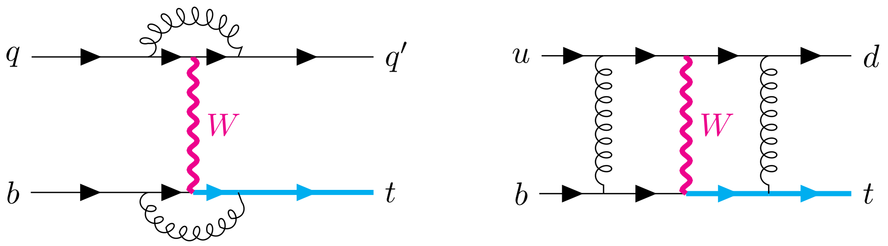

Figure 10.2: Diagrams contributing to the t-channel single top production. On the left panel, a gluon emitted by a fermion line is absorbed by the same fermion line. On the right panel, we show a diagram contributing to non-factorisable corrections since the two fermion lines are strongly interacting.

we explicitly prove the cancellation of the $1/\varepsilon$ poles by considering double-virtual, real-virtual and real-real contributions. We then discuss the evaluation of the finite part of the double-virtual contribution. We perform an analytic reduction of the loop amplitudes, retaining the exact dependence on the W boson and the top-quark mass. To evaluate the master integrals, we use the auxiliary mass flow method [126, 127]. This semi-numerical technique has recently been used to compute the two-loop helicity amplitudes for weak boson pair production in gluon fusion [128, 129]. Next, we discuss the computation of the double real-emission and real-virtual contributions. Finally, we present some numerical results for non-factorisable corrections for the LHC and the Future Circular Collider (FCC) [8, 9].

11

COLOUR STRUCTURE AND INFRARED POLE CANCELLATION

We mentioned in the Introduction that non-factorisable corrections are effectively Abelian. In this chapter, we explain the reason for that by studying the colour structure of the different amplitudes required to compute the t-channel single top production at NNLO QCD. We elucidate the simple form of the IR singularities in each of the three relevant partonic processes, namely the elastic process, the single-gluon emission, and the double-gluon emission. Finally, we demonstrate the cancellation of the $1/\varepsilon$ poles in the NNLO cross section.

11.1 COLOUR STRUCTURE

The colour structure of the non-factorisable corrections is simple. In fact, we can consider the non-factorisable QCD corrections as Abelian, which means that, for the purpose of computing non-factorisable corrections, self-interaction of gluons can be ignored. In this section, we will make this property explicit.

11.1.1 *Elastic process*

We start with the elastic process

$$1_q + 2_b \to 3_{q'} + 4_t\,, \tag{11.1}$$

where $p_i^2 = 0$, $i = 1,2,3$ and $p_4^2 = m_t^2$. It is convenient to work in the colour space to extract the colour structure of different amplitudes [130].[1] For instance, the Born amplitude $\mathcal{M}_0$ can be projected on the colour vector $|c\rangle$. The result reads

$$\langle c|\mathcal{M}_0(1_q, 2_b, 3_{q'}, 4_t)\rangle = \delta_{c_3c_1}\delta_{c_4c_2}\, A_0(1_q, 2_b, 3_{q'}, 4_t)\,, \tag{11.2}$$

where A_0 is the colour-stripped Born amplitude and c_i, $i = 1\dots4$ are colour labels of partons in Eq. (11.1). Eq. (11.2) demonstrates an obvious fact that in the single top production process there is no colour exchange between the two quark lines at leading order in QCD. Similarly, the one-loop amplitude can be decomposed into two contributions

$$\begin{aligned}\langle c|\mathcal{M}_1(1_q, 2_b, 3_{q'}, 4_t)\rangle = \frac{\alpha_s}{2\pi}\big(&\delta_{c_3c_1}\delta_{c_4c_2}\, A_1(1_q, 2_b, 3_{q'}, 4_t)\\ &+ t^a_{c_3c_1}t^a_{c_4c_2}\, B_1(1_q, 2_b, 3_{q'}, 4_t)\big)\,.\end{aligned} \tag{11.3}$$

---

[1] We use the same formalism to describe the structure of the one-loop contribution in Chapter 7.

The first term in Eq. (11.3) describes processes where a virtual gluon is emitted and absorbed by the same fermion line. The second term describes contributions where the virtual gluon couples to both fermion lines. It is this contribution to the amplitude that is relevant for the non-factorisable corrections.

The IR structure of any one-loop amplitude can be described using Catani's operator I_1 [66, 84]. The colour-stripped amplitude B_1 can be written as

$$B_1(1_q, 2_b, 3_{q'}, 4_t) = I_1(\varepsilon)\ A_0(1_q, 2_b, 3_{q'}, 4_t) + B_{1,\text{fin}}(1_q, 2_b, 3_{q'}, 4_t)\,, \tag{11.4}$$

where $B_{1,\text{fin}}$ is finite in four dimensions and $I_1(\varepsilon)$ reads

$$I_1(\varepsilon) \equiv I_1(1_q, 2_b, 3_{q'}, 4_t; \varepsilon) = \frac{1}{\varepsilon}\left[\ln\left(\frac{p_1 \cdot p_4\ p_2 \cdot p_3}{p_1 \cdot p_2\ p_3 \cdot p_4}\right) + 2\pi i\right]. \tag{11.5}$$

We provide additional details about the determination of this operator I_1 in Chapter 13. From Eq. (11.5) it follows that $I_1(\varepsilon)$ diverges as $1/\varepsilon$ at one-loop, whereas typically one-loop amplitudes exhibits $1/\varepsilon^2$ infrared singularities. This fact is a consequence of the absence of collinear divergences in non-factorisable contributions.

Similarly, the two-loop amplitude can also be split into several parts, according to their colour structures. We write it as

$$\begin{aligned}&\langle c|\mathcal{M}_2(1_q, 2_b, 3_{q'}, 4_t)\rangle \\ &\quad = \left(\frac{\alpha_s}{2\pi}\right)^2 \left(\ldots + \frac{1}{2}\{t^a, t^b\}_{c_3 c_1} \frac{1}{2}\{t^a, t^b\}_{c_4 c_2}\ B_2(1_q, 2_b, 3_{q'}, 4_t)\right),\end{aligned} \tag{11.6}$$

where, analogously, B_2 is defined as the colour-stripped, two-loop amplitude which is part of the non-factorisable corrections and which is symmetric under the exchange of the two gluons. The dots in Eq. (11.6) stand for the rest of the two-loop amplitude which describes factorisable contributions as well as those that cannot interfere with the Born amplitude, as in Fig. 11.1. The IR pole structure of B_2 can be written using the same operator I_1

$$\begin{aligned}B_2(1_q, 2_b, 3_{q'}, 4_t) = &-\frac{I_1^2(\varepsilon)}{2}\ A_0(1_q, 2_b, 3_{q'}, 4_t) + I_1(\varepsilon)\ B_1(1_q, 2_b, 3_{q'}, 4_t) \\ &+ B_{2,\text{fin}}(1_q, 2_b, 3_{q'}, 4_t)\,,\end{aligned} \tag{11.7}$$

where $B_{2,\text{fin}}$ is finite in four dimensions.

The double-virtual non-factorisable contribution is constructed by squaring the one-loop amplitude B_1, defined in Eq. (11.4), and by computing the interference of the

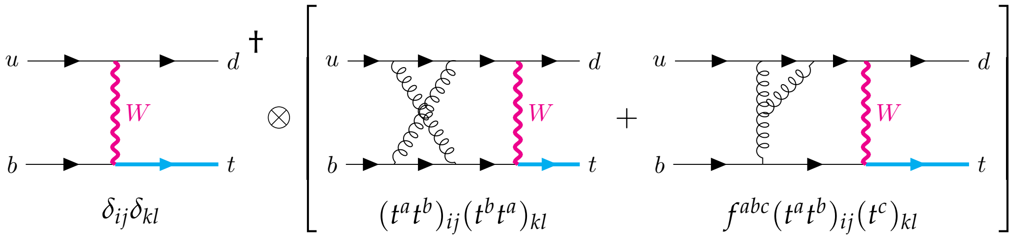
u
d
W
b
t
†
⊗
$\delta_{ij}\delta_{kl}$
u
d
W
b
t
$(t^a t^b)_{ij}(t^b t^a)_{kl}$
+
u
d
W
b
t
$f^{abc}(t^a t^b)_{ij}(t^c)_{kl}$

Figure 11.1: Diagrams with triple-gluon vertex vanishes because of colour conservation once projected on the Born amplitude.

two-loop amplitude B_2, given in Eq. (11.7), with the colour-stripped Born amplitude A_0. We find

$$\begin{aligned}
&|\mathcal{M}_1(1_q,2_b,3_{q'},4_t)|^2_{\text{nf}} + 2\text{Re}\left[\mathcal{M}_0^*(1_q,2_b,3_{q'},4_t)\,\mathcal{M}_2(1_q,2_b,3_{q'},4_t)\right]_{\text{nf}} \\
&= \frac{N^2-1}{4}\left(\frac{\alpha_s}{2\pi}\right)^2 \Big[-\text{Re}\left[I_1^2(\varepsilon)\right] |A_0(1_q,2_b,3_{q'},4_t)|^2 + |B_1(1_q,2_b,3_{q'},4_t)|^2 \\
&\qquad + 2\text{Re}\left[I_1(\varepsilon)\, A_0^*(1_q,2_b,3_{q'},4_t)\, B_1(1_q,2_b,3_{q'},4_t)\right] \\
&\qquad + 2\text{Re}\left[A_0^*(1_q,2_b,3_{q'},4_t)\, B_{2,\text{fin}}(1_q,2_b,3_{q'},4_t)\right] \Big],
\end{aligned} \tag{11.8}$$

where we have used $\text{Tr}(t^a t^b)\text{Tr}(t^a t^b) = T_F^2 \delta^{ab}\delta_{ab} = (N_c^2-1)/4$. The amplitude B_1 in Eq. (11.7) still contains implicit poles in ε. We use Eq. (11.4) to rewrite the double-virtual non-factorisable amplitude as

$$\begin{aligned}
&|\mathcal{M}_1(1_q,2_b,3_{q'},4_t)|^2_{\text{nf}} + 2\text{Re}\left[\mathcal{M}_0^*(1_q,2_b,3_{q'},4_t)\mathcal{M}_2(1_q,2_b,3_{q'},4_t)\right]_{\text{nf}} \\
&= \frac{N^2-1}{4}\left(\frac{\alpha_s}{2\pi}\right)^2 \Big[2\left(\text{Re}\left[I_1(\varepsilon)\right]\right)^2 |A_0(1_q,2_b,3_{q'},4_t)|^2 + |B_{1,\text{fin}}(1_q,2_b,3_{q'},4_t)|^2 \\
&\qquad + 4\text{Re}\left[I_1(\varepsilon)\right]\,\text{Re}\left[A_0^*(1_q,2_b,3_{q'},4_t)\, B_{1,\text{fin}}(1_q,2_b,3_{q'},4_t)\right] \\
&\qquad + 2\text{Re}\left[A_0^*(1_q,2_b,3_{q'},4_t)\, B_{2,\text{fin}}(1_q,2_b,3_{q'},4_t)\right] \Big].
\end{aligned} \tag{11.9}$$

11.1.2 *Single-real emission contributions*

We perform a similar analysis for the case of a single-real emission process

$$1_q + 2_b \to 3_{q'} + 4_t + 5_g\,. \tag{11.10}$$

Again, we decompose the tree-level amplitude into two terms

$$\begin{aligned}
\langle c|\mathcal{M}_0(1_q,2_b,3_{q'},4_t;5_g)\rangle = g_{s,b}\Big[& t^{c_5}_{c_3c_1}\delta_{c_4c_2} A_0^L(1_q,2_b,3_{q'},4_t;5_g) \\
& + t^{c_5}_{c_4c_2}\delta_{c_3c_1} A_0^H(1_q,2_b,3_{q'},4_t;5_g)\Big],
\end{aligned} \tag{11.11}$$

where we introduce the colour-stripped amplitude A_0^L (A_0^H) to describe contributions where the gluon is emitted from the light-quark or the heavy-quark line. The real-emission amplitude exhibits a soft singularity when the emitted gluon energy goes to zero. It factorises in that limit

$$\begin{aligned} S_5\, A_0^L(1_q,2_b,3_{q'},4_t;5_g) &= J(3,1;5,\varepsilon_5)\, A_0(1_q,2_b,3_{q'},4_t)\,, \\ S_5\, A_0^H(1_q,2_b,3_{q'},4_t;5_g) &= J(4,2;5,\varepsilon_5)\, A_0(1_q,2_b,3_{q'},4_t)\,, \end{aligned} \tag{11.12}$$

In Eq. (11.12), we use the soft operator S_5, already defined in Eq. (3.13) and introduce

$$J(i,j;k,\varepsilon_k) = \varepsilon_{k,\mu} J^\mu(i,j;k)\,, \tag{11.13}$$

with

$$J^\mu(i,j;k) = \frac{p_i^\mu}{p_i \cdot p_k} - \frac{p_j^\mu}{p_j \cdot p_k}\,. \tag{11.14}$$

Similarly, we decompose the one-loop five-point amplitude using the colour-space formalism. The result reads

$$\begin{aligned} \langle c|\mathcal{M}_1(1_q,2_b,3_{q'},4_t;5_g)\rangle \;&= g_{s,b}\left(\frac{\alpha_s}{2\pi}\right)\Big[t^{c_5}_{c_3c_1}\delta_{c_4c_2}\, A_1^L(5_g) + t^{c_5}_{c_4c_2}\delta_{c_3c_1}\, A_1^H(5_g) \\ &\quad + \frac{1}{2}\{t^a,t^{c_5}\}_{c_3c_1}\, t^a_{c_4c_2}\, B_1^{sL}(5_g) + \frac{1}{2}[t^a,t^{c_5}]_{c_3c_1}\, t^a_{c_4c_2}\, B_1^{aL}(5_g) \\ &\quad + \frac{1}{2}\{t^a,t^{c_5}\}_{c_4c_2}\, t^a_{c_3c_1}\, B_1^{sH}(5_g) + \frac{1}{2}[t^a,t^{c_5}]_{c_4c_2}\, t^a_{c_3c_1}\, B_1^{aH}(5_g)\Big]\,, \end{aligned} \tag{11.15}$$

where we have extended the notation for the amplitudes introduced in Eq. (11.3) to this case. Here, we distinguish between contributions where the gluon 5_g is emitted from the light-fermion or the heavy-fermion line. Additionally, we use indices s and a to differentiate between the colour-symmetric and colour-antisymmetric contributions for cases where one of the gluons interacts with the two fermion lines. For example, the colour-stripped amplitudes B_1^{sH} and B_1^{sL} do not receive contributions from diagrams with triple gluon vertices.

At NNLO, the real-virtual contribution has to be considered. It is build from the interference of the tree-level and the one-loop five-point amplitudes

$$\begin{aligned} &2\mathrm{Re}\left[\mathcal{M}_0^*(1_q,2_b,3_{q'},4_t;5_g)\mathcal{M}_1(1_q,2_b,3_{q'},4_t;5_g)\right]_{\mathrm{nf}} \\ &\quad = g_{s,b}^2\,\frac{N^2-1}{4}\left(\frac{\alpha_s}{2\pi}\right)\left(A_0^{L*}(5_g)\, B_1^{sH}(5_g) + A_0^{H*}(5_g)\, B_1^{sL}(5_g) + \mathrm{c.c.}\right)\,, \end{aligned} \tag{11.16}$$

To derive Eq. (11.16), we omitted all factorisable and colour-antisymmetric contributions, and performed the colour algebra where relevant.

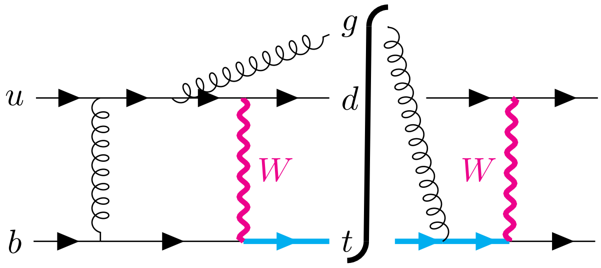

Figure 11.2: Example of diagram interference that contribute to non-factorisable, real-virtual corrections to the single-top t-channel production.

Analogously to the elastic process, the pole structure of the one-loop amplitude can be extracted using Catani's operator defined in Eq. (11.5). We can write

$$\begin{aligned} B_1^{sL(H)}(1_q,2_b,3_{q'},4_t;5_g) = \; & I_1(\varepsilon)\; A_0^{L(H)}(1_q,2_b,3_{q'},4_t;5_g) \\ & + B_{1,\mathrm{fin}}^{sL(H)}(1_q,2_b,3_{q'},4_t;5_g)\,, \end{aligned} \tag{11.17}$$

where $B_{1,\mathrm{fin}}^{sL(H)}$ is the finite part of the one-loop five-point amplitude. In addition to the explicit poles which originates from the integration over the loop momentum, the amplitude becomes singular when the emitted gluon becomes soft. These singularities factorise so that the amplitude can be written as a product of an eikonal factor and the one-loop four-point amplitude

$$\begin{aligned} S_5\, B_1^{sL}(1_q,2_b,3_{q'},4_t;5_g) &= J(3,1;5,\varepsilon_5)\; B_1(1_q,2_b,3_{q'},4_t)\,, \\ S_5\, B_1^{sH}(1_q,2_b,3_{q'},4_t;5_g) &= J(4,2;5,\varepsilon_5)\; B_1(1_q,2_b,3_{q'},4_t)\,. \end{aligned} \tag{11.18}$$

To summarise, in the soft limit, the real-virtual non-factoriasble contribution can be simply written as

$$\begin{aligned} & S_5 \left\{ 2\mathrm{Re}\, \left[\mathcal{M}_0^*(1_q,2_b,3_{q'},4_t;5_g)\mathcal{M}_1(1_q,2_b,3_{q'},4_t;5_g)\right]_{\mathrm{nf}} \right\} \\ & = -g_{s,b}^2\, \frac{N^2-1}{2} \left(\frac{\alpha_s}{2\pi}\right)\; \mathrm{Eik}_{\mathrm{nf}}(1_q,2_b,3_{q'},4_t;5_g) \\ & \qquad \times 2\mathrm{Re}\, \left[A_0^*(1_q,2_b,3_{q'},4_t)\; B_1(1_q,2_b,3_{q'},4_t)\right]\,. \end{aligned} \tag{11.19}$$

In Eq. (11.19), we have defined the soft function $\mathrm{Eik}_{\mathrm{nf}}$ as the sum of the four eikonal factors that describe gluon emission off the external legs. It reads

$$\mathrm{Eik}_{\mathrm{nf}}(1_q,2_b,3_{q'},4_t;5_g) = J^\mu(3,1;5)J_\mu(4,2;5) = \sum_{\substack{i\in[1,3]\\ j\in[2,4]}} \frac{\lambda_{ij}\; p_i\cdot p_j}{(p_i\cdot p_5)(p_j\cdot p_5)}\,, \tag{11.20}$$

where $\lambda_{ij} = 1$ if both partons with momentum p_i and p_j are in initial (final) state and $\lambda = -1$ otherwise. Once integrated over the gluon phase space, the soft function produces a $1/\varepsilon$ pole related to a soft gluon emission.

11.1.3 *Double-real emission amplitudes*

The last process we need to study is the single top production with two additional gluons. We assign the following momenta to the particles of the process

$$1_q + 2_b \to 3_{q'} + 4_t + 5_g + 6_g\,. \tag{11.21}$$

The tree-level amplitude is projected on the colour vector $\langle c|$. We obtain

$$\begin{aligned}
&\langle c|\mathcal{M}_0(1_q,2_b,3_{q'},4_t;5_g,6_g)\rangle = \\
&\quad g_{s,b}^2\Bigg[\frac{1}{2}\{t^{c_5},t^{c_6}\}_{c_3c_1}\delta_{c_4c_2}\,A_0^{sL}(5_g,6_g) + \frac{1}{2}[t^{c_5},t^{c_6}]_{c_3c_1}\delta_{c_4c_2}\,A_0^{aL}(5_g,6_g) \\
&\qquad + \frac{1}{2}\{t^{c_5},t^{c_6}\}_{c_4c_2}\delta_{c_3c_1}\,A_0^{sH}(5_g,6_g) + \frac{1}{2}[t^{c_5},t^{c_6}]_{c_4c_2}\delta_{c_3c_1}\,A_0^{aH}(5_g,6_g) \\
&\qquad + t^{c_5}_{c_3c_1}t^{c_6}_{c_4c_2}\,B_0^{5L,6H}(5_g,6_g) + t^{c_6}_{c_3c_1}t^{c_5}_{c_4c_2}\,B_0^{6L,5H}(5_g,6_g)\Bigg]\,,
\end{aligned} \tag{11.22}$$

where the first two lines contain contributions to the amplitude where both gluons are emitted from the light- or the heavy-fermion line. Similar to the real-virtual case, we split each contribution into colour-symmetric and colour-antisymmetric terms. The third line consists of contributions where gluons are emitted from different lines.

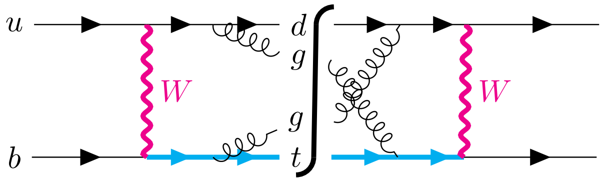

Figure 11.3: Example of diagram interference that contribute to non-factorisable, double real-emission corrections to the t-channel single top production.

The non-factorisable contributions to the double-real amplitude squared is constructed out of interferences where a gluon emitted from the light fermion line is absorbed by the heavy fermion line, and vice-versa. This requirement leads to a simple form of the non-factorisable, double-real contribution

$$\begin{aligned}
&\left|\mathcal{M}_0(1_q,2_b,3_{q'},4_t;5_g,6_g)\right|^2_{\mathrm{nf}} = g_{s,b}^4\,\frac{N^2-1}{4} \\
&\qquad \times\left(A_0^{sL}(5_g,6_g)\,A_0^{sH*}(5_g,6_g) + B_0^{5L,6H}(5_g,6_g)\,B_0^{6L,5H*}(5_g,6_g) + \text{c.c.}\right),
\end{aligned} \tag{11.23}$$

where the colour algebra has been performed and the colour-antisymmetric part of the amplitude was discarded. Analogously to the case of single-real emission, both gluons can be soft. In the limit where the gluon 6_g becomes soft, the different amplitudes in Eq. (11.23) factorise

$$\begin{aligned}
S_6\, B_0^{5L,6H}(1_q,2_b,3_{q'},4_t;5_g,6_g) &= J(4,2;6,\varepsilon_6)\; A_0^L(1_q,2_b,3_{q'},4_t;5_g)\,,\\
S_6\, B_0^{6L,5H}(1_q,2_b,3_{q'},4_t;5_g,6_g) &= J(3,1;6,\varepsilon_6)\; A_0^H(1_q,2_b,3_{q'},4_t;5_g)\,,\\
S_6\, A_0^{sL}(1_q,2_b,3_{q'},4_t;5_g,6_g) &= J(3,1;6,\varepsilon_6)\; A_0^L(1_q,2_b,3_{q'},4_t;5_g)\,,\\
S_6\, A_0^{sH}(1_q,2_b,3_{q'},4_t;5_g,6_g) &= J(4,2;6,\varepsilon_6)\; A_0^H(1_q,2_b,3_{q'},4_t;5_g)\,,
\end{aligned} \tag{11.24}$$

where J is defined in Eq. (11.13). Using these results, we write the corresponding limit of the double-real emission contribution as follows

$$\begin{aligned}
S_6\left|\mathcal{M}_0(1_q,2_b,3_{q'},4_t;5_g,6_g)\right|^2_{\rm nf} = &-g_{s,b}^4\,\frac{N^2-1}{2}\,{\rm Eik}_{\rm nf}(1_q,2_b,3_{q'},4_t;6_g)\\
&\times\left[A_0^L(1_q,2_b,3_{q'},4_t;5_g)\,A_0^{H*}(1_q,2_b,3_{q'},4_t;5_g)+{\rm c.c.}\right].
\end{aligned} \tag{11.25}$$

If the gluon 5_g also becomes soft, the double real-emission contribution factorises in the following way

$$\begin{aligned}
S_5S_6\left|\mathcal{M}_0(1_q,2_b,3_{q'},4_t;5_g,6_g)\right|^2_{\rm nf} = &\;g_{s,b}^4\,(N^2-1)\left|A_0(1_q,2_b,3_{q'},4_t)\right|^2\\
&\times{\rm Eik}_{\rm nf}(1_q,2_b,3_{q'},4_t;5_g)\;{\rm Eik}_{\rm nf}(1_q,2_b,3_{q'},4_t;6_g)\,.
\end{aligned} \tag{11.26}$$

11.2 CONSTRUCTION OF THE SUBTRACTION TERMS

In the previous section, we have demonstrated that the non-Abelian contribution to the single-top non-factorisable corrections vanishes due to colour conservation. The relevant amplitudes have been discussed, and the factorisation in the limit where gluons are soft has been made explicit.

In this section, we construct subtraction terms using the nested soft-collinear subtraction scheme [65] to regularise the soft gluon divergences. This scheme has been introduced in Chapter 3, where the definition of the different operators and objects used in the section can be found. Similar to the previous section, we consider double-real and real-virtual contributions separately.

11.2.1 *Double-real cross section*

We start with the double-real cross section. Using notations introduced in Chapter 3, we write it as

$$\begin{aligned}
2s\cdot\sigma_{\rm RR}^{\rm nf} &= \frac{1}{2!}\int[dp_5]\,[dp_6]\,F_{\rm LM}^{\rm nf}\left(1_q,2_b,3_{q'},4_t;5_g,6_g\right)\\
&\equiv\left\langle F_{\rm LM}^{\rm nf}\left(1_q,2_b,3_{q'},4_t;5_g,6_g\right)\right\rangle,
\end{aligned} \tag{11.27}$$

where the factor 1/2! is the symmetry factor due the fact that the two emitted gluons are identical. Furthermore, we have defined the following integral over the Born phase space of the non-factorisable double real-emission amplitude

$$\begin{aligned} F^{\rm nf}_{LM}\left(1_q,2_b,3_{q'},4_t;5_g,6_g\right) = &\mathcal{N}\int \mathrm{dLips}_{34}\,(2\pi)^d\,\delta^{(d)}\Big(p_1+p_2-\sum_{i=3}^{6}p_i\Big) \\ &\times\,\left|\mathcal{M}_0\left(1_q,2_b,3_{q'},4_t;5_g,6_g\right)\right|^2_{\rm nf}\,. \end{aligned} \tag{11.28}$$

In Eq. (11.28), $\mathcal{N}=1/(4N_c^2)$ stands for colour and spin average of initial partons. We note that, although we write formulas for the total cross section, the exact same reasoning would apply to any infrared-safe observable, which implies that the extension of our result to differential cross sections is straightforward. The double-real cross section suffers from soft divergences when one of the two gluons becomes soft. It can be regularised by introducing two subtraction terms

$$\begin{aligned} \langle F^{\rm nf}_{LM}\left(1_q,2_b,3_{q'},4_t;5_g,6_g\right)\rangle = &\langle S_5S_6\,F^{\rm nf}_{LM}\left(1_q,2_b,3_{q'},4_t;5_g,6_g\right)\rangle \\ &+2\,\langle S_6\left(1-S_5\right)F^{\rm nf}_{LM}\left(1_q,2_b,3_{q'},4_t;5_g,6_g\right)\rangle \\ &+\langle\left(1-S_5\right)\left(1-S_6\right)F^{\rm nf}_{LM}\left(1_q,2_b,3_{q'},4_t;5_g,6_g\right)\rangle\,, \end{aligned} \tag{11.29}$$

where we use the soft operators S_5 and S_6, defined in Eq. (3.13). In Eq. (11.29), we use the fact that the two gluons are undistinguishable and write $S_5(1-S_6)=S_6(1-S_5)$. It is convenient to define the integral of the eikonal factor over the related soft gluon phase space

$$\bar{g}_s^2\int[dp_k]\,\mathrm{Eik}_{\rm nf}(1_q,2_b,3_{q'},4_t;k_g)\equiv\frac{\alpha_s}{2\pi}\left(\frac{2E_{\rm max}}{\mu}\right)^{-2\varepsilon}K_{\rm nf}(1_q,2_b,3_{q'},4_t;\varepsilon)\,, \tag{11.30}$$

where $\bar{g}_s$ is the bare strong coupling constant and α_s is the coupling constant renormalised in the $\overline{\rm MS}$ scheme. The analytic calculation of $K_{\rm nf}(\varepsilon)\equiv K_{\rm nf}(1_q,2_b,3_{q'},4_t;\varepsilon)$ is described in Chapter 12. The integrated subtraction terms can be expressed as

$$\begin{aligned} 2s\cdot\sigma_{RR} = &\left(\frac{\alpha_s}{2\pi}\right)^2\frac{N^2-1}{2N^2}\left(\frac{2E_{\rm max}}{\mu}\right)^{-4\varepsilon}\langle K^2_{\rm nf}(\varepsilon)\,F_{\rm LM}(1_q,2_b,3_{q'},4_t)\rangle \\ &-\left(\frac{\alpha_s}{2\pi}\right)\frac{N^2-1}{2}\left(\frac{2E_{\rm max}}{\mu}\right)^{-2\varepsilon}\langle K_{\rm nf}(\varepsilon)\,(I-S_5)\,\widetilde{F}^{\rm nf}_{\rm LM}(1_q,2_b,3_q,4_t;5_g)\rangle \\ &+\langle(I-S_5)(I-S_6)\,F^{\rm nf}_{\rm LM}(1_q,2_b,3_{q'},4_t;5_g,6_g)\rangle\,. \end{aligned} \tag{11.31}$$

where we defined

$$\begin{aligned} F_{LM}\left(1_q,2_b,3_{q'},4_t\right) = &\mathcal{N}\int\mathrm{dLips}_{34}\,(2\pi)^d\,\delta^{(d)}\left(p_1+p_2-p_3-p_4\right) \\ &\times\left|\mathcal{M}_0\left(1_q,2_b,3_{q'},4_t\right)\right|^2, \end{aligned} \tag{11.32}$$

$$\begin{aligned}\widetilde{F}^{\rm nf}_{\rm LM}(1_q,2_b,3_q,4_t;5_g) = \mathcal{N}\int {\rm dLips}_{34}\,(2\pi)^d\,\delta^{(d)}\Big(p_1+p_2-\sum_{i=3}^{5}p_i\Big) \\ \times\; g_{s,b}^2\,\Big(A_0^{L*}(1_q,2_b,3_q,4_t;5_g)\,A_0^H(1_q,2_b,3_q,4_t;5_g)+\text{c.c.}\Big)\;.\end{aligned} \tag{11.33}$$

Infrared poles related to soft gluon emission are made explicit by the introduction the integrated soft function $K_{\rm nf}(\varepsilon)$.

11.2.2 *Real-virtual cross section*

Analogously to Eq. (11.28), we introduce the following quantity to describe the real-virtual contribution

$$\begin{aligned}F^{\rm nf}_{\rm LV}\,(1_q,2_b,3_{q'},4_t;5_g) = \mathcal{N}\int {\rm dLips}_{34}\,(2\pi)^d\,\delta^{(d)}\Big(p_1+p_2-\sum_{i=3}^{5}p_i\Big) \\ \times\; 2{\rm Re}\Big[\mathcal{M}_0^*(1_q,2_b,3_{q'},4_t;5_g)\,\mathcal{M}_1(1_q,2_b,3_{q'},4_t;5_g)\Big]_{\rm nf}\,.\end{aligned} \tag{11.34}$$

The emitted gluon can be soft. We regularise $F^{\rm nf}_{\rm LV}$ by subtracting the leading soft contribution, $E_5 \to 0$. We write

$$\begin{aligned}2s\cdot\sigma_{\rm RV} &= \int [dp_5]\,F^{\rm nf}_{\rm LV}\,(1_q,2_b,3_{q'},4_t;5_g) \\ &= \langle S_5F^{\rm nf}_{\rm LV}(1_q,2_b,3_{q'},4_t;5_g)\rangle + \langle (I-S_5)F^{\rm nf}_{\rm LV}(1_q,2_b,3_{q'},4_t;5_g)\rangle\,.\end{aligned} \tag{11.35}$$

We use the factorisation of the real-virtual amplitude given in Eq. (11.18) and the definition of the finite part of the four-point one-loop amplitude in Eq. (11.4) to write the integrated soft subtraction term as

$$\begin{aligned}&\langle S_5\,F^{\rm nf}_{\rm LV}\,(1_q,2_b,3_{q'},4_t;5_g)\rangle = \\ &\quad -\left(\frac{\alpha_s}{2\pi}\right)^2\frac{N^2-1}{N^2}\left(\frac{2E_{\rm max}}{\mu}\right)^{-2\varepsilon}\langle K_{\rm nf}(\varepsilon)\,{\rm Re}\,[I_1(\varepsilon)]\,F_{\rm LM}(1_q,2_b,3_{q'},4_t)\rangle \\ &\quad -\left(\frac{\alpha_s}{2\pi}\right)^2\frac{N^2-1}{2}\left(\frac{2E_{\rm max}}{\mu}\right)^{-2\varepsilon}\langle K_{\rm nf}(\varepsilon)\,\widetilde{F}^{\rm nf}_{\rm LV,\,fin}(1_q,2_b,3_{q'},4_t)\rangle\,.\end{aligned} \tag{11.36}$$

In writing Eq. (11.36), we have defined the finite quantity

$$\begin{aligned}\widetilde{F}^{\rm nf}_{\rm LV,fin}(1_q,2_b,3_{q'},4_t) = \mathcal{N}\int {\rm dLips}_{34}\,(2\pi)^d\,\delta^{(d)}(p_1+p_2-p_3-p_4) \\ \times\; 2{\rm Re}\Big[A_0^*(1_q,2_b,3_{q'},4_t)B_{1,{\rm fin}}(1_q,2_b,3_{q'},4_t)\Big]\,.\end{aligned} \tag{11.37}$$

The regulated term in Eq. (11.35) displays a $1/\varepsilon$ pole from the loop momentum integration. We make it explicit using the Catani's operator

$$\begin{aligned}&\langle (I-S_5)F_{\rm LV}^{\rm nf}(1_q,2_b,3_{q'},4_t;5_g)\rangle = \\ &\qquad \left(\frac{\alpha_s}{2\pi}\right)\frac{N^2-1}{2}\langle {\rm Re}\,[I_1(\varepsilon)]\,(I-S_5)\,\widetilde{F}_{\rm LM}^{\rm nf}(1_q,2_b,3_{q'},4_t;5_g)\rangle \\ &\qquad +\left(\frac{\alpha_s}{2\pi}\right)\frac{N^2-1}{4}\langle (I-S_5)\,\widetilde{F}_{\rm LV,\,fin}^{\rm nf}(1_q,2_b,3_{q'},4_t;5_g)\rangle\,,\end{aligned} \tag{11.38}$$

where, analogously to Eq. (11.37), we introduced the following finite quantity

$$\begin{aligned}\widetilde{F}_{\rm LV,\,fin}^{\rm nf}(1_q,2_b,3_{q'},4_t;5_g) &= \mathcal{N}\int {\rm dLips}_{34}\,(2\pi)^d\,\delta^{(d)}\Big(p_1+p_2-\sum_{i=3}^{5}p_i\Big) \\ &\quad\times \bar{g}_s^2\,\Big(A_0^{L*}(1_q,2_b,3_{q'},4_t;5_g)B_{1,\rm fin}^{sH}(1_q,2_b,3_{q'},4_t;5_g) \\ &\quad + A_0^{H*}(1_q,2_b,3_{q'},4_t;5_g)B_{1,\rm fin}^{sL}(1_q,2_b,3_{q'},4_t;5_g)+{\rm c.c.}\Big)\,.\end{aligned} \tag{11.39}$$

11.2.3 *Double-virtual cross section*

In the previous sections, we made explicit the IR poles related to unresolved emissions of soft gluons. In the case of the double-virtual correction, the poles are explicit thanks to the Catani's formula. We use the result from Eq. (11.26) and write the cross section as

$$\begin{aligned}2s\cdot\sigma_{\rm VV} &= \langle F_{\rm LVV}^{\rm nf}(1_q,2_b,3_{q'},4_t)\rangle \\ &= \mathcal{N}\int {\rm dLips}_{34}\,(2\pi)^d\,\delta^{(d)}\Big(p_1+p_2-p_3-p_4\Big)\Big\{\big|\mathcal{M}_1(1_q,2_b,3_{q'},4_t)\big|^2_{\rm nf} \\ &\qquad + 2{\rm Re}\Big[\mathcal{M}_0^*(1_q,2_b,3_{q'},4_t)\mathcal{M}_2((1_q,2_b,3_{q'},4_t)\Big]_{\rm nf}\Big\} \\ &= \left(\frac{\alpha_s}{2\pi}\right)^2\frac{N^2-1}{4}\bigg[\frac{2}{N^2}\Big\langle\big({\rm Re}\,[I_1(\varepsilon)]\,\big)^2 F_{LM}(1_q,2_b,3_{q'},4_t)\Big\rangle \\ &\qquad +2\,\langle {\rm Re}\,[I_1(\varepsilon)]\,\widetilde{F}_{\rm LV,fin}^{\rm nf}(1_q,2_b,3_{q'},4_t)\rangle+\langle\widetilde{F}_{\rm VV,fin}^{\rm nf}(1_q,2_b,3_{q'},4_t)\rangle\bigg]\,,\end{aligned} \tag{11.40}$$

where we introduced the finite-contribution

$$\begin{aligned}\widetilde{F}_{\rm VV,fin}^{\rm nf}(1_q,2_b,3_{q'},4_t) &= \mathcal{N}\int {\rm dLips}_{34}\,(2\pi)^d\,\delta^{(d)}\,(p_1+p_2-p_3-p_4) \\ &\times\Big\{\,\big|B_{1,\rm fin}(1_q,2_b,3_{q'},4_t)\big|^2+2{\rm Re}\Big[A_0^*(1_q,2_b,3_{q'},4_t)B_{2,\rm fin}(1_q,2_b,3_{q'},4_t)\Big]\Big\}\,.\end{aligned} \tag{11.41}$$

11.3 POLE CANCELLATION

The non-factorisable corrections to t-channel single top production cross section is the sum of double-virtual, real-virtual and double-real contributions

$$\sigma_{\rm nf} = \sigma_{\rm nf}^{(2g)} + \sigma_{\rm nf}^{(1g)} + \sigma_{\rm nf}^{(0g)} \,. \tag{11.42}$$

The double-real resolved contribution consists of the regulated term

$$2s \cdot \sigma_{\rm nf}^{(2g)} = \langle (I - S_5)(I - S_6) F_{\rm LM}^{\rm nf} \left(1_q, 2_b, 3_{q'}, 4_t; 5_g, 6_g \right) \rangle \,, \tag{11.43}$$

and can be numerically computed in four dimensions. The single-resolved and the elastic contributions $\sigma_{\rm nf}^{(1g)}$ and $\sigma_{\rm nf}^{(0g)}$ contain terms that are separately divergent, but whose sum is finite. To present these two contributions, it is convenient to define the following quantity

$$\mathcal{W}(1_q, 2_b, 3_{q'}, 4_t) = \left(\frac{2E_{\rm max}}{\mu} \right)^{-2\varepsilon} K_{\rm nf}(1_q, 2_b, 3_{q'}, 4_t; \varepsilon) - {\rm Re} \left[I_1(1_q, 2_b, 3_{q'}, 4_t; \varepsilon) \right] . \tag{11.44}$$

We note that $\mathcal{W}$ is free of singularities. Indeed, we will show in Chapter 12 that the divergent structure of $K_{\rm nf}$ reads

$$K_{\rm nf}(1_q, 2_b, 3_{q'}, 4_t; \varepsilon) = \frac{1}{\varepsilon} \ln \left(\frac{p_1 \cdot p_4 \; p_2 \cdot p_3}{p_1 \cdot p_2 \; p_3 \cdot p_4} \right) + \mathcal{O}(\varepsilon^0) \,. \tag{11.45}$$

Using Eq. (11.5) for $I_1(\varepsilon)$, we find

$$K_{\rm nf}(1_q, 2_b, 3_{q'}, 4_t; \varepsilon) - {\rm Re} \left[I_1(1_q, 2_b, 3_{q'}, 4_t; \varepsilon) \right] = \mathcal{O}(\varepsilon^0) \,. \tag{11.46}$$

We write the single-resolved contribution, which is the sum of the second term in Eq. (11.31) and the regulated term in Eq. (11.38), in the following way

$$\begin{aligned} 2s \cdot \sigma_{\rm nf}^{(1g)} = & - \left(\frac{\alpha_s}{2\pi} \right) \frac{N^2 - 1}{2} \langle \mathcal{W}(1_q, 2_b, 3_{q'}, 4_t)(I - S_5) \widetilde{F}_{\rm LM}^{\rm nf}(1_q, 2_b, 3_{q'}, 4_t; 5_g) \rangle \\ & + \left(\frac{\alpha_s}{2\pi} \right) \frac{N^2 - 1}{4} \langle (I - S_5) \widetilde{F}_{\rm LV,fin}^{\rm nf}(1_q, 2_b, 3_{q'}, 4_t; 5_g) \rangle \,. \end{aligned} \tag{11.47}$$

We emphasise that this expression is finite in four dimensions. Similarly, the elastic contribution, build from the sum of the first term in Eq. (11.31), the expression in Eq. (11.36), and the two-loop contribution in Eq. (11.40) can be expressed as

$$\begin{aligned} 2s \cdot \sigma_{\rm nf}^{(0g)} = & \left(\frac{\alpha_s}{2\pi} \right)^2 \frac{N^2 - 1}{2N^2} \langle \mathcal{W}^2(1_q, 2_b, 3_{q'}, 4_t) \, F_{\rm LM}(1_q, 2_b, 3_{q'}, 4_t) \rangle \\ & - \left(\frac{\alpha_s}{2\pi} \right)^2 \frac{N^2 - 1}{2} \langle \mathcal{W}(1_q, 2_b, 3_{q'}, 4_t) \, \widetilde{F}_{\rm LV,fin}^{\rm nf}(1_q, 2_b, 3_{q'}, 4_t) \rangle \\ & + \left(\frac{\alpha_s}{2\pi} \right)^2 \frac{N^2 - 1}{4} \langle \widetilde{F}_{\rm VV,fin}^{\rm nf}(1_q, 2_b, 3_{q'}, 4_t) \rangle \,. \end{aligned} \tag{11.48}$$

The pole cancellation of the non-factorisable NNLO QCD correction to t-channel single top production cross section, build from the sum of Eq. (11.43), Eq. (11.47), and Eq. (11.48), is explicit. We also note that the only amplitude that needs to be known through order $\mathcal{O}(\varepsilon)$ is the one-loop amplitude B_1, since it is needed to define the finite part of the amplitude B_2 in Eq. (11.7).

12 INTEGRATED EIKONAL FUNCTIONS

In Chapter 11, we have explained how to regulate the NNLO QCD cross section for non-factorisable corrections to t-channel single top production. In this chapter, we focus on the integrated soft subtraction terms. We present in detail the integration of the eikonal factor for one massive and one massless particle, with an arbitrary angle between their 3-momentum. Then, we give the results for the back-to-back configuration, and for two massless particles. Finally, we present a compact formula for the function $K_{\rm nf}$ introduced in the previous Chapter.

Our goal is to calculate the integrated soft function $K_{\rm nf}$ defined in Eq. (11.30). We focus on the integration of one of the eikonal factors. For two arbitrary emitters with momentum p_i and p_j, we have

$$\begin{aligned} \bar{g}_s^2 \int [dp_5] \frac{p_i \cdot p_j}{(p_i \cdot p_5)\,(p_j \cdot p_5)} &= \frac{\alpha_s}{2\pi} \left(\frac{2E_{\rm max}}{\mu}\right)^{-2\varepsilon} \frac{e^{\varepsilon\gamma_E}\Gamma(1-\varepsilon)}{\Gamma(1-2\varepsilon)} \left(-\frac{1}{2\varepsilon}\right) \\ &\quad \times \int d(\cos\theta)\, \frac{d\phi}{\pi} \big(\sin\theta\sin\phi\big)^{-2\varepsilon} \frac{\hat{p}_i \cdot \hat{p}_j}{\hat{p}_i \cdot \hat{p}_5\, \hat{p}_j \cdot \hat{p}_5} \\ &= \frac{\alpha_s}{2\pi} \left(\frac{2E_{\rm max}}{\mu}\right)^{-2\varepsilon} \frac{e^{\varepsilon\gamma_E}\Gamma(1-\varepsilon)}{\Gamma(1-2\varepsilon)} \left(-\frac{1}{2\varepsilon}\right) I_\Omega\,, \end{aligned} \tag{12.1}$$

where we define normalised 4-momenta $\hat{p}_i = p_i/E_i$. The integration over the solid angle of the emitted gluon is tedious. We describe the calculation of I_Ω for the case of a massive and a massless emitter in the next section.

12.1 ONE MASSIVE EMITTER, ONE MASSLESS – ARBITRARY ANGLE

We need to compute this integral

$$I_\Omega = (1 - \beta\vec{n}_1 \cdot \vec{n}_4) \int \frac{d\Omega_5}{(1-\vec{n}_1\cdot\vec{n}_5)(1-\beta\vec{n}_4\cdot\vec{n}_5)}\,, \tag{12.2}$$

where $d\Omega_5 = d(\cos\theta)\ d\phi/\pi\big(\sin\theta\sin\phi\big)^{-2\varepsilon}$. We emphasise that the integration over the -2ε-dimensional solid angle has already been performed in Eq. (12.1). This eikonal factor originates from the emission of a soft gluon from one massive and one massless emitter, with momenta $p_4 = E_4(1, \beta\vec{n}_4)$ and $p_1 = E_1(1, \vec{n}_1)$, respectively. The velocity of the massive particle reads $\beta = \sqrt{1 - m_t^2/E_4}$. The integral diverges in the collinear limit $\rho_{15} \to 0$. We would like to extract the pole in ε. We write

$$
\begin{aligned}
I &= \int \frac{d\Omega_5}{1 - \vec{n}_1 \cdot \vec{n}_5} \left\{ \frac{1}{1 - \beta \vec{n}_4 \cdot \vec{n}_5} - \frac{1}{1 - \beta \vec{n}_4 \cdot \vec{n}_1} \right\} + \frac{1}{1 - \beta \vec{n}_1 \cdot \vec{n}_4} \int \frac{d\Omega_5^{(d)}}{1 - \vec{n}_1 \cdot \vec{n}_5} \\
&\equiv I^{\mathrm{reg}} + I^{(\varepsilon)} .
\end{aligned} \tag{12.3}
$$

As in Ref. [131], we split the integral in two: one part which is regulated in the collinear limit ρ_{15} and one which is divergent. The computation of the latter is simple, since

$$
I^{(\varepsilon)} = \int \frac{d\Omega_5}{1 - \vec{n}_1 \cdot \vec{n}_5} = -\frac{1}{\varepsilon} . \tag{12.4}
$$

On the other hand, computation of the regulated part I^{reg} is more subtle. We note that this integral is required to $\mathcal{O}(\varepsilon)$ because of the soft pole in Eq. (12.1) and, therefore, we cannot set $\varepsilon \to 0$ in I^{reg}.

12.1.1 *Regulated integral*

To calculate the regulated term, we first derive a useful expression for the polar angle integration and then, we integrate over the azimuthal angle.

We choose the z-axis along $\vec{n}_4$. Then, the dependence on the polar angle ϕ in Eq. (12.3) only comes from the massless propagator. We need the following integral

$$
I_\phi = \int_0^\pi \frac{d\phi}{\pi} \frac{\left[\sin^2(\phi)\right]^{-\varepsilon}}{[1 - \cos\theta_1 \cos\theta] + [-\sin\theta_1 \sin\theta] \cos\phi} , \tag{12.5}
$$

where θ_1 is the angle between n_1 and n_4. After some manipulations, we find that Eq. (12.5) can be written as

$$
\begin{aligned}
I_\phi = {} & \frac{2^{2\varepsilon}}{|\cos\theta - \cos\theta_1|} \frac{\Gamma(1-2\varepsilon)}{\Gamma^2(1-\varepsilon)} \\
& \times \sum_{j=1}^{2} (1 - z_j^2)^{-2\varepsilon} \theta\left(1 - z_j^2\right) {}_2F_1\left(-\varepsilon, -2\varepsilon; 1-\varepsilon; z_j^2\right) ,
\end{aligned} \tag{12.6}
$$

where

$$
z_1 = \frac{(1-\cos\theta)(1+\cos\theta_1)}{\sin\theta_1 \sin\theta} , \qquad z_2 = \frac{(1-\cos\theta_1)(1+\cos\theta)}{\sin\theta_1 \sin\theta} . \tag{12.7}
$$

The simple form of the integral in four dimensions can be obtained from the d-dimensional result in Eq. (12.6). We recall that

$$
I_\phi^{(d=4)} = \int \frac{d\phi}{\pi} \frac{1}{1 - \vec{n}_5 \cdot \vec{n}_1} = \frac{2}{|\cos\theta - \cos\theta_1|} . \tag{12.8}
$$

We can now consider the integration over the azimuthal angle θ of the regulated integral. The regulated term in Eq. (12.3) reads

$$I^{\rm reg} = \int_{-1}^{1} d(\cos\theta)\, \sin^{-2\varepsilon}(\theta) \left\{ \frac{1}{1-\beta\cos\theta} - \frac{1}{1-\beta\cos\theta_1} \right\} I_\phi(\theta) \tag{12.9}$$

We perform the following change of variables

$$\cos\theta = 1-2x\,, \qquad \cos\theta_1 = 1-2y\,, \tag{12.10}$$

and find that the regulated integral can be expressed as

$$\begin{aligned} I^{\rm reg} &= 2^{2\varepsilon}\frac{\Gamma(1-2\varepsilon)}{\Gamma^2(1-\varepsilon)} \int_0^1 dx\, x^{-\varepsilon}(1-x)^{-\varepsilon} \\ &\times \left\{ \frac{1}{(1-\beta)+2\beta\, x} - \frac{1}{(1-\beta)+2\beta\, y} \right\} \\ &\times \left[\theta(y-x)\frac{[(1-x)y]^{2\varepsilon}}{(y-x)^{1+2\varepsilon}}\, {}_2F_1\left(-\varepsilon, -2\varepsilon; 1-\varepsilon; \frac{x}{1-x}\frac{1-y}{y}\right) + (x \leftrightarrow y) \right]. \end{aligned} \tag{12.11}$$

It is evident that the divergence at $x = y$ in the square bracket is regulated by the terms in curly brackets. We treat the two regions separately. In the first region where $y > x$, we rescale the integration variable $x = \eta y$, while in the second region, we choose $\eta = \frac{1-x}{1-y}$. We find the following expression for the regulated integral

$$\begin{aligned} I^{\rm reg} &= 2^{2\varepsilon}\frac{\Gamma(1-2\varepsilon)}{\Gamma^2(1-\varepsilon)} \int_0^1 d\eta \left\{ \frac{1}{(1-\beta)+2\beta\, y\,\eta} - \frac{1}{(1-\beta)+2\beta\, y} \right\} \\ &\times \left[\frac{(1-y\eta)^{\varepsilon}}{(1-\eta)^{1+2\varepsilon}(y\eta)^{\varepsilon}}\, {}_2F_1\left(-\varepsilon, -2\varepsilon; 1-\varepsilon; \frac{\eta(1-y)}{1-y\eta}\right) + (y \leftrightarrow (1-y)) \right]. \end{aligned} \tag{12.12}$$

Since this expression is free of divergences, it can be expanded in ε and analytically integrated order-by-order using the Maple package `HyperInt` [132]. The result of the integration is expressed in terms of multiple polylogarithm (MPL) [1] that can be simplified using the Mathematica package `PolyLogTools` [133].

12.1.2 *Results*

Using the result from the previous section, we find that the integrated eikonal function I_Ω for one massive and one massless emitters reads

$$I_\Omega = -\frac{1}{\varepsilon} + \mathcal{I}^{(0)} + \varepsilon\mathcal{I}^{(1)} + \varepsilon^2\mathcal{I}^{(2)} + \mathcal{O}(\varepsilon^3)\,, \tag{12.13}$$

---

[1] Multiple polylogarithm (MPL) are discussed in Appendix C.

where

$$
\begin{aligned}
\mathcal{I}^{(0)} &= 2\ln\left(\frac{E_4\,\rho_{14}}{m_t}\right) , \\
\mathcal{I}^{(1)} &= -2\left[\frac{1}{4}\ln^2\left(\frac{1-\beta}{1+\beta}\right) + \ln\left(\frac{\rho_{14}}{1+\beta}\right)\,\ln\left(\frac{\rho_{14}}{1-\beta}\right) + \mathrm{Li}_2\left(1-\frac{\rho_{14}}{1+\beta}\right)\right. \\
&\qquad \left. + \mathrm{Li}_2\left(1-\frac{\rho_{14}}{1-\beta}\right)\right] .
\end{aligned}
\tag{12.14}
$$

This result agree with the one found in Ref. [131]. For our purpose, the integrated eikonal factor is needed up to $\mathcal{O}(\varepsilon)$. It is in principle possible to get it to any order in the dimensional regulator ε by expanding further the integrand Eq. (12.12).

12.2 INTEGRATED SOFT FUNCTION

Using the results in Eq. (12.13), the integrated eikonal for massless partons, see, for instance, [65] and the definition of K_{nf} in Eq. (11.30), we find the following result for the function K_{nf}

$$
\begin{aligned}
K_{\mathrm{nf}}(1_q, 2_b, 3_{q'}, 4_t; \varepsilon) = &\frac{1}{\varepsilon}\ln\left(\frac{p_1\cdot p_4\;p_2\cdot p_3}{p_1\cdot p_2\;p_3\cdot p_4}\right) - \frac{1}{2}\ln^2\left(\frac{\rho_{23}}{2}\right) \\
&+ \frac{1}{2}\ln^2\left(\frac{\rho_{12}}{2}\right) - \ln\left(\frac{\rho_{14}}{1-\beta}\right)\ln\left(\frac{\rho_{14}}{1+\beta}\right) \\
&+ \ln\left(\frac{\rho_{34}}{1-\beta}\right)\ln\left(\frac{\rho_{34}}{1+\beta}\right) + \mathrm{Li}_2\left(1-\frac{\rho_{12}}{2}\right) \\
&- \mathrm{Li}_2\left(1-\frac{\rho_{23}}{2}\right) - \mathrm{Li}_2\left(1-\frac{\rho_{14}}{1-\beta}\right) \\
&- \mathrm{Li}_2\left(1-\frac{\rho_{14}}{1+\beta}\right) + \mathrm{Li}_2\left(1-\frac{\rho_{34}}{1-\beta}\right) \\
&+ \mathrm{Li}_2\left(1-\frac{\rho_{34}}{1+\beta}\right) + \mathcal{O}(\varepsilon) .
\end{aligned}
\tag{12.15}
$$

where $\beta = \sqrt{1-m_t^2/E_4^2}$ and $\rho_{ij} = 1 - \vec{n}_i\cdot\vec{n}_j$.

13 THE DOUBLE-VIRTUAL CONTRIBUTION

In this chapter, we focus on the calculation of the finite remainder of the double-virtual contributions to t-channel single top production. As discussed in Chapter 11, the finite remainder of the double-virtual contribution is defined by the subtraction of the IR poles using Catani's operator [66, 84], see Eqs. (11.5)-(11.7). In what follows, we first justify the form of the Catani's operator in our problem. Then, we discuss the computation of the amplitudes required to evaluate the double-virtual contribution. We focus on the computation of the two-loop amplitude, since the calculation of the one-loop amplitude squared is analogous.

13.1 DIVERGENCES OF THE LOOP AMPLITUDES

The IR structure of one- and two-loop amplitudes is known [66, 84]. To account for colour correlations between the different external partons, it is convenient to write an amplitude as a vector in the colour space. In this section, we use the the notations of Ref. [85], already introduced in Chapter 7. We provide a definition of the finite part of the non-factorisable contribution to the double-virtual corrections.

The starting point is the same as in Chapter 7. We write

$$|\mathcal{A}\rangle = \boldsymbol{Z}|\mathcal{F}\rangle\,, \tag{13.1}$$

where $|\mathcal{A}\rangle$ is an amplitude considered to be a vector in the colour space, $\boldsymbol{Z}$ is an operator that contains IR poles, and $|\mathcal{F}\rangle$ stands for the finite part of the amplitude. The $\boldsymbol{Z}$-operator is determined from the anomalous dimension operator $\boldsymbol{\Gamma}$, defined in Eq. (7.8). For our purpose, we want to select the part of $\boldsymbol{\Gamma}$ that contributes to non-factorisable corrections. For that, we consider each term in Eq. (7.13) and decide if it can contribute to the non-factorisable corrections.

We begin by selecting terms that contain colour correlations between the light- and the heavy-fermion lines, which means that we allow $\boldsymbol{T}_i \cdot \boldsymbol{T}_j$ with $i(j) \in \{1,3\}$ and $j(i) \in \{2,4\}$. In addition, the anomalous dimensions of the different partons do not contribute as they are related to collinear singularities. The cusp anomalous dimension from Eq. (7.13) needs to be expanded to NNLO. The result reads [87, 91]

$$\gamma_{\text{cusp}} = 4\left(\frac{\alpha_s}{4\pi}\right) + \left[\left(\frac{268}{9} - \frac{4\pi^2}{3}\right) C_A - \frac{80}{9} T_F n_f\right]\left(\frac{\alpha_s}{4\pi}\right)^2 + \mathcal{O}(\alpha_s^3)\,. \tag{13.2}$$

It is clear that the NNLO of γ_{cusp} does not contribute to non-factorisable corrections since the presence of C_A reflects the non-Abelian nature of QCD and $n_f T_F$ requires internal fermions loops. Taking into account all these constains, we find that the anomalous dimension operator takes a simple form. It reads

$$\boldsymbol{\Gamma}_{\text{nf}}(\{p_i\}, m_t, \mu) = \left(\frac{\alpha_s}{4\pi}\right) \boldsymbol{\Gamma}_{0,\text{nf}}(\{p_i\}, m_t, \mu)\,, \tag{13.3}$$

where

$$\boxed{\begin{aligned} \boldsymbol{\Gamma}_{0,\text{nf}} = 4\Bigg[&\boldsymbol{T}_1 \cdot \boldsymbol{T}_2 \ln\left(\frac{\mu^2}{-s-i\varepsilon}\right) + \boldsymbol{T}_2 \cdot \boldsymbol{T}_3 \ln\left(\frac{\mu^2}{-u-i\varepsilon}\right) \\ &+ \boldsymbol{T}_1 \cdot \boldsymbol{T}_4 \ln\left(\frac{\mu\, m_t}{m_t^2-u-i\varepsilon}\right) + \boldsymbol{T}_3 \cdot \boldsymbol{T}_4 \ln\left(\frac{\mu\, m_t}{m_t^2-s-i\varepsilon}\right)\Bigg]\,. \end{aligned}} \tag{13.4}$$

The operator $\boldsymbol{Z}$ introduced in Eq. (7.11) is expanded to NNLO. It becomes [87, 91]

$$\begin{aligned} \boldsymbol{Z}_{\text{nf}} &= 1 + \left(\frac{\alpha_s}{4\pi}\right) \boldsymbol{Z}^{(1)} + \left(\frac{\alpha_s}{4\pi}\right)^2 \boldsymbol{Z}^{(2)} + \mathcal{O}(\alpha_s^3) \\ &= 1 + \left(\frac{\alpha_s}{4\pi}\right) \frac{\boldsymbol{\Gamma}_{0,\text{nf}}}{2\varepsilon} + \left(\frac{\alpha_s}{4\pi}\right)^2 \frac{\boldsymbol{\Gamma}_{0,\text{nf}}{}^2}{8\varepsilon^2} + \mathcal{O}(\alpha_s^3)\,. \end{aligned} \tag{13.5}$$

We note that the reduced degree of divergence ($1/\varepsilon$ instead of $1/\varepsilon^2$) of the operator $\boldsymbol{Z}$ is related to the fact that $\boldsymbol{\Gamma}'_{0,\text{nf}} = 0$.

The operator $\boldsymbol{Z}_{\text{nf}}$ can be used to determine the pole structure of the one- and two-loop amplitudes. We use Eq. (13.1) and expand it in α_s. We find

$$\begin{aligned} |\mathcal{A}\rangle &= |\mathcal{A}^{(0)}\rangle + \frac{\alpha_s}{4\pi}|\mathcal{A}^{(1)}\rangle + \left(\frac{\alpha_s}{4\pi}\right)^2 |\mathcal{A}^{(2)}\rangle + \mathcal{O}(\alpha_s^3) \\ &= |\mathcal{A}^{(0)}\rangle + \frac{\alpha_s}{4\pi}\left(\boldsymbol{Z}^{(1)}|\mathcal{A}^{(0)}\rangle + \mathcal{F}^{(1)}\right) \\ &\quad + \left(\frac{\alpha_s}{4\pi}\right)^2 \left(\left[\boldsymbol{Z}^{(2)} - \boldsymbol{Z}^{(1)}\boldsymbol{Z}^{(1)}\right]|\mathcal{A}^{(0)}\rangle + \boldsymbol{Z}^{(1)}|\mathcal{A}^{(1)}\rangle + \mathcal{F}^{(2)}\right) + \mathcal{O}(\alpha_s^3)\,. \end{aligned} \tag{13.6}$$

At the first order in the strong coupling in Eq. (13.6), we find

$$|\mathcal{A}^{(1)}\rangle = \frac{\boldsymbol{\Gamma}_{0,\text{nf}}}{2\varepsilon}|\mathcal{A}^{(0)}\rangle + |\mathcal{F}^{(1)}\rangle\,. \tag{13.7}$$

We use the properties of the colour charge operator

$$\langle \boldsymbol{e}|\boldsymbol{T}_i^a|\boldsymbol{d}\rangle = T^a_{e_i d_i} \prod_{j\neq i} \delta_{e_j d_j}\,, \quad T^a_{e_i d_i} = \begin{cases} t^a_{e_i d_i} & \text{final state quark} \\ -t^a_{d_i e_i} & \text{initial state quark}\,, \end{cases} \tag{13.8}$$

the colour decomposition of the one-loop amplitude in Eq. (11.3), and the Born amplitude in Eq. (11.2), and write the finite part of the non-factorisable one-loop amplitude as[1]

$$\begin{aligned} B_{1,\mathrm{fin}}(1_q,2_b,3_{q'},4_t) &= B_1(1_q,2_b,3_{q'},4_t) \\ &\quad - \frac{1}{\varepsilon}\left[\ln\left(\frac{p_1\cdot p_4\; p_2\cdot p_3}{p_1\cdot p_2\; p_3\cdot p_4}\right) + 2\pi i\right] A_0(1_q,2_b,3_{q'},4_t)\,. \end{aligned} \tag{13.9}$$

The result in Eq. (13.9) justifies the form of the Catani's operator I_1 used in Eq. (11.5).

For the evaluation of the double-virtual finite contribution, we need the two-loop amplitude projected on the Born amplitude and the one-loop squared amplitude. We use the result of the expansion in Eq. (13.6) and the expression of $\boldsymbol{Z}$ in Eq. (13.5) to write

$$\begin{aligned} \langle \mathcal{A}^{(0)}|\mathcal{A}^{(2)}_{\mathrm{nf}}\rangle &= -\frac{1}{8\varepsilon^2}\langle \mathcal{A}^{(0)}|\boldsymbol{\Gamma}^2_{0,\mathrm{nf}}|\mathcal{A}^{(0)}\rangle + \frac{1}{2\varepsilon}\langle \mathcal{A}^{(0)}|\boldsymbol{\Gamma}_{0,\mathrm{nf}}|\mathcal{A}^{(1)}_{\mathrm{nf}}\rangle + \langle \mathcal{A}^{(0)}|\mathcal{F}^{(2)}_{\mathrm{nf}}\rangle, \\ \langle \mathcal{A}^{(1)}_{\mathrm{nf}}|\mathcal{A}^{(1)}_{\mathrm{nf}}\rangle &= \frac{1}{4\varepsilon^2}\langle \mathcal{A}^{(0)}||\boldsymbol{\Gamma}_{0,\mathrm{nf}}|^2|\mathcal{A}^{(0)}\rangle + \frac{1}{2\varepsilon}\langle \mathcal{A}^{(1)}_{\mathrm{nf}}|\boldsymbol{\Gamma}_{0,\mathrm{nf}}|\mathcal{A}^{(0)}\rangle \\ &\quad + \frac{1}{2\varepsilon}\langle \mathcal{A}^{(0)}|\boldsymbol{\Gamma}^{\dagger}_{0,\mathrm{nf}}|\mathcal{A}^{(1)}_{\mathrm{nf}}\rangle + \langle \mathcal{F}^{(1)}_{\mathrm{nf}}|\mathcal{F}^{(1)}_{\mathrm{nf}}\rangle. \end{aligned} \tag{13.10}$$

The expressions in Eq. (13.10) can be easily evaluated using the definition of the colour charge operator in Eq. (13.8). Using the standard normalisation of the Gell-Mann matrices

$$\mathrm{Tr}\left(t^a t^b\right) = \frac{1}{2}\delta^{ab}\,, \tag{13.11}$$

we find that the colour algebra reduced to the following expression

$$\langle \mathcal{A}^{(0)}|(\boldsymbol{T}_i\cdot\boldsymbol{T}_j)(\boldsymbol{T}_k\cdot\boldsymbol{T}_m)|\mathcal{A}^{(0)}\rangle = (-1)^{n_i}\frac{N_c^2-1}{4}\,, \tag{13.12}$$

where each pair of colour charge operators is restricted to non-factorisable interactions as explained earlier and n_i stands for the number of partons among $\{i,j,k,m\}$ that are in the initial state. For example, we find that the leading pole of the non-factorisable, two-loop amplitude in the Eq. (13.10) reads

$$\langle \mathcal{A}^{(0)}|\boldsymbol{\Gamma}^2_{0,\mathrm{nf}}|\mathcal{A}^{(0)}\rangle = 4(N_c^2-1)\langle \mathcal{A}^{(0)}|\mathcal{A}^{(0)}\rangle\,(\varepsilon\, I_1)^2\,. \tag{13.13}$$

Using the colour decomposition of the two-loop amplitude in Eq. (11.6), we easily find that the non-factorisable, two-loop amplitude in Eq. (13.10) reads

$$\begin{aligned} &\left[\mathcal{M}_0^*(1_q,2_b,3_{q'},4_t)\,\mathcal{M}_2(1_q,2_b,3_{q'},4_t)\right]_{\mathrm{nf}} \\ &= \frac{N^2-1}{4}\left(\frac{\alpha_s}{2\pi}\right)^2\Big[-\frac{I_1^2(\varepsilon)}{2}|A_0(1_q,2_b,3_{q'},4_t)|^2 \\ &\qquad + I_1(\varepsilon)\,A_0^*(1_q,2_b,3_{q'},4_t)\,B_1(1_q,2_b,3_{q'},4_t) \\ &\qquad + A_0^*(1_q,2_b,3_{q'},4_t)\,B_{2,\mathrm{fin}}(1_q,2_b,3_{q'},4_t)\Big]\,, \end{aligned} \tag{13.14}$$

---

[1] We emphasise that the amplitudes and the operators introduced in Chapter 11 are expanded in $\alpha_s/(2\pi)$, whereas, in this section, we work with an $\alpha_s/(4\pi)$ expansion.

which confirms Eq. (11.7) used in Chapter 11. The IR poles of the double-virtual contribution in Eq. (11.8) are easily found from the real part of the non-factorisable two-loop amplitude in Eq. (13.14) and the non-factorisable one-loop amplitude squared in Eq. (13.9).

We have explained the origin of the formula for the infrared $1/\varepsilon$ poles of the one-loop and the two-loop amplitudes used in Chapter 11. It allows us to write explicitly the poles of the double-virtual contribution, see Eq. (11.9). This is an useful result, since it provides an important cross-check on the evaluation of the amplitude.

13.2 TENSOR DECOMPOSITION

In this section, we discuss how to calculate the non-factorisable two-loop amplitude for the double-virtual contribution to t-channel single top production. We use a standard method which consists of projecting the amplitude on a basis of tensor structures to define Lorentz-invariant form factors [123, 128, 129]. Then, we discuss how these tensor structures can be evaluated using spinor helicity formalism.

The double-virtual contribution is made of the one-loop amplitude squared and the two-loop amplitude interfered with the Born amplitude. We focus on the latter. We extract the colour factor of the non-factorisable two-loop amplitude and write

$$\sum_{\text{colour}} \mathcal{A}^{(0)*}\mathcal{A}^{(2)}_{\text{nf}} = \frac{1}{4}(N_c^2-1)\, A^{(0)*}A^{(2)}_{\text{nf}} \,. \tag{13.15}$$

The colour-stripped amplitude $A^{(2)}_{\text{nf}}$ is composed of two fermion lines interacting by the exchange of two gluons and one W boson. Weak interactions treat the left- and the right-handed fermions differently. For instance, the interaction vertex of the W boson with two quarks comes with a left-handed projector. It reads

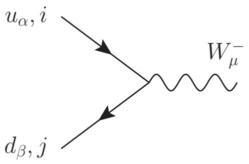

$$= -i\delta_{ij}\frac{g_W}{\sqrt{2}}\gamma_\mu \mathcal{P}_L \left(V_{\text{CKM}}\right)_{\alpha\beta} \,, \tag{13.16}$$

where $\mathcal{P}_L = (\mathbb{1}-\gamma_5)/2$ is the left-handed projector, u_α and d_β are up and down type fermions respectively, $g_W = e/\cos\theta_W$ is the weak coupling constant, $\cos\theta_W = 0.876\ldots$, and V_{CKM} is the Cabibbo–Kobayashi–Maskawa (CKM) matrix.

The treatment of γ_5 in d dimensions is a known problem and many schemes exists to deal with it [21, 134, 135]. However, in the case of non-factorisable corrections, absence of closed fermion loops allows us to use the anti-commuting γ_5 or, in other words, to consider incoming fermions to be left-handed and drop $\mathcal{P}_L$ in the W-boson interaction vertex. It is then clear that the calculation can be performed by only accounting for the vector current part of the vertex in Eq. (13.16), keeping in mind that only left-handed incoming quarks contribute to the final result.

To define form factors, we need to choose a set of tensor structures that is sufficient to write the Born, the one-loop and the two-loop amplitudes that contribute to t-channel single top production. We consider the following set of tensor structures[2]

$$\begin{aligned}
\mathcal{S}_1 &= \overline{u}_t(p_4)\; u(p_2) \times \overline{u}(p_3)\, \not{p}_4\, u(p_1)\,,\\
\mathcal{S}_2 &= \overline{u}_t(p_4)\, \not{p}_1\, u(p_2) \times \overline{u}(p_3)\, \not{p}_4\, u(p_1)\,,\\
\mathcal{S}_3 &= \overline{u}_t(p_4)\, \gamma^{\mu_1}\, u(p_2) \times \overline{u}(p_3)\, \gamma_{\mu_1}\, u(p_1)\,,\\
\mathcal{S}_4 &= \overline{u}_t(p_4)\, \gamma^{\mu_1}\not{p}_1\, u(p_2) \times \overline{u}(p_3)\, \gamma_{\mu_1}\, u(p_1)\,,\\
\mathcal{S}_5 &= \overline{u}_t(p_4)\, \gamma^{\mu_1}\gamma^{\mu_2}\, u(p_2) \times \overline{u}(p_3)\, \gamma_{\mu_1}\gamma_{\mu_2}\not{p}_4\, u(p_1)\,,\\
\mathcal{S}_6 &= \overline{u}_t(p_4)\, \gamma^{\mu_1}\gamma^{\mu_2}\not{p}_1\, u(p_2) \times \overline{u}(p_3)\, \gamma_{\mu_1}\gamma_{\mu_2}\not{p}_4\, u(p_1)\,,\\
\mathcal{S}_7 &= \overline{u}_t(p_4)\, \gamma^{\mu_1}\gamma^{\mu_2}\gamma^{\mu_3}\, u(p_2) \times \overline{u}(p_3)\, \gamma_{\mu_1}\gamma_{\mu_2}\gamma_{\mu_3}\, u(p_1)\,,\\
\mathcal{S}_8 &= \overline{u}_t(p_4)\, \gamma^{\mu_1}\gamma^{\mu_2}\gamma^{\mu_3}\not{p}_1\, u(p_2) \times \overline{u}(p_3)\, \gamma_{\mu_1}\gamma_{\mu_2}\gamma_{\mu_3}\, u(p_1)\,,\\
\mathcal{S}_9 &= \overline{u}_t(p_4)\, \gamma^{\mu_1}\gamma^{\mu_2}\gamma^{\mu_3}\gamma^{\mu_4}\, u(p_2) \times \overline{u}(p_3)\, \gamma_{\mu_1}\gamma_{\mu_2}\gamma_{\mu_3}\gamma_{\mu_4}\not{p}_4\, u(p_1)\,,\\
\mathcal{S}_{10} &= \overline{u}_t(p_4)\, \gamma^{\mu_1}\gamma^{\mu_2}\gamma^{\mu_3}\gamma^{\mu_4}\not{p}_1\, u(p_2) \times \overline{u}(p_3)\, \gamma_{\mu_1}\gamma_{\mu_2}\gamma_{\mu_3}\gamma_{\mu_4}\not{p}_4\, u(p_1)\,,\\
\mathcal{S}_{11} &= \overline{u}_t(p_4)\, \gamma^{\mu_1}\gamma^{\mu_2}\gamma^{\mu_3}\gamma^{\mu_4}\gamma^{\mu_5}\, u(p_2) \times \overline{u}(p_3)\, \gamma_{\mu_1}\gamma_{\mu_2}\gamma_{\mu_3}\gamma_{\mu_4}\gamma_{\mu_5}\, u(p_1)\,.
\end{aligned} \tag{13.17}$$

They form a complete set of structures and allow us to compute the double-virtual, non-factorisable correction to t-channel single top production. The vector-current contribution to the colour-stripped Born amplitude is found to be

$$A^{(0)}(\vec{\lambda}) = \frac{\mathcal{S}_3(\vec{\lambda})}{4(t-m_W^2)}\,, \tag{13.18}$$

where $\vec{\lambda}$ denotes the polarisation states of the external particles. Restoring the colour factors, the vector-current contribution to Born amplitude squared reads

$$\sum_{\vec{\lambda},\text{colours}} |\mathcal{A}^{(0)}(\vec{\lambda})|^2 = N_c^2 \frac{4\,s\,(s-m_t^2)}{(t-m_W^2)^2}\,. \tag{13.19}$$

The one-loop amplitude is expressed in terms of the first seven tensors in Eq. (13.17). At two loops, we aim to write the colour-stripped amplitude as

$$A_{\text{nf}}^{(2)} = \vec{f}\cdot\vec{\mathcal{S}}\,, \tag{13.20}$$

---

[2] We note that these eleven tensor structures differ slightly from the ones in Ref. [123], because we are only considering the vector part of the W boson, which is equivalent to setting $\gamma_5 = 0$ in the calculation, as explained earlier.

where $\vec{\mathcal{S}}$ stands for the vector of all eleven tensor structures and $\vec{f}$ are the *form factors*. To determine these form factors, we construct the following eleven quantities

$$Q_i = \sum_{\vec{\lambda}} \mathcal{S}_i^\dagger(\vec{\lambda})\, A_{\rm nf}^{(2)}(\vec{\lambda}), \quad i = 1, \dots, 11\,, \tag{13.21}$$

where we sum over polarisations of external state particles and use

$$\sum_{\lambda} u(p_i) \otimes \bar{u}(p_i) = \not{p}_i, \quad i = 1, 2, 3, \qquad \sum_{\lambda} u_t(p_4) \otimes \bar{u}_t(p_4) = \not{p}_4 + m_t\,. \tag{13.22}$$

We define the matrix

$$C_{ij} = \sum_{\vec{\lambda}} \mathcal{S}_i^\dagger(\vec{\lambda})\, \mathcal{S}_j(\vec{\lambda})\,, \tag{13.23}$$

and write the Q_i in the following way

$$Q_i = \sum_{\vec{\lambda}} \mathcal{S}_i^\dagger(\vec{\lambda})\, A_{\rm nf}^{(2)}(\vec{\lambda}) = \sum_j f_j \sum_{\vec{\lambda}} \mathcal{S}_i^\dagger(\vec{\lambda})\, \mathcal{S}_j(\vec{\lambda}) = \sum_j C_{ij}\, f_j\,. \tag{13.24}$$

It follows from Eq. (13.24) that the vector $\vec{Q}$ is obtained by acting on the vector $\vec{f}$ with the matrix C.

$$\vec{Q} = \hat{C}\, \vec{f}\,. \tag{13.25}$$

Therefore, the form factors are determined using the inverse matrix $\hat{C}^{-1}$ and the vector $\vec{Q}$. They read

$$\vec{f} = \hat{C}^{-1}\, \vec{Q}\,. \tag{13.26}$$

We would like to extract the dependence on ε of the tensor structures in Eq. (13.17) and express them as 4-dimensional objects. The ε dependence is provided only by the Lorentz indices since the external momenta and the spinors are four-dimensional. The d-dimensional space can be thought of in terms of two distinct spaces.[3] We split the metric

$$\eta_{\mu\nu} = \hat{\eta}_{\mu\nu} + \tilde{\eta}_{\mu\nu}\,, \tag{13.27}$$

such that

$$\hat{\eta}^\mu_\mu = \hat{\eta}^{\mu\nu}\eta_{\nu\mu} = 4, \quad \tilde{\eta}^\mu_\mu = \tilde{\eta}^{\mu\nu}\eta_{\nu\mu} = -2\varepsilon, \quad \tilde{\eta}_{\mu\sigma}\hat{\eta}^{\sigma\nu} = 0\,. \tag{13.28}$$

From this construction, it is clear that one needs at least two terms with a -2ε-part to provide any ε-term. The consequence of Eq. (13.28) is that each tensor structure in

---

[3] This idea has been first introduced by G. 't Hooft and M. Veltman in Ref. [21].

Eq. (13.17) can be written as a sum of 4-dimensional structures with explicit ε dependence. We find

$$\boxed{\begin{aligned} \mathcal{S}_{1,..,4} &= \mathcal{S}^{(4)}_{1,..,4}\,, \\ \mathcal{S}_{5,6} &= \mathcal{S}^{(4)}_{5,6} - 2\varepsilon \mathcal{S}^{(4)}_{1,2}\,, \\ \mathcal{S}_{7,8} &= \mathcal{S}^{(4)}_{7,8} - 6\varepsilon \mathcal{S}^{(4)}_{3,4}\,, \\ \mathcal{S}_{9,10} &= \mathcal{S}^{(4)}_{9,10} - 12\varepsilon \mathcal{S}^{(4)}_{5,6} + \left(12\varepsilon^2 + 4\varepsilon\right) \mathcal{S}^{(4)}_{1,2}\,, \\ \mathcal{S}_{11} &= \mathcal{S}^{(4)}_{11} - 20\varepsilon \mathcal{S}^{(4)}_{7} + \left(60\varepsilon^2 + 20\varepsilon\right) \mathcal{S}^{(4)}_{3}\,, \end{aligned}} \tag{13.29}$$

where $S_i^{(4)}$ are four-dimensional spinor structure. The spinor structures in Eq. (13.29) can be computed using spinors with fixed helicities[4]. We select only the left-handed incoming partons to restore the correct structure of the $V - A$ current.

In the next section, we will discuss the evaluation of the quantities Q_i.

13.3 FORM FACTORS AND MASTER INTEGRALS

In the previous section, we have decomposed the two-loop amplitude into tensor structures and form factors. In this section, we explain how to express these form factors through a set of master integrals. Then, we describe the evaluation of master integrals using a semi-numerical approach called the *auxiliary mass flow method* [126, 127].

The form factors defined in the previous section in Eq. (13.24) contain many two-loop Feynman integrals. We classify them into integral families using `REDUZE 2` [137]. We find that there are eighteen integral families, which can be mapped onto nine by crossing symmetry, $p_1 \leftrightarrow -p_3$. They are shown in Fig. 13.1.

An integral family is defined by propagators that integrals in the family depend upon. Any scalar products of loop momenta with external momenta can be expressed as a linear combination of the propagators that define the topology. For $2 \to 2$ scattering at two-loop, we need to include nine propagators into each family. As the result, in addition to seven propagators that naturally come from the double-box loop integrals, we need two additional ones. Then, in each topology, two-loop integrals are written as

$$I(a_1, \ldots, a_9) = \int \left(\prod_{n=1}^{2} e^{\epsilon \gamma_E} \frac{\mathrm{d}^d k_n}{i\pi^{d/2}} \right) \frac{1}{D_1^{a_1} D_2^{a_2} \cdots D_9^{a_9}}\,, \tag{13.30}$$

where D_i, $i = 1 \ldots 9$, are propagators defining the integral family. In Table 13.1, these propagators are shown for each integral family.

---

[4] For a review of this formalism, we refer the reader to Ref. [136].

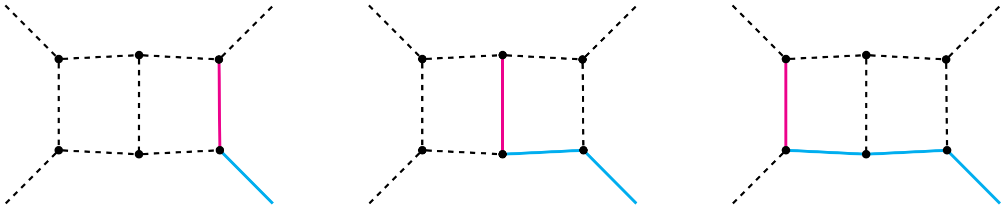

(a) planar no. 1 (b) planar no. 2 (c) planar no. 3

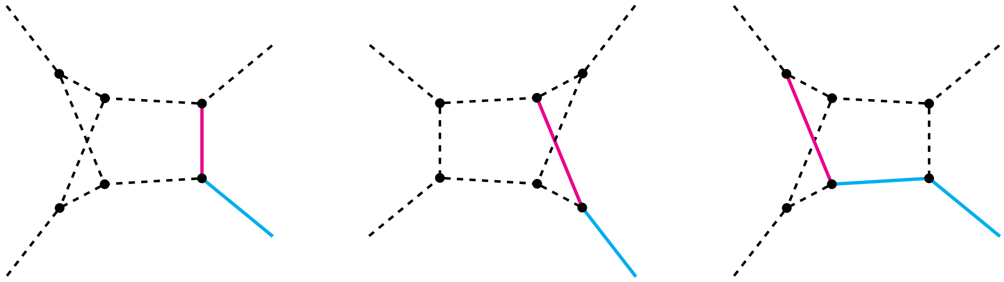

(d) non-planar no. 1 (e) non-planar no. 2 (f) non-planar no. 3

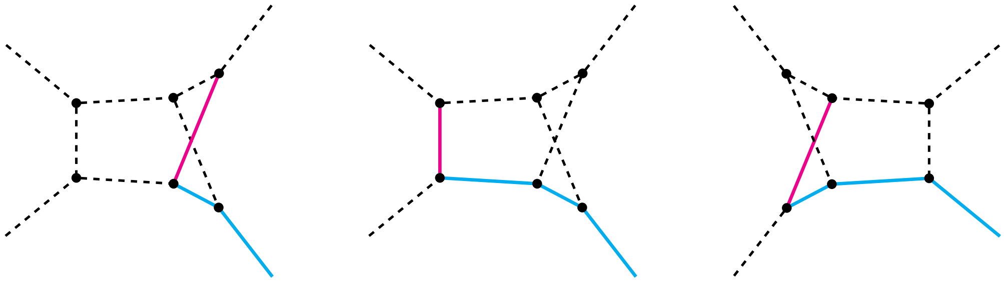

(g) non-planar no. 4 (h) non-planar no. 5 (i) non-planar no. 6

Figure 13.1: The nine integral families that form the two-loop amplitude projections Q_i. Dashed lines stand for massless external legs or propagators. Massive legs or propagators are represented with solid line and the colour indicates to which particle it refers; blue corresponds to the top quark and pink to the W boson.

In each integral family, we perform an analytic reduction of Feynman integrals to master integrals using `KIRA` [138], a computer program which implements Laporta's reduction algorithm [139]. Each integral which contributes to the two-loop amplitude can be expressed as a linear combination of these master integrals. The reduction is performed in four days on twenty cores for the most difficult integral families. In total, we find that there are 428 master integrals, whose evaluation is discussed in the next section.

13.4 NUMERICAL EVALUATION OF THE MASTER INTEGRALS

In this section, we discuss the calculation of the 428 master integrals required to compute the two-loop amplitude for the non-factorisable corrections to t-channel single top

Name		Definition
planar	1	$k_1^2, (k_1-p_1)^2, (k_1+p_2)^2, (k_2+p_3)^2, (k_1+k_2-p_1+p_3)^2, (k_2-p_1-p_2+p_3)^2, k_2^2-m_W^2, k_1\cdot p_3, k_2\cdot p_2$
	2	$k_1^2, k_2^2, (k_1-p_1)^2, (k_1+p_2)^2, (k_2+p_3)^2, (k_2-p_1-p_2+p_3)^2-m_t^2, (k_1+k_2-p_1+p_3)^2-m_W^2, k_1\cdot p_3, k_2\cdot p_2$
	3	$k_2^2, (k_1-p_1)^2, (k_2+p_3)^2, (k_1+k_2-p_1+p_3)^2, (k_1+p_2)^2-m_t^2, (k_2-p_1-p_2+p_3)^2-m_t^2, k_1^2-m_W^2, k_1\cdot p_3, k_2\cdot p_2$
non-planar	1	$k_2^2, (k_2-p_1)^2, (k_1+p_3)^2, (k_1-k_2+p_3)^2, (k_1-k_2-p_2+p_3)^2, (k_1-p_1-p_2+p_3)^2, k_1^2-m_W^2, k_2\cdot p_2, k_2\cdot p_3$
	2	$k_1^2, k_2^2, (k_1-p_1)^2, (k_1+p_2)^2, (k_2+p_3)^2, (k_1-k_2+p_2-p_3)^2, (k_1-k_2-p_1)^2-m_W^2, k_2\cdot p_1, k_2\cdot p_2$
	3	$k_1^2, k_2^2, (k_1+p_3)^2, (k_1-k_2+p_3)^2, (k_1-k_2-p_2+p_3)^2, (k_1-p_1-p_2+p_3)^2-m_t^2, (k_2-p_1)^2-m_W^2, k_2\cdot p_2, k_2\cdot p_3$
	4	$k_1^2, k_2^2, (k_1-p_1)^2, (k_1+p_2)^2, (k_1-k_2-p_1)^2, (k_1-k_2+p_2-p_3)^2-m_t^2, (k_2+p_3)^2-m_W^2, k_2\cdot p_1, k_2\cdot p_2$
	5	$k_2^2, (k_1-p_1)^2, (k_2+p_3)^2, (k_1-k_2-p_1)^2, (k_1+p_2)^2-m_t^2, (k_1-k_2+p_2-p_3)^2-m_t^2, k_1^2-m_W^2, k_2\cdot p_1, k_2\cdot p_2$
	6	$k_1^2, k_2^2, (k_2-p_1)^2, (k_1+p_3)^2, (k_1-k_2-p_2+p_3)^2-m_t^2, (k_1-p_1-p_2+p_3)^2-m_t^2, (k_1-k_2+p_3)^2-m_W^2, k_2\cdot p_2, k_2\cdot p_3$

Table 13.1: Definitions of the integral families. The propagators are defined by the loop momenta k_1 and k_2 and the external momenta p_1, p_2, and p_3 as defined in Eq. (11.1). Three of them are planar and six are non-planar. The nine integral families that contribute to the Q_i but which are not defined here can be obtained by the crossing symmetry $p_1 \leftrightarrow -p_3$.

production.

Since the analytic calculation of master integral is currently not possible,[5] we decided to evaluate the master integrals using the auxiliary mass flow method [126, 127]. We adapt the procedure to our process as follows. We consider the mass of the W boson, which only appears internally in one propagator, as a free complex parameter.[6] We write

$$m_W^2 \to m_W^2(1+x)\,, \tag{13.31}$$

---

[5] The analytic computation of the master integrals of the two-loop, non-factorisable amplitude for the t-channel single top production has been the subject of two recent papers [124, 125]. Nevertheless, both studies report incomplete results.

[6] The auxiliary mass flow method as originally presented in Ref. [126, 127] introduces an auxiliary mass to every propagators, massless or massive.

where $\operatorname{Im} x < 0$ to respect the Feynman prescription in the propagator. We generate differential equations for master integrals with respect to x using integration-by-parts (IBP) relations and find

$$\partial_x \boldsymbol{I} = \boldsymbol{M}(x, \varepsilon)\boldsymbol{I}\,. \tag{13.32}$$

To solve these equations, we need boundary conditions. To find them, we compute integrals at $x = -i\infty$. At this point, the mass of the W boson is very large in comparison to s, t and m_t^2, simplifying the analytic computation of the master integrals. Once the boundary conditions are available, it becomes possible, for any phase-space point, to solve the differential equation in Eq. (13.32) iteratively to reach the point $x = 0$ which corresponds to the physical value of the W boson mass. We will now explain this procedure in detail.

The value $x = -i\infty$, chosen to determine boundary conditions to solve the differential equation in Eq. (13.32), is a singular point. Therefore, we expect the following form for the solution to the differential equation around $y = 1/x = 0$

$$\boldsymbol{I} = \sum_j^M \varepsilon^j \sum_k^N \sum_l \boldsymbol{c}_{jkl}\, y^k \ln^l y + \mathcal{O}(\varepsilon^{M+1}) + \mathcal{O}(y^{N+1})\,, \tag{13.33}$$

where the value of M is fixed by the desired order of the ε-expansion of the different master integrals and by the singularity structure of the matrix $\boldsymbol{M}$. This Ansatz can be used to move away from the singular point $y = 0$. The size of the first step is not completely arbitrary. Indeed, it cannot be larger than the distance to the closest singularity of the differential equations in Eq. (13.32) in the y complex plane. In addition, the numerical precision attained in this first step depends on the value of y and the order of the expansion N and, therefore, it is preferable to keep it small.

Once we have moved away from the boundary, we move through a grid of regular points. At each of such points, the master integrals can be expanded in Taylor series. From the regular point x_0, we consider the following Ansatz

$$\boldsymbol{I} = \sum_j^M \varepsilon^j \sum_{k=0}^N \boldsymbol{c}_{jk}(x - x_0)^k + \mathcal{O}(\varepsilon^{M+1}) + \mathcal{O}((x - x_0)^{N+1})\,. \tag{13.34}$$

We approach the point $x = 0$, step-by-step, by numerically solving the differential equation, determining coefficients of the Taylor expansion and matching them to each other. As mentionned earlier, the maximal size of the step we can perform is determined by the closest singularity in the complex plane. We illustrate this principle in Fig. 13.2. From the first regular point (blue), we can move closer to the physical value (green) with a step size smaller than the distance from x_0 to the closest singularity, denoted with a dashed half-circle. After this step, we have are at the second blue point. Since the closest

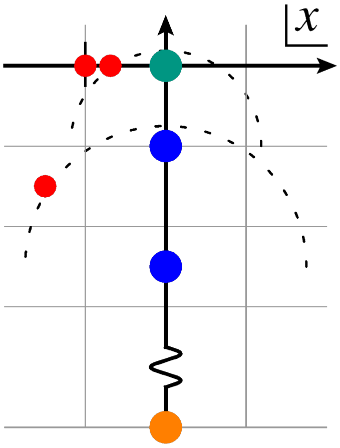

Figure 13.2: Illustration of the auxiliary mass flow method. We start at the irregular point in orange where $x = -i\infty$, move in the complex plane to regular points, denoted in blue. The step size is determined by how far is the closest singularity of the differential equation.

singularity is further away than the physical point, one additional step is enough to conclude the evaluation.

In practice, we will choose only a fraction $1/n$, $n \in N$ of the maximal allowed step size. The error on the final results due to the truncation of the Taylor series scales as $(1/n)^{N+1}$. Increasing n or N will give more accurate results at the price of a larger number of steps or more coefficients to determine when solving the differential equation, respectively.

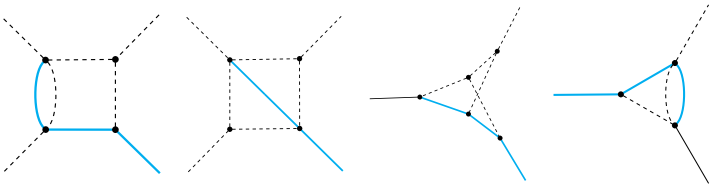

Figure 13.3: Example of integrals required at the boundary $m_W^2 \to -i\infty$ that are difficult to calculate analytically . Dashed lines stand for massless legs and propagators, whereas solid lines stand for massive legs or propagators. We denote in blue the lines that corresponds to m_t.

As we already mentioned, integrals at the boundary $y = 0$ are simpler to calculate. Nevertheless, a few of these integrals are still difficult to compute analytically. We illustrate some of them in Fig. 13.3. For those integrals, we proceed in an analogous way to the what has been done for m_W and consider the *internal* top-quark mass m_t to be a free complex parameter. We write

$$m_t^2 \to m^2(1+w)\,, \tag{13.35}$$

where $\operatorname{Im} w < 0$. We derive differential equations by differentiating the master integrals with respect to w. The steps are then analogous to what has been described for the W boson mass. There is, however, one difference in this case. Since we have shifted only the internal top-quark mass, the internal and the external top-quark masses are different. As the result, solutions to the differential equations display unphysical branches in the limit $w \to 0$. These branches should be discarded. We proceed in the following way. For the last step, the Ansatz for the master integrals is analogous to Eq. (13.33). We write it as

$$\boldsymbol{I} = \sum_j^M \varepsilon^j \sum_k^N \sum_l \boldsymbol{c}_{jkl} w^{k+l\varepsilon} + \mathcal{O}(\varepsilon^{M+1}) + \mathcal{O}(w^{N+1})\,. \tag{13.36}$$

Then, the physical result for $w = 0$ corresponds to the branch $k = 0$ and $l = 0$.

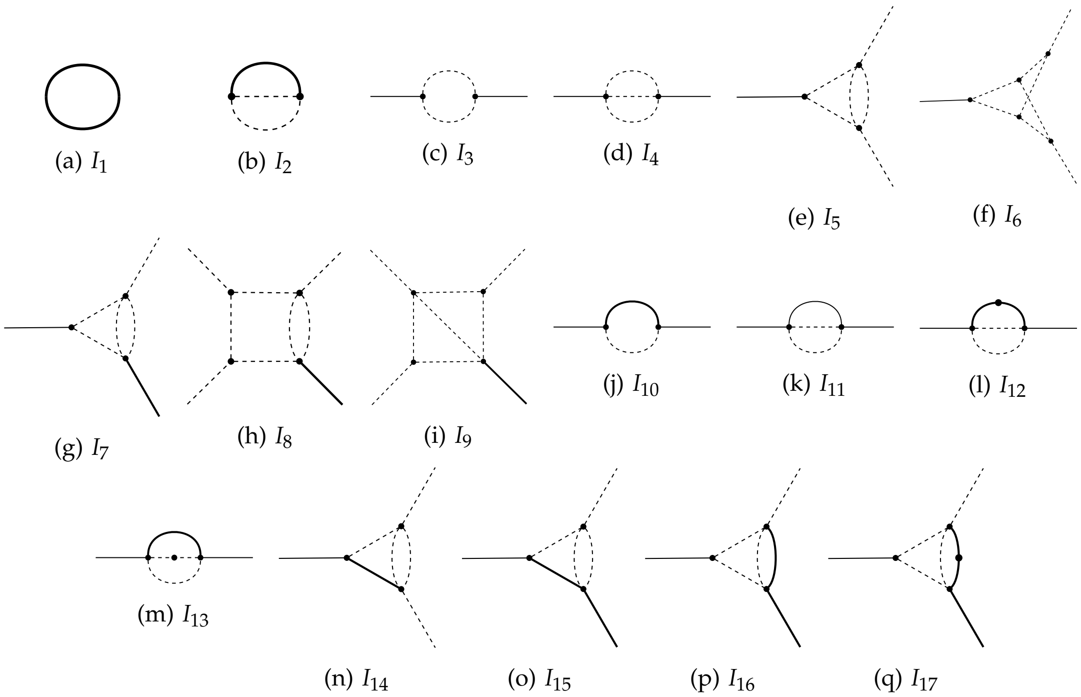
(a) I_1 (b) I_2 (c) I_3 (d) I_4 (e) I_5 (f) I_6 (g) I_7 (h) I_8 (i) I_9 (j) I_{10} (k) I_{11} (l) I_{12} (m) I_{13} (n) I_{14} (o) I_{15} (p) I_{16} (q) I_{17}

Figure 13.4: Integrals that are required as boundary conditions to evaluate the 428 master integrals. Dashed lines stand for massless legs or propagators, whereas solid line represents massive legs or propagators with mass m_t.

In summary, we perform the numerical evaluation of the master integrals in two steps, as illustrated in Fig. 13.5a. First, we solve the differential equations to move away

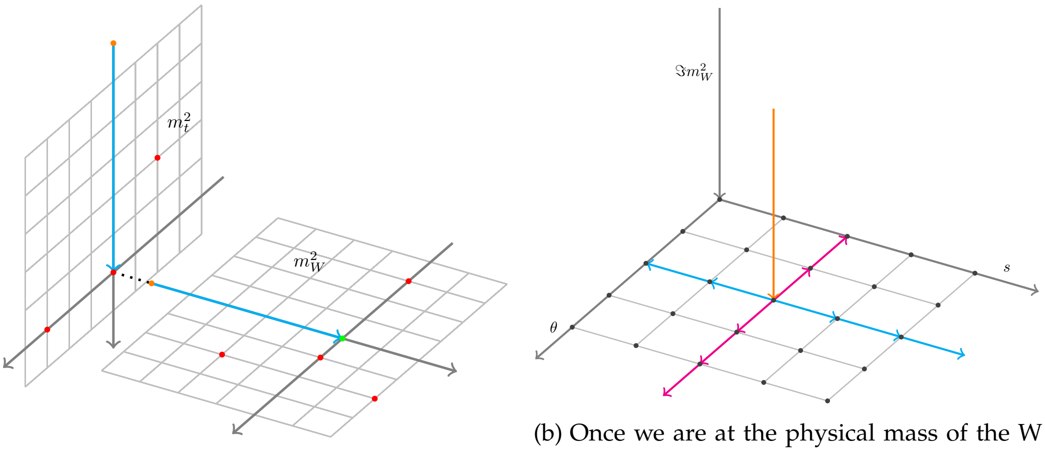

(a) Differential equations are first solved for m_t and, then, for m_W.

(b) Once we are at the physical mass of the W boson, we can move in the phase space using differential equations with respect to s and t.

Figure 13.5: Description of the displacement in the parameter space.

from the boundary $m^2 = -i\infty$ to get to its physical value and, then, use this result as a boundary condition to solve the differential equations in Eq. (13.32) to go to the physical value of the W mass. We find that we only need a small set of integrals at the boundary where $m^2 = -i\infty$ and $m_W^2 = -i\infty$, shown in Fig. 13.4. Most of the integrals needed are available in the literature [140–144]. Few of them were not available to sufficiently high order in ε and two of them, I_{16} and I_{17}, were not found. An overview of the calculation of these two integrals is given in Appendix C.

For phenomenology, we need to evaluate the two-loop amplitude at several phase-space points, parametrised by the Mandelstam variables (s, t). In Refs. [128, 129], the evaluation of the master integrals at each phase-space point was done in the following way: the integrals at the boundary $m_W^2 \to -i\infty$ are evaluated at a specific phase-space points and then, we solve the differential equations to go to the physical value of the W boson as described in the previous section. We consider an alternative approach by generating differential equations for the master integrals with respect to the Mandelstam variables s and t. We use these equations to move from a physical point to other points in the phase space. This is illustrated in Fig. 13.5b. We note that a similar approach has already been used in Refs. [145–147].

13.5 NUMERICAL RESULTS

The 428 master integrals can be evaluated to 20 digits precision within half an hour on a single core for one kinematic point. The evaluation of the master integrals is checked in two ways. First, we compare the results from the auxiliary mass flow method with the evaluations obtained with `pySecDec` [148, 149] at a physical phase-space point[7]. A good agreement is found for the majority of the master integrals. Nevertheless, we were not able to produce a meaningful result for few of them, such as non-planar, double-box integrals. Then, the second numerical check that we can perform is a self-consistency check. The evaluation of the master integrals at some phase-space point (s_1, t_1) obtained from the direct integration of the boundary $m_W \to -i\infty$ is compared to the value obtained from the phase-space point (s_2, t_2) which is then transported to (s_1, t_1) using differential equations in s and t, as described in Fig. 13.5b. This procedure has been successfully applied to all master integrals for several phase-space points with an agreement of 20 digits.

The two-loop amplitude is evaluated at all phase-space points and its poles are compared to the prediction from Eq. (13.10). In Table 13.2, we present the agreement between the evaluation of the two-loop amplitude to the pole prediction for a typical phase-space point. The agreement is of 14 digits at $\mathcal{O}(\varepsilon^{-2})$ and of 13 digits at $\mathcal{O}(\varepsilon^{-1})$. It is reasonable to assume that we lose one digit per ε order and, therefore, we expect 12 correct digits for the finite part of the amplitude. In Table 13.3, we provide additional evaluations of the two-loop amplitude.

	ε^{-2}	ε^{-1}
$\langle \mathcal{A}^{(0)} \vert \mathcal{A}^{(2)}_{\text{nf}} \rangle$	$-229.0940408654660 - 8.9781633332241640i$	$-301.1802988944764 - 264.1773596529505i$
IR poles	$-229.0940408654665 - 8.9781633332241973i$	$-301.1802988944791 - 264.1773596529535i$

Table 13.2: Comparison of the two-loop amplitude evaluation and the pole prediction at a typical phase space point $s \approx 104337$ GeV^2 and $t \approx -5179.68$ GeV^2.

$\langle \mathcal{A}^{(0)} \vert \mathcal{A}^{(2)}_{\text{nf}} \rangle (s,t)$	ε^{-2}	ε^{-1}	ε^{0}
$(104337.30, -5179.6797)$	$-229.09404 - 8.9781633i$	$-301.18030 - 264.17736i$	$380.61217 + 307.59053i$
$(51824.679, -16060.887)$	$-8.2985887 - 4.8234599i$	$-7.2779624 - 22.421862i$	$42.503179 + 59.484685i$
$(2728123.9, -69809.245)$	$-5061.2720 - 83.997993i$	$34392.588 - 1255.7061i$	$-1507.7598 + 18782.966i$

Table 13.3: Evaluations of the two-loop amplitude at three different phase-space points.

The non-factorisable, double-virtual contribution to the cross section for t-channel single top production in proton-proton collision can be written as

$$d\sigma^{VV,ub}_{pp\to d+t} = \sum_{\substack{i,j=u,b\\ i\neq j}} \int dx_1\, dx_2\, f_i(x_1,\mu_R)\, d\hat{\sigma}^{VV}_{ij\to d+t}(x_1,x_2,\mu_R)\, f_j(x_2,\mu_R)\,, \tag{13.37}$$

---

[7] We chose $s = (500 \text{ GeV})^2$ and $t = -(100 \text{ GeV})^2$

where we set the flavour of the light quarks to be $q = u$ and $q' = d$. We use the PDF `NNPDF31_lo_as_0118` [95, 96], set the factorisation scale to $\mu_F = m_t$, the masses of the top quark and the W boson to $m_t = 173$ GeV and $m_W = 80.379$ GeV, and the Fermi constant to $G_F = 1.16637 \times 10^{-5}\ \ \text{GeV}^{-2}$.

We build the partonic cross section from the finite part of the amplitude defined from the subtraction of Catani's operator in Eq. (13.10). It reads

$$\hat{\sigma}^{VV}_{ij\to d+t} = \frac{1}{8N_c^2\, s} \int [dp_3][dp_4] \langle \mathcal{F}|\mathcal{F}\rangle \, (2\pi)^4 \delta^{(4)}\left(p_1 + p_2 - p_3 - p_4\right) , \tag{13.38}$$

where the finite amplitude squared reads

$$\langle \mathcal{F}|\mathcal{F}\rangle = \langle \mathcal{A}^{(0)}|\mathcal{A}^{(0)}\rangle + \left(\frac{\alpha_s}{4\pi}\right)^2 \left[\langle \mathcal{F}^{(1)}_{\text{nf}}|\mathcal{F}^{(1)}_{\text{nf}}\rangle + 2\text{Re}\left\{\langle \mathcal{A}^{(0)}|\mathcal{F}^{(2)}_{\text{nf}}\rangle\right\}\right] . \tag{13.39}$$

To evaluate the non-factorisable corrections, we need to generate a set of phase space points that describes well the kinematics of t-channel single top production. We assume that the double-virtual and the Born contributions are not radically different and train the Vegas integrator on the latter. Then, we extract ten lists of $10,000$ phase-space points from the grid that has been adapted to the Born contribution. For each phase-space points, we evaluate the 428 master integrals as described in the previous section. Using these sets of points, we can estimate the double-virtual cross section.

Interestingly, the evaluation of the double-virtual contribution can provide insights into the actual magnitude of the non-factorisable corrections. Indeed, it appears that, in non-factorisable corrections, real-emission corrections are suppressed compared to the double-virtual ones. This can be justified in the following way: we consider an expansion of the cross section in the top-quark transverse momentum

$$\sigma = \sigma_0 + \frac{p_{t,\text{top}}}{\sqrt{s}}\, \sigma_1 + \mathcal{O}\left(p^2_{t,\text{top}}/s\right) , \tag{13.40}$$

where σ_0 corresponds to the contribution where $p_{t,\text{top}} = 0$, or equivalently, for *massless* partons, $p_1^\mu = p_3^\mu$ and $p_2^\mu = p_4^\mu$. Then, we consider the real-emission amplitude where a gluon is emitted off the light-quark line. To contribute to σ_0, the gluon has to be soft. However, in this case, the real-emission amplitude vanishes since

$$S_5 A_0^L(1_q, 2_b, 3_{q'}, 4_t; 5_g) = (\frac{p_3^\mu}{p_3 \cdot p_5} - \frac{p_1^\mu}{p_3 \cdot p_5}) A_0(1_q, 2_b, 3_{q'}, 4_t) = \mathcal{O}(m_t) , \tag{13.41}$$

where we use the notation introduced in Chapter 11 and Eqs. (11.12)-(11.14). Therefore, the real-emission corrections do not contribute to σ_0. The same argument holds for any amplitudes which are part of real-emission contributions. As the result, the double-virtual contribution is expected to be dominant in non-factorisable corrections. In addition, we note that σ_0 is free of IR poles since they are provided by the emission of soft gluon. Nevertheless, the top quark is massive, and, thus, we expect a milder suppression of the real-emission contributions in the case of t-channel single-top production.

14 CALCULATION OF THE REAL-EMISSION AMPLITUDES

In this chapter, we discuss the calculation of the real-emission amplitudes that contribute to non-factorisable corrections to t-channel single top production. First, we explain how the tree-level amplitudes are obtained. Then, we elaborate on the one-loop five-point amplitude and the efforts made to improve its numerical stability.

14.1 TREE-LEVEL AMPLITUDES

The real-emission, tree-level amplitudes are generated with `QGRAF` [79] and the Dirac algebra is performed with `FORM` [73–76]. At NNLO, we need single- and double-real emission amplitudes.[1] The double-real emission amplitude corresponds to the process

$$q(p_1) + b(p_2) \to q'(p_3) + t(p_4) + g(p_5) + g(p_6)\,. \tag{14.1}$$

The single top production is characterised by the presence of the W boson vertex, described in Eq. (13.16). Similar to the treatment of the double-virtual contribution in Sec. 13.2, we use the anticommutating γ_5 to force the initial state partons to be left-handed. We use spinor helicity formalism [150] to write

$$P_L\, u(p_i) = u_L(p_i) = |i]\,, \quad \text{for light-like } p_i\,, \tag{14.2}$$

where, for the considered process, $i = 1, 2, 3$. Spinors that describe massive partons can also be written as spinors with fixed helicities by decomposing their momentum into two light-like momenta. For instance,

$$p_4^\mu = p_4^{\flat\,\mu} + \frac{m_t^2}{2n \cdot p_4}\, n^\mu\,, \tag{14.3}$$

where we introduced the light-like momentum $p_4^{\flat\,\mu}$ and the reference vector n^μ which is arbitrary. The spinors that describe left- and the right-handed top quarks can be written as

$$\bar{u}_L(p_4) = \langle 4^\flat| + \frac{m_t}{[n4^\flat]}[n| \quad \text{and} \quad \bar{u}_R(p_4) = [4^\flat| + \frac{m_t}{\langle n4^\flat\rangle}\langle n|\,. \tag{14.4}$$

---

[1] The single-real emission amplitude contributes once interfered with the one-loop five-point amplitude.

We use this representation for the massive sponors to write the Born amplitude as

$$\begin{aligned} A_0(1_q^L, 2_b^L, 3_{q'}^L, 4_t^L) &= \frac{g_W^2}{t - m_W^2} \langle 3 4^\flat \rangle [21] \,, \\ A_0(1_q^L, 2_b^L, 3_{q'}^L, 4_t^R) &= \frac{g_W^2}{t - m_W^2} \frac{m_t}{\langle n 4^\flat \rangle} \langle 3 n \rangle [21] \,, \end{aligned} \tag{14.5}$$

where $t = (p_1 - p_3)^2$. It is clear that if we chose $n^\mu = p_3^\mu$, right-handed top quarks do not contribute to the Born amplitude. This choice also simplifies the expression for single- and double-real emission amplitudes.

Single- and double-real emission amplitudes can be numerically evaluated using the spinor helicity formalism. The non-factorisable, real-emission contribution is then obtained by interfering the diagrams where gluons are emitted off the light-fermion line with the ones where gluons are emitted off the heavy-fermion line, and vice-versa, as illustrated in Fig. 11.3. To check our results, we compare the evaluation of the double-real emission cross section to `MadGraph5_aMC@NLO` [77] for resolved kinematics.

14.2 ONE-LOOP FIVE-POINT AMPLITUDE

In this section, we described the calculation of the one-loop five-point amplitude $\mathcal{M}_1(1_q, 2_b, 3_{q'}, 4_t, 5_g)$, introduced in Eq. (11.16). This amplitude is needed up to finite order in ε.

As discussed in Chapter 11, we discard colour-antisymmetric contributions. We generate the diagrams using `QGRAF` [79] and perform the Dirac algebra with `FORM` [73–76]. We use the same notation as in Chapter 11 and split the 24 diagrams that contribute to the real-emission, one-loop amplitude into two categories: one where the gluon is emitted from the light-fermion line (B_1^{sL}), and the other where the gluon is emitted by the heavy-fermion line (B_1^{sH}), see Fig. 14.1 for examples. We first discuss the treatment of the spinor chains and, then, the calculation of the one-loop tensor integrals.

As already explained in Chapter 13, we take care of γ_5 in this case by selecting left-handed incoming partons. We work in the spinor helicity formalism and we split the metric into four-dimensional and -2ε-dimension parts, see Eq. (13.28). The ε dependence is extracted and we are left with 4-dimensional helicity spinor chains which can be evaluated at any phase-space points. We find that there are two spinor structures per helicity configuration. For instance, if both the emitted gluon and the top-quark are left-handed, we find that the amplitude depends on the following two helicity spinor chains

$$\langle 4^\flat 5_g \rangle^2 \langle 1_q 3_{q'} \rangle [4^\flat 1_q][1_q 2_b], \qquad \langle 4^\flat 5_g \rangle \langle 3_{q'} 5_g \rangle [1_q 2_b] \,. \tag{14.6}$$

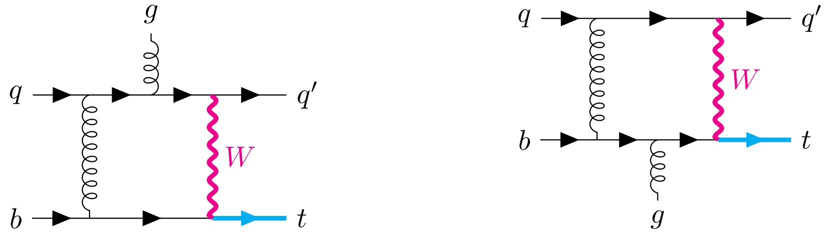

(a) B_1^{sL} (b) B_1^{sH}

Figure 14.1: Two of the one-loop five-point diagrams required to compute the real-virtual contribution to t-channel single top production. We split them into B_1^{sL} where the gluon is emitted from the light-fermion line and B_1^{sH} where the gluon is emitted from the heavy-fermion line.

Since both the top quark and the gluon have two physical polarisations, there are four different helicity configurations in total, leading to eight spinor structures.[2]

Among the 24 diagrams, eight lead to tensor pentagon integrals. We write the five-point amplitude as

$$B_1^{sX} = \sum_i \sum_{r=0}^{3} c^X_{5,i,r}(\varepsilon)\, I_{5,i}[k^{\mu_1} \cdots k^{\mu_r}] + \sum_i \sum_{r=0}^{2} c^X_{4,i,r}(\varepsilon)\, I_{4,i}[k^{\mu_1} \cdots k^{\mu_r}]\,, \tag{14.7}$$

where we split the contribution of the tensor box integrals and of the tensor pentagon integrals. In Eq. (14.7), the integrals are defined as

$$I_{n,i}[k^{\mu_1} \cdots k^{\mu_r}] = \int \frac{\mathrm{d}^d k}{(2\pi)^d} \frac{\prod_{j=1}^{r} k^{\mu_j}}{\prod_{l=1}^{n} D_{i,l}}\,, \tag{14.8}$$

where i stands for the topology, $D_{i,l} = (k - q_{i,l})^2 - m^2_{i,l}$, and $q_{i,l} = \sum_{a=1}^{l} p_a$ with p_a being the external momenta. The masses $m_{i,l}$ are either zero, m_t, or m_W.

To reduce the tensor pentagon integrals, it is convenient to work with the van Neerven-Vermaseren (vNV) basis [152]. A short overview of this concept can be found in Ref. [153]. The vNV basis $\{v_i^\mu\}$, whose construction is based on the Schouten identity, are defined such that $v_i \cdot p_j = \delta_{ij}$, where p_i are the external momenta. In four dimensions, the basis vectors read

$$v_i^\mu = \frac{\delta^{p_1 \dots \mu \dots p_4}_{p_1\, p_2\, p_3\, p_4}}{\Delta(p_1 \dots p_4)}\,, \tag{14.9}$$

where

$$\Delta(p_1 \dots p_4) = \delta^{p_1 \dots p_4}_{p_1 \dots p_4} \equiv \det|\delta^\mu_\nu| \prod_{i,j=1}^{4} p_{i\mu} p_j^\nu\,, \tag{14.10}$$

---

[2] This is the expected number for a five-point amplitude with four helicity configurations [151].

is the Gram determinant. In the definition of the vector v_i^μ in Eq. (14.9), the Lorentz index μ is at the i^{th} place in the upper indices. Note that in both Eq. (14.9) and Eq. (14.10), we simplify notations by replacing an index of a tensor which is contracted with an external momenta by the momenta itself.

The vectors of the vNV basis can be used to rewrite the loop momentum in the tensor loop integrals defined in Eq. (14.8). The most difficult tensor integrals that we need to reduce are rank 3, pentagon integrals. These integrals are free of rational terms and, therefore, it is sufficient to consider the contribution from the physical space of the loop momentum [153, 154]. Since the physical space is four-dimensional, we can use the basis defined in Eq. (14.9). The loop momentum in this basis reads

$$k^\mu = \sum_{i=1}^{4} (k \cdot q_i)\, v_i^\mu \,, \tag{14.11}$$

In this basis, the loop momentum is expressed with the propagators of the tensor integral $I_{5,i}$ in Eq. (14.8). It reads

$$\begin{aligned} k^\mu = &\frac{1}{2}(D_{5,1} - D_{5,5})v_1^\mu + \frac{1}{2}(D_{5,2} - D_{5,1})v_2^\mu + \frac{1}{2}(D_{5,3} - D_{5,2})v_3^\mu \\ &+ \frac{1}{2}(D_{5,4} - D_{5,3})v_4^\mu + \mathcal{V}^\mu \,, \end{aligned} \tag{14.12}$$

where $\mathcal{V}^\mu$ depends on the seven scales of this calculation. When one of the loop momentum in the numerator of the rank r, tensor integral $I_{5,i}$ is expressed in the vNV basis, the first four terms in Eq. (14.12) leads to rank $r-1$, box integrals, on which we can use the standard Passarino-Veltman reduction [80]. The last term in Eq. (14.12) leads to a rank $r-1$, pentagon integrals, on which we repeat the procedure.

At this point, we are left with only scalar pentagon, box, triangle and bubble integrals. Scalar pentagon integrals can be expressed as a sum of scalar box integrals in four dimensions [155]. The one-loop five-point amplitude defined in Eq. (14.7) becomes

$$B_1^{sX} = \sum_i \hat{c}_{4,i}^X(\varepsilon)\, I_{4,i} + \sum_i \hat{c}_{3,i}^X(\varepsilon)\, I_{3,i} + \sum_i \hat{c}_{2,i}^X(\varepsilon)\, I_{2,i} + \mathcal{O}(\varepsilon)\,. \tag{14.13}$$

We find a minimal set of 109 master integrals.

We would like to chose a convenient basis of master integrals that simplifies the one-loop five-point amplitude. We know from Chapter 11 that non-factorisable contributions are free of collinear singularities and, therefore, display a mild degree of divergence, starting at $1/\varepsilon^2$. Thus, we know that the degree of divergence of the one-loop five-point amplitude is at most $1/\varepsilon$, since another pole $1/\varepsilon$ will be provided by the integration over the emitted-gluon phase space. We would like to make this property explicit by choosing a basis of finite box integrals. We follow the reasoning of Ref. [156]. As an example, we consider the following scalar box integral

$$I_{4,1} = \int \frac{\mathrm{d}^d k}{(2\pi)^d} \frac{1}{k^2 (k-p_1)^2 (k-p_1-p_2)^2 (k-p_1-p_2+p_5)^2} \,. \tag{14.14}$$

This integral is IR divergent if the loop momentum becomes soft, $k \to 0$, or if, for instance, the loop momentum k is collinear to p_1. We introduce a numerator to make $I_{4,1}$ finite and define

$$F_{4,1} = \int \frac{\mathrm{d}^d k}{(2\pi)^d} \frac{\mathrm{Tr}\left((-\not{p}_1)(\not{k}-\not{p}_1)(\not{k}-\not{p}_1-\not{p}_2)(\not{p}_5)\right)}{k^2 (k-p_1)^2 (k-p_1-p_2)^2 (k-p_1-p_2+p_5)^2} = \mathcal{O}(\varepsilon^0) \,. \tag{14.15}$$

The trace that we introduced in Eq. (14.15) can be computed. We find

$$\begin{aligned} \mathrm{Tr}\big((-\not{p}_1)(\not{k}-\not{p}_1)(\not{k}-\not{p}_1-\not{p}_2)(\not{p}_5)\big) = {} & -s_{12}\left(s_{12}+s_{15}-s_{34}\right) \\ & + \left(s_{12}+s_{15}-s_{34}\right) k^2 - \left(s_{12}-s_{34}\right)\left(k-p_1\right)^2 \\ & + \left(s_{12}+s_{15}\right)\left(k-p_1-p_2\right)^2 - s_{12}\left(k-p_1-p_2+p_5\right)^2 \,, \end{aligned} \tag{14.16}$$

where we recognise the different propagators of the scalar box integral $I_{4,1}$. As the result, the finite box integral $F_{4,1}$ is expressed as a linear combination of triangle scalar integrals and the initial box integral $I_{4,1}$.

We apply this procedure to all divergent box integrals such that B_1^{sX} becomes

$$B_1^{sX} = \sum_i \bar{c}^X_{4,i}\, F_{4,i} + \sum_i \bar{c}^X_{3,i}\, I_{3,i} + \sum_i \hat{c}^X_{2,i}(\varepsilon)\, I_{2,i} + \mathcal{O}(\varepsilon) \,. \tag{14.17}$$

Since the scalar box integrals $F_{4,i}$ are finite, we are able to set $\varepsilon \to 0$ in the coefficients $\bar{c}^X_{4,i}$. This reduces drastically their complexity. In addition, we observe that the coefficients $\bar{c}^X_{3,i}$ become ε-independent. We emphasise that the poles of the amplitude are only provided by the triangle integrals. Indeed, since non-factorisable amplitudes are free of UV divergences at NNLO, the sum over the bubble integrals is finite.

The change of basis that we have just described makes the amplitudes B_1^{sL} and B_1^{sH} more concise. Nevertheless, we need to go further to ensure the numerical stability of the amplitudes in the whole phase-space, especially the region where the emitted gluon is soft. In addition to the two masses, there is five scales that need to be chosen. To avoid large cancellations during the numerical evaluation, we choose the following variables

$$s_{12}, \quad s_{23}, \quad \delta_1 = s_{34} - s_{12}, \quad \delta_2 = s_{45} - m_t^2, \quad \delta_3 = s_{15} \,. \tag{14.18}$$

These variables are convenient since, in the limit where the gluon goes soft, the variables δ_1, δ_2, and δ_3 vanish.

Similar to the tree-level amplitudes, the one-loop amplitudes B_1^{sL} and B_1^{sH} can be numerically evaluated within the helicity spinor formalism. The one-loop scalar integrals are evaluated using `QCDLoop` [157, 158].

This ends the computation of the real-emission amplitudes. Once combined with the double-virtual corrections computed in Chapter 13, we have the complete non-factorisable corrections to t-channel single top production. In the next chapter, we present numerical results that are relevant for the LHC and the Future Circular Collider (FCC).

15 RESULTS

We consider proton-proton collisions at 13 TeV. The t-channel single top production cross section is written as

$$\mathrm{d}\sigma_{pp\to X+t} = \sum_{i,j} \int \mathrm{d}x_1\, \mathrm{d}x_2\, f_i(x_1, \mu_F)\, f_j(x_2, \mu_F)\, \mathrm{d}\hat{\sigma}_{ij\to X+t}\left(x_1, x_2, \mu_R\right) , \tag{15.1}$$

where i and j stand for the parton types. We set the CKM matrix to be the identity matrix. As the result, only $j(i) = b$ and $i(j) = u, c, \bar{d}, \bar{s}$ contribute. The vacuum expectation value of the Higgs field is set to $v = 246.2$ GeV. The masses of the process evaluate to $m_t = 173.0$ GeV and $m_W = 80.379$ GeV. We use the `CT14_lo` PDFs for the LO cross section and `CT14_nnlo` PDFs [159] for the non-factorisable corrections and we set the factorisation scale to $\mu_F = m_t$. The running of the strong coupling constant is performed by a routine from `NNPDF` [96, 159]. It gives, for example, $\alpha_s(m_t) = 0.108$. We find that the t-channel single top production cross section evaluates to

$$\boxed{\frac{\sigma_{pp\to X+t}}{1\ \text{pb}} = 117.96 + 0.26 \left(\frac{\alpha_s(\mu_R)}{0.108}\right)^2 ,} \tag{15.2}$$

where the first term corresponds to the LO cross-section and the second to the non-factorisable contributions. However, in writing Eq. (15.2), we have emphasised that there is no clear choice for the renormalisation scale of the non-factorisable contribution.[1] Indeed, since these kind of corrections first occur at NNLO, we do not have any indication from lower orders. The proximity of the quark scattering occuring in the t-channel to the deep-inelastic scattering (DIS) could indicate that the renormalisation scale should be close to the typical transverse momentum value of the process, which corresponds to $\mu_R = 40$ GeV. For this choice of scale, the non-factorisable corrections are enhanced and reach $\mathcal{O}(0.35\%)$.

We find that the real-emission contribution reduces the double-virtual contribution by $\mathcal{O}(24\%)$. As we argued in Eq. (13.40), the virtual contribution is indeed dominant in the non-factorisable corrections. As expected, the suppression is also milder than it would be for a massless top quark. [2]

---

[1] The renormalisation scale only appears in the running of the strong coupling constant, since non-factorisable contribution is free of UV divergences at NNLO QCD.

		$\mu_R = m_t$		$\mu_R = 40$ GeV	
$p_\perp^{t,\text{cut}}$	σ_{LO} (pb)	$\sigma^{\text{nf}}_{\text{NNLO}}$ (pb)	δ_{NNLO} [%]	$\sigma^{\text{nf}}_{\text{NNLO}}$ (pb)	δ_{NNLO} [%]
0 GeV	118.01	$0.26^{-0.04}_{+0.06}$	$0.22^{-0.04}_{+0.05}$	0.40	0.34
20 GeV	115.09	$0.26^{-0.04}_{+0.06}$	$0.23^{-0.04}_{+0.05}$	0.41	0.36
40 GeV	109.56	$0.27^{-0.05}_{+0.06}$	$0.25^{-0.04}_{+0.06}$	0.43	0.39
60 GeV	104.63	$0.28^{-0.05}_{+0.06}$	$0.26^{-0.04}_{+0.06}$	0.43	0.41

Table 15.1: Dependence of the non-factorisable corrections on a cut on the transverse momentum of the top quark for 13 TeV proton-proton collisions. The factorisation scale is set to $\mu_F = m_t$. Each row corresponds to a value of the cut given in the first column. In the second column, we report the LO cross section. In the third and fifth columns, we present the non-factorisable contributions in picobarn at $\mu_R = m_t$ and $\mu_R = 40$ GeV, respectively. We refer the reader to the main text for further information.

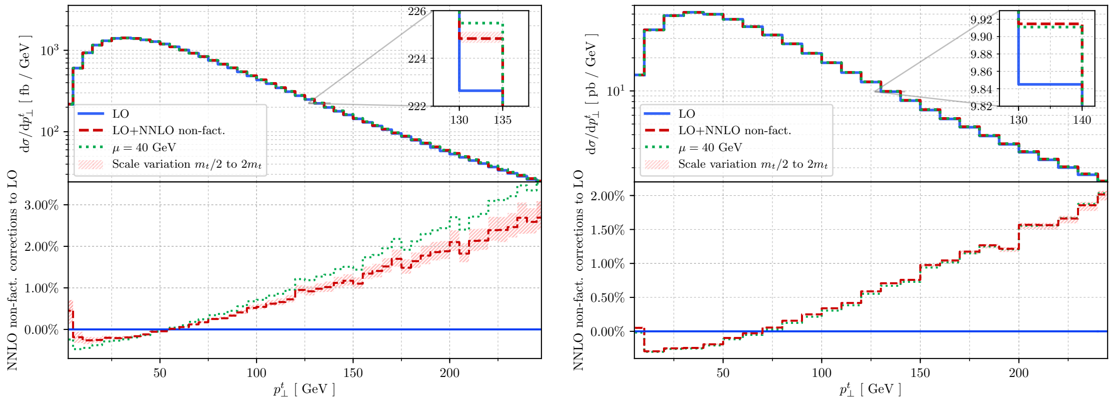

(a) 13 TeV

(b) 100 TeV

Figure 15.1: Distribution of the top-quark transverse momentum. We report the LO distribution evaluated at $\mu_F = m_t$ with a blue solid line. Non-factorisable corrections are plotted with a red dashed line for $\mu = m_t$ and the scale variation is indicated by the lighter red bands. In green dotted line, we show the corrections at $\mu = 40$ GeV.

In Table 15.1, we plot the dependence of the non-factorisable corrections on a cut on the transverse momentum of the top quark. Each row of the Table 15.1 corresponds to a value of the cut. The third and fourth columns correspond to the non-factorisable corrections

---

[2] Indeed, we argued that, for $m_t = 0$, the real-emission contributions are suppressed by a factor $\mathcal{O}(p^2_{t,\text{top}}/s)$. The typical partonic energy is about $\sqrt{s} = 300$ GeV. The suppression for $m_t = 0$ would be $p^2_{t,\text{top}}/s \approx 2\%$.

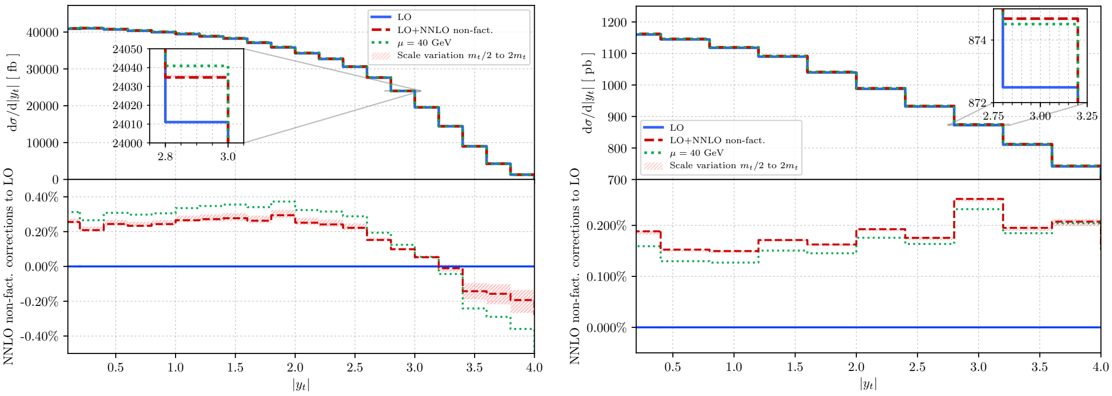

(a) 13 TeV (b) 100 TeV

Figure 15.2: Distribution of the top-quark rapidity. We report the LO distribution evaluated at $\mu_f = m_t$ with a blue solid line. Non-factorisable corrections are plotted with a red dashed line for $\mu = m_t$ and the scale variation is indicated by the lighter red bands. In green dotted line, we show the corrections at $\mu = 40$ GeV.

at $\mu_R = m_t$ with, to the right of the central value, the corrections using $\mu_R = 2m_t$ and $\mu_R = m_t/2$, respectively. In the third column, we show the non-factorisable contribution in picobarns and, in the fourth column, we give the corrections relative to the Born cross section in percent. The last two columns show the same quantities for $\mu_R = 40$ GeV.

		$\mu_R = m_t$		$\mu_R = 40\,\text{GeV}$	
$p_\perp^{t,\text{cut}}$	σ_{LO} (pb)	$\sigma^{\text{nf}}_{\text{NNLO}}$ (pb)	δ_{NNLO} [%]	$\sigma^{\text{nf}}_{\text{NNLO}}$ (pb)	δ_{NNLO} [%]
0 GeV	2367.02	$3.79^{-0.63}_{0.84}$	$0.16^{-0.03}_{0.04}$	5.95	0.25
20 GeV	2317.03	$3.89^{-0.64}_{0.86}$	$0.17^{-0.03}_{0.04}$	6.11	0.26
40 GeV	2216.61	$4.14^{-0.69}_{0.92}$	$0.19^{-0.03}_{0.04}$	6.50	0.29
60 GeV	2121.88	$4.28^{-0.71}_{0.95}$	$0.20^{-0.03}_{0.04}$	6.71	0.32

Table 15.2: Dependence of the non-factorisable corrections on a cut on the transverse momentum of the top quark for 100 TeV proton-proton collisions. The factorisation scale is set to $\mu_F = m_t$. Each lines corresponds to a value of the cut, given in the first column. The second column reports the LO cross section. In the third and fifth columns, we present non-factorisable contributions in picobarn at $\mu_R = m_t$ and $\mu_R = 40$ GeV, respectively. We refer the reader to the main text for additional informations.

We observe that, from $p_\perp^{t,cut} = 0$ to $p_\perp^{t,cut} = 60$ GeV, the LO cross section decreases by $\mathcal{O}(11\%)$, while the non-factorisable corrections increase by $\mathcal{O}(8\%)$. These values can be compared with the factorisable corrections given in Table 7 of Ref. [6] for a similar

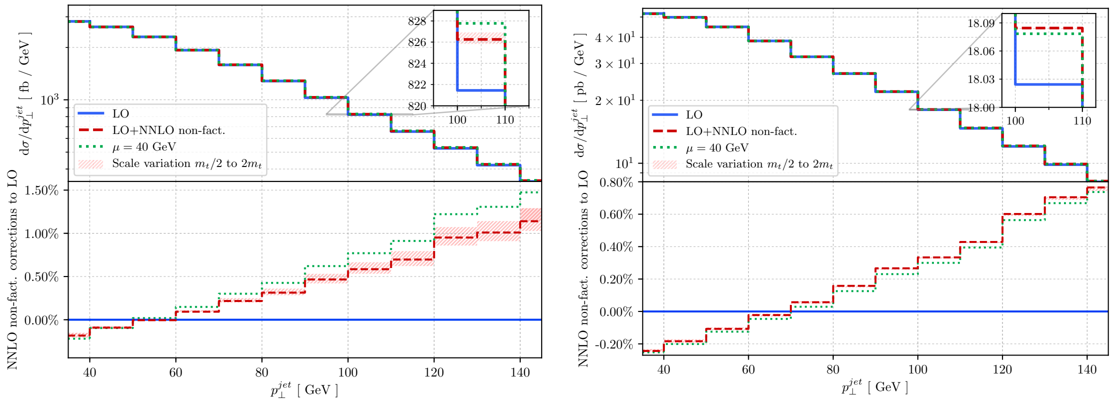

(a) 13 TeV

(b) 100 TeV

Figure 15.3: Distribution of the leading-jet transverse momentum. We report the LO distribution evaluated at $\mu_F = m_t$ with a blue solid line. Non-factorisable corrections are plotted with a red dashed line for $\mu = m_t$ and the scale variation is indicated by the lighter red bands. In green dotted line, we show the corrections at $\mu = 40$ GeV.

choice of PDFs and scales.[3] We note that NNLO factorisable corrections decrease the NLO cross section by a factor $\mathcal{O}(0.7\%)$. As a consequence, the non-factorisable corrections, although smaller, are quite comparable to the factorisable corrections. At most, the non-factorisable corrections reach $\mathcal{O}(0.4\%)$ for $p_\perp^{t,cut} = 60$ GeV and $\mu_R = 40$ GeV.

For the computation of the observable distributions, we set $\mu = \mu_F = \mu_R = m_t$ and vary this value by a factor two. We emphasise again that this choice is not thought to be optimal, but it allows a comparison with studies of the factorisable corrections found in the literature. For this reason, we also include results for $\mu = 40$ GeV.

In Fig. 15.1, we show the distribution of the transverse momentum of the top quark. From $p_\perp^t = 0$ to $p_\perp^t = 50$ GeV, the corrections are small and negative.[4]. Then, the corrections increase linearly, reaching $\mathcal{O}(2\%)$ at 200 GeV. We note that the factorisable corrections to the same distribution, shown in Fig. 11 from Ref. [6], have a similar shape, but are larger by a factor $3 - 10$. We also note that the factorisable corrections vanish around 30 GeV, while the non-factorisable ones vanish around 50 GeV. This means that the non-factorisable corrections are, in fact, dominant in a region close to the peak of the distribution.

---

[3] We note that the collider energy is fixed to 14 GeV in Ref. [6], but this difference does not invalidate the comparison.

[4] We note that we observe the same behaviour for the double-virtual contribution.

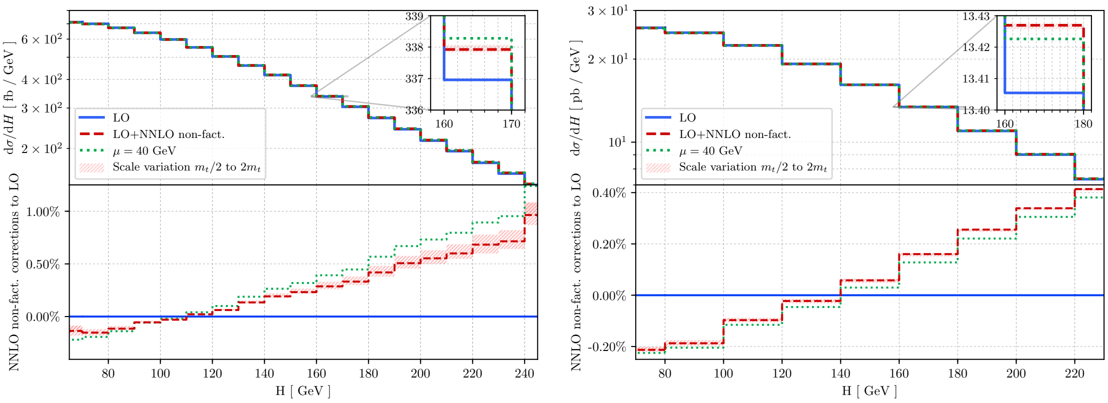

(a) 13 TeV

(b) 100 TeV

Figure 15.4: Distribution of the sum of transverse momenta H. We report the LO distribution evaluated at $\mu_F = m_t$ with a blue solid line. Non-factorisable corrections are plotted with a red dashed line for $\mu = m_t$ and the scale variation is indicated by the lighter red bands. In green dotted line, we show the corrections at $\mu = 40$ GeV.

The distribution of the top-quark rapidity is shown in Fig. 15.2a. The non-factorisable corrections are almost constant for $|y_t| \leq 2.5$, changing the LO distribution by $\mathcal{O}(0.25\%)$. They then rapidly decrease and change sign at $|y_t| = 3$. It is interesting to note that factorisable corrections to the top-quark rapidity vanish around $|y_t| \sim 1.2$. Again, one concludes that non-factorisable corrections are dominant in some parts of the phase space.

We will now consider observables related to jets. We use the k_T-algorithm [160] with $p_\perp^{\text{jet}} > 30$ GeV and $\Delta R = 0.4$. We also define the following quantity

$$H = p_\perp^t + \sum_{i=1}^{n_{jet}} p_\perp^{jet,i}, \tag{15.3}$$

where n_{jet} stands for the number of jets in the event.

The distribution of the leading-jet transverse momentum is shown in Fig. 15.3a. The non-factorisable corrections are negative up to $p_\perp^{\text{jet}} = 50$ GeV where they vanish. The corrections reach $\mathcal{O}(1.2\%)$ at $p_\perp^{\text{jet}} = 140$ GeV. The corrections to the sum of the transverse momenta H, defined in Eq. (15.3), present a similar behaviour. In Fig. 15.5a, we see that the corrections to the leading jet rapidity are constant up to $|y_{\text{jet}}| = 2$, and change sign at $|y_{\text{jet}}| = 3.5$.

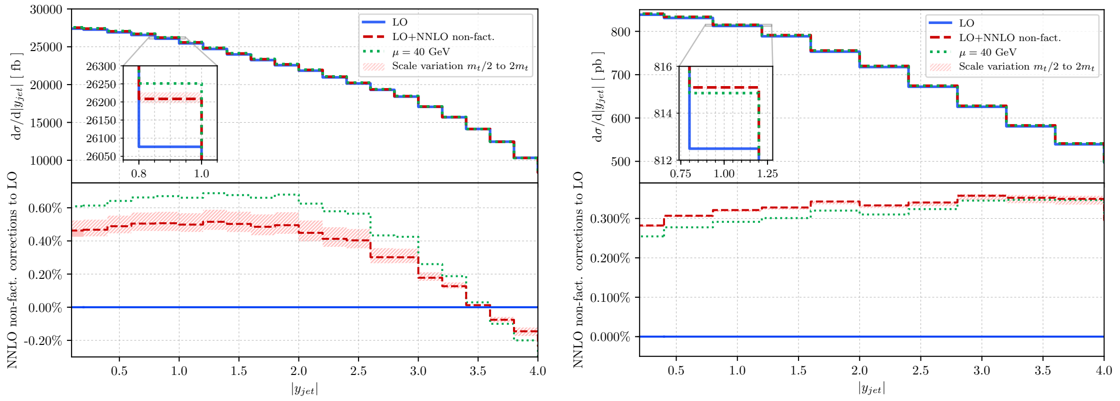

(a) 13 TeV

(b) 100 TeV

Figure 15.5: Distribution of the leading-jet rapidity. We report the LO distribution evaluated at $\mu_F = m_t$ with a blue solid line. The non-factorisable corrections are plotted with a red dashed line for $\mu = m_t$ and the scale variation is indicated by the lighter red bands. In green dotted line, we show the distribution at $\mu = 40$ GeV.

The same results have been computed for the Future Circular Collider (FCC) [8, 9], where protons will collide with a centre-of-mass energy of 100 TeV. We keep the same setting as before, and find

$$\boxed{\frac{\sigma_{pp\to X+t}}{1\text{ pb}} = 2367.0 + 3.8\left(\frac{\alpha_s(\mu_R)}{0.108}\right)^2.} \tag{15.4}$$

At the FCC, the non-factorisable corrections amount to $\mathcal{O}(0.16\%)$ of the LO cross section, for $\mu_R = m_t$. These corrections increase to $\mathcal{O}(0.25\%)$ for $\mu_R = 40$ GeV. In Table 15.2, which is the counterpart of Table 15.1, we show the dependence of the non-factorisable corrections to the value of the cut imposed on the transverse momentum of the top quark. We observe the same behaviour as in Table 15.1, but amplified, since the LO cross section decrease by $\mathcal{O}(10\%)$ when we impose $p_\perp^{t,cut} = 60$ GeV, whereas the non-factorisable corrections grow by $\mathcal{O}(25\%)$. The corrections stay larger for $\mu_R = 40$ GeV, and reach $\mathcal{O}(0.3\%)$ for moderate $p_\perp^{t,cut}$ values. It would be desirable to compare these values with the factorisable corrections, as it is difficult to predict the effect of such an increase of the centre-of-mass collision energy on them.

For each distribution presented earlier, we provide its 100 TeV counterpart. In Fig. 15.1b, we see that the non-factorisable corrections to the top-quark transverse momentum display as similar behaviour to the one observed in Fig. 15.1a. The corrections are shifted as they vanish around $p_\perp^t = 70$ GeV. The same observation is made for the distribution of the transverse momentum of the leading jet and to the sum of the transverse momenta

H. Indeed, both of them are shifted as they vanish at $p_\perp^{\text{jet}} = 70$ GeV and $p_\perp^{\text{top}} = 140$ GeV, respectively. The corrections to the rapidity of the top quark, in Fig. 15.2b, and to the rapidity of the leading jet, in Fig. 15.5b, are almost flat over the whole range of rapidity displayed, which goes up to $y_{\text{top,jet}} = 4$. These corrections amount to 0.2% and 0.35%, respectively.

We observe some common features at 100 GeV. First, the corrections depend less on the choice of renormalisation scale, since the lighter red band is nearly undistinguishable and the $\mu = 40$ GeV distribution is close to the $\mu = m_t$ one. In addition, distributions related to transverse momenta present interesting features. At the tail of the distributions, the 100 GeV corrections are systematically smaller than at 13 GeV. On the other hand, in small transverse momentum region, the corrections have the same relative importance. This could be explained by the fact that the real-emission corrections are suppressed when the collision energy is increased, whereas the leading terms of the virtual contribution stay unaffected.

16 CONCLUSION

We have calculated the non-factorisable corrections to t-channel single top production at the LHC and the FCC [8, 9]. This contribution, which first appears at NNLO, has been neglected in previous studies because it is colour-suppressed compared to the factorisable corrections. Nevertheless, it appears that the factorisable corrections to t-channel single top production are relatively small. Therefore, non-factorisable corrections could be comparable.

In Chapter 11, we made explicit the absence of non-Abelian interactions in non-factorisable corrections and demonstrated the IR pole cancellation using the nested soft-collinear subtraction scheme [65]. The pole structure shows a mild degree of divergence, as the non-factorisable contribution does not exhibit collinear singularities. In Chapter 12, we calculated the subtraction term related to soft-gluon emissions. It turns out that the integrated soft function can be written in a relatively compact form. In Chapter 13, we focused on the double-virtual contribution. We used a standard approach to calculate the two-loop amplitude [123, 128, 129]. We projected the amplitude onto a minimal set of tensor structures to define form factors, which are reduced to master integrals via an analytic reduction. We then used the auxiliary mass flow method [126, 127] to evaluate the master integrals over the phase space. We have shown that this approach is sufficiently reliable to give results relevant for phenomenology. Then, in Chapter 14, we explained how the double-real and real-virtual contributions were determined. The calculation turned out to be non-trivial due to the presence of several scales and high-rank tensor integrals. We also explained how we ensured the numerical stability of the amplitudes, especially in the limit where emitted gluons are soft. Finally, we presented numerical results relevant for the LHC and the FCC.

We find that non-factorisable corrections amount to $\mathcal{O}(0.4\%)$ of the inclusive cross-section and can reach $\mathcal{O}(2)$ percents for some distributions at the LHC. We conclude that the non-factorisable corrections are certainly small, but in fact quite comparable to the factorisable corrections. The importance of the virtual effects in the non-factorisable corrections has been emphasised. In addition, we observed that such effects are not suppressed when the collision energy is increased. It would be desirable to compare the magnitude of the non-factorisable corrections with the factorisable ones at the FCC.

Part III

NON-FACTORISABLE DOUBLE-VIRTUAL CONTRIBUTION TO HIGGS PRODUCTION IN WBF – BEYOND THE EIKONAL APPROXIMATION

The non-factorisable, double-virtual contribution to Higgs boson production in weak boson fusion (WBF) at LHC has been computed in the eikonal approximation in Ref. [7]. We extend this calculation to the next-to-leading order in the forward limit of the tagging jets. It turns out these contributions are sizeable as they decrease earlier estimates of the non-factorisable corrections by $\mathcal{O}(20\%)$.

This part of the thesis is based on Ref. [161]

17 INTRODUCTION

Studying the production of the Higgs boson at the LHC is essential for gaining a better understanding of the properties of the only scalar particle predicted by the SM. Given the large number of events involving the Higgs boson that will be observed during the HL-LHC [2], we can expect significant improvements in the accuracy of our current measurements. However, in order to take full advantage of these experimental advances, theoretical predictions also need to be refined. Fortunately, recent years have seen major developments related to the Higgs sector [162], with the aim of potentially uncovering physics beyond the Standard Model (BSM).

The WBF is one of the major Higgs production channels at the LHC. It has been studied by ATLAS [163, 164] and CMS [165, 166] collaborations. The measured cross section agrees with the SM prediction with 20% accuracy, as shown in the second line of Fig. 17.1.

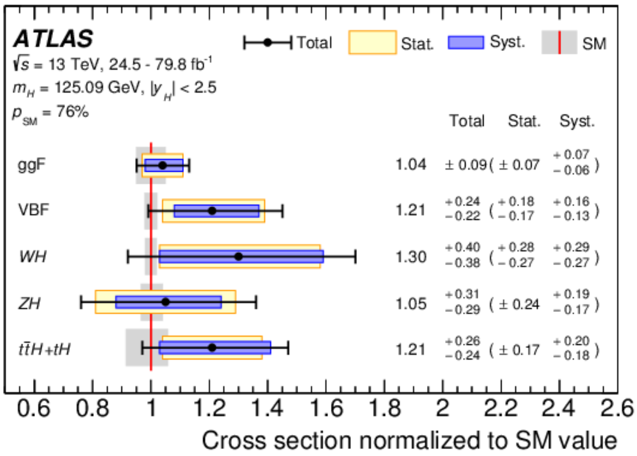

Figure 17.1: Cross sections of the main Higgs production channels at the LHC. The Higgs boson production channels are sorted by importance; the gluon fusion, shown on the first line, is the dominant one. The grey bands indicate the theoretical uncertainties, whereas the black intervals stand for the total experimental ones. Figure from Ref. [164].

Corrections to Higgs boson production in WBF are understood to an advanced level. Fully differential cross sections are known including NLO QCD [167, 168], NNLO QCD [32, 33], and mixed EW-QCD corrections [169]. The total cross section is known up to N^{3}LO QCD corrections [34]. However, all these studies have been carried out in the so called structure function approximation [170], where non-factorisable corrections are neglected.

As discussed in Part II, non-factorisable corrections first appear at NNLO QCD. They are gauge invariant by themselves and colour-suppressed compared to their factorisable counterpart. Nevertheless, it has been demonstrated by studying the double-virtual contribution to Higgs boson production in WBF in the eikonal approximation [7] that, for this process, these corrections are enhanced by a factor π^2, originating from the exchange of Glauber gluons. The authors of this paper show that the double-virtual contribution changes the Born cross-section by $\mathcal{O}(1\%)$[1].

The double-virtual contributions is known to be dominant in non-factorisable corrections, see Eq. (13.40). It is therefore essential to get a better understanding of this contribution. However, the exact evaluation of the five-point, two-loop amplitude is currently impossible. We cannot apply the technique that we used in the case of t-channel single top production in Part II because i) the reduction of the two-loop amplitude to master integrals is difficult, ii) the number of master integrals would be substantially larger, and iii) we would need to evaluate the master integrals for a considerable amount of phase-space points. We take a different approach and follow Ref. [7] by working around the forward limit of the tagging jets.

In this part of the thesis, we want to go beyond the eikonal approximation by including next-to-leading order terms in the eikonal expansion. First, we investigate how to extend the calculation done in Ref. [7] by working on t-channel massless single top production, whose physics is close to the WBF one. We derive the sub-eikonal contributions from the exact amplitude and present two techniques for approximating the loop integrals to reproduce this result. Finally, we compute the double-virtual contribution to the Higgs production in WBF including next-to-leading terms in the eikonal approximation using the expansion by regions [172–174].

---

[1] Later, the results of this paper were extended to the double-Higgs production [171].

18 MASSLESS SINGLE TOP PRODUCTION – A TOY MODEL

In this chapter, we explore the physics of t-channel massless single top production, which closely relates to Higgs production in weak boson fusion (WBF). More precisely, we investigate how to compute the non-factorisable, double-virtual corrections in the forward limit, where the transverse momentum of the process is much smaller than the collision energy in the partonic centre-of-mass frame. We focus on the one-loop amplitude, with the intention of extending the calculation to the two-loop amplitude in a subsequent stage.

We start our analysis by computing the leading and the next-to-leading contributions from the exact one-loop amplitude. Then, we consider different methods to calculate the one-loop amplitude in the forward limit. The eikonal term is readily obtained by following the approach of Ref. [7], but computing the next-to-eikonal terms is more challenging. We will consider two approaches. The first one involves resolving differential equations, while the second one is based on the expansion by regions technique [172–175].

18.1 ONE-LOOP AMPLITUDE IN THE FORWARD LIMIT

We consider t-channel massless single top production

$$u(p_1) + b(p_2) \to d(p_3) + t(p_4)\,, \tag{18.1}$$

where, to be closer to the physics of Higgs boson production in WBF, we consider all external partons to be massless, $p_i^2 = 0$, $i = 1 \ldots 4$. We consider the non-factorisable correction to the one-loop amplitude.[1] Two of the four contributing diagrams are shown in Fig. 18.1. The other two diagrams are obtained by the crossing-symmetry $p_1 \leftrightarrow -p_3$.

For the rest of this chapter, we consider that the partons with momenta p_1 and p_2 are incoming, whereas the ones with momenta p_3 and p_4 are outgoing. The Mandelstam variables read

$$s = (p_1 + p_2)^2\,, \quad t = (p_1 - p_3)^2\,, \quad u = (p_2 - p_3)^2\,, \tag{18.2}$$

such that $s + t + u = 0$.

---

[1] The non-factorisable, one-loop amplitude starts contributing at NNLO QCD, see Chapter 11.

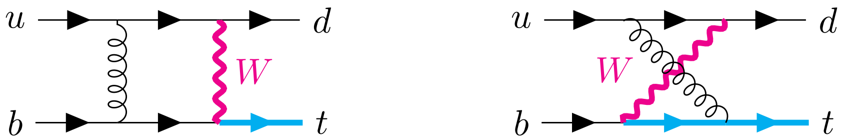

(a) Planar

(b) Crossed

Figure 18.1: Example of planar (left) and crossed (right) diagrams contributing to the one-loop amplitude for the process described in Eq. (18.1).

The determination of the one-loop amplitude for the process described in Eq. (18.1) is straightforward. We generate the diagrams using `QGRAF` [79] and perform the Dirac algebra with `FORM` [73, 76]. We use spinor helicity formalism since only left-handed partons contribute to the process. The different spinor structures can be simplified to the Born one. To reduce the one-loop tensor integrals to scalar integrals, we use Passarino-Veltman reduction [80]. Then, we use `PackageX` [81] to express every scalar tadpole, bubble, triangle and box integrals in terms of logarithmic and dilogarithmic functions.

We focus on the forward limiit of the tagging jets where they are only slightly scattering. In this configuration, we can assume that

$$s \gg t \sim m_W^2 \,. \tag{18.3}$$

We write the one-loop, non-factorisable amplitude as

$$M^{(1)} = t^A_{i_3 i_1} t^A_{i_4 i_2} \mathcal{A}^{(1)} \,, \tag{18.4}$$

and expand the colour-stripped one-loop amplitude $\mathcal{A}^{(1)}$ including next-to-leading terms in the eikonal expansion. We find

$$\begin{aligned}\mathcal{A}^{(1)} = & \frac{\alpha_s(\mu)}{\pi}\Bigg\{ -\frac{1}{\varepsilon}\left(i\pi + \frac{t}{s}\right) + i\pi\ln\left(\frac{(t-m_W^2)^2}{\mu^2 m_W^2}\right) - i\pi\frac{m_W^2}{s} \\ & + \frac{m_W^2 - t}{s}\left[\frac{2\pi^2}{3} + \ln^2\left(\frac{s}{m_W^2-t}\right) + 2\mathrm{Li}_2\left(\frac{t}{m_W^2-t}\right)\right] \\ & + \frac{2m_W^2}{s} + \frac{t}{s}\ln\left(\frac{s}{\mu^2}\right) + \frac{m_W^2}{s}\ln\left(\frac{s}{m_W^2}\right) \\ & \qquad + \frac{t^2 + 2t\,m_W^2 - m_W^4}{s\,t}\ln\left(1 - \frac{t}{m_W^2}\right) + \mathcal{O}\left(\frac{t^2}{s^2}\right)\Bigg\}\mathcal{A}^{(0)} \,,\end{aligned} \tag{18.5}$$

where the strong coupling has been renormalised in the $\overline{\text{MS}}$ scheme. In Eq. (18.5), we have defined the colour-stripped Born amplitude as

$$\mathcal{A}^{(0)} = -g_W^2 \frac{1}{2}\frac{[12]\langle 34\rangle}{t - m_W^2} \,, \tag{18.6}$$

where $g_W = e/\cos\theta_W$ is the weak coupling constant and $\cos\theta_W = 0.876\ldots$. We note that the pole in ε in Eq. (18.5) corresponds to what we expect from the Catani's operator [66, 84]. Indeed, from Eq. (13.9), we find

$$\mathcal{A}^{(1)} = \frac{\alpha_s(\mu)}{\pi}\frac{1}{\varepsilon}\left(i\pi + \frac{t}{s} + \mathcal{O}\left(\frac{t^2}{s^2}\right)\right)\mathcal{A}^{(0)} + \mathcal{O}\left(\varepsilon^0\right) . \tag{18.7}$$

The finite part of $\mathcal{A}^{(1)}$ in Eq. (18.5) presents interesting features. First, the leading-order term consists of a single logarithm. We observe that, as for the case of Higgs boson production in WBF [7], the one-loop amplitude is purely imaginary in the eikonal approximation. Then, the other terms in Eq. (18.5) correspond to the next-to-leading order in the eikonal approximation, suppressed by a factor $t/s \sim m_W/s$. With the exception of one term, all of them are purely real. Since the one-loop amplitude contributes once squared, such real terms start contributing only at order $\mathcal{O}\left(p_t^4/s^2\right)$, which is strongly suppressed.[2]

Eventually, we want to determine the sub-eikonal contribution to Higgs boson production in WBF. To mimic the two weak boson propagators, characteristic of this process, we consider the amplitude of the massless t-channel single top production with a dot on the W boson propagator. This is close to a configuration where both weak bosons have a small transverse momentum and where the Higgs boson is not very energetic. The one-loop amplitude is easily obtained by deriving $\mathcal{A}^{(1)}$ with respect to m_W^2. We find

$$\begin{aligned}\dot{\mathcal{A}}^{(1)} =& \frac{\tilde{\alpha}_s(\mu)}{\pi}\Bigg[-\frac{1}{\varepsilon}\left(i\pi + \frac{t}{s}\right) + i\pi\left(\ln\left(\frac{(t-m_W^2)^2}{\mu^2 m_W^2}\right) - \left(1 + \frac{t}{m_W^2}\right)\right) \\ &+ \frac{2m_W^2}{s} - \frac{t}{s}\left(1 + i\pi + \frac{t}{m_W^2} + \ln\left(\frac{\mu^2}{m_W^2}\right)\right) + 2\frac{m_W^2}{s}\ln\left(\frac{s}{m_W^2}\right) \\ &+ \frac{m_W^4 - 2m_W^2\, t + 3t^2}{s\,t}\ln\left(1 - \frac{t}{m_W^2}\right) + \mathcal{O}\left(\frac{t^2}{s^2}\right)\Bigg]\dot{\mathcal{A}}^{(0)} ,\end{aligned} \tag{18.8}$$

where $\dot{\mathcal{A}}^{(0)}$ is the Born amplitude in Eq. (18.6) with a dot on the W boson propagator.

Both results in Eqs. (18.5)-(18.8) are compact. It is clear that Higgs boson production in WBF has a larger number of scales and, thus, we expect a more consequent expression. It would be desirable to develop methods to derive such results by directly expanding loop amplitudes in the forward limit. First, we will reproduce the idea from Ref. [7] and calculate the eikonal contribution by combining the four diagrams that compose the one-loop amplitude. However, this approach is not easily generalised to higher order in the t/s-expansion and we would like to consider different ways to derive the sub-eikonal contribution. The first method that we will investigate involves reducing the one-loop amplitude to master integrals and, then, approximating these master integrals in the forward limit using differential equations. The second method is based on the expansion by regions technique [173, 174, 176].

---

[2] For simplicity, we do not consider the $\mathcal{O}(\varepsilon)$ terms in this analysis. However, one should keep in mind that they are required to evaluate non-factorisable corrections.

18.2 THE EIKONAL CONTRIBUTION

In this section, we determine the leading-order terms in Eq. (18.5), following the calculation done for WBF in Ref. [7].

The one-loop amplitude is made of four diagrams, shown in Fig. 18.2. In each of them, we assign the loop momentum k to the gluon propagator. We consider the limit where the outgoing jets are very energetic compared to the momentum in the transverse plane to the incoming momenta p_1, p_2. In light-cone coordinates, they read

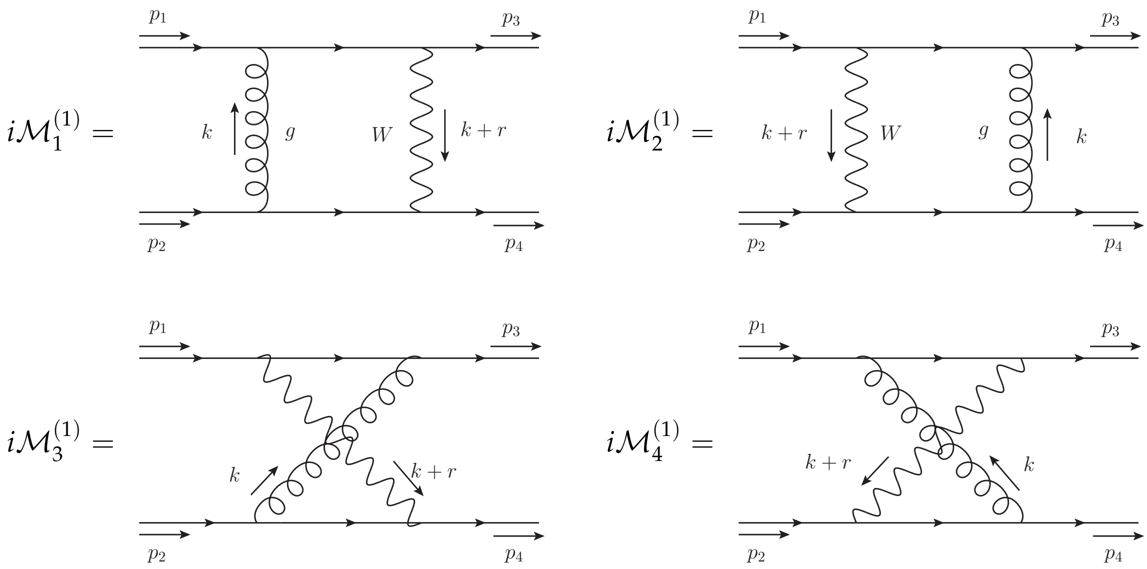

Figure 18.2: Definition of the four diagrams. The external momenta are on-shell. The transverse momentum is defined as $r = p_1 - p_3$. The diagrams $\mathcal{M}_3^{(1)}$ and $\mathcal{M}_4^{(1)}$ are respectively related to $\mathcal{M}_1^{(1)}$ and $\mathcal{M}_2^{(1)}$) by the momentum mapping $p_1 \leftrightarrow -p_3$.

$$p_1 = \left(\sqrt{s/2}, 0, \vec{0}\right), \qquad p_2 = \left(0, \sqrt{s/2}, \vec{0}\right) . \tag{18.9}$$

To separate teh physics of the null components from that of the transverse plane, we perform a Sudakov decomposition of the loop momentum

$$k = \alpha p_1 + \beta p_2 + k_\perp , \tag{18.10}$$

In this coordinate system, the kinematic limit that we consider translates to $\alpha \sim \beta \ll \sqrt{s}$. In addition, we assume that $k_\perp \sim r_\perp \ll \sqrt{s}$, which is the small scale of our problem. This allows an expansion of the fermion propagators in their eikonal form

$$\frac{1}{\not{k} + \not{p}_{1,2} + i\varepsilon} = \frac{\not{k} + \not{p}_{1,2}}{(k + p_{1,2})^2 + i\varepsilon} \approx \frac{\not{p}_{1,2}}{2k \cdot p_{1,2} + i\varepsilon} = \frac{\gamma^\mp}{2k^\mp + i\varepsilon}\,. \tag{18.11}$$

The second equality of Eq. (18.11) is obtained by assuming that $k^2 \ll k \cdot p_1$. If the loop momentum and $p_{1,2}$ have a relative sign, the location of the pole changes

$$\frac{1}{\not{k} - \not{p}_{1,2} + i\varepsilon} \approx \frac{-\not{p}_{1,2}}{-2k \cdot p_{1,2} + i\varepsilon} = \frac{\gamma^\mp}{2k^\mp - i\varepsilon}\,. \tag{18.12}$$

We consider the first diagram in Fig. 18.2

$$i\mathcal{M}_1^{(1)} = \mathcal{C} \int \frac{d^dk}{(2\pi)^d} \frac{\langle 3|\gamma^\mu(\not{k} + \not{p}_1)\gamma^\nu|1]\langle 4|\gamma_\mu(\not{k} - \not{p}_2)\gamma_\nu|2]}{k^2(k^2 + 2k \cdot p_1)(k^2 - 2k \cdot p_2)[(k + r)^2 - m_W^2]}\,, \tag{18.13}$$

where $\mathcal{C} = g_s^2\, g_W^2/2\, t^a_{21} t^a_{43}$ contains the coupling and the colour factors. In Eq. (18.13), we use the fact that only left-handed incoming partons contribute. Since we are only interested in the leading-order contribution, we can drop the loop momentum in the currents in Eq. (18.13) and use Eq. (18.11) to rewrite the two fermion propagators in their eikonal form

$$i\mathcal{M}_1^{(1)} \approx \mathcal{C} \int \frac{d^dk}{(2\pi)^d} \frac{\langle 3|\gamma^\mu\gamma^-\gamma^\nu|1]\langle 4|\gamma_\mu\gamma^+\gamma_\nu|2]}{k^2(2k^- + i\varepsilon)(2k^+ - i\varepsilon)[(k + r)^2 - m_W^2]}\,. \tag{18.14}$$

Similarly, the third diagram becomes

$$\mathcal{M}_3^{(1)} \approx -\mathcal{C} \int \frac{d^dk}{(2\pi)^d} \frac{\langle 3|\gamma^\nu\gamma^-\gamma^\mu|1]\langle 4|\gamma_\mu\gamma^+\gamma_\nu|2]}{k^2(2k^- - i\varepsilon)(2k^+ - i\varepsilon)[(k + r)^2 - m_W^2]}\,, \tag{18.15}$$

where we use Eq. (18.12) to expand the first fermion propagator and the fact that $p_3 \approx p_1$ in the eikonal approximation. Except an overall sign, the only difference with the result from the first diagram in Eq. (18.14) comes from the sign of the Feynman prescription on one of the eikonal propagator. The sum of the two diagrams is conveniently expressed as

$$\begin{aligned} i\mathcal{M}_1^{(1)} + \mathcal{M}_3^{(1)} \approx \mathcal{C} \int \frac{d^dk}{(2\pi)^d} & \frac{J_{31}^{\mu\nu} J_{\mu\nu,42}}{k^2(2k^+ - i\varepsilon)[(k + r)^2 - m_W^2]} \\ & \times \left[\frac{1}{2k^- + i\varepsilon} - \frac{1}{2k^- - i\varepsilon}\right]\,, \end{aligned} \tag{18.16}$$

where we introduce the following notations for the two fermion currents

$$J_{31}^{\mu\nu} = \langle 3|\gamma^\mu\gamma^-\gamma^\nu|1]\,, \qquad J_{\mu\nu,42} = \langle 4|\gamma_\mu\gamma^+\gamma_\nu|2]\,. \tag{18.17}$$

Note that, to write Eq. (18.16), we perfom the replacement $J_{31}^{\mu\nu} \leftrightarrow J_{31}^{\nu\mu}$ that will be justified later. The integral in Eq. (18.16) can be simplified since

$$\frac{1}{2k^+ \pm i\varepsilon} = \mathcal{P}\frac{1}{2k^+} \mp i\pi\delta(2k^+)\,, \tag{18.18}$$

where $\mathcal{P}$ denotes the principal value [177]. This expression means that the propagator is real except when k^+ vanishes. In this case, there is a pole in the complex plane of k^+ which leads to a residue once integrated. The sign of the residue is determined by the location of the pole in either the upper or the lower half of the complex plane.

Then, using Eq. (18.18), the square bracket in Eq. (18.16) can be written as

$$\frac{1}{2k^- + i\varepsilon} - \frac{1}{2k^- - i\varepsilon} = 2\mathrm{Im}\left\{\frac{1}{2k^+ + i\varepsilon}\right\} = -2i\pi\delta(2k^+) = -i\pi\delta(k^+)\,. \tag{18.19}$$

The combinaison of the propagators becomes a Dirac delta function that force the plus component of the loop momentum to vanish. The sum of the first and the third diagram becomes

$$i\mathcal{M}_1^{(1)} + \mathcal{M}_3^{(1)} \approx \mathcal{C} J_{31}^{\mu\nu} J_{\mu\nu,42} \int \frac{d^dk}{(2\pi)^d} \frac{-i\pi\delta(k^+)}{k^2(2k^+ - i\varepsilon)[(k+r)^2 - m_W^2]}\,. \tag{18.20}$$

An analogous derivation can be performed for the two other diagrams. We find

$$i\mathcal{M}_2^{(1)} + \mathcal{M}_4^{(1)} \approx -\mathcal{C} J_{42}^{\mu\nu} J_{\mu\nu,42} \int \frac{d^dk}{(2\pi)^d} \frac{-i\pi\delta(k^+)}{k^2(2k^+ + i\varepsilon)[(k+r)^2 - m_W^2]}\,. \tag{18.21}$$

We can now combine Eqs. (18.20)-(18.21) to write the full amplitude as

$$\begin{aligned} i\mathcal{M}^{(1)} &= \mathcal{C} J_{31}^{\mu\nu} J_{\mu\nu,42} \int \frac{d^dk}{(2\pi)^d} \frac{-i\pi\delta(k^+)}{k^2[(k+r)^2 - m_W^2]} \left[\frac{1}{2k^+ - i\varepsilon} - \frac{1}{2k^+ + i\varepsilon}\right] \\ &= \mathcal{C} J_{31}^{\mu\nu} J_{\mu\nu,42} \int \frac{d^dk}{(2\pi)^d} \frac{\pi^2\delta(k^+)\delta(k^-)}{k^2[(k+r)^2 - m_W^2]}\,. \end{aligned} \tag{18.22}$$

The loop integral is therefore reduce to the integral over the transverse plane. This can be made explicit by expressing the measure in light-cone coordinates[3]

$$d^dk = dk_+\,dk_-\,d^{d-2}\mathbf{k}_\perp\,. \tag{18.23}$$

Then, Eq. (18.22) becomes

$$i\mathcal{M}^{(1)} = \pi^2\,\mathcal{C}\,J_{31}^{\mu\nu} J_{\mu\nu,42} \int \frac{d^{d-2}\mathbf{k}_\perp}{(2\pi)^d} \frac{1}{{\mathbf{k}_\perp}^2[(\mathbf{k}_\perp + \mathbf{r}_\perp)^2 + m_W^2]}\,, \tag{18.24}$$

---

[3] We denote Euclidian vector with bold symbol such that $k_\perp^2 = -{\mathbf{k}_\perp}^2$

where we use the fact that the null components of r cannot contribute in $k \cdot r$ because of the two Dirac functions and the fact that at leading order $r^2 \approx -\mathbf{r}_\perp{}^2$.

The two currents can also be further simplified. We consider the upper current $J_{31}^{\mu\nu} = \langle 3|\gamma^\mu\gamma^-\gamma^\nu|1]$. We use the Dirac equation

$$\langle 3|\not{p}_3 = 0\,, \tag{18.25}$$

and the fact that, at leading order, $p_3 \approx p_1$, to write

$$\langle 3|\not{p}_3 \approx \langle 3|\gamma_- = 0\,. \tag{18.26}$$

Therefore, the upper current necessarily reads

$$J_{31}^{\mu\nu} \to \langle 3|\gamma^+\gamma^-\gamma^\nu|1]\,. \tag{18.27}$$

We note that the first Dirac matrix in Eq. (18.27) cannot be $\gamma_\perp$ since p_3 does not have a transverse component at leading order. To go further, we derive the anti-commutation relation for the light-cone Dirac matrices

$$\{\gamma^+,\gamma^-\} = \frac{1}{2}\{\gamma^0+\gamma^3,\gamma^0-\gamma^3\} = \frac{1}{2}\left(2\eta^{00}-2\eta^{33}\right)\mathbb{1} = 2\mathbb{1}\,. \tag{18.28}$$

Using the anti-commutation relation in Eq. (18.28) and the Dirac equation in Eq. (18.26), we find

$$J_{31}^{\mu\nu} \to 2\langle 3|\gamma^\nu|1]\,. \tag{18.29}$$

The same reasoning is applied to $J_{42}^{\mu\nu}$. We note that this reasoning also justify the permutation of the Lorentz index in Eq. (18.16).

Once the fermion currents are simplified using Eq. (18.29), the one-loop amplitude in Eq. (18.24) becomes

$$\mathcal{M}^{(1)} = i\frac{g_s^2}{4\pi}\, t_{31}^a\, t_{42}^a\, \chi^{(1)}\, \mathcal{A}^{(0)}\,, \tag{18.30}$$

where we use the expression of the colour-stripped Born amplitude $\mathcal{A}^{(0)}$ defined in Eq. (18.6) and define

$$\chi^{(1)} = \frac{1}{(2\pi)^{-2\varepsilon}}\int \frac{d^{d-2}\mathbf{k}_\perp}{\pi}\,\frac{t-m_W^2}{\mathbf{k}_\perp{}^2[(\mathbf{k}_\perp+\mathbf{r}_\perp)^2+m_W^2]}\,. \tag{18.31}$$

Apart from the choice of regulator for the loop integral, this result matches the one in Ref. [7]. We can perform the Euclidian loop integral by introducing Feynman parameters and considering spherical coordinates. We find

$$\chi^{(1)} = \frac{\pi^{-\varepsilon}}{(2\pi)^{-2\varepsilon}}\,\frac{\Gamma(1+\varepsilon)\Gamma(-\varepsilon)}{\Gamma(1-\varepsilon)}\,\frac{t-m_W^2}{(m_W^2)^{1+\varepsilon}}\,{}_2F_1\left(1,1+\varepsilon;1-\varepsilon;-\rho\right)\,. \tag{18.32}$$

We use this result and we renormalise the strong coupling in the $\overline{\text{MS}}$ scheme. Then, the one-loop amplitude in Eq. (18.30) becomes

$$\mathcal{A}^{(1)} = \frac{\alpha_s(\mu)}{\pi}\left[-\frac{i\pi}{\varepsilon} + i\pi \ln\left(\frac{(t-m_W^2)^2}{\mu^2 m_W^2}\right) + \mathcal{O}\left(\frac{t}{s}\right)\right]\mathcal{A}^{(0)}\,, \tag{18.33}$$

where we use ${\mathbf{r}_\perp}^2 = -t + \mathcal{O}(t/s)$. This result matches what we found from the expansion of the exact analytic amplitude in Eq. (18.5).

We would like to go beyond the eikonal contribution. The computation that we followed from Ref. [7] is straightforward and give the correct expression. Nevertheless, it is not clear how one can extend this procedure to higher order in t/s-expansion. In the following sections, we present different ways to approximate Feynman integrals in this limit.

18.3 APPROXIMATION OF THE MASTER INTEGRALS USING DIFFERENTIAL EQUATIONS

In this section, we consider that it is possible to reduce the one-loop amplitude to master integrals, but that the latters are difficult to compute exactly. We approximate them in the limit $t \ll s$ using differential equations build from IBP relations, as discussed for the computation of the two-loop triangle integrals in Appendix C.

The reduction of the one-loop amplitude is performed with `Kira` [178]. We find two integral families, one planar and one crossed. The integrals of the crossed family can be mapped to the ones of the planar family by crossing symmetry $p_1 \leftrightarrow -p_3$, see Fig. 18.1. We focus on the planar family. It is defined by the following set of propagators

$$\left\{k^2, (k+p_2)^2, (k-p_1)^2, (k-p_1+p_3)^2 - m_W^2\right\}\,. \tag{18.34}$$

Five master integrals belong to this integral family. They are diagrammatically represented on Fig. 18.3. We would like to find the expression of these five master integrals in the limit where $t \sim m_W^2$ and $t \ll s$. We consider the following scaleless ratios

$$x = -\frac{t}{s}\,, \qquad \rho = -\frac{t}{m_W^2}\,. \tag{18.35}$$

In the limit we are considering, x is a small parameter. On the other hand, since $t \sim m_W^2$, we need to determine the exact dependence on ρ. We can differentiate the set of master integrals with respect to x and ρ using `LiteRed` [179]. The differential equation reads[4]

$$d\vec{I} = M_x(x,\rho,\varepsilon)\vec{I}\, dx + M_\rho(x,\rho,\varepsilon)\vec{I}\, d\rho\,, \tag{18.36}$$

---

[4] We note that, for simplicity, we have set the scale $t = -1$. It can be reconstructed at the end of the calculation by dimensional analysis.

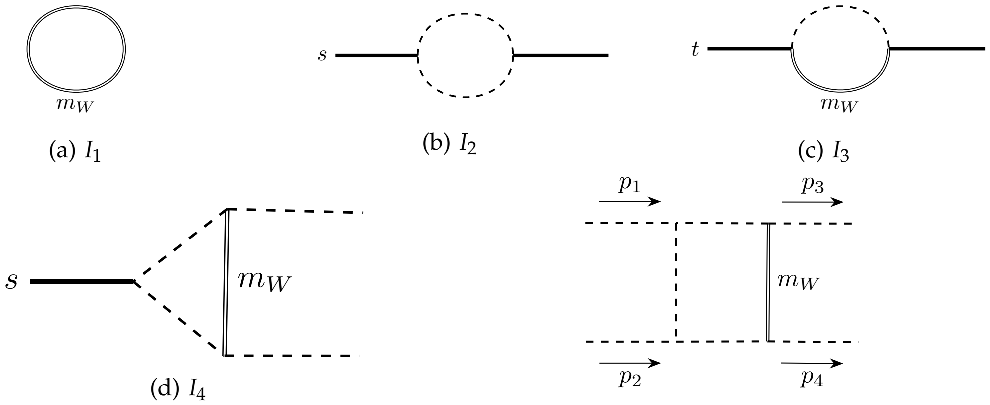

(a) I_1 (b) I_2 (c) I_3 (d) I_4 (e) I_5

Figure 18.3: Master integrals of the first integral family. The double lines indicate massive W boson propagators. Dashed lines are related to massless propagators and on-shell legs. Solid lines are used to denote off-shell legs.

where

$$M_x = \begin{bmatrix} 0 & 0 & 0 & 0 & 0 \\ 0 & \frac{\varepsilon}{x} & 0 & 0 & 0 \\ 0 & 0 & 0 & 0 & 0 \\ \frac{\rho^2(\varepsilon-1)}{\rho+x} & \frac{\rho(1-2\varepsilon)}{\rho+x} & 0 & \frac{\rho-\varepsilon x+x}{\rho x+x^2} & 0 \\ \frac{\rho^3(\varepsilon-1)(\rho x+\rho+3x-1)}{(\rho+1)^2(x-1)(\rho+x)} & \frac{\rho(1-2\varepsilon)x}{(x-1)(\rho+x)} & \frac{2\rho^2(1-2\varepsilon)}{(\rho+1)^2(x-1)} & \frac{\rho\varepsilon}{(x-1)(\rho+x)} & \frac{\varepsilon x+x-1}{(x-1)x} \end{bmatrix}, \tag{18.37}$$

and

$$M_\rho = \begin{bmatrix} \frac{\varepsilon-1}{\rho} & 0 & 0 & 0 & 0 \\ 0 & 0 & 0 & 0 & 0 \\ \frac{1-\varepsilon}{\rho+1} & 0 & -\frac{1-2\varepsilon}{\rho^2+\rho} & 0 & 0 \\ -\frac{\rho(\varepsilon-1)x}{\rho+x} & \frac{(2\varepsilon-1)x}{\rho+x} & 0 & \frac{\varepsilon(\rho+2x)}{\rho(\rho+x)} & 0 \\ -\frac{\rho^2(\varepsilon-1)x}{(\rho+1)(\rho+x)} & -\frac{(2\varepsilon-1)x(\rho+2x)}{(\rho+1)(\rho+x)} & 0 & -\frac{\rho\varepsilon}{\rho^2+\rho x+\rho+x} & \frac{2\varepsilon+1}{\rho^2+\rho} \end{bmatrix}. \tag{18.38}$$

We consider that the master integrals defined in Fig. 18.3 assume the following form

$$I_i \sim \sum_{n=-\infty}^{\infty} x^{n+m\varepsilon} \ln^k(x)\, g^{(i)}_{nmk}(\rho,\varepsilon)\,, \tag{18.39}$$

where the possible values of n, m, and k are fully defined by the form of the differential equation in x defined in Eq. (18.37) and the desired order of expansion. Once the x dependence is fixed, we are left with only few functions $g^{(i)}_{nmk}(\rho,\varepsilon)$. Using the second differential equation in ρ, defined in Eq. (18.38), we built differential equations that relate these different building blocks.

As an example, it is clear from Eq. (18.37) that the first master integral does not depend on x. Thus,

$$I_1 = g^{(1)}_{000}(\rho, \varepsilon)\,. \tag{18.40}$$

Then, the ρ-dependent function is determined by the second differential equation. We find

$$\frac{dI_1}{d\rho} = \frac{d}{d\rho} g^{(1)}_{000}(\rho, \varepsilon) = \frac{-1+\varepsilon}{\rho} g^{(1)}_{000}(\rho, \varepsilon)\,. \tag{18.41}$$

Therefore,

$$g^{(1)}_{000}(\rho, \varepsilon) = c_1(\varepsilon)\rho^{-1+\varepsilon}\,, \tag{18.42}$$

which is the correct expression for the one-loop tadpole integral. Similarly, we find with ease that

$$\begin{aligned} I_2 &= c_2(\varepsilon)x^{\varepsilon}\,, \\ I_3 &= \left(\frac{\rho}{1+\rho}\right)^{2\varepsilon-1} \left[c_3(\varepsilon) + c_1(\varepsilon)\rho^{1-\varepsilon} {}_2F_1\left(2-2\varepsilon, 1-\varepsilon, 2-\varepsilon, -\rho\right)\right]\,. \end{aligned} \tag{18.43}$$

Up to now, we found the integrals in their exact form. The situation is different for the fourth integral, which has a non-trivial dependence on x. From Eq. (18.37), we read

$$\frac{dI_4}{dx} = \Big[(\varepsilon-1)\rho + \mathcal{O}(x)\Big] I_1 + \Big[(1-2\varepsilon) + \mathcal{O}(x)\Big] I_2 + \left[\frac{1}{x} - \frac{\varepsilon}{\rho} + \mathcal{O}(x)\right] I_4\,, \tag{18.44}$$

where we approximate the equation using $x \ll \rho \sim 1$. The form of this equation indicates that I_4 has the following x dependence in the $x \to 0$ limit

$$I_4 = x g^{(4)}_{100}(\rho, \varepsilon) + x\ln(x) g^{(4)}_{101}(\rho, \varepsilon) + x^{1+\varepsilon} g^{(4)}_{110}(\rho, \varepsilon) + \mathcal{O}(x^2)\,, \tag{18.45}$$

where we discard $\mathcal{O}(x^2)$ terms since they do not contribute to the next-to-leading order in the eikonal approximation of the one-loop amplitude. By plugging this Ansatz in Eq. (18.37), we see that two of the g's are fixed by the previous master integral g's. We find

$$g^{(4)}_{101}(\rho, \varepsilon) = c_1(\varepsilon)(\varepsilon-1)\rho^{\varepsilon}\,, \quad g^{(4)}_{110}(\rho, \varepsilon) = c_2(\varepsilon)\frac{1-2\varepsilon}{\varepsilon}\,. \tag{18.46}$$

The last one, $g^{(4)}_{100}(\rho, \varepsilon)$, is a new building block that needs to be determined using the differential equation in ρ. From Eq. (18.38), we find

$$\frac{d}{d\rho} g^{(4)}_{100}(\rho, \varepsilon) = c_1(\varepsilon)(1-\varepsilon)\rho^{-1+\varepsilon} + \frac{\varepsilon}{\rho} g^{(4)}_{100}(\rho, \varepsilon)\,. \tag{18.47}$$

This differential equation be solved and lead to a new integration constant $c_4(\varepsilon)$

$$g^{(4)}_{100}(\rho,\varepsilon) = \rho^{\varepsilon}\left(c_4(\varepsilon) + (1-\varepsilon)c_1(\varepsilon)\ln(\rho)\right) . \tag{18.48}$$

The last integral is the box integral I_5. We note that, in this case, we need to include the $\mathcal{O}(x^2)$ terms, since after reduction of the one-loop amplitude, I_5 comes with $\mathcal{O}(1/x)$ coefficients. In the $x \to 0$ limit, we find that the differential equation with respect to x reads

$$\begin{aligned} \frac{dI_5}{dx} =& \left[\frac{(1-\rho)\rho^2(\varepsilon-1)}{(1+\rho)^2} + \frac{\rho(1+\rho+2\rho^2)(1-\varepsilon)}{(1+\rho)^2}x + \mathcal{O}(x^2)\right] I_1 \\ &+ \left[(2\varepsilon-1)x + \mathcal{O}(x^2)\right] I_2 + \left[\frac{2\rho^2(2\varepsilon-1)}{(1+\rho)^2}\right] I_3 - \left[\varepsilon + \mathcal{O}(x)\right] I_4 \\ &+ \left[\frac{1}{x} - \varepsilon - \varepsilon x\right] I_5 . \end{aligned} \tag{18.49}$$

We look at the different x terms present in the equation and suppose the following Ansatz for I_5

$$\begin{aligned} I_5 = x g^{(5)}_{100}(\rho,\varepsilon) + x\ln(x) g^{(5)}_{101}(\rho,\varepsilon) + x^2 g^{(5)}_{200}(\rho,\varepsilon) + x^{2+\varepsilon} g^{(5)}_{210}(\rho,\varepsilon) \\ + x^2\ln(x) g^{(5)}_{201}(\rho,\varepsilon) + \mathcal{O}(x^3) . \end{aligned} \tag{18.50}$$

Four of the five coefficients are directly fixed by the previous expressions. We find

$$\begin{aligned} g^{(5)}_{101}(\rho,\varepsilon) &= c_1(\varepsilon)(\varepsilon-1)\rho^{\varepsilon} \\ g^{(5)}_{201}(\rho,\varepsilon) &= -\varepsilon\left(c_1(\varepsilon)\rho^{\varepsilon}(\varepsilon-1) + g^{(5)}_{101}(\rho,\varepsilon)\right) \\ g^{(5)}_{210}(\rho,\varepsilon) &= c_2(\varepsilon)\frac{2(\varepsilon-1)}{1+\varepsilon} \\ g^{(5)}_{200}(\rho,\varepsilon) &= c_1(\varepsilon)\frac{\rho^{\varepsilon}(1+\rho+2\rho^2)(1-\varepsilon)}{(1+\rho)^2} + \frac{2\rho^2(2\varepsilon-1)}{(1+\rho)^2} g^{(3)}_{000}(\rho,\varepsilon) \\ &\quad + \varepsilon\left(c_1(\varepsilon)\rho^{\varepsilon}(\varepsilon-1) - g^{(4)}_{100}(\rho,\varepsilon) - g^{(5)}_{100}(\rho,\varepsilon) + g^{(5)}_{101}(\rho,\varepsilon)\right) . \end{aligned} \tag{18.51}$$

The last coefficient is determined by the second differential equation, keeping only the x terms

$$\frac{dg^{(5)}_{100}(\rho,\varepsilon)}{d\rho} = \frac{1+2\varepsilon}{\rho(1+\rho)} g^{(5)}_{100}(\rho,\varepsilon) + \frac{\rho^{\varepsilon}}{(1+\rho)}\left[c_1(\varepsilon)(1-\varepsilon)(1-\varepsilon\ln(\rho)) - c_4(\varepsilon)\varepsilon\right] . \tag{18.52}$$

The solution to this differential equation can be expressed as hypergeometric functions

$$\begin{aligned} g^{(5)}_{100}(\rho,\varepsilon) = \left(\frac{\rho}{1+\rho}\right)^{1+2\varepsilon} \Bigg[\frac{\rho^{-\varepsilon}}{\varepsilon}\Bigg(c_1(\varepsilon)(1-\varepsilon)\, {}_3F_2\left(-2\varepsilon, -\varepsilon, -\varepsilon; 1-\varepsilon, 1-\varepsilon; -\rho\right) \\ + {}_2F_1\left(-2\varepsilon, -\varepsilon; 1-\varepsilon; -\rho\right)\left(c_4(\varepsilon)\varepsilon - c_1(\varepsilon)(\varepsilon-1)(\varepsilon\ln(\rho)-1)\right)\Bigg) + c_5(\varepsilon)\Bigg] . \end{aligned} \tag{18.53}$$

We have found a solution for each of the master integrals of the planar topology in the limit $t \ll s$. The ρ dependence is kept exact through the determination of the function g. Each of these building blocks is associated with a x branch. We find that only one branch is to be computed since the others are fixed by integrals in lower sector. As the result, we have one integration constant for each integrals that can be computed in a convenient limit.

18.3.1 *Boundary conditions*

To fix the five integration constants, we need to compute the master integrals in some convenient limit. In addition to the $x \to 0$ limit that we are considering since the beginning, we consider the large m_W limit, which is equivalent to $\rho \to 0$. The Feynman integrals become easier to calculate. We focus on the determination of $c_5(\varepsilon)$.

We can determine the integration constants by calculating the integral I_5 in the limit $x \to 0$ and $\rho \to 0$ using the standard Feynman parametrisation. We report such computations in Appendix D. We find that

$$c_5(\varepsilon) = \mathcal{O}(\varepsilon)\,. \tag{18.54}$$

Nevertheless, such computation, even if it is less tedious than the original integral, can be difficult for two-loop integrals. We would like to exploit the structure of the differential equations solution. Indeed, most of the expression is fixed by other integration constants as the $g^{(i)}_{nmk}(\rho)$ are shuffled between the different master integrals. For instance, the integral I_5 in Eq. (18.50) is fully determined up to the branch x. It would be counterproductive to compute again the branches $x\ln(x)$, x^2, $x^{2+\varepsilon}$ and $x^2\ln x$. In addition, by looking at the solution in Eq. (18.53), we know that, in fact, we only need the branch $x\rho^{1+2\varepsilon}$ of I_5.

For this purpose, we find that it is convenient to use the Mellin-Barnes representation of the W boson propagator. Indeed, since the dependence on m_W is only present in the propagator, it allows us to write it as a massless propagator and a factor of the mass. Formally, the idea behind this method is to use the following identity

$$\frac{1}{(X+Y)^\lambda} = \frac{1}{\Gamma(\lambda)}\frac{1}{2\pi i}\int_{-i\infty}^{i\infty} dz\,\Gamma(\lambda+z)\Gamma(-z)\frac{Y^z}{X^{\lambda+z}}\,, \tag{18.55}$$

where the integration contour has to pass between the *left poles*, $\Gamma(\cdots+z)$, and the *right poles*, $\Gamma(\cdots-z)$. The integration contour is then closed to the left-hand side or to the right-hand side complex part of the complex plane. We refer the reader to Ref. [176] for an introduction on the Mellin-Barnes representation and its use to compute loop integrals.

We consider the integral I_5 where we use the Eq. (18.55) on the massive W boson propagator and invert the order of integration

$$\begin{aligned} I_5 = &- \frac{1}{2\pi i}\int_{-i\infty}^{i\infty} dz\; (m_W^2)^z\, \Gamma(1+z)\Gamma(-z) \\ &\times \int \frac{d^dk}{i\pi^{d/2}} \frac{(-1)^{1+z}}{(k^2)^{1+z}(k+p_4)^2(k-p_3)^2(k+p_1-p_3)^2}\,. \end{aligned} \tag{18.56}$$

The integration becomes simpler since we need to calculate a massless box integral with non-integer exponents. We combine the propagators pairwise by introducing two Feynman parameters. We find

$$\begin{aligned} I_5 = &\frac{1}{2\pi i}\int_{-i\infty}^{i\infty} dz\; (m_W^2)^z\, \Gamma(-z)\frac{\Gamma(-\varepsilon-z)\Gamma(-\varepsilon)\Gamma(2+z+\varepsilon)}{\Gamma(-2\varepsilon-z)} \\ &\times \int_0^1 dx \int_0^1 dy\; \frac{1}{[-s(1-y)x-t(1-x)y]^{2+z+\varepsilon}}\,. \end{aligned} \tag{18.57}$$

We use Eq. (18.55) to write the denominator of Eq. (18.58) in its Mellin-Barnes representation. The x and y integration is easily performed as we recognise the integral form of the beta function. We find

$$\begin{aligned} I_5 = &\frac{1}{(2\pi i)^2}\int_{-i\infty}^{i\infty} dz\; (m_W^2)^z\, \Gamma(-z)\frac{\Gamma(-\varepsilon-z)\Gamma(-\varepsilon)}{\Gamma(-2\varepsilon-z)}\int_{-i\infty}^{i\infty} dz_2\; \Gamma(-z_2) \\ &\times \Gamma(2+z+\varepsilon+z_2)\left(\frac{t}{s}\right)^{z_2+2+z+\varepsilon}\frac{\Gamma(-1-\varepsilon-z-z_2)^2\Gamma(1+z_2)^2}{\Gamma(-\varepsilon-z)^2}\,. \end{aligned} \tag{18.58}$$

We are left with the integration over the two Mellin-Barnes variables. We start with z_2. The integrand in Eq. (18.58) has two sets of poles of order 2, $0+n$ and $-1-\varepsilon-z+n$, with $n \in \mathbb{N}$. Since we want to find the branch x of I_5, it is clear that we need to consider the second set of poles. In addition, we want to find the result only for the branch $\rho^{1+2\varepsilon}$. It means that we have to consider the pole in $z=-1-2\varepsilon$. However, once the integration over z_2 has been performed, it is easy to see that the integrand is not divergent at $z=-1-2\varepsilon$. We conclude that the branch $x\rho^{1+2\varepsilon}$ does not contribute to I_5 and, therefore, $c_5(\varepsilon)=0$.

This result agrees with the one found using Feynman parameters. We note that the Mellin-Barnes representation greatly simplifies the calculation and is more systematic. We report a similar calculation for $c_4(\varepsilon)$ in Sec. D.2. For more complicated cases, such calculations can be facilitated by the collection of Mathematica codes `MB tools` [180–182].

To summarise, we find the following boundary constants

$$\boxed{\begin{aligned} c_1(\varepsilon) &= \frac{1}{\varepsilon} + 1 + \left(1 + \frac{\pi^2}{12}\right)\varepsilon + \left(1 + \frac{\pi^2}{12} + \frac{\psi(1)}{6}\right)\varepsilon^2 + \mathcal{O}(\varepsilon^3)\,, \\ c_2(\varepsilon) &= \frac{1}{\varepsilon} + 2 + i\pi + \left(4 + 2i\pi - \frac{7}{12}\pi^2\right)\varepsilon + \mathcal{O}(\varepsilon^2)\,, \\ c_3(\varepsilon) &= \mathcal{O}(\varepsilon^2)\,, \\ c_4(\varepsilon) &= -\frac{1}{\varepsilon^2} - \frac{i\pi}{\varepsilon} + \frac{5\pi^2}{12} + \mathcal{O}(\varepsilon)\,, \\ c_5(\varepsilon) &= 0\,, \end{aligned}} \tag{18.59}$$

which completes the determination of the master integrals of the first integral family in the $x \to 0$ limit. A similar analysis can be performed for the crossed topology. Then, by expanding the reduction table to the required x dependence, we check that the next-to-eikonal contribution to the one-loop massless single top production, shown in Eq. (18.5), is correctly reproduced.

We have shown that the master integrals that compose the non-factorisable contribution to t-channel massless single-top one-loop amplitude can be expanded in the forward limit. We have computed the master integrals up to the sub-eikonal terms, allowing us to reproduce the result for the one-loop amplitude which has been derived in Eq. (18.5). Nevertheless, this method relies on the fact that loop amplitudes can be reduced to master integrals. In the next section, we take a different approach and study the master integral using the *expansion by regions*.

18.4 EXPANSION BY REGIONS

The expansion by regions is used to approximate multi-loop integrals, in the case where they depend on scales that are very different in size [172–174]. Since we are considering that the fermion currents are nearly not scattering, leading to the hierarchy $t \ll s$, this method is appropriate for our problem.

In this section, we consider again the master integral I_5. We use the expansion by regions to derive its leading order expression in the limit $t \ll s$. Then, we show how one can compute higher-order contributions.

The box integral I_5, shown in Fig. 18.3e, reads

$$I_5 = \int \frac{d^d k}{i\pi^{d/2}} \frac{1}{(k^2 - m^2)(k^2 - 2k \cdot p_1)(k^2 + 2k \cdot p_2)(k - r)^2}\,, \tag{18.60}$$

where we define $r = p_1 - p_3$. We characterise the small scale of our problem with a parameter $\lambda \ll 1$. In the forward limit, we have

$$m_W^2 \sim t \sim \lambda\,, \qquad s \sim 1\,. \tag{18.61}$$

The regions are defined by the scaling of the loop momentum k, whose components are independent from each other. Similar to the computation of the eikonal contribution in Sec. 18.2, it is convenient to use the Sudakov decomposition

$$k^\mu = \alpha p_1^\mu + \beta p_2^\mu + k_\perp^\mu\,. \tag{18.62}$$

The two incoming 4-momenta p_1 and p_2 define the null components and the transverse plane is spanned by the Euclidian 2-vector $\mathbf{k}_\perp$ such that

$$k_\perp^2 = -\mathbf{k}_\perp{}^2 \tag{18.63}$$

We can determine the scale of the transverse momentum r^μ using its Sudakov decomposition

$$r^\mu = \alpha_r p_1^\mu + \beta_r p_2^\mu + r_\perp^\mu\,. \tag{18.64}$$

The different components can be expressed in term of the Mandelstam variables. For instance,

$$2p_1 \cdot r = s\beta_r = -2p_1 \cdot p_3 = t \implies \beta_r = \frac{t}{s}\,, \tag{18.65}$$

and similarly

$$2p_2 \cdot r = s\alpha_r = 2p_1 \cdot p_2 - 2p_2 \cdot p_3 = s + u = -t \implies \alpha_r = -\frac{t}{s}\,. \tag{18.66}$$

Finally, the transverse component is fixed by the norm of r

$$r^2 = \alpha_r\beta_r - \mathbf{r}_\perp{}^2 = t \implies \mathbf{r}_\perp{}^2 = -t(1 + \frac{t}{s})\,. \tag{18.67}$$

Each component of r^μ is now explicitely 0 as $t \to 0$ since $r^\mu \sim (\lambda, \lambda, \sqrt{\lambda})$.

Regions are defined by the scaling of α, β and $\mathbf{k}_\perp$. They can be determined in several ways. One of them is to use the Mathematica package `asy.m` [174, 175]. This computer program works with the Symmanzik polynomials $\mathcal{U}$ and $\mathcal{F}$ and provides all possible scaling of the Feynman parameters which lead to non-vanishing integrals. Each of this set is associated to a region. In the case of I_5, we find that the different regions are

$$\begin{aligned}
(h):&\quad \alpha \sim 1, \quad \beta \sim 1, \quad k_\perp \sim 1 \\
(1c):&\quad \alpha \sim 1, \quad \beta \sim \lambda, \quad k_\perp \sim \sqrt{\lambda} \\
(2c):&\quad \alpha \sim \lambda, \quad \beta \sim 1, \quad k_\perp \sim \sqrt{\lambda}\,.
\end{aligned} \tag{18.68}$$

where the first region corresponds to k being hard and the last two are regions where k is collinear to either p_1 or p_2. The scaling of I_5 is clearly defined in each region. We find

$$I_5^{(h)} \sim 1\,, \qquad I_5^{(1c)} \sim \lambda^{-1}\,, \qquad I_5^{(2c)} \sim \lambda^{-1}\,. \tag{18.69}$$

Other scalings, like the soft region $k \sim (\lambda, \lambda, \sqrt{\lambda})$, results in scaleless integrals which are set to 0 in the $\overline{\text{MS}}$ scheme. In the rest of this section, we compute the integral I_5 in each of these regions.

18.4.1 *Hard region*

In the hard region, all the components of the loop momentum are large $k \sim (1, 1, 1)$ and the integral I_5 drastically simplifies. Using Eq. $(A.28)$ from Ref. [176], we find that the leading term of the hard region reads

$$\boxed{\begin{aligned} I_5^{(h)} &= \int \frac{d^dk}{i\pi^{d/2}} \frac{1}{(k^2+2k\cdot p_1)(k^2-2k\cdot p_2)(k^2)^2} \\ &= \frac{1}{(-s)^{2+\varepsilon}} \frac{\Gamma(-\varepsilon)^2\Gamma(1+\varepsilon)}{(1+\varepsilon)\Gamma(-2\varepsilon)} + \mathcal{O}(\lambda)\,. \end{aligned}} \tag{18.70}$$

As expected, the hard region provides sub-leading contributions.

18.4.2 *First collinear region*

The collinear regions correspond to the loop momentum k being collinear to the incoming momenta p_1 and p_2. We compute the first collinear region characterised by $k \sim (1, \lambda, \sqrt{\lambda})$ and, then, by symmetry, deduce the expression for the second one. Each of these regions require a special treatment because they display unregulated divergences. We follow Ref. [173] and regulate the integral by introducing auxiliary parameters to the exponents to both fermion propagators. The integral I_5 reads

$$\begin{aligned} &I_5^{(1c)}(\lambda_1, \lambda_2) \\ &= \int \frac{d^dk}{i\pi^{d/2}} \frac{1}{(k^2-m^2)(k^2+2k\cdot p_2)^{1+\lambda_2}(k^2-2k\cdot p_1)^{1+\lambda_1}(k-\beta_r p_2 - r_\perp)^2}\,, \end{aligned} \tag{18.71}$$

where the W boson propagator has been expanded, keeping only the $\mathcal{O}(\lambda)$ terms. Since $k^2 \ll k\cdot p_2$, we expand the first fermion propagator

$$\frac{1}{(k^2+2k\cdot p_2)^{1+\lambda_2}} = \frac{1}{\Gamma(1+\lambda_2)} \sum_{n=0}^{\infty} \frac{\Gamma(1+\lambda_2+n)}{\Gamma(1+n)} \frac{(k^2)^n}{(2p_2\cdot k)^{1+n+\lambda_2}}\,. \tag{18.72}$$

We use Eq. (18.72) to rewrite Eq. (18.73) and see that I_5 scales as $I_5 \sim x^{1+\lambda_1+n}$. We consider the leading order term $n = 0$. It reads

$$I_5^{(1c)} = \int \frac{d^dk}{i\pi^{d/2}} \frac{1}{(k^2 - m^2)(2k\cdot p_2)^{1+\lambda_2}(k^2 - 2k\cdot p_1)^{1+\lambda_1}(k - \beta_r p_2 - r_\perp)^2} \,. \tag{18.73}$$

The loop integral is easily performed by introducting Feynman parameters. We find

$$\begin{aligned} I_5^{(1c)} = \frac{1}{(-s)^{1+\lambda_2}} \frac{1}{(m^2)^{1+\varepsilon+\lambda_1}} & \frac{\Gamma(\lambda_1 - \lambda_2)\Gamma(1+\varepsilon+\lambda_1)\Gamma(-\varepsilon-\lambda_1)}{\Gamma(1+\lambda_1)\Gamma(1-\varepsilon-\lambda_2)} \\ & \times {}_2F_1\left(1+\varepsilon+\lambda_1, 1; 1-\varepsilon-\lambda_2; -\rho\right) \,. \end{aligned} \tag{18.74}$$

As explained, this expression is singular as $\lambda_1 - \lambda_2 \to 0$. This pole is expected to cancel to the one in the second collinear region. We would like to make this pole explicit and to sum this result with the one from the second collinear region. Then, we will be able to safely consider the limit $\lambda_1, \lambda_2 \to 0$.

First, we change variables $\lambda_1 = \delta$ and $\lambda_2 = -\delta$ such that the pole is located at $\delta \to 0$. To expand Eq. (18.74) in δ, we write the hypergeometric function in its integral form. Since the integral is regulated as $\delta \to 0$, we can safely expand the integrand in δ and integrate order by order. It reads

$$\begin{aligned} {}_2F_1\left(1, 1+\varepsilon+\delta; 1-\varepsilon+\delta; -\rho\right) &= \frac{\Gamma(1-\varepsilon+\delta)}{\Gamma(1+\varepsilon+\delta)\Gamma(-2\varepsilon)} \int_0^1 \frac{dz\, z^{\varepsilon+\delta}}{(1-z)^{1+2\varepsilon}(1+\rho z)} \\ &= \frac{\Gamma(1-\varepsilon+\delta)}{\Gamma(1+\varepsilon+\delta)} \left[\frac{\Gamma(1+\varepsilon)}{\Gamma(1-\varepsilon)} {}_2F_1\left(1, 1+\varepsilon; 1-\varepsilon; -\rho\right) \right. \\ & \left. \quad + \frac{\delta}{\Gamma(-2\varepsilon)} \int_0^1 dz\, \frac{z^\varepsilon (1-z)^{-2\varepsilon-1}}{1+\rho z} \ln(z) + \mathcal{O}(\delta^2) \right] . \end{aligned} \tag{18.75}$$

We remark that the integral at order $\mathcal{O}(\delta)$ is free of divergences as $\varepsilon \to 0$, since the limit $z \to 1$ is regulated by the logarithm. We can, therefore, expand in ε and integrate order by order

$$\begin{aligned} {}_2F_1\left(1, 1+\varepsilon+\delta; 1-\varepsilon+\delta; -\rho\right) &= \frac{\Gamma(1-\varepsilon+\delta)}{\Gamma(1+\varepsilon+\delta)\Gamma(-2\varepsilon)} \left[\frac{\Gamma(1+\varepsilon)\Gamma(-2\varepsilon)}{\Gamma(1-\varepsilon)} \right. \\ \times\, {}_2F_1\left(1, 1+\varepsilon; 1-\varepsilon; -\rho\right) &+ \left. \frac{\delta}{1+\rho} \left(\mathrm{Li}_2(-\rho) - \frac{\pi^2}{6} + \mathcal{O}(\varepsilon) \right) + \mathcal{O}(\delta^2) \right] . \end{aligned} \tag{18.76}$$

Using this result in Eq. (18.74), we find that, in the first collinear region, the master integral I_5 reads

$$\boxed{\begin{aligned} I_5^{(1c)} &= \frac{\Gamma(-\varepsilon-\delta)\Gamma(2\delta)}{\Gamma(1+\delta)\Gamma(-2\varepsilon)}\frac{1}{(-s-i\epsilon)^{1-\delta}}\frac{1}{(m^2)^{1+\varepsilon+\delta}}\left[\frac{\Gamma(1+\varepsilon)\Gamma(-2\varepsilon)}{\Gamma(1-\varepsilon)}\right.\\ &\left.\times\,{}_2F_1\left(1,1+\varepsilon;1-\varepsilon;-\rho\right)+\frac{\delta}{1+\rho}\left(\mathrm{Li}_2(-\rho)-\frac{\pi^2}{6}+\mathcal{O}(\varepsilon)\right)+\mathcal{O}(\delta^2)\right].\end{aligned}} \tag{18.77}$$

It can be checked that the second collinear sector is obtained by switching $\lambda_1 \leftrightarrow \lambda_2$, or equivalently $\delta \to -\delta$, such that

$$I_5^{(2c)}(\delta) = I_5^{(1c)}(-\delta)\,. \tag{18.78}$$

Once summed, the results from the two collinear regions provide the leading order of the integral I_5

$$I_5 = \lim_{\delta\to 0}\left(I_5^{(1c)}(\delta) + I_5^{(2c)}(\delta)\right)\,. \tag{18.79}$$

We successfully derived the leading order of the master integral I_5. Nevertheless, to determine the next-to-eikonal contribution to the one-loop amplitude, we need to compute the next-to-leading order terms.

18.4.3 *Next-to-leading order of the master integrals*

In this section, we explain how the next-to-leading order contributions can be obtained using the expansion by regions. Again, we focus on the master integral I_5 of the first integral family.

We have already computed the leading-order term of I_5 by considering the first and the second collinear regions, see Eq.(18.79). We would like now to calculate the next-to-leading contribution in the x expansion. At this order, we need to consider the hard contribution, calculated in Eq. (18.70). Then, we need to expand the collinear regions to the next-to-leading order. We focus on this task.

First, to compute the next-to-leading order of I_5 in the first collinear region, we need to consider the $n = 1$ term in the fermion propagator expansion (18.72). It reads

$$\frac{1}{(k^2+2k\cdot p_2)^{1-\delta}} = \frac{1}{(2k\cdot p_2)^{1-\delta}} - (1-\delta)\frac{k^2}{(2k\cdot p_2)^{2-\delta}} + \mathcal{O}\left((k^2)^2\right)\,. \tag{18.80}$$

Similarly, to write Eq. (18.73), we have expanded the W boson propagator to the leading order. We have neglected the component $\alpha_r p_1^\mu$ of r^μ and have used $r_\perp^2 = -\mathbf{r}_\perp{}^2 =$

$t(1-x) = t + \mathcal{O}(x)$, where $x = -t/s$. To understand how to expand this propagator to sub-leading orders, we introduce the following variable

$$\tilde{r}_\perp = \frac{r_\perp}{\sqrt{1-x}}\,, \tag{18.81}$$

such that $\tilde{r}_\perp^2 = t$ which corresponds to the approximation we are making at leading order. It means that the leading order propagator can be unambiguously written as

$$\frac{1}{(k-r)^2} = \frac{1}{(k-\beta_r p_2 - \tilde{r}_\perp)^2} + \mathcal{O}(\lambda^0)\,. \tag{18.82}$$

It is now clear how we should expand $\tilde{r}_\perp$ since

$$\tilde{r}_\perp = \frac{r_\perp}{\sqrt{1-x}}\left(1 + (\sqrt{1-x} - 1)\right) = \frac{r_\perp}{\sqrt{1-x}}\left(1 - \frac{x}{2}\right) + \mathcal{O}(x^2)\,. \tag{18.83}$$

Therefore, the expansion of the W boson propagator to the next-to-leading order reads

$$\frac{1}{(k-r)^2} = \frac{1}{k^2 - \beta_r 2k\cdot p_2 + t - 2k\cdot\tilde{r}_\perp} + x\frac{2k\cdot p_1 - k\cdot\tilde{r}_\perp}{[(k-\beta_r p_2 - \tilde{r}_\perp)^2]^2} + \mathcal{O}(x^2)\,. \tag{18.84}$$

The scalar product appearing on the numerator of Eqs. (18.80)-(18.84) can be rewritten in terms of the propagator of the first topology, see Eq. (18.34). We find

$$\begin{aligned}
k^2 &= (k^2 - m^2) + m^2 \\
2k\cdot p_1 &= -(k^2 - 2k\cdot p_1) + (k^2 - m^2) + m^2 \\
k\cdot r_\perp &= -\frac{1}{2}(k - \beta_r p_2 - r_\perp)^2 + \frac{1}{2}(t + m_W^2) + \frac{1}{2}(k^2 - m^2) - \frac{1}{2}\beta_r(2k\cdot p_2)\,,
\end{aligned} \tag{18.85}$$

where in the last equation we have neglected higher-order contribution $\mathcal{O}(\lambda^2)$.

The contributions from the expansion of the fermion propagator in Eq. (18.80) and the expansion of the W boson propagator in Eq. (18.84) provide the next-to-leading order contribution to I_5 in the collinear regions. Tensor integrals that appear after the expansion of the propagators are reduced to scalar integrals using Eq. (18.85).

To simplify the calculation and to make it more systematic, we can set IBP relations for these integrals. We emphasise that, in this case, we need to derive IBP relations for integrals with propagators raised to non-integer exponents. We proceed in the following way. We use `LiteRed` [179] to generate the IBP relations. Since this computer program use symbolic placeholders for the exponents of the propagators, it is easy to shift them with the regulators λ_1 and λ_2. Then, we use `FiniteFlow` to solve the system of linear equations and find the master integrals.

Once solve, the system of equations reveals that the triangle integral I_4 and the box integral I_5, computed in the collinear region, are the only two master integrals needed. We can, therefore, express all the integrals present at NLO in terms of those. For example, the next-to-leading order of I_5 in the first collinear region is found to be

$$\boxed{I_5^{(1c),\mathrm{NLO}} = \left[\delta(1-\varepsilon)-\varepsilon+\mathcal{O}(\delta^2)\right] I_4^{(1c)} + x\left[\delta(1+\varepsilon)-\varepsilon+\mathcal{O}(\delta^2)\right] I_5^{(1c)},} \tag{18.86}$$

where the triangle integral I_4 in the first collinear region is easily derived. It reads

$$I_4^{(1c)}(\delta) = (-s)^{-1+\delta}(m_W^2)^{-\delta-\varepsilon}\frac{\Gamma(2\delta)\Gamma(\delta+\varepsilon)\Gamma(1-\delta-\varepsilon)}{\Gamma(1+\delta)\Gamma(1+\delta-\varepsilon)} + \mathcal{O}(\lambda)\,. \tag{18.87}$$

The second collinear region in obtained by symmetry, see Eq. (18.78). Once the two collinear regions are combined with the hard contribution, given in Eq. (18.70), we get the next-to-leading order term of the master integral I_5. A similar calculation is performed for the second integral family. Then, we proceed in the same way as in Sec. 18.3. We expand the reduction table to the required order in x and use the approximate results of the master integrals. We find the expected result, derived from the exact amplitude in Eq. (18.5).

The expansion by regions offers a convenient way to understand how the loop momentum scales with respect to the other scale of the considered integral. In fact, it offers a convenient framework to extend the results of Ref. [7]. Indeed, one of the main idea of this reference is that one can benefits from major simplification when the diagrams are combined, see Sec. 18.2. It should be possible to consider build on this idea and use the expansion by regions to compute higher-order terms, following what has been discussed in this section.

In the next chapter, we apply this idea to compute the non-factorisable, double-virtual contribution to Higgs boson production in WBF in the forward limit.

19 SUB-EIKONAL CORRECTIONS TO THE HIGGS PRODUCTION IN WBF

In this chapter, we study non-factorisable corrections to the double virtual contribution to Higgs boson production in weak boson fusion. We extend the calculation of Ref. [7] by computing the next-to-leading term in the eikonal expansion. We provide numerical results and estimate the accuracy of our result.

We note that, in this chapter, we closely follow Ref. [161].

19.1 KINEMATICS

We consider Higgs boson production in weak boson fusion

$$q(p_1) + q(p_2) \to q(p_3) + q(p_4) + H(p_H)\,. \tag{19.1}$$

We consider all quarks to be massless, $p_i^2 = 0$, $i = 1, \dots, 4$, and the Higgs boson is on-shell, $p_H^2 = m_H^2$. Experimentally, events with two nearly forwarded jets are selected to reduce the background. To describe this situation, we proceed in the same way as in Sec. 18.4 and consider the Sudakov decomposition of the outgoing jet momenta. They read

$$\begin{aligned} p_3 &= \alpha_3 p_1 + \beta_3 p_2 + p_{3,\perp}\,, \\ p_4 &= \alpha_4 p_1 + \beta_4 p_2 + p_{4,\perp}\,. \end{aligned} \tag{19.2}$$

In the forward limit, we have that $\alpha_3 \sim \beta_4 \sim 1$ and $p_{3,\perp}^2/s \sim p_{4,\perp}^2/s \sim \lambda$ where $\lambda \ll 1$ is the small parameter of the problem. Since p_3 and p_4 are on-shell, we find[1]

$$\beta_3 = \frac{\mathbf{p}_{3,\perp}^2}{s\alpha_3}\,, \quad \alpha_4 = \frac{\mathbf{p}_{4,\perp}^2}{s\beta_4}\,, \tag{19.3}$$

so that $\beta_3 \sim \alpha_4 \sim \lambda$. The momenta that flow through the weak boson propagators are

$$\begin{aligned} q_1 &= p_1 - p_3 = \delta_3 p_1 - \beta_3 p_2 - p_{3,\perp}\,, \\ q_2 &= p_2 - p_4 = -\alpha_4 p_1 + \delta_4 p_2 - p_{4,\perp}\,, \end{aligned} \tag{19.4}$$

where we defined $\delta_3 = 1 - \alpha_3$ and $\delta_4 = 1 - \beta_4$. Because $\alpha_3 \sim \beta_4 \sim 1$, the scaling of δ_3 and δ_4 is not transparent and needs to be determined. Thanks to the energy-momentum conservation,

$$p_H = q_1 + q_2\,. \tag{19.5}$$

---

[1] As in Chapter 18, we denote Euclidian vectors with bold symbol.

Using the fact that the Higgs is produced on-shell, we find

$$\delta_3\delta_4 s = m_H^2 + \frac{\mathbf{p}_{3,\perp}^2}{\alpha_3} + \frac{\mathbf{p}_{4,\perp}^2}{\beta_4} + 2\mathbf{p}_{3,\perp}\cdot\mathbf{p}_{4,\perp} - \frac{\mathbf{p}_{3,\perp}^2\mathbf{p}_{4,\perp}^2}{\alpha_3\beta_4 s}\,. \tag{19.6}$$

This equation can be used to defined the smallness of δ_3 and δ_4. Indeed, the contribution to the cross section mainly comes from $p_{3,4,\perp} \sim m_V$ where we use $V = W, Z$ to denote quantities related to weak gauge bosons. This leads to the following hierarchy

$$\delta_3\delta_4 \sim \frac{m_V^2}{s} \sim \frac{m_H^2}{s} \sim \frac{\mathbf{p}_{3,\perp}^2}{s} \sim \frac{\mathbf{p}_{4,\perp}^2}{s} \sim \lambda \ll 1\,, \tag{19.7}$$

where we use the fact that m_V and m_H are numerically close to each other in the SM. Assuming that we are interested in the central production of the Higgs boson, we write

$$\delta_3 \sim \delta_4 \sim \sqrt{\lambda} \gg \lambda\,. \tag{19.8}$$

Finally, we note that the variables δ_3 and δ_4 can be written as

$$\delta_{3,4} = \sqrt{\frac{\mathbf{p}_{H,\perp}^2 + m_H^2}{s}}\,e^{\pm y_H} + \mathcal{O}(\lambda)\,, \tag{19.9}$$

where y_H is the rapidity of the Higgs boson in the partonic centre-of-mass frame. From this equation, it is clear that kinematic configurations with large y_H may violate the assumed scaling.

19.2 ONE-LOOP AMPLITUDE

We start our analysis with the one-loop amplitude. Unlike the case of the single top production, both Z and W bosons contribute to the Higgs production in WBF. As we will see, through the next-to-leading order in the eikonal expansion, the Lorentz-structure of the one- and two-loop amplitudes coincide with the Born one. Therefore, for simplicity, we consider only the vector part of the weak boson coupling, $-ig_V\gamma^\mu$, and take the left-handed external fermions. The generalisation of our result to $V = W$ and $V = Z$ with their helicity-dependent couplings is straightforward.

The one-loop amplitude can be written as

$$\mathcal{M}_1 = g_s^2\, g_W^2\, g_{VVH}\, t^a_{i_3i_1} t^a_{i_4i_2}\, \mathcal{A}_1\,, \tag{19.10}$$

where we set the coupling of the weak bosons and the Higgs boson to be $ig_{VVH}\, g_{\mu\nu}$. In Eq. (19.10), we defined the colour-stripped one-loop amplitude

$$\mathcal{A}_1 = \int \frac{d^dk_1}{(2\pi)^d}\frac{1}{d_1d_3d_4} J_{\mu\nu}(k_1, -k_1 - q_1)\, \tilde{J}^{\mu\nu}(-k_1, k_1 - q_2)\,, \tag{19.11}$$

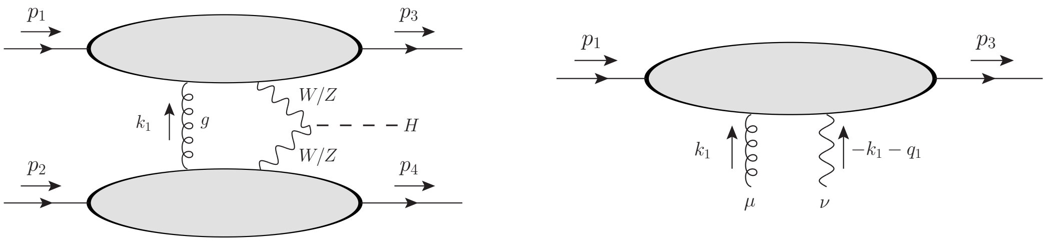

Figure 19.1: To compute the one-loop amplitude, shown on the left, we consider the two quark currents separately. The convention for momentum assignment is described for the upper current on the right. The lower current is defined in an analogous way.

where we use a simplified notation for the boson propagators

$$d_1 = k_1^2 + i\epsilon, \quad d_3 = (k_1 + q_1)^2 - m_V^2 + i\epsilon, \quad d_4 = (k_1 - q_2)^2 - m_V^2 + i\epsilon\,, \tag{19.12}$$

and the fermion currents, defined following the convention in Fig. 19.1, read

$$\begin{aligned} J^{\mu\nu}(k_1, -k_1 - q_1) &= \langle 3| \left[\frac{\gamma^\nu (\not{p}_1 + \not{k}_1)\gamma^\mu}{\rho_1(k_1)} + \frac{\gamma^\mu (\not{p}_3 - \not{k}_1)\gamma^\nu}{\rho_3(-k_1)} \right] |1]\,, \\ \tilde{J}^{\mu\nu}(-k_1, k_1 - q_2) &= \langle 4| \left[\frac{\gamma^\nu (\not{p}_2 + \not{k}_1)\gamma^\mu}{\rho_2(k_1)} + \frac{\gamma^\nu (\not{p}_4 - \not{k}_1)\gamma_\mu}{\rho_4(-k_1)} \right] |2]\,. \end{aligned} \tag{19.13}$$

The currents $J^{\mu\nu}$ and $\tilde{J}^{\mu\nu}$ contain the fermion propagators which read

$$\rho_i(k) = \frac{1}{(p_i + k)^2 + i\epsilon}\,. \tag{19.14}$$

At this stage, we would like to use the expansion by regions [172–174], as done in the previous chapter in Sec. 18.4. We consider the Sudakov decomposition of the loop momentum

$$k_1 = \alpha_1 p_1 + \beta_1 p_2 + k_{1,\perp}\,. \tag{19.15}$$

The loop integral measure becomes

$$\frac{d^d k_1}{(2\pi)^d} = \frac{s}{2} \frac{d\alpha_1}{2\pi} \frac{d\beta_1}{2\pi} \frac{d^{d-2}\mathbf{k}_{1,\perp}}{(2\pi)^{d-2}}\,. \tag{19.16}$$

To understand the scaling of the loop momentum components, we proceed in the following way. The inverse propagators of the colour-stripped one-loop amplitude in Eq. (19.11) are linear in α_1 and β_1. If we perform the integration over one of these variables, for instance α_1, we get a contribution from the poles. Then, once the residue from one of the poles has been computed, the dependence in the second variable, in this case β_1, in the other propagators is at most quadratic. If we assume that the transverse components of k_1 are either of the order of the partonic centre-of-mass energy or of the order of the transverse momentum, then, the possible scales of β_1 are unambiguously defined, and, consequently, the scale of α_1. The regions that we found in this way are listed in Table 19.1. Following the order of the list in Table 19.1, we identify the Glauber, the Glauber-soft, the soft, the collinear, and the hard regions.

Region	α_1	β_1	$\mathbf{k}_{1,\perp}$
a	λ	λ	$\sqrt{\lambda}$
b	λ	$\sqrt{\lambda}$	$\sqrt{\lambda}$
c	$\sqrt{\lambda}$	$\sqrt{\lambda}$	$\sqrt{\lambda}$
d	1	λ	$\sqrt{\lambda}$
e	1	1	1

Table 19.1: Relevant regions for the non-factorisable, one-loop amplitude. Each column is related to one component of the loop momentum $k_1 = (\alpha_1, \beta_1, \mathbf{k}_{1,\perp})$, as defined in Eq. (19.15). We do not list symmetric regions.

It is easy to determine the scaling of the one-loop amplitude in the different regions. We find

$$\mathcal{M}^{(a)} \sim \lambda^{-2}, \quad \mathcal{M}^{(b)} \sim \lambda^{-2}, \quad \mathcal{M}^{(c)} \sim \lambda^{-2}, \quad \mathcal{M}^{(d)} \sim \lambda^{-3/2}, \quad \mathcal{M}^{(e)} \sim 1\,. \tag{19.17}$$

In the regions a), b) and c), the one-loop amplitude has the same scaling as the Born amplitude, i. e. λ^{-2}. These regions provide the leading order contribution in the eikonal approximation. We aim to determine the next-to-leading order corrections. Therefore, we have to consider these three regions to the next-to-leading order and the region d) to the leading order. The hard region can obviously be ignored for our purpose.

We will now consider the amplitude $\mathcal{A}_1$ in the relevant regions. To simplify the notation, we introduce definitions for various quantities in the plane transverse to the light-like momenta p_1 and p_2

$$\begin{aligned} &\Delta_1 = -\mathbf{k}_{1,\perp}^2,\ \Delta_{3,1} = -(\mathbf{k}_{1,\perp} - \mathbf{p}_{3,\perp})^2 - m_V^2,\ \Delta_{4,1} = -(\mathbf{k}_{1,\perp} + \mathbf{p}_{4,\perp})^2 - m_V^2\,, \\ &\Theta_{3,1} = -\left(\mathbf{k}_{1,\perp}^2 - 2\mathbf{k}_{1,\perp}\cdot\mathbf{p}_{3,\perp}\right)\,, \qquad \Theta_{4,1} = -\left(\mathbf{k}_{1,\perp}^2 + 2\mathbf{k}_{1,\perp}\cdot\mathbf{p}_{4,\perp}\right)\,. \end{aligned} \tag{19.18}$$

These definitions will be common to all the regions.

19.2.1 *Glauber region*

In the Glauber region, the inverse propagators of the one-loop amplitude $\mathcal{A}_1$ scales as $\mathcal{O}(\lambda)$ at the leading order. As mentioned earlier, we need to calculate the amplitude up to the next-to-leading order in the eikonal approximation in this region. Therefore, we keep terms in the propagators which scale as $\lambda^{3/2}$ and neglect the ones that scale as $\mathcal{O}(\lambda^2)$. We find

$$\begin{aligned}
&d_1 \approx \Delta_1 + i\varepsilon, \quad d_3 \approx s\delta_3(\beta_1 - \beta_3) + \Delta_{3,1} + i\epsilon\,, \\
&d_4 \approx -s\delta_4(\alpha_1 + \alpha_4) + \Delta_{4,1} + i\epsilon\,, \\
&\rho_1(k_1) \approx s\beta_1 + \Delta_1 + i\epsilon\,, \qquad\qquad \rho_2(-k_1) \approx -s\alpha_1 + \Delta_1 + i\epsilon\,, \\
&\rho_3(-k_1) \approx -s\alpha_3\beta_1 + \Theta_{3,1} + i\epsilon\,, \quad \rho_4(k_1) \approx s\beta_4\alpha_1 + \Theta_{4,1} + i\epsilon\,.
\end{aligned} \tag{19.19}$$

We use Eq. (19.19) and the definition of $\mathcal{A}_1$ in Eq. (19.11) to express the one-loop amplitude in the Glauber region. It reads

$$\mathcal{A}_1^{(a)} = -\frac{s}{2}\int \frac{d^{d-2}\mathbf{k}_{1,\perp}}{(2\pi)^{d-2}}\,\frac{1}{\Delta_1\Delta_{3,1}\Delta_{4,1}}\,\Phi^{\mu\nu}\,\tilde{\Phi}_{\mu\nu}\,, \tag{19.20}$$

where the fermion currents factorise. In Eq. (19.20), we defined the currents as

$$\begin{aligned}
\Phi^{\mu\nu} = &\int\limits_{-\sigma}^{\sigma} \frac{d\beta_1}{2\pi i}\,\frac{\Delta_{3,1}}{s\delta_3(\beta_1-\beta_3)+\Delta_{3,1}} \\
&\qquad\times \langle 3|\left[\frac{\gamma^\nu(\not{p}_1 + \not{k}_{1,\perp})\gamma^\mu}{s\beta_1 + \Delta_1 + i\epsilon} + \frac{\gamma^\mu(\not{p}_3 - \not{k}_{1,\perp})\gamma^\nu}{-s\alpha_3\beta_1 + \Theta_{3,1} + i\epsilon}\right]|1]\,,
\end{aligned} \tag{19.21}$$

$$\begin{aligned}
\tilde{\Phi}^{\mu\nu} = &\int\limits_{-\sigma}^{\sigma} \frac{d\alpha_1}{2\pi i}\,\frac{\Delta_{4,1}}{-s\delta_4(\alpha_1+\alpha_4)+\Delta_{4,1}} \\
&\qquad\times \langle 4|\left[\frac{\gamma^\nu(p_2 + \not{k}_{1,\perp})\gamma_\mu}{-s\alpha_1 + \Delta_1 + i\epsilon} + \frac{\gamma^\nu(p_4 - \not{k}_{1,\perp})\gamma_\mu}{s\beta_4\alpha_1 + \Theta_{4,1} + i\epsilon}\right]|2]\,.
\end{aligned} \tag{19.22}$$

In Eqs. (19.21)-(19.22), we have performed the replacement $k_1 \to k_{1,\perp}$ in the numerators since the null components of k_1 which scale as λ cannot contribute the $\mathcal{O}(\sqrt{\lambda})$ relative corrections. In addition, we have limited the integration by introducing an auxiliary parameter $\sigma \ll \sqrt{\lambda}$ that limits α_1 and β_1 to the Glauber region. In addition, we impose that

$$\lambda \ll \sigma \ll \sqrt{\lambda}\,, \tag{19.23}$$

such that the same cut-off parameter can be used in the Glauber-soft region, where one of the null components of k_1 scales as $\sqrt{\lambda}$.

The numerator of the currents in Eqs. (19.21)-(19.22) can be further simplified. We recall that we need to compute $\mathcal{O}(\sqrt{\lambda})$ relative corrections. As the result, if we consider the transverse momentum $\not{k}_{1,\perp} \sim \sqrt{\lambda}$ in one of the current, then the other current has to be considered to the leading order. However, at leading order, the currents become

$$\langle 4|\gamma^\mu \not{p}_{2,4}\gamma^\nu|2] \approx 4p_2^\mu p_2^\nu\,, \qquad \langle 3|\gamma^\mu \not{p}_{3,1}\gamma^\nu|1] \approx 4p_1^\mu p_1^\nu\,. \tag{19.24}$$

Once the leading order current is contracted with the other current, the transverse component $k_{1,\perp}$ vanishes, since

$$\not{p}_i \not{k}_{1,\perp} \not{p}_i = 0, \quad i = 1, 2, \tag{19.25}$$

because $p_{1,2} \cdot k_{1,\perp} = 0$ and $p_{1,2}^2 = 0$. The integrand of Eqs. (19.21)-(19.22) can be further simplified. We use the fact that $\beta_1 \in [-\sigma, \sigma]$ and $\alpha_1 \in [-\sigma, \sigma]$ to write

$$\begin{aligned} \frac{\Delta_{3,1}}{s\delta_3(\beta_1 - \beta_3) + \Delta_{3,1} + i\epsilon} &\approx 1 + \frac{s\delta_3(\beta_3 - \beta_1)}{\Delta_{3,1}} + \mathcal{O}(\lambda), \\ \frac{\Delta_{4,1}}{-s\delta_4(\alpha_1 + \alpha_4) + \Delta_{4,1} + i\epsilon} &\approx 1 + \frac{s\delta_4(\alpha_4 + \alpha_1)}{\Delta_{4,1}} + \mathcal{O}(\lambda), \end{aligned} \tag{19.26}$$

where we neglect $\mathcal{O}(\lambda)$ corrections.

We use Eq. (19.26) and the simplification of the numerators discussed earlier to rewrite the currents $\Phi^{\mu\nu}$ and $\tilde{\Phi}^{\mu\nu}$. We focus on the former. It is convenient to define

$$\Phi^{\mu\nu} = \frac{2p_1^\mu \langle 3|\gamma^\nu|1]}{s} \Phi, \tag{19.27}$$

where

$$\Phi = \int_{-\sigma}^{\sigma} \frac{d\beta_1}{2\pi i} \left(1 + \frac{s\delta_3(\beta_3 - \beta_1)}{\Delta_{3,1}}\right) \left[\frac{1}{\beta_1 + \frac{\Delta_1}{s} + i\epsilon} + \frac{1}{-\beta_1 + \frac{\Theta_{3,1}}{s\alpha_3} + i\epsilon}\right]. \tag{19.28}$$

The integration is performed using Cauchy's residue theorem. We note that there are poles in the upper half of the complex plane and in the lower one. We use

$$\int_{-\sigma}^{\sigma} \frac{d\beta_1}{2\pi i} \frac{1}{\pm\beta_1 - z_a + i\epsilon} = -\frac{1}{2} + \mathcal{O}(z_a/\sigma), \tag{19.29}$$

and

$$\begin{aligned} \int_{-\sigma}^{\sigma} \frac{d\beta_1}{2\pi i} \beta_1 \left(\frac{1}{\beta_1 - z_a + i\epsilon} + \frac{1}{-\beta_1 - z_b + i\epsilon}\right) \\ = -\frac{1}{2}(z_a - z_b) + \mathcal{O}(z_a^2/\sigma, z_b^2/\sigma). \end{aligned} \tag{19.30}$$

We note that Eqs. (19.29)-(19.30) are valid for $|z_a| < \sigma$. These result are found by closing the integration contour in the plane where there is no pole and by integrating over the half-circle of radius σ. Using the results in Eq. (19.29) and Eq. (19.30), we find

$$\Phi = (-1) \left[1 + \frac{\delta_3}{2\Delta_{3,1}} (2s\beta_3 + \Delta_1 - \Theta_{3,1})\right]. \tag{19.31}$$

Similarly, the lower current in Eq. (19.22) is defined as

$$\tilde{\Phi}^{\mu\nu} = \frac{2p_2^\mu \langle 4|\gamma^\nu|2]}{s}\tilde{\Phi} . \tag{19.32}$$

We easily find that

$$\tilde{\Phi} = (-1)\left[1 + \frac{\delta_4}{2\Delta_{4,1}}\left(2s\beta_4 + \Delta_1 - \Theta_{4,1}\right)\right] . \tag{19.33}$$

Altogether, the contribution of the Glauber region to the non-factorisable, one-loop amplitude $\mathcal{A}_1$ reads

$$\begin{aligned}\mathcal{A}_1^{(a)} = -\langle 3|\gamma^\mu|1]\langle 4|\gamma_\mu|2] \int \frac{d^{d-2}\mathbf{k}_{1,\perp}}{(2\pi)^{d-2}} \frac{1}{\Delta_1\Delta_{3,1}\Delta_{4,1}} \\ \times\left(1 + \frac{\delta_3}{2\Delta_{3,1}}\left(2s\beta_3 + \Delta_1 - \Theta_{3,1}\right) + \frac{\delta_4}{2\Delta_{4,1}}\left(2s\beta_4 + \Delta_1 - \Theta_{4,1}\right)\right) .\end{aligned} \tag{19.34}$$

19.2.2 *Glauber-soft region*

We consider now the Glauber-soft region. As mentioned earlier, the contribution from this region naively start at λ^{-2}. However, we will now argue that there is an additional $\sqrt{\lambda}$ suppression which implies that we only need to consider the leading order contribution in this region.

First, we demonstrate that the loop momentum in the numerator can be discarded. According to the scaling of the loop momentum k_1 described in Table 19.1, we can perform the following replacement $k_1 \to \beta_1 p_2 + k_{1,\perp}$ in the numerator of both currents. Then, if we consider the $\mathcal{O}(\sqrt{\lambda})$ relative correction in $J^{\mu\nu}$, the other current has to be considered at leading order, $\tilde{J}^{\mu\nu} \sim p_2^\mu p_2^\nu$. It is clear that the contribution from k_1 vanishes. On the other hand, if we consider the $\mathcal{O}(\sqrt{\lambda})$ relative correction in $\tilde{J}^{\mu\nu}$, the argument differs. We note that, in the numerator of $\tilde{J}^{\mu\nu}$, the loop momentum is independent of α_1 and the sign of the loop momentum is different in the two propagators. Therefore, once we integrate over α_1, the contribution from the loop momentum k_1 in the numerator of $\tilde{J}^{\mu\nu}$ vanishes.

Then, we use the fact that $\beta_1 \gg \Delta_1/s, \Theta_{3,1}/s$ to write the current $J^{\mu\nu}$ as

$$\begin{aligned}J^{\mu\nu}(k_1, -q_1 - k_1) &\approx p_1^\mu p_1^\nu \left(\frac{1}{s\beta_1 + \Delta_1 + i\epsilon} + \frac{\alpha_3}{-s\alpha_3\beta_1 + \Theta_{3,1} + i\epsilon}\right) \\ &\approx -\frac{p_1^\mu p_1^\nu}{s\beta_1^2}\left(\Delta_1 + \Theta_{3,1}\right) ,\end{aligned} \tag{19.35}$$

where we remind the reader that the poles in $\beta_1 = -\Delta_1/s$ and $\beta_1 = \Theta_{3,1}/s/\alpha_3$ are outside of the integration region, $\mathbb{R} - [-\sigma, \sigma]$. We see that, for the scaling $k_1 \sim (\lambda, \sqrt{\lambda}, \sqrt{\lambda})$, the current $J^{\mu\nu}$ in Eq. (19.35) does not scale as $\lambda^{-1/2}$, but as $\mathcal{O}(1)$. We conclude that the Glauber-soft region starts contributing at $\lambda^{-3/2}$.

We use the expansion of the current $J^{\mu\nu}$ in Eq. (19.35) and consider the rest of the amplitude $\mathcal{A}_1$ at the leading order. We find

$$\mathcal{A}_1^{(b)} = -\langle 3|\gamma_\mu|1]\langle 4|\gamma^\mu|2] \int \frac{d^{d-2}\mathbf{k}_{1,\perp}}{(2\pi)^{d-2}} \frac{1}{\Delta_1 \Delta_{3,1} \Delta_{4,1}} \Delta\Phi \, \tilde{\Phi} \,, \tag{19.36}$$

where

$$\Delta\Phi = \left(-\frac{\Delta_1}{s} - \frac{\Theta_{3,1}}{s} \right) \int\limits_{-\infty}^{\infty} \frac{d\beta_1}{2\pi i} \frac{(\theta(\beta_1 - \sigma) + \theta(-\sigma - \beta_1))\Delta_{3,1}}{(s\delta_3 \beta_1 + \Delta_{3,1} + i\epsilon)\, \beta_1^2} \,. \tag{19.37}$$

The calculation of the integral in Eq. (19.37) is easily performed. We find

$$\Delta\Phi = \frac{\delta_3}{2\Delta_{3,1}} \left(\Delta_1 + \Theta_{3,1} \right) \,. \tag{19.38}$$

This concludes the calculation for the Glauber-soft region where $k_1 \sim (\lambda, \sqrt{\lambda}, \sqrt{\lambda})$. There is a symmetric region which scales as $k_1 \sim (\sqrt{\lambda}, \lambda, \sqrt{\lambda})$. We proceed in a analogous way and find

$$\Delta\tilde{\Phi} = \frac{\delta_4}{2\Delta_{4,1}} \left(\Delta_1 + \Theta_{4,1} \right) \,. \tag{19.39}$$

We combine the result from the Glauber region in Eq. (19.34) with the one from the two Glauber-soft regions. We find

$$\begin{aligned} \mathcal{A}_1^{a\&b} = -\langle 3|\gamma^\mu|1]\langle 4|\gamma_\mu|2] & \int \frac{d^{d-2}\mathbf{k}_{1,\perp}}{(2\pi)^{d-2}} \frac{1}{\Delta_1 \Delta_{3,1} \Delta_{4,1}} \\ & \times \left(1 + \frac{\delta_3}{\Delta_{3,1}} (s\beta_3 - \Theta_{3,1}) + \frac{\delta_4}{\Delta_{4,1}} (s\alpha_4 - \Theta_{4,1}) \right) \,. \end{aligned} \tag{19.40}$$

19.2.3 *Soft and collinear regions*

We consider the soft region where $k_1 \sim (\sqrt{\lambda}, \sqrt{\lambda}, \sqrt{\lambda})$. Naively, we have seen that we need to expand the contribution of this region to the next-to-leading order in the eikonal approximation. We will now argue that, in fact, this contribution is suppressed by a factor $\mathcal{O}(\sqrt{\lambda})$ per current and, thus, does not contribute at $\mathcal{O}(\lambda^{-3/2})$. Indeed, at leading order, the currents vanish. For instance, in the soft region, the upper current $J^{\mu\nu}$ reads

$$\begin{aligned} J^{\mu\nu}(k_1, -q_1 - k_1) &\approx p_1^\mu p_1^\nu \left(\frac{1}{s\beta_1 + i\epsilon} + \frac{\alpha_3}{-s\alpha_3\beta_1 + i\epsilon} \right) \\ &= p_1^\mu p_1^\nu (-2i\pi)\delta(\beta_1) \to 0 \,, \end{aligned} \tag{19.41}$$

where the pole in $\beta_1 = 0$ has been ignored because it was already considered in the Glauber region. The same argument holds for the second current $\tilde{J}^{\mu\nu}$. Therefore, the contribution from the soft region can be ignored.

Similarly, we can ignore the contribution from the collinear regions. We have seen earlier that the collinear regions start contributing at $\mathcal{O}(\lambda^{-3/2})$, which implies that every terms that make up the one-loop amplitude have to be considered to the leading order. As the result, for the scaling $k_1 \sim (\lambda, 1, \sqrt{\lambda})$, the currents read

$$\begin{aligned} J^{\mu\nu}(k_1,k_2) &= \langle 3| \left[\frac{\gamma^\nu(\slashed{p}_1 + \beta_1 \slashed{p}_2)\gamma^\mu}{\beta_1 s + i\epsilon} + \frac{\gamma^\mu(\slashed{p}_1 - \beta_1 \slashed{p}_2)\gamma^\nu}{-\beta_1 s + i\epsilon} \right] |1] \\ &= \langle 3|\gamma^\mu \slashed{p}_2 \gamma^\nu + \gamma^\nu \slashed{p}_2 \gamma^\mu |1] = 2\langle 3| p_2^\mu \gamma^\nu + p_2^\nu \gamma^\mu - g^{\mu\nu} \slashed{p}_2 |1], \\ \tilde{J}^{\mu\nu}(k_1,k_2) &= \langle 4| \left[(1+\beta_1) \frac{\gamma^\nu \slashed{p}_2 \gamma^\mu}{\rho_2(k_1)} + (1-\beta_1) \frac{\gamma^\nu \slashed{p}_2 \gamma^\mu}{\rho_4(-k_1)} \right] |2]\,. \end{aligned} \tag{19.42}$$

We see that the contraction of the currents in Eq. (19.42) vanishes and, therefore, the collinear region do not contribute at $\mathcal{O}(\lambda^{-3/2})$. The same argument holds for the symmetric region.

19.2.4 *Final result*

We conclude that only two regions are required to compute the non-factorisable one-loop contribution to the Higgs boson production at the next-to-leading order in the eikonal approximation, namely the Glauber region and the Glauber-soft region in Eq. (19.40). Interestingly, this result can be computed directly from the following current

$$\Phi = \int \frac{d\beta_1}{2\pi i} \frac{\Delta_{3,1}}{s\delta_3(\beta_1 - \beta_3) + \Delta_{3,1} + i\epsilon} \left[\frac{1}{\beta_1 + \frac{\Delta_1}{s} + i\epsilon} + \frac{1}{-\beta_1 + \frac{\Theta_{3,1}}{s\alpha_3} + i\epsilon} \right], \tag{19.43}$$

where this expression is obtained by following the same first steps described in Sec. 19.2.1 up to Eq. (19.28), except that we do not perform the expansion shown in Eq. (19.26). Then, we close the contour in the upper half-plane, we only need to consider the residue of the pole $\beta_1 = \Theta_{3,1}/s/\alpha_3$. We find

$$\Phi = (-1) \frac{\Delta_{3,1}}{\Delta_{3,1} + \delta_3(\Theta_{3,1} - s\beta_3)}\,. \tag{19.44}$$

A similar expression is found for $\tilde{\Phi}$. Then, once expanded in δ_3 and δ_4, we recover the result in Eq. (19.40).

Finally, the one-loop amplitude $\mathcal{M}_1$ can be written as

$$\mathcal{M}_1 = i\,\frac{g_s^2}{4\pi}\, T^a_{i_3 i_1} T^a_{i_4 i_2}\, \mathcal{M}_0\, \mathcal{C}_1\,, \tag{19.45}$$

where we define the Born amplitude as

$$\mathcal{M}_0 = i g_W^2 g_{VVH} \frac{\langle 3|\gamma^\mu|1]\langle 4|\gamma_\mu|2]}{(q_1^2 - m_V^2)(q_2^2 - m_V^2)} \,. \tag{19.46}$$

In Eq. (19.45), we define $\mathcal{C}_1$ which contains the integral over the transverse components of the loop momentum. It reads

$$\boxed{\begin{aligned} \mathcal{C}_1 = \int \frac{d^{d-2}\mathbf{k}_{1,\perp}}{\pi(2\pi)^{-2\epsilon}} & \frac{(\mathbf{p}_{3,\perp}^2 + m_V^2)(\mathbf{p}_{4,\perp}^2 + m_V^2)}{\Delta_1 \Delta_{3,1} \Delta_{4,1}} \\ & \times \left[1 - \delta_3 \left(\frac{m_V^2}{\mathbf{p}_{3,\perp}^2 + m_V^2} + \frac{m_V^2}{\Delta_{3,1}} \right) - \delta_4 \left(\frac{m_V^2}{\mathbf{p}_{4,\perp}^2 + m_V^2} + \frac{m_V^2}{\Delta_{4,1}} \right) \right] . \end{aligned}} \tag{19.47}$$

19.3 TWO-LOOP AMPLITUDE

The calculation we have just performed at the one-loop level can be straightforwardly extended to the computation of the next-to-leading order corrections to the two-loop amplitude in the eikonal approximation. We write the latter as

$$\mathcal{M}_2 = -i g_s^4 \, g_W^2 \, g_{VVH} \left(\frac{1}{2} \{t^a, t^b\} \right)_{i_3 i_1} \left(\frac{1}{2} \{t^a, t^b\} \right)_{i_4 i_2} \mathcal{A}_2 \,, \tag{19.48}$$

where the colour-stripped two-loop amplitude is defined as

$$\begin{aligned} \mathcal{A}_2 = & \frac{1}{2!} \int \frac{d^d k_1}{(2\pi)^d} \frac{d^d k_2}{(2\pi)^d} \frac{1}{d_1 d_2 d_3 d_4} J_{\mu\nu\alpha}(k_1, k_2, -k_{12} - q_1) \\ & \qquad \times \tilde{J}^{\mu\nu\alpha}(-k_1, -k_2, k_{12} - q_2) \,. \end{aligned} \tag{19.49}$$

In Eq. (19.48), we account for identical gluons in the final state and defined $k_{12} = k_1 + k_2$. In Eq. (19.49), the inverse boson propagators are defined as

$$\begin{aligned} & d_1 = k_1^2 + i\epsilon \,, \qquad d_2 = k_2^2 + i\epsilon \,, \\ & d_3 = (k_{12} + q_1)^2 - m_V^2 + i\epsilon \,, \qquad d_4 = (k_{12} - q_2)^2 - m_V^2 + i\epsilon \,, \end{aligned} \tag{19.50}$$

and the currents follow the convention in Fig. 19.2. They read

$$\begin{aligned} & J_{\mu\nu\alpha}(k_1, k_2, -k_{12} - q_1) = \langle 3| \Bigg\{ \\ & \frac{\gamma^\alpha(\not{p}_1 + \not{k}_{12})\gamma^\nu(\not{p}_1 + \not{k}_1)\gamma^\mu}{\rho_1(k_{12})\rho_1(k_1)} + \frac{\gamma^\alpha(\not{p}_1 + \not{k}_{12})\gamma^\mu(\not{p}_1 + \not{k}_2)\gamma^\nu}{\rho_1(k_{12})\rho_1(k_2)} \\ & + \frac{\gamma^\nu(\not{p}_3 - \not{k}_2)\gamma^\alpha(\not{p}_1 + \not{k}_1)\gamma^\mu}{\rho_3(-k_2)\rho_1(k_1)} + \frac{\gamma^\mu(\not{p}_3 - \not{k}_1)\gamma^\alpha(\not{p}_1 + \not{k}_2)\gamma^\nu}{\rho_3(-k_1)\rho_1(k_2)} \\ & + \frac{\gamma^\nu(\not{p}_3 - \not{k}_2)\gamma^\mu(\not{p}_3 - \not{k}_{12})\gamma^\alpha}{\rho_3(-k_2)\rho_3(-k_{12})} + \frac{\gamma^\mu(\not{p}_3 - \not{k}_1)\gamma^\nu(\not{p}_3 - \not{k}_{12})\gamma^\alpha}{\rho_3(-k_1)\rho_3(-k_{12})} \Bigg\} |1] \,, \end{aligned} \tag{19.51}$$

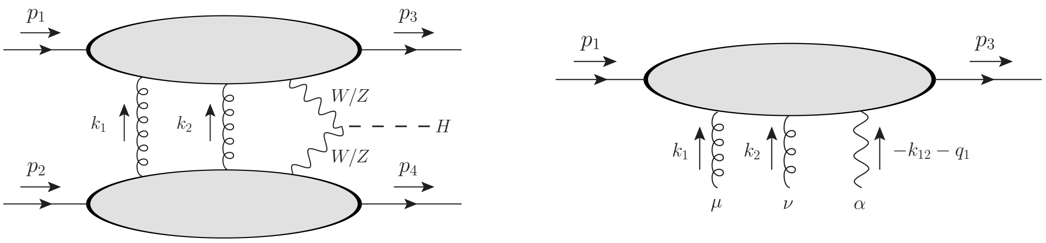

Figure 19.2: Similar to the computation of the one-loop amplitude, we think of the two-loop amplitude, shown on the left, in terms of the two quark currents that make it up. The convention for momentum assignment are presented for the upper current on the right. The lower current is defined in an analogous way.

and

$$
\begin{aligned}
&\tilde{J}_{\mu\nu\alpha}(-k_1, -k_2, k_{12} - q_2) = \langle 4| \Bigg\{ \\
&\frac{\gamma^\alpha(\slashed{p}_2 - \slashed{k}_{12})\gamma^\nu(\slashed{p}_2 - \slashed{k}_1)\gamma^\mu}{\rho_2(-k_{12})\rho_2(-k_1)} + \frac{\gamma^\alpha(\slashed{p}_2 - \slashed{k}_{12})\gamma^\mu(\slashed{p}_2 - \slashed{k}_2)\gamma^\nu}{\rho_2(-k_{12})\rho_2(-k_2)} \\
&+ \frac{\gamma^\nu(\slashed{p}_4 + \slashed{k}_2)\gamma^\alpha(\slashed{p}_2 - \slashed{k}_1)\gamma^\mu}{\rho_4(k_2)\rho_2(-k_1)} + \frac{\gamma^\mu(\slashed{p}_4 + \slashed{k}_1)\gamma^\alpha(\slashed{p}_2 - \slashed{k}_2)\gamma^\nu}{\rho_4(k_1)\rho_2(-k_2)} \\
&+ \frac{\gamma^\nu(\slashed{p}_4 + \slashed{k}_2)\gamma^\mu(\slashed{p}_4 + \slashed{k}_{12})\gamma^\alpha}{\rho_4(k_2)\rho_4(k_{12})} + \frac{\gamma^\mu(\slashed{p}_4 + \slashed{k}_1)\gamma^\nu(\slashed{p}_4 + \slashed{k}_{12})\gamma^\alpha}{\rho_4(k_1)\rho_4(k_{12})} \Bigg\} |2] \,.
\end{aligned}
\tag{19.52}
$$

We consider the Sudakov decomposition of both loop momenta

$$
k_i = \alpha_i p_1 + \beta_i p_2 + k_{i,\perp}\,, \quad i = 1, 2\,. \tag{19.53}
$$

We extend the definitions of the quantities which depend on the transverse components of the loop momenta

$$
\begin{aligned}
&\Delta_i = -\mathbf{k}_{i,\perp}^2\,, \;\; \Delta_{3,i} = -(\mathbf{k}_{i,\perp} - \mathbf{p}_{3,\perp})^2 - m_V^2\,, \;\; \Delta_{4,i} = -(\mathbf{k}_{i,\perp} + \mathbf{p}_{4,\perp})^2 - m_V^2\,, \\
&\Theta_{3,i} = -\left(\mathbf{k}_{i,\perp}^2 - 2\mathbf{k}_{i,\perp}\cdot\mathbf{p}_{3,\perp}\right)\,, \;\; \Theta_{4,i} = -\left(\mathbf{k}_{i,\perp}^2 + 2\mathbf{k}_{i,\perp}\cdot\mathbf{p}_{4,\perp}\right)\,,
\end{aligned}
\tag{19.54}
$$

where $i \in \{1, 2, 12\}$. Similarly, we define $\alpha_{12} = \alpha_1 + \alpha_2$, $\beta_{12} = \beta_1 + \beta_2$ for later purpose.

At two-loop level, the scaling of each loop momentum is given by the same kinematic regions, defined in Table 19.1. Naturally, we expect that the Glauber region where $\alpha_1 \sim \beta_1 \sim \alpha_2 \sim \beta_2 \sim \lambda$ and $|\mathbf{k}_{1,\perp}| \sim |\mathbf{k}_{2,\perp}| \sim \sqrt{\lambda}$ to provide the leading contribution. Then, analogously to the one-loop case, we expect the sub-leading corrections to be provided by either one or both loop momenta being in the Glauber-soft region. In what follows, we will talk about it as the mixed region and there is several configurations that we will now discuss.

First of all, for all these configurations, we can discard the loop momentum on the numerator of the currents in Eq. (19.51) and Eq. (19.52) for the same reasons as in the one-loop case. Then, among the different combinations of scaling of the loop momenta, only the one where one of both β's scaling as $\sqrt{\lambda}$ and both α's scale as λ (and vice versa) contributes. Indeed, if one of the α's and one of the β's scale as $\sqrt{\lambda}$, then k_{12} is soft. In this case, both currents in Eqs. (19.51)-(19.52) receive $\mathcal{O}(\sqrt{\lambda})$ relative corrections, leading to an overall scaling λ^{-1}. As the result, if we consider corrections to one of the currents, then the other current has to be considered to the leading order.

Following the observation made at one-loop order in Eq. (19.43), we expand the propagators such that they contain both the leading and the sub-leading terms of the Glauber region and only the leading order terms in the mixed region because we already have $\mathcal{O}(\sqrt{\lambda})$ relative corrections from one of the current. We find

$$\begin{aligned}
&d_{1,2} \approx \Delta_{1,2} + i\epsilon\,, \qquad d_3 \approx s\delta_3(\beta_{12} - \beta_3) + \Delta_{3,12} + i\epsilon\,,\\
&d_4 \approx -s\delta_4(\alpha_{12} + \alpha_4) + \Delta_{4,12} + i\epsilon\,,\\
&\rho_1(k_i) \approx s\beta_i + \Delta_i + i\epsilon\,, \qquad \rho_3(k_i) \approx s\alpha_3\beta_3 + \Theta_{3,i} + i\epsilon\,,\\
&\rho_2(k_i) \approx s\alpha_i + \Delta_i + i\varepsilon\,, \qquad \rho_4(k_i) \approx s\beta_4\alpha_i + \Theta_{4,i} + i\epsilon\,.
\end{aligned} \tag{19.55}$$

The colour-stripped two-loop amplitude in this region is expressed as

$$\mathcal{A}_2^{a\&b} = \frac{1}{2!}\langle 3|\gamma^\alpha|1]\langle 4|\gamma_\alpha|2] \int \frac{d^{d-2}\mathbf{k}_{1,\perp}}{(2\pi)^{d-2}} \frac{d^{d-2}\mathbf{k}_{2,\perp}}{(2\pi)^{d-2}} \frac{1}{\Delta_1\Delta_2\Delta_{3,12}\Delta_{4,12}}\, \Phi\, \tilde{\Phi}\,, \tag{19.56}$$

where the integration over the α's and the β's factorise. In Eq. (19.56), we defined

$$\begin{aligned}
\Phi = \int \frac{d\beta_1}{2\pi i}\frac{d\beta_2}{2\pi i}\frac{\Delta_{3,12}}{s\delta_3(\beta_{12}-\beta_3)+\Delta_{3,12}+i\epsilon}&\left\{\frac{1}{(\beta_{12}+\frac{\Delta_{12}}{s}+i\varepsilon)(\beta_1+\frac{\Delta_1}{s}+i\epsilon)}\right.\\
+\frac{1}{(\beta_{12}+\frac{\Delta_{12}}{s}+i\epsilon)(\beta_2+\frac{\Delta_2}{s}+i\epsilon)}&+\frac{1}{(-\beta_2+\frac{\Theta_{3,2}}{s\alpha_3}+i\epsilon)(\beta_1+\frac{\Delta_1}{s}+i\epsilon)}\\
+\frac{1}{(-\beta_1+\frac{\Theta_{3,1}}{s\alpha_3}+i\epsilon)(\beta_2+\frac{\Delta_2}{s}+i\epsilon)}&+\frac{1}{(-\beta_2+\frac{\Theta_{3,2}}{s\alpha_3}+i\epsilon)(-\beta_{12}+\frac{\Theta_{3,12}}{s\alpha_3}+i\epsilon)}\\
\left.+\frac{1}{(-\beta_1+\frac{\Theta_{3,1}}{s\alpha_3}+i\epsilon)(-\beta_{12}+\frac{\Theta_{3,12}}{s\alpha_3}+i\epsilon)}\right\}&,
\end{aligned} \tag{19.57}$$

and

$$\begin{aligned}\tilde{\Phi} = \int \frac{d\alpha_1}{2\pi i}\frac{d\alpha_2}{2\pi i}\frac{\Delta_{4,12}}{-s\delta_4(\alpha_4+\alpha_{12})+\Delta_{4,12}+i\epsilon}&\Bigg\{\frac{1}{(-\alpha_{12}+\frac{\Delta_{12}}{s}+i\varepsilon)(-\alpha_1+\frac{\Delta_1}{s}+i\epsilon)}\\ +\frac{1}{(-\alpha_{12}+\frac{\Delta_{12}}{s}+i\varepsilon)(-\alpha_2+\frac{\Delta_2}{s}+i\epsilon)}&+\frac{1}{(\alpha_2+\frac{\Theta_{4,2}}{s\beta_4}+i\varepsilon)(-\alpha_1+\frac{\Delta_1}{s}+i\epsilon)}\\ +\frac{1}{(\alpha_1+\frac{\Theta_{4,1}}{s\beta_4}+i\varepsilon)(-\alpha_2+\frac{\Delta_2}{s}+i\epsilon)}&+\frac{1}{(\alpha_2+\frac{\Theta_{4,2}}{s\beta_4}+i\varepsilon)(\alpha_{12}+\frac{\Theta_{4,12}}{s\beta_4}+i\epsilon)}\\ +\frac{1}{(\alpha_1+\frac{\Theta_{4,1}}{s\beta_4}+i\varepsilon)(\alpha_{12}+\frac{\Theta_{4,12}}{s\beta_4}+i\epsilon)}\Bigg\}&. \end{aligned} \tag{19.58}$$

Before integrating, it is convenient to rewrite the terms in curly bracket in Eq. (19.57) as

$$\begin{aligned}\Big\{\dots.\Big\} \to & \frac{\frac{\Delta_1}{s}+\frac{\Delta_2}{s}-\frac{\Delta_{12}}{s}}{(\beta_{12}+\frac{\Delta_{12}}{s}+i\epsilon)(\beta_1+\frac{\Delta_1}{s}+i\epsilon)(\beta_2+\frac{\Delta_2}{s}+i\epsilon)}\\ &+\frac{\frac{\Theta_{3,1}}{\alpha_3 s}+\frac{\Theta_{3,2}}{\alpha_3 s}-\frac{\Theta_{3,12}}{\alpha_3 s}}{(-\beta_{12}+\frac{\Theta_{3,12}}{\alpha_3 s}+i\epsilon)(-\beta_1+\frac{\Theta_{3,1}}{\alpha_3 s}+i\epsilon)(-\beta_2+\frac{\Theta_{3,2}}{\alpha_3 s}+i\epsilon)}\\ &+\left(\frac{1}{\beta_1+\frac{\Delta_1}{s}+i\epsilon}+\frac{1}{-\beta_1+\frac{\Theta_{3,1}}{s\alpha_3}+i\epsilon}\right)\left(\frac{1}{\beta_2+\frac{\Delta_2}{s}+i\epsilon}+\frac{1}{-\beta_2+\frac{\Theta_{3,2}}{s\alpha_3}+i\epsilon}\right).\end{aligned} \tag{19.59}$$

We consider the integration of each term in Eq. (19.59) separately. The first one is trivially zero because all the poles are located in the lower half of the complex plane

$$\begin{aligned}\Phi_1 = & \int \frac{d\beta_1}{2\pi i}\frac{d\beta_2}{2\pi i}\frac{\Delta_{3,12}}{s\delta_3(\beta_{12}-\beta_3)+\Delta_{3,12}+i\epsilon}\\ &\times\frac{\frac{\Delta_1}{s}+\frac{\Delta_2}{s}-\frac{\Delta_{12}}{s}}{(\beta_{12}+\frac{\Delta_{12}}{s}+i\epsilon)(\beta_1+\frac{\Delta_1}{s}+i\epsilon)(\beta_2+\frac{\Delta_2}{s}+i\epsilon)}=0\,.\end{aligned} \tag{19.60}$$

The second term of Eq. (19.59) can be integrated by closing the integration contour in the lower half of the complex plane for both β_1 and β_2. We find

$$\begin{aligned}\Phi_2 = & \int \frac{d\beta_1}{2\pi i}\frac{d\beta_2}{2\pi i}\frac{\Delta_{3,12}}{s\delta_3(\beta_{12}-\beta_3)+\Delta_{3,12}+i\epsilon}\\ &\times\frac{\frac{\Theta_{3,1}}{\alpha_3 s}+\frac{\Theta_{3,2}}{\alpha_3 s}-\frac{\Theta_{3,12}}{\alpha_3 s}}{(-\beta_{12}+\frac{\Theta_{3,12}}{\alpha_3 s}+i\epsilon)(-\beta_1+\frac{\Theta_{3,1}}{\alpha_3 s}+i\epsilon)(-\beta_2+\frac{\Theta_{3,2}}{\alpha_3 s}+i\epsilon)}\\ &=\frac{\delta_3(\Theta_{3,1}+\Theta_{3,2}-\Theta_{3,12})}{\Delta_{3,12}}\,.\end{aligned} \tag{19.61}$$

Finally, the third term of Eq. (19.59) is easily evaluated by closing the contour in the upper half of the complex plane. It reads

$$\begin{aligned}\Phi_3 &= \int \frac{d\beta_1}{2\pi i}\frac{d\beta_2}{2\pi i}\frac{\Delta_{3,12}}{s\delta_3(\beta_{12}-\beta_3)+\Delta_{3,12}+i\epsilon}\\ &\times\left(\frac{1}{\beta_1+\frac{\Delta_1}{s}+i\epsilon}+\frac{1}{-\beta_1+\frac{\Theta_{3,1}}{s\alpha_3}+i\epsilon}\right)\left(\frac{1}{\beta_2+\frac{\Delta_2}{s}+i\epsilon}+\frac{1}{-\beta_2+\frac{\Theta_{3,2}}{s\alpha_3}+i\epsilon}\right)\\ &= \frac{\Delta_{3,12}}{s\delta_3(\frac{\Theta_{3,1}}{s}+\frac{\Theta_{3,2}}{s}-\beta_3)+\Delta_{3,12}} \approx 1-\frac{\delta_3(\Theta_{3,1}+\Theta_{3,2}-s\beta_3)}{\Delta_{3,12}}\,.\end{aligned} \tag{19.62}$$

The current Φ is given by the sum of Eq. (19.60), Eq. (19.61), and Eq. (19.62). We find

$$\Phi = \sum_{i=1}^{3}\Phi_i = 1-\frac{\delta_3(\Theta_{3,12}-s\beta_3)}{\Delta_{3,12}}\,. \tag{19.63}$$

Similarly, the other current is found to be

$$\tilde{\Phi} = 1-\frac{\delta_3(\Theta_{4,12}-s\alpha_4)}{\Delta_{4,12}}\,. \tag{19.64}$$

The contribution from the Glauber and the mixed regions to the two-loop amplitude in Eq. (19.56) becomes

$$\begin{aligned}\mathcal{A}_2^{a\&b} &= -\frac{1}{2!}\langle 3|\gamma^\alpha|1]\langle 4|\gamma_\alpha|2]\int\frac{d^{d-2}\mathbf{k}_{1,\perp}}{(2\pi)^{d-2}}\frac{d^{d-2}\mathbf{k}_{2,\perp}}{(2\pi)^{d-2}}\frac{1}{\Delta_1\Delta_2\Delta_{3,12}\Delta_{4,12}}\\ &\times\left[1+\frac{\delta_3}{\Delta_{3,12}}\left(s\beta_3-\Theta_{3,12}\right)+\frac{\delta_4}{\Delta_{4,12}}\left(s\alpha_4-\Theta_{4,12}\right)\right]\,.\end{aligned} \tag{19.65}$$

Similar to Eq. (19.45), the non-factorisable, two-loop amplitude factorises to the Born. We write the amplitude $\mathcal{M}_2$ from Eq. (19.48) as

$$\mathcal{M}_2 = -\frac{1}{2}\frac{g_s^4}{(4\pi)^2}\left(\frac{1}{2}\{T^a,T^b\}\right)_{i_3i_1}\left(\frac{1}{2}\{T^a,T^b\}\right)_{i_4i_2}\mathcal{M}_0\,\mathcal{C}_2\,, \tag{19.66}$$

where the integral over the transverse components of the loop momenta reads

$$\boxed{\begin{aligned}\mathcal{C}_2 &= \int\frac{d^{d-2}\mathbf{k}_{1,\perp}}{\pi(2\pi)^{-2\epsilon}}\frac{d^{d-2}\mathbf{k}_{2,\perp}}{\pi(2\pi)^{-2\epsilon}}\frac{(\mathbf{p}_{3,\perp}^2+m_V^2)(\mathbf{p}_{4,\perp}^2+m_V^2)}{\Delta_1\Delta_2\Delta_{3,12}\Delta_{4,12}}\\ &\times\left[1-\delta_3\left(\frac{m_V^2}{\mathbf{p}_{3,\perp}^2+m_V^2}+\frac{m_V^2}{\Delta_{3,12}}\right)-\delta_4\left(\frac{m_V^2}{\mathbf{p}_{4,\perp}^2+m_V^2}+\frac{m_V^2}{\Delta_{4,12}}\right)\right]\,.\end{aligned}} \tag{19.67}$$

The result in Eq. (19.66) contains the contribution of both the Glauber and the mixed regions. Similar to the one-loop case, the soft and the collinear region do not contribute at two-loop level. The arguments are analogous to the one-loop case and they rely on additional suppressions that occur only when one first combines the diagrams before integrating. For instance, if one of the loop momentum is soft and the other one is in the Glauber region, then k_{12} is also soft. In this case, both currents receive $\mathcal{O}(\sqrt{\lambda})$ corrections. Indeed, if we consider the current in Eq. (19.59), we see that the last term, which is dominant as it naively scales as $\lambda^{-3/2}$, is in fact additionally suppressed once the pole in $\beta_1 = 0$ has been ignored, in analogy to Eq. (19.41). Since the same argument holds for the other current $\tilde{\Phi}$, this region only start at $\mathcal{O}(\lambda^{-1})$.

19.4 IR POLE CANCELLATION AND FINITE REMAINDER

The loop integrals in the transverse plane $\mathcal{C}_1$ in Eq. (19.47) and $\mathcal{C}_2$ in Eq. (19.67) are calculated analytically using differential equations method, introduced in Appendix C.[2] $\mathcal{C}_1$ is required to $\mathcal{O}(\varepsilon)$ because $\mathcal{M}_1$, which will contribute once squared, has a $1/\varepsilon$ pole of soft origin.[3] On the other hand, the $\mathcal{C}_2$ up to finite order in ε. The final expression for $\mathcal{C}_1$ and $\mathcal{C}_2$ contains at most dilogarithm functions.[4].

When we have discussed the evaluation of the double-virtual contribution to t-channel single top production in Sec. 13.5, we argued that real-emission contribution are suppressed by a factor $p_\perp^2/s \sim \lambda$ if the limit where the top quark is massless. In the case of the WBF, this suppression is exact because the external partons are massless. Thus, the double-virtual contribution is free of infrared pole of soft origin up to the next-to-leading order in the eikonal approximation. This can also be seen from the form of the Catani's operator applied to non-factorisable corrections, see Eq. (18.7). As explained in Ref. [7], the poles that we get are related to the fact that the exchanged gluons are static [184]. These poles are expected to cancel at the level of the cross section. We write

$$d\hat{\sigma}_{\rm nf}^{\rm NNLO} = \frac{N_c^2-1}{4N_c^2}\,\alpha_s^2\,\mathcal{C}_{\rm nf}\;d\hat{\sigma}^{\rm LO}\,, \tag{19.68}$$

where

$$\mathcal{C}_{\rm nf} = \mathcal{C}_1^2 - \mathcal{C}_2\,. \tag{19.69}$$

We find that the two coefficients assume the following expansions in ε

$$\begin{aligned}\mathcal{C}_1 &= -\frac{1}{\varepsilon} + \mathcal{C}_{1,0} + \varepsilon\,\mathcal{C}_{1,1} + \mathcal{O}(\varepsilon^2)\,,\\ \mathcal{C}_2 &= \frac{1}{\varepsilon^2} - \frac{2}{\varepsilon}\mathcal{C}_{1,0} + \mathcal{C}_{2,0} + \mathcal{O}(\varepsilon)\,.\end{aligned} \tag{19.70}$$

---

[2] We report the reader to the Appendix of Ref. [161] for details about the analytic calculation of $\mathcal{C}_1$ and $\mathcal{C}_2$.

[3] See Chapter 13 for a discussion about the pole structure of the double-virtual contribution for non-factorisable corrections.

[4] We point out that the analytic expressions of these functions in the eikonal approximation ($\delta_{3,4} \to 0$) has been recently calculated [183].

The pole cancellation is explicit and we write the coefficient of the non-factorisable, double-virtual contribution as

$$\boxed{\mathcal{C}_{\text{nf}} = \mathcal{C}_{1,0}^2 - 2\,\mathcal{C}_{1,1} - \mathcal{C}_{2,0}\,.} \tag{19.71}$$

The analytic expression of $\mathcal{C}_{\text{nf}}$ can be found in the ancillary file of Ref. [161].

19.5 NUMERICAL RESULTS

Our results can be checked in different ways. First, at leading order in the eikonal limit, i. e. $\delta_{3,4} = 0$, we compare numerically the expression of $\mathcal{C}_{\text{nf}}$ to the one computed in Ref. [7] and find agreement. Then, it is interesting to determine the accuracy of the sub-eikonal contribution by comparing it to the exact amplitude. Since this is obviously not possible at two-loop level, we focus on the one-loop amplitude.

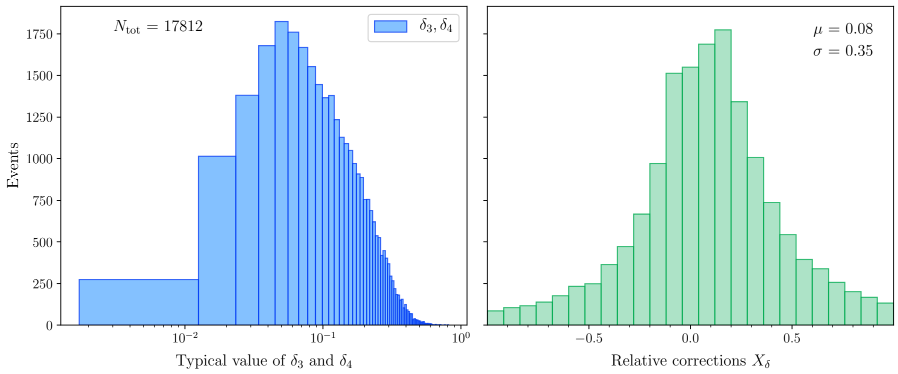

Figure 19.3: On the left, we show the distribution of the typical values of δ_3 and δ_4 for points passing the WBF cuts and $y_H < 1$ in the partonic centre-of-mass frame. On the right, we show the distribution of X_δ as defined in Eq. (19.72).

Using the van Neerven-Vermaseren basis[5] [152] and the Passarino-Veltman reduction [80], we reduce the one-loop amplitude $\mathcal{A}^{(1)}$ to a set of scalar integral, which are evaluated at any phase-space points using `LoopTools` [185]. We define the following quantity

$$X_\delta = \frac{\mathcal{A}_1 - \mathcal{A}_1^{a\&b}}{\mathcal{A}_1^{a\&b} - \mathcal{A}_1^{(0)}}\,, \tag{19.72}$$

where we defined the one-loop amplitude in the eikonal approximation as

$$\mathcal{A}_1^{(0)} = -\langle 3|\gamma^\mu|1]\langle 4|\gamma_\mu|2] \int \frac{d^{d-2}\mathbf{k}_{1,\perp}}{(2\pi)^{d-2}} \frac{1}{\Delta_1\Delta_{3,1}\Delta_{4,1}}\,, \tag{19.73}$$

---

[5] The van Neerven-Vermaseren has already been introduced in Chapter 14.

which is given by Eq. (19.45) with $\delta_{3,4} = 0$. We expect $X_\delta \sim \sqrt{\lambda}$. The standard deviation of the distribution of X_δ also allows an estimation of the neglected contributions $\mathcal{O}(\lambda)$. To evaluate X_δ, we generate a list of phase-space points that pass WBF cuts [186] and evaluate X_δ for each of them.

We consider the standard WBF cuts where both jet should satisfy $p_{\text{jet},\perp} > 25$ GeV and have an invariant mass of at least 600 GeV. Then, we required that $y_{\text{jet}} < 4.5$ and that $|y_{j_1} - y_{j_2}| > 4.5$. In addition, the jets should be in opposite hemisphere, which is equivalent to $y_{j_1} y_{j_2} < 0$. Finally, to stay in the part of the phase space that corresponds to our approximation, we impose that $|y_h| < 1$ in the partonic centre-of-mass frame, such that δ_3 and δ_4, defined in Eq. (19.9), stay smaller than one. By doing so, we exclude around $\mathcal{O}(5\%)$ of points which were passing the WBF cuts.[6]

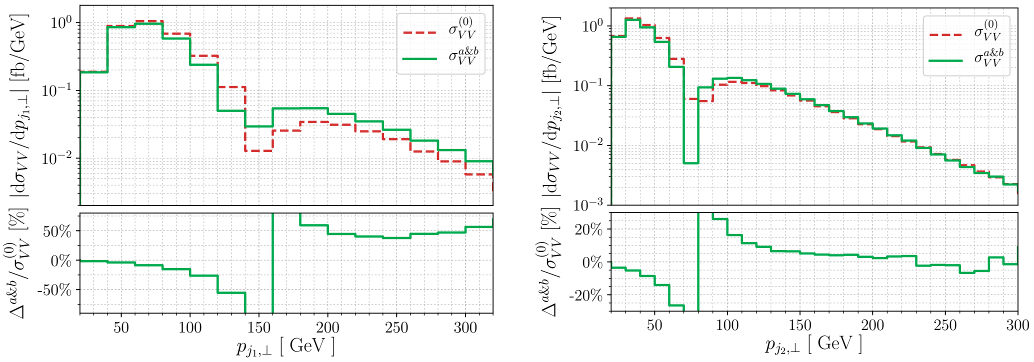

Figure 19.4: Double-virtual contribution to the absolute value of the transverse momentum distribution of the leading jet (left) and the sub-leading jet (right) in the forward limit. The leading-order contribution is plotted with a red dashed line and the sub-leading one with a green solid line. On the lower panes, we show the next-to-leading order corrections, normalised to the eikonal contribution.

On the left pane of Fig. 19.3, we see that, for most of the points, $\delta_{3,4} \sim \sqrt{\lambda} \sim 0.1$, which justifies the choice of expansion variables. On the right pane, we show the distribution of X_δ. We see that this distribution is centered around 8%, which means that the sub-eikonal corrections reproduce the evaluation of the one-loop amplitude in the forward limit. As expected, $X_\delta \sim \sqrt{\lambda}$. Then, for the majority of the points, the $\mathcal{O}(\lambda)$ terms that have been neglected amounts for $\mathcal{O}(0.3)$ of the sub-eikonal correction.

---

[6] Note that, in general, the square root in Eq. (19.9) evaluates to $\mathcal{O}(0.1)$.

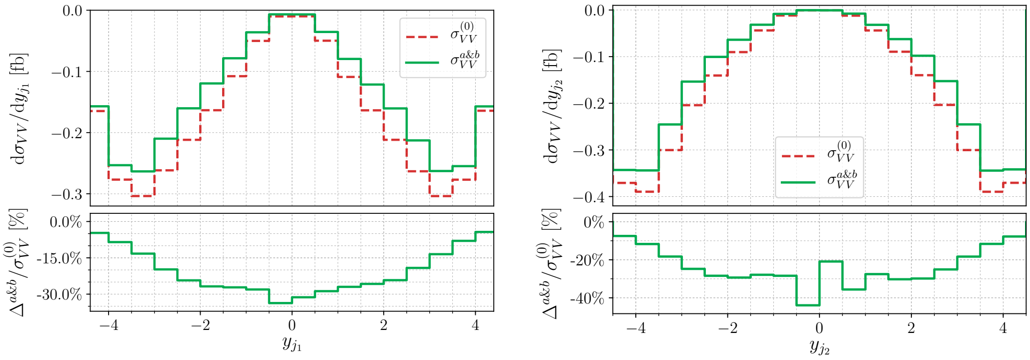

Figure 19.5: Double-virtual contribution to the rapidity distributions of the transverse momentum distribution of the leading jet (left) and the sub-leading jet (right) in the forward limit. The leading-order contribution is plotted with a red dashed line and the sub-leading one with a green solid line. On the lower panes, we show the next-to-leading order corrections, normalised to the eikonal contribution.

The non-factorisable, double-virtual contribution to Higgs boson production in WBF cross section reads

$$d\sigma = \sum_{i,j} \int dx_1\, dx_2\, f_i(x_1, \mu_F)\, d\hat{\sigma}_{nf}^{\mathrm{NNLO}}(x_1, x_2, \mu_R)\, f_j(x_2, \mu_F)\,, \tag{19.74}$$

where we consider dynamical renormalisation and factorisation scales, set to the same value

$$\mu_F = \mu_R = \frac{m_H}{2}\left(1 + \frac{4p_{H,\perp}^2}{m_H^2}\right)^{1/4}. \tag{19.75}$$

Again, for the same reasons stated in Part II, one can question that this choice of scale, which is standard for WBF studies [186], is appropriate to describe non-factorisable corrections.

We find that, in the forward limit, the non-factorisable corrections to the double-virtual contribution evaluates to

$$\boxed{\sigma_{VV} = (-3.1 + 0.53)\ \text{fb}\,,} \tag{19.76}$$

where the first number corresponds to the eikonal contribution and the second one is the corrections from the sub-eikonal terms. We note that, unlike the leading-order contribution, to evaluate the next-to-leading order corrections, we have to impose an additional cut on the Higgs rapidity in the *partonic* centre-of-mass frame to stay in the

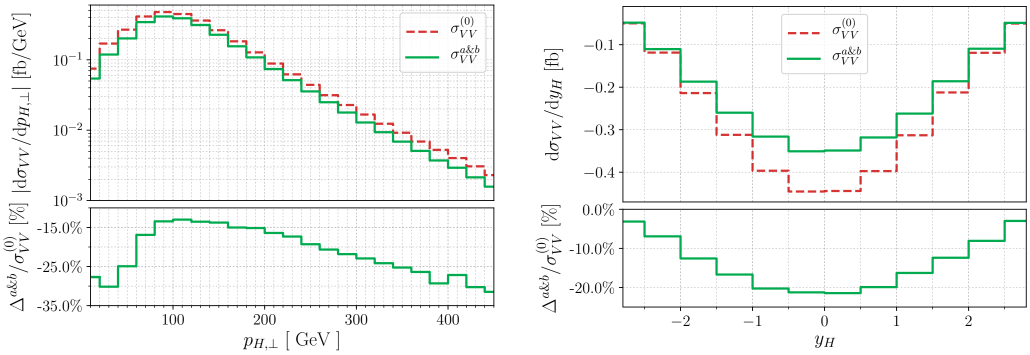

Figure 19.6: Double-virtual contribution to the absolute value of the transverse momentum of the Higgs boson (left) and to its rapidity distribution (right) in the forward limit. The leading-order contribution is plotted with a red dashed line and the sub-leading one with a green solid line. On the lower panes, we show the next-to-leading order corrections, normalised to the eikonal contribution.

forward limit, see Eq. (19.9). We find that the sub-eikonal corrections reduce the leading contribution by 17%.

In Fig. 19.4, we show the absolute value of the jet transverse momentum distributions. As observed in Ref. [7], the eikonal contribution to the transverse momentum of the leading jet and the sub-leading jet change sign around $p_{j_1,\perp} \sim 2m_V$ and $p_{j_2,\perp} \sim m_V$. For $p_{j_1,\perp} < 80$ GeV, the sub-leading contribution amounts for less than $\mathcal{O}(10\%)$, whereas the tail of the leading-jet distribution is enhanced by a constant corrections $\mathcal{O}(50\%)$. The sub-leading jet is less affected by the sub-leading contribution since, if we exclude the region where the corrections change sign, it amounts for less than $\mathcal{O}(10\%)$.

The jet-rapidity distributions, shown in Fig. 19.5, present similar characteristics. The next-to-leading order corrections reduce the leading-order contribution by $\mathcal{O}(10\%)$ around the peaks $|y_{\text{jet}}| \sim 4$. For small rapidity values, the corrections are larger as they reach $\mathcal{O}(30\%)$ for $|y_{\text{jet}}| \sim 1$. Nevertheless, contributions from this part of the phase are negligible.

In Fig. 19.6, we show observables related to the Higgs boson. The next-to-leading order corrections to the distribution of the Higgs boson transverse momentum are always larger than $\mathcal{O}(15\%)$. For small $p_{H,\perp}$, the correction reaches 30%. For large $p_{H,\perp}$, the corrections are linearly growing and also reach 30% for $p_{H,\perp} = 400$ GeV. The peak of the Higgs boson rapidity distribution is centered at $y_H \sim 0$, where the sub-eikonal contribution amounts for $\mathcal{O}(20\%)$. These corrections become less than $\mathcal{O}(10\%)$ for $|y_H| > 2$.

20 CONCLUSION

We have computed the non-factorisable, double-virtual contribution to Higgs boson production in WBF in the forward limit including next-to-leading order contribution. Unlike the t-channel single top production, the evaluation of the exact two-loop amplitude is currently infeasible. As a starting point, we referred to the calculation performed in Ref. [7] and aimed to expand upon their approach to compute sub-leading contributions.

In Chapter 18, we have studied t-channel massless single top production as a toy model. The physics of this process is indeed close to the one of Higgs boson production, but simpler because there is only two particles in the final state. By expanding the exact one-loop amplitude in the forward limit, we observed that it can be expressed in a concise form up to the next-to-leading order in the eikonal expansion. First, we computed the leading-order term following the approach outlined in Ref. [7] for this specific case. Then, we studied two methods to calculate the sub-leading corrections.

First, we demonstrated that the master integrals, which the one-loop amplitude can be reduced to, can be calculated in the forward limit using differential equations. By expanding the reduction table to the appropriate order, we successfully recovered the correct result. However, this method assumes that a reduction of the loop amplitude is possible.

To delve further, we examined the same master integrals using the expansion by regions technique [172–174]. Unlike the differential equations method, it turns out that the expansion by region can be conveniently used to work directly on Feynman diagrams. It allows us to extend the idea used in Ref. [7] to take profit of simplifications that occurs once the diagrams are summed.

In Chapter 19, we implemented the aforementioned approach to analyse the double-virtual contribution to Higgs boson production in WBF in the forward limit of the tagging jets. We showed that, among the multiple regions that would naively contribute to the next-to-leading order in the eikonal expansion, only two are actually needed.

As the result, we obtained a concise expression for the double-virtual contribution, which naturally extends the eikonal result derived in Ref. [7]. Comparing it to the t-channel massless single top production, we found that the sub-leading corrections are more significant, scaling as m_H/s or $p_{\perp,H}/s$. With realistic WBF cuts [186], we determined that the eikonal contribution decreases by $\mathcal{O}(20)$ percent, resulting in a permille corrections to the total cross section.

We note that a recent work [187] has focused on calculating the double-real and real-virtual, non-factorisable contribution to Higgs boson production in WBF. However, these contributions are highly suppressed due to the WBF cuts. Considering our findings in conjunction with the result of this reference, we conclude that the current understanding of non-factorisable effects in Higgs boson production in WBF is suitable for studying Higgs production in WBF during the HL-LHC.

21 CONCLUSION

In this thesis, we studied three problems related to precision exploration of Higgs bosons and top quarks at the Large Hadron Collider.

In Part I, we investigated the production of the Higgs boson in association with a charm quark jet. This process is considered as one of the most promising ways to measure the Yukawa coupling of the charm quark [4]. There are two mechanisms that contribute to this process: interaction of the Higgs boson with the charm quark and production of the Higgs boson in gluon fusion. For a massless charm quark, the interference between these two mechanisms vanishes. However, since the charm quark is massive, this interference does not vanish and, numerically, comprises $\mathcal{O}(10\%)$ of the Yukawa coupling contribution.

We showed that computing the NLO QCD corrections to this interference is an interesting problem. Indeed, it requires a redefinition of the parton distribution functions to account for massive partons in the initial state and forces us to explore unconventional infrared soft and collinear limits of the interference. We explained how to extract the logarithms of the charm quark mass from the different contributions using the nested soft-collinear subtraction scheme [65] and analysed their impact on the interference at NLO QCD. Although NLO QCD corrections are large, it is unlikely that they significantly affect the prospects of extracting the charm Yukawa coupling from $pp \to H + \mathrm{jet}_c$.

In Part II and Part III, we studied the non-factorisable corrections to single top and Higgs boson production in weak boson fusion. These corrections arise because of the exchange of gluons between the colliding partons, whereas, at Born level, only an exchange of a colourless boson occurs. The non-factorisable contributions were omitted in the previous studies of NNLO QCD corrections to single top and WBF processes because they are colour suppressed.

In Part II, we investigated non-factorisable effects in t-channel single top production. We have shown that the computation of real-emission contributions are simpler in non-factorisable corrections since the gluons are effectively Abelian. We employed the auxiliary mass flow method [126, 127] tailored to our problem, and successfully computed the challenging double-virtual contribution. We observed that the non-factorisable corrections are rather small but can be comparable to the NNLO QCD factorisable ones. We have shown that the virtual contributions are dominant for such corrections and that they become even more important when the centre-of-mass collision energy is increased. Computation of non-factorisable corrections formally completes the NNLO QCD description of the single top production process.

In Part III, we studied the double-virtual contribution to Higgs boson production in weak boson fusion. Because of the higher complexity of Feynman integrals in this process, exact calculation of non-factorisable corrections in this case is not feasible. Building upon the approach introduced in Ref. [7], we computed the double-virtual corrections to this process in the forward limit including next-to-leading terms in the eikonal expansions. It turns out that these corrections are quite important; they reduce earlier estimates of the non-factorisable corrections for this process at the LHC by $\mathcal{O}(20)$ percent.

Part IV

APPENDIX

A ON THEORETICAL PREDICTIONS IN PARTICLE PHYSICS

In this chapter, we present a brief and intentionally simplified overview of the journey from the mathematical formulation of the Standard Model to a theoretical prediction of physical quantities.

A.1 FEYNMAN RULES IN QCD

The Standard Model Lagrangian provides a mathematical framework for describing elementary particles' kinematics and their interactions. A complete derivation of the rules that can be extracted from this Lagrangian is the subject of many textbooks [177, 188, 189]. In this section, we follow these references and focus on the QCD Lagrangian. It reads

$$\mathcal{L}_{\text{QCD}} = -\frac{1}{4} G^A_{\mu\nu} G^{\mu\nu}_A + \sum_{\text{flavours}} \bar{\psi}_i \left(i \not{D}_{ij} + m_f \right) \psi_j - \frac{1}{2\lambda} \left(\partial_\mu A^A_\mu \right)^2 + \mathcal{L}_{\text{ghost}} , \tag{A.1}$$

where $i, j = 1, \ldots, N_c$ and $A = 1, \ldots, N_c^2 - 1$, where N_c is the number of colours. In the Standard Model, $N_c = 3$. We emphasise that we use the Einstein summation convention and, therefore, summation over pair of indices is always implied. The dynamic of the quarks field ψ is governed by the covariant derivative

$$D^\mu_{ij}(x) = \partial^\mu \delta_{ij} + i g_s \, t^A_{ij} A^{\mu,A}(x) , \tag{A.2}$$

which is defined such that the gauge symmetry $SU(3)_c$ holds locally. The object t^A_{ij} are the representation of the generator of the related Lie algebra also known as Gell-Mann matrices [190]. The gluon field $A^{\mu,A}$ dynamic and self-interaction is dictated by the strength field tensor

$$G^A_{\mu\nu} = \partial_\mu A^A_\nu - \partial_\nu A^A_\mu - g_s f^{ABC} A^B_\mu A^C_\nu , \tag{A.3}$$

where the structure constant f^{ABC} is an antisymmetric tensor. It is characteristic of the commutator defining the corresponding Lie algebra

$$[t^A, t^B] = i f^{ABC} \, t^C . \tag{A.4}$$

Finally, the last term in the QCD Lagragian in Eq. (A.1) is the gauge fixing term. It is required to eliminate the unphysical polarisations of the gluon field. It is standard to work in Feynman gauge with $\lambda = 1$ and it will be assumed in what follows. Note that this gauge is insufficient to fully cure the unphysical degree of freedom. The term $\mathcal{L}_{\text{ghost}}$ in Eq. (A.1), which contains additional Grassmann fields c and $\bar{c}$ named ghosts, needs to be added to the theory

$$\mathcal{L}_{\text{ghost}} = \partial_\mu \bar{c}^A \partial^\mu c^A + g_s f^{ABC} \left(\partial^\mu \bar{c}^A\right) A_\mu^B c^C \,. \tag{A.5}$$

We see that ghosts are intimately related to the non-Abelian nature of QCD as their interaction with the gluon field is proportional to the structure constant f^{abc}.

From the QCD Lagrangian, it is possible to extract different Feynman rules such as the propagator of the gluon

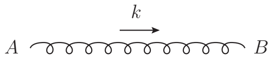

$$= \frac{i\eta_{\mu\nu}\delta_{AB}}{k^2 + i0} \,. \tag{A.6}$$

which is here represented in momentum space. As the Lagrangian describes a theory where the particles interact, one can derive interaction vertices such as the fermion-fermion-gluon vertex

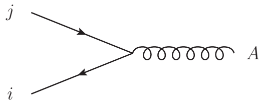

$$= i g_s \, t_{ij}^A \,, \tag{A.7}$$

or the triple gluon vertex

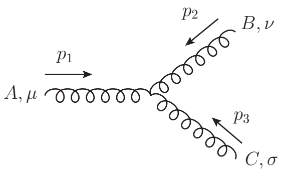

$$= -g_s f^{ABC} \Big[\eta^{\mu\nu}(p_1 - p_2)^\sigma + \eta^{\nu\sigma}(p_2 - p_3)^\mu + \eta^{\sigma\mu}(p_3 - p_1)^\nu \Big] \,. \tag{A.8}$$

Using elementary Feynman rules, one can describe any interactions in Nature by drawing Feynman diagrams. The sum of all Feynman diagrams representing a process is a complex number called the *amplitude*. It is clear that there is an infinite amount of diagrams that can describe a process and, therefore, an exact computation of the amplitude is impossible. We assume that the coupling constant is small enough to perform a *perturbative expansion*. Diagrams with the least amount of interactions make up the *Born* amplitude. Radiative corrections to this leading-order term are then classified into *real-emission contributions*, where additional particles are present in the final state, and into *virtual contributions*, where the Born diagram are dressed with loop corrections.

A.2 UV DIVERGENCES

Virtual and real-emission corrections can display divergences. For instance, the following diagram

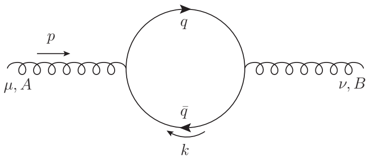

$$= g_s^2 T_F\, \delta_{AB} \varepsilon_\mu \varepsilon_\nu \int \frac{d^d k}{(2\pi)^d} \mathrm{Tr} \left\{ \frac{1}{\not{k}} \gamma^\mu \frac{1}{\not{k} + \not{p}} \gamma^\nu \right\} , \tag{A.9}$$

is divergent as the energy of the quark pair becomes infinite. This kind of divergences is called ultraviolet (UV) divergences. The renormalisation of the bare parameter of the theory, such as the masses, the couplings and the wave-function normalisations, curses these divergences. The price to pay is the introduction of a renormalisation scale μ_R, on which all the renormalised parameters will depend. The dependence of the couplings on the renormalisation scale is dictated by the β function

$$\mu \frac{d}{d\mu_R} g(\mu_R) = \beta(g) \,. \tag{A.10}$$

In QED, it simply reads

$$\beta(\alpha) = \frac{2\alpha^2(\mu_R)}{3\pi} + \mathcal{O}(\alpha^4) \,, \tag{A.11}$$

where $\alpha = e^2/(4\pi)$ and e is the electric charge. It is clear that the coupling becomes infinitely large as $\mu_R \to \infty$. The situation is different for QCD since

$$\beta(\alpha_s) = \frac{\alpha_s}{\pi} \left(-\frac{11}{3} N_c + \frac{n_f}{3} \right) + \mathcal{O}(\alpha_s^4) \,, \tag{A.12}$$

where n_f is the number of quarks flavors. Since $n_f < 11N_c/2$ in the SM, the beta function is negative. Consequently, the larger the renormalisation scale, the weaker the strong coupling. This is known as the *asymptotic freedom* [191, 192]. At sufficiently high-energy values, or, equivalently, small distances, quarks can be considered as free particles. However, there exists a pole at low energy values where the strong coupling constant diverges. This pole, called a Landau pole, is situated around $\Lambda_{QCD} \sim \mathcal{O}(100)$ MeV, which corresponds to the mass of the pions. At this energy level, the coupling is so strong that the quarks cannot be separated. This is known as *colour confinement*.

If we work at an energy scale $\Lambda_{QED} \gg Q \gg \Lambda_{QCD}$, both the strong and the weak couplings are small and can be chosen as expansion parameters. Again, for conciseness, we only consider the expansion in the strong coupling

$$|\mathcal{M}(q_1, \dots, q_n)|^2 = \sum_{n=0}^{\infty} \left(\frac{\alpha_s}{2\pi} \right)^n |\mathcal{M}^{(n)}(q_1, \dots, q_n)| \,. \tag{A.13}$$

The amplitude of a process can be directly related to its likelihood. The smaller is the norm of the amplitude, the more unlikely is the considered process.

A.3 PREDICTIONS FOR HADRONIC CROSS SECTION

We need to relate the amplitude to physical quantities that can be measured. The essential quantity computed for collider physics is the physical cross-section. In the case of the LHC, we are colliding two protons. The *factorisation theorem* [49] states that

$$\sigma = \sum_{i,j} \int dx_1\, dx_2\, f_i(x_1, \mu_F)\, f_j(x_2, \mu_F)\, d\hat{\sigma}_{ij}(x_1, x_2) \left[1 + \mathcal{O}\left(\frac{\Lambda_{\mathrm{QCD}}}{Q}\right)\right] . \tag{A.14}$$

where σ is the physical cross section σ, $f_i(x_1, \mu_F)$ are the parton distribution functions, and $\hat{\sigma}$ is the partonic cross section. The PDFs, which are empirically determined, describe the distribution of partons (light quarks, gluons, and photons) in the proton at the factorisation scale μ_F. The indices i and j runs over the parton types. The multiplicative factor on the right-hand side of Eq. (A.14) reminds us that this formula is valid only if the non-perturbative effect can be neglected.

The partonic cross section can be calculated order by order in the expansion of the coupling constant α_s by considering the appropriate set of Feynman diagrams. Tremendous efforts have been made to improve the precision of the partonic cross section. Today, corrections to most of the processes of interest for the LHC are known to the NNLO in the strong coupling constant.

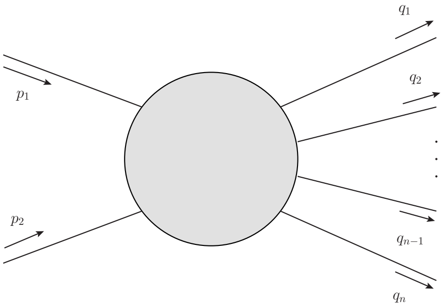

Figure A.1: Generic process where two incoming partons produce n outgoing particles.

To understand how to compute the partonic cross section, we consider a generic process where two incoming partons produce n outgoing particles

$$p_1^\mu = x_1 P_1^\mu, \quad p_2^\mu = x_2 P_2^\mu , \tag{A.15}$$

where P_1^μ and P_2^μ are the proton 4-momenta and x_1 and x_2 are the Bjorken x momentum fractions. The outgoing momenta are denoted $q_1, \ldots, q_n$. This is illustrated in Fig. A.1. The partonic cross section is computed from the integration of the amplitude $\mathcal{M}$ over the phase space of the outgoing particles

$$d\hat{\sigma}_{ij} = \frac{1}{2\hat{s}} \int d\text{Lips}(q_1, \ldots, q_n)\, |\mathcal{M}(q_1, \ldots, q_n)|^2 \mathcal{F}_{kin}(q_1, \ldots, q_n)\,, \tag{A.16}$$

where $\mathcal{F}_{kin}$ is some IR-safe observable which will be defined later and $\hat{s} = x_1 x_2 s$ is the partonic invariant mass. The Lorentz invariant phase space dLips can be defined as

$$\begin{aligned} d\text{Lips} &= \prod_{i=1}^{n} \left\{ \frac{d^d q_i}{(2\pi)^{d-1}} \delta_+ \left(q_i^2 - m_i^2\right) \right\} (2\pi)^4 \delta^{(4)} \left(p_1 + p_2 - \sum_{i=1}^{n} q_i \right) \\ &\equiv \prod_{i=1}^{n} [dq_i] (2\pi)^4 \delta^{(4)} \left(p_1 + p_2 - \sum_{i=1}^{n} q_i \right) , \end{aligned} \tag{A.17}$$

where $q_i^2 = m_i^2$ defined the mass of the outgoing particles. We have introduced a convenient notation for the individual phase space integral. It reads

$$[dq_i] = \frac{d^d q_i}{(2\pi)^{d-1}} \delta_+ \left(q_i^2 - m_i^2\right) = \frac{d^{d-1} \vec{q}_i}{2E_i (2\pi)^3}\,, \tag{A.18}$$

where the delta function $\delta_+(q_i^2 - m^2)$ selects the solution where the energy of the particle is positive and the energy is $E_i = \sqrt{m_i^2 + \vec{q}_i^{\,2}}$. The integration over the outgoing particle phase space is not straightforward as both the squared matrix element $|\mathcal{M}|^2$ and the Lorentz-invariant phase space dLips suffer from IR singularities. These singularities occurs when a particle is soft or collinear to an other particle. For instance, the emission of a gluon from a massless quark presents both type of IR divergences

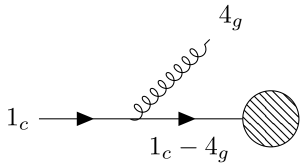

$$\propto \int \frac{[dp_4]}{p_1 \cdot p_4} \propto \int_0^\infty \frac{dE_4}{E_4} \int_{-1}^{1} \frac{d\cos\theta}{1 - \cos\theta}\,. \tag{A.19}$$

Unlike the UV divergences, the IR divergences cannot be removed. However, the *KLN theorem* [193, 194] states that for any IR-safe observable, the IR singularities cancel once both real corrections, where an additional particle is present in the final state, and virtual corrections, where the emitted particle is absorbed in the same diagram, are summed.

This feature leads to the development of subtraction schemes where the IR singularities are made explicit in every pieces of the calculations [65, 195–197]. All these schemes aim to provide a suitable way to absorb collinear emissions from initial state partons into the PDFs and to combine poles related to soft and collinear emission contributions from final state particles with the poles of the virtual contribution. These poles are made explicit by introducing a regulator, which is usually done by working in $d = 4 - 2\varepsilon$ dimensions. Once the poles are combined and the cancellation is manifest, the regulator can be dropped, resulting in quantities that can be handled numerically. As an example, in the first section of Chapter 3, we report the general NLO corrections to Higgs boson production at the LHC in the nested soft-collinear subtraction scheme, following Ref. [65].

Finally, we aim to produce theoretical predictions for physical cross sections and distributions of infrared-safe observables. We evaluate the cross section by integrating Eq. (A.14) using a Vegas integrator [78]. We randomly generate kinematical configurations to cover the complete phase space. For a given integrand, the Vegas integrator first determine numerically a change of variables that flatten the integrand and, then, perform the integration using Monte-Carlo technique. Similarly, we produce distributions of observable that can be compared to actual measurements at a particle collider.

B DETAILED INTEGRATION OF THE SOFT-QUARK EIKONAL FUNCTIONS

In this chapter, we present in details the integration of the eikonal functions originating from soft-quark singularities, discussed in Chapter 6.

B.1 INTEGRAL FROM THE SOFT-COLLINEAR SUBTRACTION TERM IN SECTOR 41 - cg CHANNEL

The cg-channel, real-emission contribution displays a soft-collinear singularity in the massless charm-quark limit when the emitted gluon 4_g is both collinear to the incoming charm quark 1_c and that its energy is zero. We consider a massive charm quark and regulate the cross section using the nested soft-collinear subtraction scheme [65], similar to Eq. (5.2) in the gg channel. The soft-collinear subtraction term in sector 41 is given by

$$\langle C_{41} S_4 F_{\mathrm{LM}}(1_c, 2_g, 3_c, 4_g)\rangle = -g_s^2 \langle\, F_{\mathrm{LM}}(1_c, 2_g, 3_c) C_{41} \int [dp_4]\, f_{\mathrm{soft}} \rangle\,, \tag{B.1}$$

where f_{soft} is the conventional soft function [50]. It reads

$$f_{\mathrm{soft}} = -C_A \frac{p_1 \cdot p_2}{p_1 \cdot p_4\, p_2 \cdot p_4} + (C_A - 2C_F) \frac{p_1 \cdot p_3}{p_1 \cdot p_4\, p_3 \cdot p_4} + C_F \frac{m_c^2}{(p_1 \cdot p_4)^2}\,. \tag{B.2}$$

The operator C_{41} acts on the eikonal functions. In this quasi-singular limit, the soft function in Eq. (B.2) reads

$$C_{41} f_{\mathrm{soft}} = -2C_F \frac{E_1}{E_4} \frac{1}{p_1 \cdot p_4} + C_F \frac{m_c^2}{(p_1 \cdot p_4)^2}\,. \tag{B.3}$$

Note that the two first eikonal functions in Eq. (B.2) are now combined and that the colour factor C_A disappeared. The integrated subtraction term to be computed is then

$$\begin{aligned} \langle C_{41} S_4 F_{\mathrm{LM}}(1_c, 2_g, 3_c, 4_g)\rangle &= -g_s^2 C_F \langle F_{\mathrm{LM}}(1_c, 2_g, 3_c)\rangle \\ &\quad \times \int [dp_4] \left(\frac{m_c^2}{(p_1 \cdot p_4)^2} - 2\frac{E_1}{E_4} \frac{1}{p_1 \cdot p_4} \right), \end{aligned} \tag{B.4}$$

where the phase-space measure needs to be considered in $d = 4 - 2\varepsilon$ since the subtraction term displays soft singularity. It reads

$$\int [dp_4] = \int \frac{d\Omega_{d-2}}{2(2\pi)^{d-1}} \int_0^{E_{\max}} dE_4\, E_4^{1-2\varepsilon} \int_{-1}^{1} d(\cos\theta) \sin^{-2\varepsilon}\theta\,. \tag{B.5}$$

The integration over the energy is trivially performed and provides a $1/\varepsilon$ pole. The mass of the emitter protects the gluon from developing another pole in ε from collinear singularity. Instead, the integral over the solid angle will result in a logarithm of the charm-quark mass. We consider the two eikonal functions with normalised 4-momenta $n_i = p_i/E_i$, $i = 1, 4$. They read

$$I_1 = \int_{-1}^{1} d(\cos\theta)\,(\sin^2\theta)^{-\varepsilon}\,\frac{1}{n_1 \cdot n_4}\,, \tag{B.6}$$

$$I_2 = \int_{-1}^{1} d(\cos\theta)\,(\sin^2\theta)^{-\varepsilon}\,\frac{m_c^2}{E_1^2}\frac{1}{(n_1 \cdot n_4)^2}\,. \tag{B.7}$$

We emphasise that the charm-quark mass is still present in the scalar product since

$$n_1 \cdot n_4 = E_1 E_4 (1 - \beta\cos\theta)\,, \tag{B.8}$$

where the velocity of the incoming parton is $\beta = \sqrt{1 - m_c^2/E_1^2}$.

It is clear that the integrals in Eq. (B.7) are singular when $\beta \to 1$. We would like to extract the leading logarithms of m_c in these two integrals and to set $m_c \to 0$, or equivalently $\beta \to 1$, in any other terms. We start with I_1. It reads

$$I_1 = \int_{-1}^{1} d(\cos\theta)\,\frac{(1 - \cos^2\theta)^{-\varepsilon}}{1 - \beta\cos\theta}\,. \tag{B.9}$$

We perform the change of variable $\cos\theta = 1 - 2\eta$ and find

$$I_1 = 2\int_0^1 d\eta\,\frac{[4\eta(1-\eta)]^{-\varepsilon}}{1 - \beta(1 - 2\eta)} = \frac{1}{\beta}\int_0^1 d\eta\,\frac{[4\eta(1-\eta)]^{-\varepsilon}}{\Delta + \eta}\,, \tag{B.10}$$

where we have defined

$$\Delta = \frac{1-\beta}{2\beta}\,. \tag{B.11}$$

This new variable Δ is a small parameter in the limit $\beta \to 1$. The factor β in front of the integral in Eq. (B.10) is safely set to one.

We know that the dependence of I_1 in Δ is logarithmic. Indeed, for $\Delta = 0$, the integrand behaves as $d\eta/\eta \sim d\ln\eta$. However, for large values of $\eta \gg \Delta$, the integral behaves as if $\Delta = 0$. We would like to take profit of this fact by supposing the existence of a parameter δ such that $\Delta \ll \delta \ll 1$ which splits the integration domain in two

$$I_1 = I_1\,\theta\,(\delta - \eta) + I_1\,\theta\,(\eta - \delta)\ . \tag{B.12}$$

The introduction of this additional parameter simplifies the computation of the integral. Once summed, the dependence on δ in the two parts of the integral has to vanish. We consider each part of the integral, keeping in mind that $\Delta \ll \delta \ll 1$. In the calculation, we discard any terms that vanish as $\delta \to 0$.

We consider the first term in Eq. (B.12). Since $\eta \ll 1$, Eq. (B.10) becomes

$$I_1\,\theta\,(\delta-\eta) = \int_0^\delta d\eta\,\frac{[4\eta(1-\eta)]^{-\varepsilon}}{\Delta+\eta} \approx 2^{-2\varepsilon}\int_0^\delta d\eta\,\frac{\eta^{-\varepsilon}}{\Delta+\eta}\,. \tag{B.13}$$

We change variable $s = \eta/\Delta$ and split the integral in two

$$\begin{aligned} I_1\,\theta\,(\delta-\eta) &= (4\Delta)^{-\varepsilon}\int_0^{\delta/\Delta} ds\,\frac{s^{-\varepsilon}}{1+s} \\ &= (4\Delta)^{-\varepsilon}\left[\int_0^\infty ds\,\frac{s^{-\varepsilon}}{1+s} - \int_{\delta/\Delta}^\infty ds\,\frac{s^{-\varepsilon}}{1+s}\right]. \end{aligned} \tag{B.14}$$

The first integral in Eq. (B.14) is calculated by changing variable $u = 1/(1+s)$ and in the second integral we use $\delta/\Delta \gg 1$. We find

$$I_1\,\theta\,(\delta-\eta) = 2^{-2\varepsilon}\left[\Delta^{-\varepsilon}\Gamma(\varepsilon)\Gamma(1-\varepsilon) - \frac{1}{\varepsilon}\delta^{-\varepsilon}\right]. \tag{B.15}$$

We consider now the second part of Eq. (B.12). We use the fact that $\eta \gg \Delta$ to write

$$\begin{aligned} I_1\,\theta\,(\eta-\delta) &= \int_\delta^1 d\eta\,\frac{[4\eta(1-\eta)]^{-\varepsilon}}{\Delta+\eta} \approx 2^{-2\varepsilon}\int_\delta^1 d\eta\,\eta^{-\varepsilon-1}(1-\eta)^{-\varepsilon} \\ &= 2^{-2\varepsilon}\int_\delta^1 d\eta\,\eta^{-\varepsilon-1}\left[(1-\eta)^{-\varepsilon}-1\right] + 2^{-2\varepsilon}\int_\delta^1 d\eta\,\eta^{-\varepsilon-1}. \end{aligned} \tag{B.16}$$

We have split the integral into two terms such that the first part is not divergent as $\varepsilon \to 0$. Thus, δ does not regulate any singularities. It means that the dependence on δ in the first part of this integral is linear. By consequence, we set $\delta = 0$ in this first part. In contrast, the second part of the integral in Eq. (B.16) is divergent as $\delta \to 0$ and therefore, it produces a logarithmic dependence on δ. We find that Eq. (B.16) becomes

$$I_1\,\theta\,(\eta-\delta) = 2^{2\varepsilon}\left[\frac{1}{\varepsilon}\delta^{-\varepsilon} + \frac{\Gamma(-\varepsilon)\Gamma(1-\varepsilon)}{\Gamma(1-2\varepsilon)}\right]. \tag{B.17}$$

As expected, by adding the result from Eq. (B.15) and Eq. (B.17), we find that the integral I_1 does not depend on the parameter δ

$$I_1 = \int_0^1 d\eta\,\frac{[4\eta(1-\eta)]^{-\varepsilon}}{\Delta+\eta} = (4\Delta)^{-\varepsilon}\Gamma(-\varepsilon)\Gamma(1-\varepsilon) + 2^{-2\varepsilon}\frac{\Gamma(-\varepsilon)\Gamma(1-\varepsilon)}{\Gamma(1-2\varepsilon)}\,. \tag{B.18}$$

The integral over the solid angle I_1 needs to be expanded to $\mathcal{O}(\varepsilon)$ since the integral over the energy of the emitted gluon has generated a $1/\varepsilon$ pole. We expand Eq. (B.18) in ε and find

$$\boxed{\begin{aligned} I_1 = 2\ln\left(\frac{2E_1}{m_c}\right) + \left[\frac{\pi^2}{3} - 4\ln(2)\ln\left(\frac{2E_1}{m_c}\right) + 2\ln^2\left(\frac{2E_1}{m_c}\right)\right]\varepsilon \\ + \mathcal{O}(\varepsilon^2) + \mathcal{O}(m_c)\,. \end{aligned}} \tag{B.19}$$

where, in the $m_c \to 0$ limit,

$$\ln(\Delta) = \ln\left(\frac{1-\beta}{2\beta}\right) = -2\ln\left(\frac{2E_1}{m_c}\right) + \mathcal{O}(m_c)\,. \tag{B.20}$$

The second integral in Eq. (B.7) that we need to determine the soft-collinear subtraction term can be treated in a similar way. It reads

$$\begin{aligned} I_2 &= \frac{m_c^2}{E_1^2}\int_{-1}^{1} d(\cos\theta)\,\frac{(\sin^2\theta)^{-\varepsilon}}{(1-\beta\cos\theta)^2} = \frac{m_c^2}{E_1^2}\frac{1}{2^{1+2\varepsilon}}\frac{1}{\beta^2}\int_0^1 d\eta\,\frac{(\eta(1-\eta))^{-\varepsilon}}{[\Delta+\eta]^2} \\ &\equiv \frac{m_c^2}{E_1^2}\frac{1}{2^{1+2\varepsilon}\beta^2}\tilde{I}_2\,, \end{aligned} \tag{B.21}$$

where we factored out the kinematic dependences to focus on the extraction of the logarithm from the quasi-collinear limit. We proceed in the same way as for I_1 by introducing a new parameter $\Delta \ll \delta \ll 1$

$$\tilde{I}_2 = \tilde{I}_2\,\theta(\delta-\eta) + \tilde{I}_2\,\theta(\eta-\delta) \tag{B.22}$$

We start with the first region where $0 < \eta < \delta$. We use this approximation to rewrite $\tilde{I}_2$ as

$$\begin{aligned} \tilde{I}_2\,\theta(\delta-\eta) &= \frac{1}{\Delta^2}\int_0^{\delta} d\eta\,\frac{\eta^{-\varepsilon}}{[1+\eta/\Delta]^2} \\ &\approx \Delta^{-1-\varepsilon}\left[\int_0^{\infty} ds\,\frac{s^{-\varepsilon}}{[1+s]^2} - \int_{\delta/\Delta}^{\infty} ds\,s^{-\varepsilon-2}\right]\,, \end{aligned} \tag{B.23}$$

where we have changed variable $s = \eta/\Delta$ and have used the fact that $1 \ll \delta/\Delta$. The first part of the integral reduces to a beta function once we change of variable $u = 1/(1+s)$ and the second part of the integral does not present any difficulties. We find that the integral in Eq. (B.23) can be written as

$$\tilde{I}_2\,\theta(\delta-\eta) = \Delta^{-1-\varepsilon} - \frac{1}{1+\varepsilon}\delta^{-1-\varepsilon}\,. \tag{B.24}$$

We consider now the integral over the second domain $[\delta, 1]$. In this region, we use the fact that $\eta \gg \Delta$ and we find

$$\begin{aligned}\tilde{I}_2\,\theta(\eta-\delta) &= \int_\delta^1 d\eta\,\eta^{-\varepsilon-2}(1-\eta)^{-\varepsilon} \\ &= \int_\delta^1 d\eta\,\eta^{-\varepsilon-2}\left[(1-\eta)^{-\varepsilon}-1\right] + \int_\delta^1 d\eta\,\eta^{-\varepsilon-2},\end{aligned} \tag{B.25}$$

where again the first integral is free of divergences as $\varepsilon \to 0$ and, therefore, the dependence in δ is at least linear. We set $\delta \to 0$ in the first integral and the second part provides $\mathcal{O}(\ln\delta)$ contribution. We find

$$\tilde{I}_2\,\theta(\eta-\delta) = \frac{\Gamma(-\varepsilon-1)\Gamma(1-\varepsilon)}{\Gamma(-2\varepsilon)} + \frac{1}{1+\varepsilon}\delta^{-1-\varepsilon}. \tag{B.26}$$

The integral I_2 from Eq. (B.21) is found by adding the result from Eq. (B.24) and the one from Eq. (B.26). It reads

$$I_2 = \frac{1}{2^{1+2\varepsilon}}\frac{1}{\beta^2}\frac{m_c^2}{E_1^2}\left[\Delta^{-1-\varepsilon} + \frac{\Gamma(-\varepsilon-1)\Gamma(1-\varepsilon)}{\Gamma(-2\varepsilon)}\right], \tag{B.27}$$

which is indeed independent of δ. In the massless charm-quark limit, the expansion of the integral in

$$\boxed{I_2 = 2 + 4\ln\left(\frac{E_1}{m_c}\right)\varepsilon + \mathcal{O}(\varepsilon^2) + \mathcal{O}(m_c).} \tag{B.28}$$

This ends the extraction of the logarithm of m_c in the case of a soft-collinear eikonal functions. In the next section, we apply a similar technique to the calculation of the integrated soft eikonal function issued from quasi-soft quark limit.

B.2 INTEGRATED QUASI-SOFT QUARK EIKONAL FUNCTIONS

In this section, we compute the following integrated eikonal function

$$I_{AB}^{(m_A,m_B)} = \int \frac{d^3\vec{p}}{(2\pi)^3 E_{\vec{p}}}\theta(E_{\max}-E_{\vec{p}})\frac{p_A\cdot p_B}{(p_A\cdot p)(p_B\cdot p)}, \tag{B.29}$$

where $p^2 = m^2$, $p_A^2 = m_A^2$ and $p_B^2 = m_B^2$. We consider this integral in the limit where $E_{\max} \gg m$ and $m \sim m_A \sim m_B$. We note that we have seen this integral in the treatment of the gg-channel real-emission contribution in Eq. (5.7). We will need both $I_{AB}^{(0,0)}$ and $I_{AB}^{(m,0)}$. We start by integrating the former.

First, we extract the energy dependence of the eikonal function

$$I_{AB}^{(0,0)} = \int \frac{d^3\vec{p}}{(2\pi)^3 2E_{\vec{p}}^3}\theta(E_{\max} - E_{\vec{p}})\frac{\bar{p}_A \cdot \bar{p}_B}{(\bar{p}_A \cdot \bar{p})(\bar{p}_B \cdot \bar{p})}\,. \tag{B.30}$$

where we define the normalised 4-vectors of the emitters as

$$\bar{p}_{A,B} = (1, \vec{n}_{A,B})^t\,, \qquad \bar{p} = (1, \beta\,\vec{n})^t\,. \tag{B.31}$$

We introduce a Feynman parametrisation of the denominator

$$\frac{1}{(\bar{p}_A \cdot \bar{p})(\bar{p}_B \cdot \bar{p})} = \int_0^1 \frac{dy}{\left[\bar{p} \cdot (\bar{p}_A y + \bar{p}_B(1-y))\right]^2}\,. \tag{B.32}$$

This is convenient to define a new 4-vector that depends on y. It reads

$$\begin{aligned} p_{AB}(y) &= (1, \vec{n}_A y + \vec{n}_B(1-y)) \\ &\equiv (1, \eta_y \vec{n}_{AB})\,, \end{aligned} \tag{B.33}$$

where we have defined

$$\eta_y = |\vec{n}_A y + \vec{n}_B(1-y)|\,. \tag{B.34}$$

We expand the phase-space measure, perform the integration over the azimuthal angle θ and change variable $\beta = \sqrt{1 - m_c^2/E_{\vec{p}}^2}$. We find that Eq. (B.30) becomes

$$I_{AB}^{(0,0)} = \frac{\mathfrak{s}^2}{2\pi^2}\int_0^{\beta_{\max}} \frac{d\beta\, \beta^2}{1-\beta^2}\int_0^1 \frac{dy}{1-\beta^2\eta_y^2}\,, \tag{B.35}$$

where we defined the constant $\mathfrak{s} \equiv \sin(\theta_{AB}/2)$ and where the integration boundary is $\beta_{\max}^2 = 1 - m^2/E_{\max}^2$.

To be able to integrate Eq. (B.35) over y, we need to understand the y dependence of η_y. We use its definition in Eq. (B.34) to write

$$\eta_y^2 = |y\vec{n}_A + (1-y)\vec{n}_B|^2 = 1 - 4y(1-y)\mathfrak{s}^2\,. \tag{B.36}$$

We focus on the y integration in Eq. (B.35). It reads

$$I_y = \int_0^1 \frac{dy}{1 - \beta(1 - 4y(1-y)\mathfrak{s}^2)}\,. \tag{B.37}$$

We use the symmetry of the integrand to reduce the integration to the range $y \in [0, 1/2]$ with a factor 2 as a trade-off. This allows, then, the following change of variable $1 - z^2 = 4y(1-y)$. The integral $I_{AB}^{(0,0)}$ in Eq. (B.35) becomes

$$I_{AB}^{(0,0)} = \frac{\mathfrak{s}}{4\pi^2}\int_0^{\beta_{\max}} \frac{d\beta\,\beta}{1-\beta^2}\frac{1}{\sqrt{1-\beta^2\mathfrak{c}^2}}\ln\left(\frac{\sqrt{1-\beta^2\mathfrak{c}^2}+\beta\mathfrak{s}}{\sqrt{1-\beta^2\mathfrak{c}^2}-\beta\mathfrak{s}}\right)\,. \tag{B.38}$$

We are left with the integration over β. We notice that

$$\frac{\partial}{\partial\beta}\ln\left(\frac{\sqrt{1-\beta^2\mathfrak{c}^2}+\beta\mathfrak{s}}{\sqrt{1-\beta^2\mathfrak{c}^2}-\beta\mathfrak{s}}\right)=\frac{2\mathfrak{s}}{\sqrt{1-\beta^2\mathfrak{c}^2}(1-\beta^2)}\,. \tag{B.39}$$

Therefore,

$$I_{AB}(0,0)=\frac{1}{16\pi^2}\int_0^{\beta_{\max}}d\beta\,\beta\,\frac{\partial}{\partial\beta}\left[\ln^2\left(\frac{\sqrt{1-\beta^2\mathfrak{c}^2}+\beta\mathfrak{s}}{\sqrt{1-\beta^2\mathfrak{c}^2}-\beta\mathfrak{s}}\right)\right]\,. \tag{B.40}$$

We perform an integration by part so that Eq. (B.40) becomes

$$\begin{aligned}I_{AB}(0,0)=\frac{1}{16\pi^2}\Bigg\{&\beta_{\max}\ln^2\left(\frac{\sqrt{1-\beta_{\max}^2\mathfrak{c}^2}+\beta_{\max}\mathfrak{s}}{\sqrt{1-\beta_{\max}^2\mathfrak{c}^2}-\beta_{\max}\mathfrak{s}}\right)\\&-\int_0^{\beta_{\max}}d\beta\ln^2\left(\frac{\sqrt{1-\beta^2\mathfrak{c}^2}+\beta\mathfrak{s}}{\sqrt{1-\beta^2\mathfrak{c}^2}-\beta\mathfrak{s}}\right)\Bigg\}\,,\end{aligned} \tag{B.41}$$

where $\beta_{\max}=\sqrt{1-m^2/E_{\max}^2}$. The argument of the first logarithm is expanded in the limit where $m\ll E_{\max}$

$$\begin{aligned}\frac{\sqrt{1-\beta_{\max}^2\mathfrak{c}^2}+\beta_{\max}\mathfrak{s}}{\sqrt{1-\beta_{\max}^2\mathfrak{c}^2}-\beta_{\max}\mathfrak{s}}&=\frac{\left(\sqrt{1-\beta_{\max}^2\mathfrak{c}^2}+\beta_{\max}\mathfrak{s}\right)^2}{1-\beta_{\max}^2}\\&=\frac{E_{\max}^2}{m^2}\left(\sqrt{1-\beta_{\max}\mathfrak{c}}+\beta_{\max}\mathfrak{s}\right)^2\approx\frac{4\mathfrak{s}^2E_{\max}^2}{m^2}\,.\end{aligned} \tag{B.42}$$

We focus on the second part of Eq. (B.41). It reads

$$I_\beta\equiv\int_0^{\beta_{\max}}d\beta\ln^2\left(\frac{\sqrt{1-\beta^2\mathfrak{c}^2}+\beta\mathfrak{s}}{\sqrt{1-\beta^2\mathfrak{c}^2}-\beta\mathfrak{s}}\right)\,. \tag{B.43}$$

We lower the degree of the logarithm by taking the derivative of the integrand with respect to $\mathfrak{s}$

$$\begin{aligned}\frac{\partial I_\beta}{\partial\mathfrak{s}}&=\int_0^{1-\delta}d\beta\,2\ln\left(\frac{\sqrt{1-\beta^2\mathfrak{c}^2}+\beta\mathfrak{s}}{\sqrt{1-\beta^2\mathfrak{c}^2}-\beta\mathfrak{s}}\right)\frac{2\beta}{\sqrt{1-\beta^2\mathfrak{c}}}\\&=-\frac{4}{\mathfrak{c}^2}\int_0^{1-\delta}d\beta\frac{\partial}{\partial\beta}\left[\sqrt{1-\beta^2\mathfrak{c}^2}\right]\ln\left(\frac{\sqrt{1-\beta^2\mathfrak{c}^2}+\beta\mathfrak{s}}{\sqrt{1-\beta^2\mathfrak{c}^2}-\beta\mathfrak{s}}\right)\,,\end{aligned} \tag{B.44}$$

where we introduce the small parameter $\delta = 1 - \beta_{\max}$. The result in Eq. (B.44) is integrated by part

$$\begin{aligned}
\frac{\partial I_\beta}{\partial \mathfrak{s}} &\approx -\frac{4}{\mathfrak{c}^2}\left\{\mathfrak{s}\ln\left(\frac{2\mathfrak{s}^2}{\delta}\right) - 2\mathfrak{s}\int_0^{1-\delta}\frac{d\beta}{1-\beta^2}\right\} \\
&= -\frac{4}{\mathfrak{c}^2}\left\{\mathfrak{s}\ln\left(\frac{2\mathfrak{s}^2}{\delta}\right) - 2\mathfrak{s}\int_0^{1-\delta} d\beta\left[\frac{1}{1-\beta} - \frac{1}{1+\beta}\right]\right\} \\
&= -\frac{4}{\mathfrak{c}^2}\left\{\mathfrak{s}\ln\left(\frac{2\mathfrak{s}^2}{\delta}\right) - 2\mathfrak{s}\ln\frac{2}{\delta}\right\} = -\frac{4\mathfrak{s}}{\mathfrak{c}^2}\ln\left(\mathfrak{s}^2\right) ,
\end{aligned} \tag{B.45}$$

where on the first line we have approximated the argument of the logarithm in the limit $\delta \ll 1$. It is now possible to calculate the integral in Eq. (B.43) by integrating the result of Eq. (B.45). We choose $\mathfrak{s} = 0$ as the boundary condition since from Eq. (B.43), we see that $I_\beta(\mathfrak{s} = 0) = 0$

$$I_\beta = -4\int_0^{\mathfrak{s}} \frac{dx\, x}{1-x^2}\ln(x^2) = -2\int_{1-\mathfrak{s}^2}^{1}\frac{dx}{x}\ln(1-x) = 2\left(\frac{\pi^2}{6} - \mathrm{Li}_2\left(\mathfrak{c}^2\right)\right) \tag{B.46}$$

Finally, the integral from Eq. (B.41) takes a simple form

$$\boxed{I_{AB}^{(0,0)} = \frac{1}{16\pi^2}\left\{\ln^2\left(\frac{4\mathfrak{s}^2 E_{\max}^2}{m^2}\right) - \frac{\pi^2}{3} + 2\mathrm{Li}_2\left(\mathfrak{c}^2\right)\right\} ,} \tag{B.47}$$

where

$$\begin{aligned}
\mathfrak{s}^2 &= \sin^2\left(\frac{\theta_{AB}}{2}\right) = \frac{1-\cos\theta_{AB}}{2} \\
\mathfrak{c}^2 &= \cos^2\left(\frac{\theta_{AB}}{2}\right) = \frac{1+\cos\theta_{AB}}{2} .
\end{aligned}$$

We also need to consider the case where the quasi-soft quark is emitted from a massive parton with $m_A = m$. The direct integration is difficult and we need to find a way to circumvent it. We start over from Eq. (B.35) and integrate first over β

$$I_{AB}^{(0,0)} = \frac{\mathfrak{s}^2}{4\pi^2}\int_0^1 \frac{dy}{1-\eta_y^2}\left\{\ln\left(\frac{1+\beta_{\max}}{1-\beta_{\max}}\right) - \frac{1}{\eta_y}\ln\left(\frac{1+\beta_{\max}\eta}{1-\beta_{\max}\eta_y}\right)\right\} . \tag{B.48}$$

The limit $\beta_{\max} \to 1$ cannot be taken because of the argument of the first logarithm. We rewrite the logarithms

$$\begin{aligned}
&\ln\left(\frac{1+\beta_{\max}}{1-\beta_{\max}}\right) - \frac{1}{\eta_y}\ln\left(\frac{1+\beta_{\max}\eta_y}{1-\beta_{\max}\eta_y}\right) \\
&= -\frac{1-\eta_y}{\eta_y}\ln\left(\frac{1+\beta_{\max}\eta_y}{1-\beta_{\max}\eta_y}\right) - \ln\left(\frac{1+\beta_{\max}\eta_y}{1+\beta_{\max}}\right) + \ln\left(\frac{1-\beta_{\max}\eta_y}{1-\beta_{\max}}\right) ,
\end{aligned} \tag{B.49}$$

and we use the following equation

$$\ln\left(\frac{1-\beta_{\max}\eta_y}{1-\beta_{\max}}\right)=\ln\left(\frac{1-\beta_{\max}^2\eta_y^2}{1-\beta_{\max}^2}\right)-\ln\left(\frac{1+\beta_{\max}}{1+\beta_{\max}\eta_y}\right), \tag{B.50}$$

to rewrite the integral that we have just computed in Eq. (B.35) as

$$\begin{aligned} I_{AB}^{(0,0)} =& \frac{\mathfrak{s}^2}{4\pi^2}\int_0^1 dy\left[-\frac{1}{(1+\eta_y)\eta_y}\ln\left(\frac{1+\beta_{\max}\eta_y}{1-\beta_{\max}\eta_y}\right)\right. \\ &\left.+\frac{1}{1-\eta_y^2}\ln\left(\frac{1-\beta_{\max}^2\eta_y^2}{1-\beta_{\max}^2}\right)-\frac{2}{1-\eta_y^2}\ln\left(\frac{1+\beta_{\max}\eta_y}{1+\beta_{\max}}\right)\right]. \end{aligned} \tag{B.51}$$

Despite a more complex integrand, we have isolated the singularity in one logarithm whose argument is free of square roots. The Eq. (B.51) is approximated using $E_{\max} \gg m$. It reads

$$\begin{aligned} I_{AB}^{(0,0)} =& \frac{\mathfrak{s}^2}{4\pi^2}\int_0^1 dy\left[-\frac{1}{(1+\eta_y)\eta_y}\ln\left(\frac{1+\eta_y}{1-\eta_y}\right)\right. \\ &\left.+\frac{1}{1-\eta_y^2}\ln\left(\frac{1-\beta_{\max}^2\eta_y^2}{1-\beta_{\max}^2}\right)-\frac{2}{1-\eta_y^2}\ln\left(\frac{1+\eta_y}{2}\right)\right]. \end{aligned} \tag{B.52}$$

We consider the argument of the second logarithm where it is not safe to set $\beta_{\max} \to 1$. We make explicit the mass dependence

$$\frac{1-\beta_{\max}^2\eta_y^2}{1-\beta_{\max}^2}=\frac{m^2/E_{\max}^2+\beta_{\max}^2(1-\eta_y^2)}{m^2/E_{\max}^2}=\frac{\xi^2+4y(1-y)\mathfrak{s}^2}{\xi^2}, \tag{B.53}$$

and we defined the ratio $\xi = m^2/E_{\max}^2$ and sent $\beta_{\max} \to 1$ since ξ acts as a regulator of the divergences in $y = 0$ and $y = 1$ in the argument of the logarithm. We need the following integral

$$I_y=\frac{1}{16\pi^2}\int_0^1 dy\,\frac{1}{y(1-y)\mathfrak{s}^2}\ln\left(\frac{\xi^2+4y(1-y)}{\xi^2}\right). \tag{B.54}$$

This integral diverges as $y \to 0$ and $y \to 1$. Similar to what has been done in the beginning of this chapter to compute the integration soft-collinear eikonal function, we introduce a small parameter $\xi \ll \Lambda \ll 1$ to split the integration domain in three parts. The first integral we are considering reads

$$\begin{aligned} I_1 = \int_0^\Lambda \frac{dy}{y(1-y)}\ln\left(\frac{\xi^2+4y(1-y)\mathfrak{s}^2}{\xi^2}\right) &\approx \int_0^\Lambda \frac{dy}{y}\ln\left(1+\frac{4y\mathfrak{s}^2}{\xi^2}\right) \\ &= \frac{1}{2}\ln^2\left(\frac{4\mathfrak{s}^2\Lambda}{\xi^2}\right)+\frac{\pi^2}{6}+\mathcal{O}(\Lambda). \end{aligned} \tag{B.55}$$

The second integral is defined as

$$\begin{aligned}
I_2 &= \int_{1-\Lambda}^{1} \frac{dy}{y(1-y)} \ln\left(\frac{\xi^2 + 4y(1-y)\mathfrak{s}^2}{\xi^2}\right) \\
&\approx \int_{1-\Lambda}^{1} \frac{dy}{1-y} \ln\left(1 + \frac{4(1-y)\mathfrak{s}^2}{\xi^2}\right) .
\end{aligned} \tag{B.56}$$

We recognise that this is exactly the integral I_1. Finally, the last integral reads

$$\begin{aligned}
I_3 &= \int_{\Lambda}^{1-\Lambda} \frac{dy}{y(1-y)} \ln\left(\frac{\xi^2 + 4y(1-y)\mathfrak{s}^2}{\xi^2}\right) \\
&\approx \int_{\Lambda}^{1-\Lambda} dy \left(\frac{1}{y} + \frac{1}{1-y}\right) \left[\ln\left(\frac{4\mathfrak{s}^2}{\xi^2}\right) + \ln(y) + \ln(1-y)\right] \\
&= -\frac{\pi^2}{3} - \ln^2\left(\frac{4\mathfrak{s}^2\Lambda}{\xi^2}\right) + \ln^2\left(\frac{4\mathfrak{s}^2}{\xi^2}\right) .
\end{aligned} \tag{B.57}$$

As expected, the dependence on Λ vanishes once the three integral are summed. We find that Eq. (B.54) becomes

$$I_y = \frac{1}{16\pi^2} \ln^2\left(\frac{4\mathfrak{s}^2 E_{\mathrm{max}}^2}{m^2}\right) . \tag{B.58}$$

Plugging this result in the expression for the massless integral, we find that Eq. (B.52) reads

$$\begin{aligned}
I_{AB}^{(0,0)} =& \frac{\mathfrak{s}^2}{4\pi^2} \int_0^1 dy \Bigg[-\frac{1}{(1+\eta_y)\eta_y} \ln\left(\frac{1+\eta_y}{1-\eta_y}\right) \\
& \qquad - \frac{2}{1-\eta_y^2} \ln\left(\frac{1+\eta_y}{2}\right)\Bigg] + \frac{1}{16\pi^2} \ln^2\left(\frac{4\mathfrak{s}^2 E_{\mathrm{max}}^2}{m^2}\right) .
\end{aligned} \tag{B.59}$$

By direct comparison with the final result of the first part in Eq. (B.47), we find

$$\begin{aligned}
&\frac{\mathfrak{s}^2}{4\pi^2} \int_0^1 dy \left[-\frac{1}{(1+\eta_y)\eta_y} \ln\left(\frac{1+\eta_y}{1-\eta_y}\right) - \frac{2}{1-\eta_y^2} \ln\left(\frac{1+\eta_y}{2}\right)\right] \\
&= \frac{1}{16\pi^2} \left[2\mathrm{Li}_2\left(\mathfrak{c}^2\right) - \frac{\pi^2}{3}\right]
\end{aligned} \tag{B.60}$$

This result will be used in the computation of the integral $I_{AB}^{(m,0)}$. We start from Eq. (B.29) and expand the phase-space measure. We find

$$I_{AB}^{(m,0)} = \frac{1 - \beta_A \cos\theta_{AB}}{4\pi^2} \int_m^{E_{\mathrm{max}}} \frac{dE_{\vec{p}}}{E_{\vec{p}}} \beta \int_{-1}^{1} \frac{d(\cos\theta)}{2} \int_0^1 \frac{dy}{\left[1 - \beta\eta_y \cos\theta\right]^2} . \tag{B.61}$$

where we use the definition from Eq. (B.34). We send $\beta_A \to 1$ in the prefactor and change the integration over the energy to an integration over β

$$I_{AB}^{(m,0)} = \frac{1-\cos\theta_{AB}}{4\pi^2} \int_0^{\beta_{\max}} \frac{d\beta\,\beta^2}{1-\beta^2}\beta \int_{-1}^{1} \frac{d(\cos\theta)}{2} \int_0^1 \frac{dy}{\left[1-\beta\eta_y\cos\theta\right]^2} . \tag{B.62}$$

After integration over the azimuthal angle, we find the same integral that in Eq. (B.35). We perform the integration over β and use the known result in Eq. (B.52). We remind the result for convenience

$$\begin{aligned} I_{AB}^{(m,0)} =& \frac{\mathfrak{s}^2}{4\pi^2}\int_0^1 dy \left[-\frac{1}{(1+\eta_y)\eta_y}\ln\left(\frac{1+\eta_y}{1-\eta_y}\right) \right. \\ & \left. + \frac{1}{1-\eta_y^2}\ln\left(\frac{1-\beta_{\max}^2\eta_y^2}{1-\beta_{\max}^2}\right) - \frac{2}{1-\eta_y^2}\ln\left(\frac{1+\eta_y}{2}\right)\right] . \end{aligned} \tag{B.63}$$

In this case, the norm η_y is different from the one in Eq. (B.52) as it depends on the velocity of one of the emitter. The norm of η_y reads

$$\begin{aligned} \eta_y^2 &= \beta_A^2 y^2 + (1-y)^2 + 2\beta_A y(1-y)\cos\theta_{AB} \\ &= 1 - 2y(1-y)(1-\cos\theta_{AB}) - \zeta_A^2 y(y+(1-y)\cos\theta_{AB}) , \end{aligned} \tag{B.64}$$

where we defined $\zeta_A = \frac{m_A}{E_A}$. Similar to Eq. (B.53), we expand the argument of the second logarithm in Eq. (B.63) which is divergent as $\beta_{\max} \to 1$. Then, Eq. (B.63) becomes

$$\begin{aligned} I_{AB}^{(m,0)} =& \frac{1}{16\pi^2}\left(2\mathrm{Li}_2\left(\mathfrak{c}^2\right) - \frac{\pi^2}{3}\right) \\ & + \frac{\mathfrak{s}^2}{4\pi^2}\int_0^1 \frac{dy}{y}\,\frac{\ln\left(\frac{\mathfrak{z}^2+4y(1-y)\mathfrak{s}^2+\zeta_A^2 y(1-y)\cos\theta_{AB}}{\mathfrak{z}^2}\right)}{4\mathfrak{s}^2(1-y)+\zeta_A^2(y+(1-y)\cos\theta_{AB})} . \end{aligned} \tag{B.65}$$

This last integral is again calculated by introducing an auxiliary parameter $\Lambda \ll 1$ which split the integration domain in three parts, $[0,1] = [0,\Lambda] \cup [\Lambda, 1-\Lambda] \cup [1-\Lambda, 1]$. The first integral reads

$$I_1 = \frac{\mathfrak{s}^2}{4\pi^2}\int_0^{\Lambda}\frac{dy}{y}\frac{1}{4\mathfrak{s}^2+\zeta_A^2\cos\theta_{AB}}\ln\left(\frac{\mathfrak{z}^2+4y\mathfrak{s}^2+\zeta_A^2 y\cos\theta_{AB}}{\mathfrak{z}^2}\right) . \tag{B.66}$$

We recall that $\zeta_A = m/E_A \ll 1$ so the integrand simplifies. We find

$$I_1 = \frac{1}{16\pi^2}\int_0^{\Lambda}\frac{dy}{y}\ln\left(\frac{\mathfrak{z}^2+4y\mathfrak{s}^2}{\mathfrak{z}^2}\right) = \frac{1}{16\pi^2}\left[\frac{1}{2}\ln^2\left(\frac{4\mathfrak{s}^2\Lambda}{\mathfrak{z}^2}\right) + \frac{\pi^2}{6}\right] . \tag{B.67}$$

The second integral reads

$$I_2 = \frac{\mathfrak{s}^2}{4\pi^2}\int_{1-\Lambda}^{1} dy \frac{1}{4\mathfrak{s}^2(1-y)+\zeta_A^2}\ln\left(\frac{\mathfrak{z}^2+4\mathfrak{s}^2(1-y)+\zeta_A^2}{\mathfrak{z}^2}\right) . \tag{B.68}$$

We change the integration variable $\mathfrak{f} = 4\mathfrak{s}^2(1-y) + \xi_A^2$ and find

$$\begin{aligned} I_2 &= \frac{1}{16\pi^2}\int_{\xi_A}^{4\mathfrak{s}^2} \frac{d\mathfrak{f}}{\mathfrak{f}} \ln\left(\frac{\xi^2 + f}{\xi^2}\right) = I_1 - \frac{1}{16\pi^2}\int_0^{\xi_A^2} \frac{d\mathfrak{f}}{\mathfrak{f}} \ln\left(1 + \frac{\mathfrak{f}}{\xi^2}\right) \\ &= \frac{1}{16\pi^2}\left[\frac{1}{2}\ln^2\left(\frac{4\mathfrak{s}^2\Lambda}{\xi^2}\right) + \frac{\pi^2}{6} + \mathrm{Li}_2\left(-\frac{\xi_A^2}{\xi^2}\right)\right] . \end{aligned} \tag{B.69}$$

The third integral reads

$$I_3 = \frac{1}{16\pi^2}\int_{\Lambda}^{1-\Lambda} \frac{dy}{y(1-y)} \ln\left(\frac{4y(1-y)\mathfrak{s}^2}{\xi^2}\right) , \tag{B.70}$$

which is the same as Eq. (B.57). Once the three parts are combined, the dependence on Λ cancel as expected and we find the desired result

$$\boxed{I_{AB}^{(m,0)} = \frac{1}{16\pi^2}\left[2\mathrm{Li}_2\left(\mathfrak{c}^2\right) - \frac{\pi^2}{3} + \mathrm{Li}_2\left(-\frac{E_{\max}^2}{E_A^2}\right) + \ln^2\left(\frac{4\mathfrak{s}^2 E_{\max}^2}{m^2}\right)\right] .} \tag{B.71}$$

We note that this result differ from Eq. (B.47) by only one term.

C

BOUNDARY INTEGRALS

In this chapter, we present the calculation of the two-loop triangle integrals I_{16} and I_{17}, shown in Fig. 13.4. These integrals are required for the computation of boundary conditions for the master integrals for t-channel single top production. Unfortunately, they were not found in the literature and need to be evaluated up to order $\mathcal{O}(\varepsilon^5)$ and $\mathcal{O}(\varepsilon^6)$, respectively.

To compute these two-loop triangle integrals, we follow the standard procedure for multi-loop Feynman integrals [198]. First, we use `LiteRed` [179, 199] to reduce the desired integrals to a basis of master integrals. Then, we differentiate these master integrals with respect to the kinematic invariants and use IBP relations to build a system of ordinary differential equations. Next, we use the Mathematica package `CANONICA` [200] to change the integral basis to bring the differential equation into *canonical form*. In this form, the solution to the differential equation is easily expressed through harmonic polylogarithms (HPLs) [201]. Finally, we consider a convenient kinematical limit where the master integrals are easy to calculate, allowing us to compute the integration constants.

C.1 LOOP-INTEGRAL CALCULATIONS USING DIFFERENTIAL EQUATIONS

To numerically evaluate the 428 master integrals using the auxiliary mass flow method, we need a set of 17 integrals at the boundary $m_W^2 \to -i\infty$ and the internal top-quark mass $m_t^2 \to m^2 \to -i\infty$, as explained in Chapter 13. Two of them were not found in the literature, namely I_{16} and I_{17}, shown in Fig. C.1. They read

$$I_{16} = \int \prod_{j=1}^{2} \left(\frac{d^d k_j}{i\pi^{d/2}} \right) \frac{1}{(k_2^2 - m^2)(k_1 - k_2)^2 (p_1 - k_1)^2 (p_2 + k_1)^2}, \tag{C.1}$$

$$I_{17} = \int \prod_{j=2}^{2} \left(\frac{d^d k_j}{i\pi^{d/2}} \right) \frac{1}{(k_2^2 - m^2)^2 (k_1 - k_2)^2 (p_1 - k_1)^2 (p_2 + k_1)^2}, \tag{C.2}$$

where $p_1^2 = m^2$, $p_2^2 = 0$ and $(p_1 + p_2)^2 = s$.

We would like to calculate these integrals analytically through the order $\mathcal{O}\left(\varepsilon^5\right)$ and $\mathcal{O}\left(\varepsilon^6\right)$, respectively. Direct calculations of I_{16} and I_{17} using Feynman parameters leads to complicated integrals. Instead, we use differential equations Ref. [198] which allows a

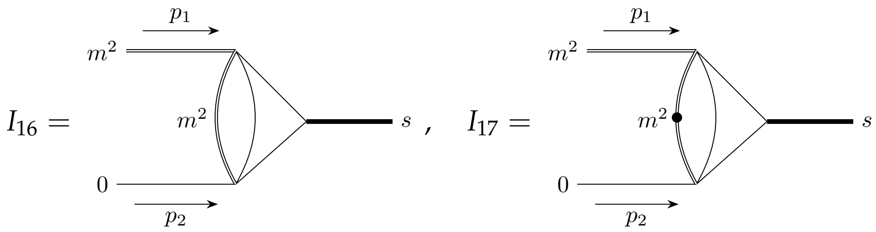

Figure C.1: Two-loop triangle integrals required as boundary conditions by the auxiliary mass flow method to evaluate the two-loop amplitude. Double lines stand for massive propagators and legs with mass m^2. Massive leg with $p^2 = s$ is denoted by a thick line. Simple solid lines are massless. Dots indicate that the propagator is squared.

simpler and more systematic approach.

The two-loop triangle integrals I_{16} and I_{17} depend only on the Mandelstam variable $s = (p_1 + p_2)^2$ and the squared mass m^2. We decided to differentiate the integrals with respect to the dimensionless ratio $x = s/m^2$, set $m \to 1$, and reconstruct the mass dependence at the end of the calculation by dimensional analysis. By doing this and using IBP relations, we build the differential equation

$$\partial_x \vec{I} = \mathcal{M}(x, \varepsilon) \vec{I}, \tag{C.3}$$

where $\mathcal{M}$ is a matrix that depends on x and ε, and a vector of master integrals reads

$\vec{I} = \Big\{$ 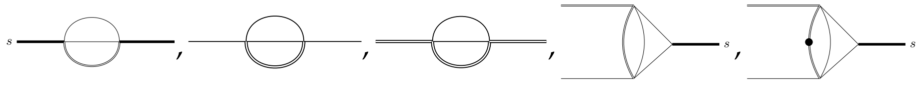 $\Big\}$. (C.4)

The determination of the master integrals and the differentiation is performed using `LiteRed` [179, 199].

The first three master integrals in $\vec{I}$ are easy to compute analytically. Indeed, they contain a massless internal bubble which is well-known

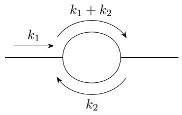

$$= \int \frac{d^d k_2}{i\pi^{d/2}} \frac{1}{(k_2)^2 (k_1 + k_2)^2} = \Gamma(\varepsilon)\beta(1-\varepsilon, 1-\varepsilon)(-k_1^2)^{-\varepsilon} \tag{C.5}$$

As the result, we are left with an one-loop integration where the massless internal topology has been replaced by a simple propagator $1/(-k_1^2)^\varepsilon$ and some ε-dependent factors. After the second loop integration, we find

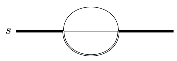

$$= -\Gamma(-1+\varepsilon)\Gamma(\varepsilon)\beta(1-\varepsilon, 1-\varepsilon)(-x)^{-\varepsilon}(m^2)^{1-\varepsilon} \tag{C.6}$$

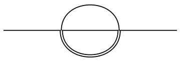

$$= -\Gamma(-1+2\varepsilon)\beta(1-\varepsilon,1-\varepsilon)\beta(\varepsilon,2-2\varepsilon)(m^2)^{1-2\varepsilon} \tag{C.7}$$

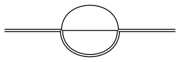

$$= -\Gamma(-1+2\varepsilon)\beta(1-\varepsilon,1-\varepsilon)\beta(3-4\varepsilon,\varepsilon)(m^2)^{1-2\varepsilon}\,. \tag{C.8}$$

The next step is called *fuchsification*. It consists in a change of master integral basis, defined by the matrix $\mathcal{F}$, such that the differential equation in Eq. (C.3) becomes

$$\partial_x \vec{J} = \varepsilon\, \mathcal{M}'(x)\, \vec{J}\,, \tag{C.9}$$

where $\vec{J}$ is a linear transformation of $\vec{I}$ such that $\vec{I} = \mathcal{F}\vec{J}$ and the Fuchsian matrix $\mathcal{M}'$ reads

$$\mathcal{M}' = \frac{1}{x}\begin{pmatrix} 1 & 0 & 0 & 0 & 0 \\ 0 & 0 & 0 & 0 & 0 \\ 0 & 0 & 0 & 0 & 0 \\ \frac{1}{10} & \frac{3}{10} & -\frac{5}{7} & 4 & 9 \\ 0 & -\frac{1}{10} & \frac{1}{7} & 0 & 1 \end{pmatrix} + \frac{1}{1-x}\begin{pmatrix} 0 & 0 & 0 & 0 & 0 \\ 0 & 0 & 0 & 0 & 0 \\ 0 & 0 & 0 & 0 & 0 \\ 0 & 0 & 0 & -1 & -6 \\ 0 & 0 & 0 & 1 & 4 \end{pmatrix}. \tag{C.10}$$

The differential equation in Eq. (C.9) is said to be in the canonical form or in ε-form. We found the canonical basis using `CANONICA` [200].

C.2 SOLUTION TO THE DIFFERENTIAL EQUATION IN CANONICAL FORM

We would like to solve the differential equations in Eq. (C.9). The first important point to notice is that the matrix $\mathcal{M}'$ is singular at $x = 0$, $x = 1$ and $x \to \infty$. These three singularities are related to special physical points. Indeed, the singularity at $x = 0$ corresponds to the kinematical limit $s = 0$ where the centre-of-mass energy vanishes. The singularity at $x = 1$ corresponds to $s = m^2$ which is the production threshold. Finally, the singular point $x \to \infty$ corresponds to the kinematical region where $s \gg m^2$.

It is clear that, if we integrate once the differential equation in Eq. (C.9), we get logarithms of x and $1-x$ with a factor ε. The next order in ε is obtained by a consecutive integration. These integrals are commonly known as harmonic polylogarithms (HPLs) [201]. They are defined as

$$H_{m_\omega}(x) = \int_0^x dt\, f_a(t) H_{m_{\omega-1}}(t)\,, \tag{C.11}$$

where

$$H_0(x) \equiv \ln(x)\,, \quad H_1(x) \equiv -\ln(1-x)\,, \quad H_{-1}(x) \equiv \ln(1+x)\,, \tag{C.12}$$

and

$$f_0(x) \equiv \frac{1}{x}, \quad f_1(x) \equiv \frac{1}{1-x}, \quad f_{-1}(x) \equiv \frac{1}{1+x}. \tag{C.13}$$

The numbers -1, 1 and 0 are call *letters* and the set $\{-1, 0, 1\}$ is called the *alphabet*. In Eq. (C.11), the vector m_ω is a ω-dimensional vector whose entries are the letters of the alphabet, and a is a letter. The two vectors in Eq. (C.11) are related in the following way

$$m_\omega = (a, m_{\omega-1}). \tag{C.14}$$

The solution to the differential equations in canonical form, as shown in Eq. (C.9), can be conveniently expressed using HPL, whose alphabet is $\{0, 1\}$[1]. However, at each order in ε, we obtain integration constants, one for each master integrals, which need to be fixed by considering the master integrals I in a convenient kinematical limit.

C.3 TWO-LOOP TRIANGLE INTEGRALS AT THE BOUNDARY

Unlike the sunrise integrals, the two-loop triangle integrals I_{16} and I_{17} do not have a massless sub-topology, which makes the integration more challenging. In this section, we demonstrate how to overcome this difficulty by using dispersion integrals. First, we review the concept of dispersion integral by deriving the dispersion integrals for an one-loop bubble integral with a massive internal propagator. Then, we apply this method to compute the integral I_{16} and I_{17} in the limit $x \to 0$.

C.3.1 *Dispersion integrals – bubble with one massive propagator*

Dispersion integrals relate a kinematic-dependent function $F(q^2)$ to its imaginary part through Cauchy theorem. A review can be found in Ref. [204]. The dispersion integral for $F(q^2)$ reads

$$F(q^2) = \frac{1}{\pi} \int_{q_0^2}^{\infty} ds \frac{\operatorname{Im} F(s + i\epsilon)}{s - q^2 - i\epsilon}, \tag{C.15}$$

where $\operatorname{Im} F$ denotes the imaginary part of F and q_0^2 is the energy threshold. In complex analysis, q_0^2 stands for the start of the branch cut on the real axis in the complex plane.

---

[1] We note that, when the letters of the alphabet are not restricted to the set $\{-1, 0, 1\}$, we speak about multiple polylogarithm (MPL). There is a different sign convention between MPL and HPL. There are equal to each other up to $(-1)^p$ where p is the number of letter 1 in m_ω of the HPL. [133, 202]. One can deal with MPL using the Mathematica package HPL [203].

In this subsection, we will compute the dispersion integral for a bubble with one massive propagator and off-shell legs. This results can be found in Ref. [205]. In this case, the function $F(q^2)$ reads

$$F(q^2) =$$

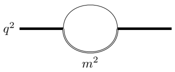

$$= \int \frac{d^dk}{i\pi^{d/2}} \frac{1}{(k^2-m^2)(k-q)^2} \,. \tag{C.16}$$

To compute the dispersion integral, we need to obtain an expression for the imaginary part of the bubble integral. This can be easily done using Cutkosky's rules [206]. The imaginary part of the diagram is given by the sum over all possible cuts of the diagram's propagator. To cut a propagator means to force it be on-shell. Graphically,

$$2\text{Im}\,\left(F(q^2)\right) =$$

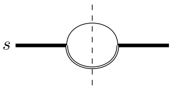

$$= \int \frac{d^dk}{i\pi^{d/2}} \left[2\pi i\,\theta(k^0)\delta(k^2-m^2)\right] \left[2\pi i\,\theta(q^0-k^0)\delta((q-k)^2)\right] \,. \tag{C.17}$$

This integral can be calculated by splitting it into an integration over the energy k^0 and an integration over the momentum $\vec{k}$. It reads

$$\begin{aligned}\text{Im}\,\left(F(q^2)\right) = -\frac{2\pi^2}{i\pi^{d/2}} \int_0^{q_0} dk^0 \int d^{d-1}\vec{k}\,\delta\left((k^0)^2-\vec{k}^2-m^2\right) \\ \times\,\delta\left((k^0)^2-\vec{k}^2-2q\cdot k+q^2\right) \,.\end{aligned} \tag{C.18}$$

As the integrand is invariant under Lorentz transformations, we can choose the frame where $q = (q^0, \vec{0})$. We switch to spherical coordinates and perform the integral over the solid angle. We find

$$\begin{aligned}\text{Im}\,\left(F(q^2)\right) = \frac{4\pi^{3/2}i}{\Gamma\left(\frac{d-1}{2}\right)} \int_0^{q_0} dk^0 \int_0^\infty dr\, r^{d-2}\delta\left((k^0)^2-r^2-m^2\right) \\ \times\,\delta\left((k^0)^2-r^2-2q^0k^0+(q^0)^2\right) \,.\end{aligned} \tag{C.19}$$

The integration over r can be performed and we restore the Lorentz invariance by going back in a general frame

$$\boxed{\text{Im}\,\left(F(q^2)\right) = \frac{2\pi^{3/2}i}{\Gamma\left(\frac{3}{2}-\varepsilon\right)} \frac{(q^2-m^2)^{1-2\varepsilon}}{(4q^2)^{1-\varepsilon}} \,.} \tag{C.20}$$

As a check, the dispersion integral can be used to find the result of the bubble integral $F(q^2)$

$$\begin{aligned}F\left(q^2\right) &= \frac{1}{\pi}\int_{m^2}^\infty ds\, \frac{\text{Im}\,F(s+i\epsilon)}{s-q^2-i\epsilon} \\ &= \frac{2^{-1+2\varepsilon}\pi^{1/2}}{\Gamma\left(3/2-\varepsilon\right)}(m^2)^{-\varepsilon}\frac{\Gamma\left(\varepsilon\right)\Gamma\left(2-2\varepsilon\right)}{\Gamma\left(2-\varepsilon\right)}\,{}_2F_1\left(1,\varepsilon;2-\varepsilon;\frac{q^2+i\epsilon}{m^2}\right) \,.\end{aligned} \tag{C.21}$$

This result, which is numerically cross-checked using `PySecDec` [148], is indeed the formula for the one-loop bubble with one massive propagator and off-shell legs.

C.3.2 *Application to the two-loop triangle integrals I_{16} and I_{17}*

In the previous section, we derived the dispersion integral for a bubble integral with a massive propagator and off-shell legs. In this section, we use this result to compute the two-loop triangle integrals I_{16} and I_{17}.

Using the Eq. (C.20), the two-loop triangle integral I_{16} can be written as

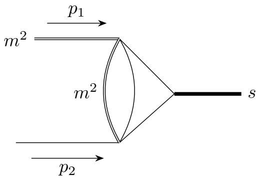

$$= \frac{-2\pi^{1/2}}{\Gamma\left(\frac{3}{2}-\varepsilon\right)} \int_{m^2}^{\infty} d\lambda \, \frac{\left(\lambda - m^2\right)^{1-2\varepsilon}}{(4\lambda)^{1-\varepsilon}} \Bigg($$

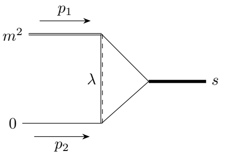

$$\Bigg) \, . \tag{C.22}$$

We see that the dispersion representation for the bubble integral derived in the previous section allows us to express the two-loop integral I_{16} as a convolution of an one-loop integral with a propagator with squared mass λ with the bubble's spectral density. This one-loop triangle integral is calculated in the limit $x \to 0$.

We find

$$I_{1L}(\lambda) =$$

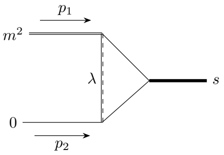

$$= \mathcal{I}_1 - (-s - i\epsilon)^{-\varepsilon} \, \mathcal{I}_2 + \mathcal{O}(x) \, , \tag{C.23}$$

where

$$\mathcal{I}_1 = \frac{\Gamma(1+\varepsilon)}{\varepsilon} \lambda^{-1-\varepsilon} \frac{1}{1-\varepsilon} \, {}_2F_1\left(1+\varepsilon, 1; 2-\varepsilon; \frac{m^2}{\lambda}\right) \, , \tag{C.24}$$

$$\mathcal{I}_2 = \Gamma(1+\varepsilon) \, \frac{1}{\lambda\varepsilon} \frac{\Gamma(1-\varepsilon)^2}{\Gamma(2-2\varepsilon)} \, {}_2F_1\left(1, 1-\varepsilon; 2-2\varepsilon; \frac{m^2}{\lambda}\right) \, . \tag{C.25}$$

Using this result in Eq. (C.22), we find the expression for I_{16} at the boundary $x \to 0$. It reads

$$\begin{aligned} I_{16}^{(0)} &= \frac{-2\pi^{1/2}}{\Gamma\left(\frac{3}{2}-\varepsilon\right)} \int_{m^2}^{\infty} d\lambda \, \frac{(\lambda - m^2)}{(4\lambda)^{1-\varepsilon}} I_{1L}(\lambda) \\ &= \frac{-2^{-1+2\varepsilon} i \sqrt{\pi}}{\Gamma\left(\frac{3}{2}-\varepsilon\right)} \left[\frac{\Gamma(1+\varepsilon)}{\varepsilon(1-\varepsilon)} \mathcal{A}_{16} - (-s - i\epsilon)^{-\varepsilon} \frac{\Gamma(1+\varepsilon)}{\varepsilon} \frac{\Gamma(1-\varepsilon)^2}{\Gamma(2-2\varepsilon)} \mathcal{B}_{16} \right] \, , \end{aligned} \tag{C.26}$$

where we defined

$$\mathcal{A}_{16} = \int_{m^2}^{\infty} d\lambda \, \frac{(\lambda - m^2)^{1-2\varepsilon}}{\lambda^2} \, {}_2F_1\left(1+\varepsilon, 1; 2-\varepsilon; \frac{m^2}{\lambda}\right) , \tag{C.27}$$

$$\mathcal{B}_{16} = \int_{m^2}^{\infty} d\lambda \, \frac{(\lambda - m^2)^{1-2\varepsilon}}{\lambda^{2-\varepsilon}} \, {}_2F_1\left(1, 1-\varepsilon; 2-2\varepsilon; \frac{m^2}{\lambda}\right) . \tag{C.28}$$

We need to compute these two integrals. We change the integration variable to $x = m^2/\lambda$. The integral $\mathcal{A}_{16}$ becomes

$$\mathcal{A}_{16} = (m^2)^{-2\varepsilon}\, \Gamma(2\varepsilon)\, \Gamma(2-2\varepsilon)\; {}_3F_2\left(1, 1+\varepsilon, 2\varepsilon; 2-\varepsilon, 2; 1\right) . \tag{C.29}$$

This integral can be expanded using the Mathematica package `HypExp` [207]. We find

$$\begin{aligned}\mathcal{A}_{16} = (m^2)^{-2\varepsilon}\Bigg[& \frac{1}{2\varepsilon} + \left(1 - \frac{\pi^2}{6}\right) + \varepsilon\left(3 + \frac{2\pi^2}{3} - 5\zeta_3\right) + \varepsilon^2\Bigg(10\zeta(3) + 9 \\ & + \pi^2 - \frac{13\pi^4}{36}\Bigg) + \varepsilon^3\Bigg(10\zeta(3) - 5\pi^2\zeta(3) - 75\zeta(5) + 27 + 3\pi^2 \\ & + \frac{79\pi^4}{90}\Bigg) + \varepsilon^4\Bigg(30\zeta(3) + 10\pi^2\zeta(3) - 25\zeta(3)^2 + 150\zeta(5) \\ & + 81 + 9\pi^2 + \frac{31\pi^4}{30} - \frac{317\pi^6}{540}\Bigg) + \varepsilon^5\Bigg(90\zeta(3) + 10\pi^2\zeta(3) \\ & - \frac{31\pi^4\zeta(3)}{6} + 50\zeta(3)^2 + 150\zeta(5) - 75\pi^2\zeta(5) - 1005\zeta(7) \\ & + 243 + 27\pi^2 + \frac{31\pi^4}{10} + \frac{781\pi^6}{630}\Bigg) + \mathcal{O}\left(\varepsilon^6\right)\Bigg] .\end{aligned} \tag{C.30}$$

Similarly, we find that the integral $\mathcal{B}$ reads

$$\begin{aligned}\mathcal{B}_{16} = (m^2)^{-\varepsilon}\Bigg[& \frac{1}{\varepsilon} + \left(1 - \frac{\pi^2}{6}\right) + \varepsilon\left(3 + \frac{2\pi^2}{3} - 6\zeta_3\right) + \varepsilon^2\Bigg(14\zeta(3) + 9 \\ & + \frac{\pi^2}{3} - \frac{37\pi^4}{120}\Bigg) + \varepsilon^3\Bigg(2\zeta(3) - \frac{7\pi^2\zeta(3)}{3} - 75\zeta(5) + 27 + \pi^2 \\ & + \frac{43\pi^4}{60}\Bigg) + \varepsilon^4\Bigg(6\zeta(3) + \frac{16\pi^2\zeta(3)}{3} - 12\zeta(3)^2 + 156\zeta(5) \\ & + 81 + 3\pi^2 + \frac{\pi^4}{10} - \frac{1759\pi^6}{5040}\Bigg) + \varepsilon^5\Bigg(18\zeta(3) + \frac{2\pi^2\zeta(3)}{3} \\ & - \frac{73\pi^4\zeta(3)}{60} + 26\zeta(3)^2 + 6\zeta(5) - 26\pi^2\zeta(5) - \frac{5733\zeta(7)}{8} \\ & + 243 + 9\pi^2 + \frac{3\pi^4}{10} + \frac{5521\pi^6}{7560}\Bigg) + \mathcal{O}\left(\varepsilon^6\right)\Bigg] .\end{aligned} \tag{C.31}$$

Analogously, we use dispersion integrals to get an expression for I_{17} at the boundary $x \to 0$. However, we do not apply the Cutkosky's rule to obtain the imaginary part of the bubble integral with a dotted propagator. Instead, we use IBP relations to rewrite it through a bubble integral and a massive tadpole integral using `LiteRed` [179, 199]. We find

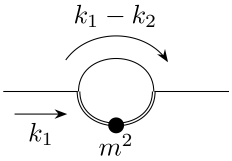

$$= \frac{d-3}{k_1^2-m^2}$$

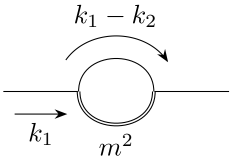

$$+ \frac{d-2}{2m^2}\frac{1}{k_1^2-m^2}$$

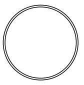

$$. \qquad \text{(C.32)}$$

Using the dispersion relation for the bubble integral, we obtain the following representation for the integral I_{17}

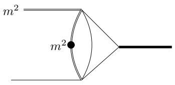

$$= \frac{2\sqrt{\pi}i}{\Gamma\left(\frac{3}{2}-\varepsilon\right)}(1-2\varepsilon)$$

$$\times \left\{ \int_{m^2}^{\infty} d\lambda \frac{(\lambda-m^2)^{-2\varepsilon}}{(4\lambda)^{1-\varepsilon}}\right.$$

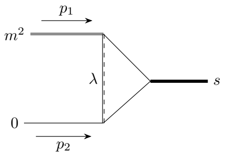

$$\left. - \int_{m^2}^{\infty} d\lambda \frac{(\lambda-m^2)^{-2\varepsilon}}{(4\lambda)^{1-\varepsilon}} \right\} \qquad \text{(C.33)}$$

$$- (1-\varepsilon)(m^2)^{-\varepsilon}\Gamma(\varepsilon-1)$$

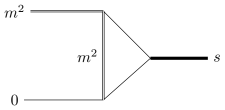

$$.$$

We note that in writing Eq. (C.33), we used the analytic expression for the massive tadpole

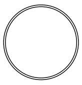

$$= \Gamma(\varepsilon-1)\,(m^2)^{-\varepsilon}. \qquad \text{(C.34)}$$

After few manipulations, the integral I_{17} at the boundary $x \to 0$ is expressed as

$$\boxed{\begin{aligned} I_{17}^{(0)} = \frac{2^{-1+2\varepsilon}\sqrt{\pi}i}{\Gamma\left(\frac{3}{2}-\varepsilon\right)}(1-2\varepsilon)&\left[\frac{\Gamma(1+\varepsilon)}{\varepsilon}\left\{\frac{1}{1-\varepsilon}\mathcal{A}_{17} - (-s)^{-\varepsilon}\frac{\Gamma(1-\varepsilon)^2}{\Gamma(2-2\varepsilon)}\mathcal{B}_{17}\right\}\right. \\ &\left. - (m^2)^{-\varepsilon}\beta(1-2\varepsilon,\varepsilon)\, I_{1L}(m^2)\right] - (1-\varepsilon)\Gamma(\varepsilon-1)\,(m^2)^{-\varepsilon} I_{1L}(m^2)\,, \end{aligned}} \qquad \text{(C.35)}$$

where

$$\begin{aligned}
\mathcal{A}_{17} = (m^2)^{-1-2\varepsilon}\bigg[&\frac{\pi^2}{6} + \varepsilon\left(5\zeta_3 - \frac{\pi^2}{6}\right) + \varepsilon^2\bigg(\frac{13\pi^4}{36} - 5\zeta(3)\bigg) \\
&+ \varepsilon^3\bigg(5\pi^2\zeta(3) + 75\zeta(5) - \frac{13\pi^4}{36}\bigg) + \varepsilon^4\bigg(25\zeta(3)^2 \\
&- 5\pi^2\zeta(3) - 75\zeta(5) + \frac{317\pi^6}{540}\bigg) + \varepsilon^5\bigg(\frac{31\pi^4\zeta(3)}{6} \\
&- 25\zeta(3)^2 + 75\pi^2\zeta(5) - \frac{317\pi^6}{540} + 1005\zeta(7)\bigg) \\
&+ \varepsilon^6\bigg(25\pi^2\zeta(3)^2 - \frac{31\pi^4\zeta(3)}{6} + 750\zeta(3)\zeta(5) \\
&- 75\pi^2\zeta(5) - 1005\zeta(7) + \frac{13499\pi^8}{15120}\bigg) + \mathcal{O}(\varepsilon^7)\bigg],
\end{aligned} \tag{C.36}$$

and

$$\begin{aligned}
\mathcal{B}_{17} = (m^2)^{-1-\varepsilon}\bigg[&\frac{\pi^2}{6} + \varepsilon\left(6\zeta_3 - \frac{\pi^2}{3}\right) + \varepsilon^2\bigg(\frac{37\pi^4}{120} - 12\zeta(3)\bigg) \\
&+ \varepsilon^3\bigg(\frac{7\pi^2\zeta(3)}{3} + 75\zeta(5) - \frac{37\pi^4}{60}\bigg) + \varepsilon^4\bigg(12\zeta(3)^2 \\
&- \frac{14\pi^2\zeta(3)}{3} - 150\zeta(5) + \frac{1759\pi^6}{5040}\bigg) + \varepsilon^5\bigg(\frac{73\pi^4\zeta(3)}{60} \\
&- 24\zeta(3)^2 + 26\pi^2\zeta(5) + \frac{5733\zeta(7)}{8} - \frac{1759\pi^6}{2520}\bigg) \\
&+ \varepsilon^6\bigg(-\frac{73\pi^4\zeta(3)}{30} + \frac{13\pi^2\zeta(3)^2}{3} - 52\pi^2\zeta(5) \\
&+ 186\zeta(3)\zeta(5) - \frac{5733\zeta(7)}{4} + \frac{88871\pi^8}{259200}\bigg) + \mathcal{O}(\varepsilon^7)\bigg].
\end{aligned} \tag{C.37}$$

This ends the computation of the boundary conditions for the integrals I_{16} and I_{17}. We note that the analytic expressions for the two-loop triangle integrals I_{16} and I_{17}, which are not reported here, are checked numerically using `pySecDec` [148, 149].

D DETERMINATION OF THE BOUNDARY CONDITIONS FOR THE MASSLESS SINGLE-TOP MASTER INTEGRALS.

In Sec. 18, we derived solutions for the five master integrals of the planar topology. In this Appendix, we compute the integration constant $c_5(\varepsilon)$ by a convenient limits. In addition to the small transverse momentum approximation $x \to 0$, we consider that the limit where m_W is very large so that $\rho \to 0$.

We are conscious that even computing the integral in some convienient limit can be cumbersome at two-loop. Therefore, we want to find another way. We note that to fix the integration constants, one does not need to fully compute the integrals. Indeed, these constants are indeed related to branches in x and ρ. For instance, to fix $c_4(\varepsilon)$, we only need to know the branch x of the integral $I(4)$. Therefore, the Mellin-Barnes representation can be especially useful.

D.1 FIXING $c_5(\varepsilon)$ USING FEYNMAN PARAMETRISATION

The integral we want to compute is the following

$$I_5 = \int \frac{d^d k}{i\pi^{d/2}} \frac{1}{k^2(k+p_1)^2(k+p_1+p_2)((k+p_3)^2-m_W^2)} \,. \tag{D.1}$$

We introduce Feynman parametrisation and perform the integration over the loop momentum k'. We get

$$\begin{aligned} I_5 = \Gamma(2+\varepsilon) \int_0^1 dx_1 \int_0^{1-x_1} dx_2 \int_0^{1-x_1-x_2} dx_3 \\ \times \frac{1}{\left[-sx_2(1-x_1-x_2-x_3)+x_3(m_W^2-tx_1)\right]^{2+\varepsilon}} \,. \end{aligned} \tag{D.2}$$

We see that, in this case, we can safely consider the limit $m_W^2 \gg -t$ to drastically simplify the calculation. After integration over x_3, the integral reads

$$\begin{aligned} I_5^{\rho\to 0} &= \Gamma(1+\varepsilon) \int_0^1 dx_1 \int_0^1 dx_2 \frac{(1-x_1-x_2)^{-1-\varepsilon}}{m_W^2+sx_2} \left[(-sx_2)^{-1-\varepsilon} - (m_W^2)^{-1-\varepsilon}\right] \\ &\equiv I_5^{(m_W)} + I_5^{(s)} \,. \end{aligned} \tag{D.3}$$

We can compute separately the two terms in the integral. The first one can be integrated without further ado

$$\begin{aligned} I_5^{(m_W)} &= -\Gamma(1+\varepsilon)(m_W^2)^{-1-\varepsilon}\int_0^1 dx_2 \int_0^{1-x_2} dx_1 \, \frac{(1-x_1-x_2)^{-1-\varepsilon}}{m_W^2+sx_2} \\ &= \Gamma(\varepsilon)(m_W^2)^{-1-\varepsilon}\int_0^1 dx_2 \, \frac{(1-x_2)^{-\varepsilon}}{m_W^2+sx_2} \\ &= \frac{\Gamma(\varepsilon)}{1-\varepsilon}(m_W^2)^{-2-\varepsilon}{}_2F_1(1,1;2-\varepsilon;-s/m_W^2)\,. \end{aligned} \tag{D.4}$$

The second part of the integral requires slightly more attention

$$\begin{aligned} I_5^{(s)} &= \Gamma(1+\varepsilon)(-s)^{-1-\varepsilon}\int_0^1 dx_1 \int_0^{1-x_1} dx_2 \, \frac{(1-x_1-x_2)^{-1-\varepsilon}}{m_w^2+sx_2} x_2^{-1-\varepsilon} \\ &= -\Gamma(\varepsilon)(-s)^{-1-\varepsilon}\int_0^1 dx_2 \, \frac{(1-x_2)^{-\varepsilon}}{m_W^2+sx_2}\frac{1}{x_2^{1+\varepsilon}}\,. \end{aligned} \tag{D.5}$$

The integration over x_2 will produce a pole in ε. We make it explicit by introducting a subtraction term

$$\begin{aligned} I_5^{(s)} &= -\Gamma(\varepsilon)(-s)^{-1-\varepsilon}\bigg\{\int_0^1 dx_2 \left[\frac{(1-x_2)^{-\varepsilon}}{m_W^2+sx_2} - \frac{(1-x_2)^{-\varepsilon}}{m_W^2}\right] \\ &\qquad\qquad + (m_W^2)^{-1}\int_0^1 dx_2 \, x_2^{-1-\varepsilon}(1-x_2)^{-\varepsilon}\bigg\} \\ &= -\frac{\Gamma(\varepsilon)\beta(-\varepsilon,1-\varepsilon)}{(-s)^{1+\varepsilon}m_W^2} - \frac{\Gamma(\varepsilon)\Gamma(1-\varepsilon)^2}{(-s)^{\varepsilon}(m_W^2)^2}\frac{{}_2F_1(1,1-\varepsilon;2-2\varepsilon;-s/m_W^2)}{\Gamma(2-2\varepsilon)}\,, \end{aligned} \tag{D.6}$$

Combining the results from Eq. (D.4) and Eq. (D.6), we find

$$\begin{aligned} I_5^{\rho\to 0} = &-\frac{\Gamma(\varepsilon)\beta(-\varepsilon,1-\varepsilon)}{(-s)^{1+\varepsilon}m_W^2} - \frac{\Gamma(\varepsilon)\Gamma(1-\varepsilon)^2}{(-s)^{\varepsilon}(m_W^2)^2}\frac{{}_2F_1(1,1-\varepsilon;2-2\varepsilon;,-s/m_W^2)}{\Gamma(2-2\varepsilon)} \\ &+\frac{\Gamma(\varepsilon)}{1-\varepsilon}(m_W^2)^{-2-\varepsilon}{}_2F_1(1,1;2-\varepsilon;-s/m_W^2)\,. \end{aligned} \tag{D.7}$$

In order to fix $c_5(\varepsilon)$, we need to match our results to the solution we found for I_5 in Eq. (18.50). We assume an expansion in ε for the integration constant

$$c_5(\varepsilon) = \frac{c_5^{(-2)}}{\varepsilon^2} + \frac{c_5^{(-1)}}{\varepsilon^1} + c_5^{(0)} + \mathcal{O}(\varepsilon)\,, \tag{D.8}$$

and find

$$\boxed{c_5^{(-2)} = 0\,, \qquad c_5^{(-1)} = 0\,, \qquad c_5^{(0)} = 0\,.} \tag{D.9}$$

D.2 FIXING $c_4(\varepsilon)$ USING MELLIN-BARNES REPRESENTATION

The triangle integral I_4 reads

$$I_4 = \int \frac{d^d k}{i\pi^{d/2}} \frac{1}{(k^2 - m_W^2)(k-p_1)^2(k+p_2)^2} \,. \tag{D.10}$$

We can apply Eq. (18.55) to the massive propagator. After permuting the integration over z and the one over the loop momentum k, we find

$$\begin{aligned} I_4 = & -\frac{1}{2\pi i}\int_{-i\infty}^{i\infty} dz\ (m_W^2)^z \Gamma(1+z)\Gamma(-z) \\ & \qquad \times \int \frac{d^d k}{i\pi^{d/2}} \frac{1}{(-k^2)^{1+z}(k-p_1)^2(k+p_2)^2} \,. \end{aligned} \tag{D.11}$$

The integral over the loop momentum k becomes easy as it consists on a massless triangle integral with arbitrary exponents. We use the results $(A.28)$ from Ref. [176] to write

$$\int \frac{d^d k}{i\pi^{d/2}} \frac{1}{(-k^2)^{1+z}(k-p_1)^2(k+p_2)^2} = \frac{\Gamma(-z-\varepsilon)^2\Gamma(1+z-\varepsilon)}{\Gamma(1-z-\varepsilon)} \frac{1}{(-s)^{1+z-\varepsilon}} \tag{D.12}$$

Using this result, the triangle integral I_4 reads

$$I_4 = -\frac{1}{2\pi i}\frac{1}{(-s)^{1+\varepsilon}} \int_{-i\infty}^{i\infty} dz \left(\frac{m_W^2}{-s}\right)^z \frac{\Gamma(-z)\Gamma(1+\varepsilon+z)\Gamma(1+z)\Gamma(-\varepsilon-z)^2}{\Gamma(1-2\varepsilon-z)} \,. \tag{D.13}$$

The integration contour can be chosen such that $-1 < \Re(z) < \Re(\varepsilon)$. Then, we close it to the positive z axis. The poles of the integrand are defined by the poles of the different gamma functions. For instance, $\Gamma(-z)$ has simple poles in $z = n$, $n \in \mathbb{N}$. The integration contour will be equal to the sum of the different residues calculated at each poles

$$\begin{aligned} \oint dz\ f(z) &= \int_{-i\infty}^{i\infty} dz\ f(z) + \int_C dz\ f(z) \\ &= -2\pi i \sum_{\{z_0\}} \mathrm{Res}(f(z), z = z_0) \,, \end{aligned} \tag{D.14}$$

where $f(z)$ represents the integrand and $\{z_0\}$ the set of all pole present within the close path of integration in the complex plane. Note the minus sign in front of the sum as the contour integral goes clockwise.

We give few remarks about the residue of gamma functions. The residue of the function $\Gamma(z)$ at a pole $z_0 = -n$, $n \in \mathbb{N}$ reads

$$\begin{aligned} \mathrm{Res}(\Gamma(z), z = z_0) &= \lim_{z\to -n}(z+n)\Gamma(z) = \lim_{z\to -n} \frac{\Gamma(z+n+1)}{z(z+1)\dots(z+n-1)} \\ &= \frac{1}{-n(-n+1)\dots(-1)} = \frac{(-1)^n}{n!} \end{aligned} \tag{D.15}$$

Going back to the triangle integral I_4, we now see that we will get a term per pole present within the contour. Each of this term will comes with a definite branch in x. If we look at the kinematic dependence of the integrand, it reads

$$\begin{aligned} f(z) &= -\frac{1}{2\pi i}\frac{1}{(-s)^{1+\varepsilon}}\left(-\frac{m_W^2}{s}\right)^z \frac{\Gamma(-z)\Gamma(1+\varepsilon+z)\Gamma(1+z)\Gamma(-\varepsilon-z)^2}{\Gamma(1-2\varepsilon-z)} \\ &= -\frac{1}{2\pi i}(-x)^{1+z+\varepsilon}\rho^{-z}\frac{\Gamma(-z)\Gamma(1+\varepsilon+z)\Gamma(1+z)\Gamma(-\varepsilon-z)^2}{\Gamma(1-2\varepsilon-z)}\,. \end{aligned} \tag{D.16}$$

The constant $c_4(\varepsilon)$ that need to be fixed comes with $x\rho^\varepsilon$. We notice that this branch is produce by the pole of order two, $z_0 = -\varepsilon$. Indeed,

$$2\pi i\,\mathrm{Res}(f(z), z=-\varepsilon) = x\rho^\varepsilon\Gamma(\varepsilon)(2\psi(1-\varepsilon) - \ln(\rho) - \psi(\varepsilon) + \ln(-x) + \gamma_E)\,, \tag{D.17}$$

where $\psi(z)$ is the digamma function defined as

$$\psi(z) = \frac{\Gamma'(z)}{\Gamma(z)}\,. \tag{D.18}$$

As $x > 0$, we can analytically continue $\ln(-x) = \ln(x) + i\pi$ in Eq. (D.17). Then, the factor in front of $\rho^\varepsilon x$ reads

$$\Gamma(\varepsilon)(-\ln(\rho) + 2\psi(1-\varepsilon) - \psi(\varepsilon) + \ln(x) + i\pi + \gamma_E)\,. \tag{D.19}$$

We can drop the superfluous kinematic dependent terms $\ln(x)$ and $\ln(\rho)$ and apply the same normalisation of the loop momentum measure to determine the integration constant

$$\boxed{\begin{aligned} c_4(\varepsilon) &= e^{\varepsilon\gamma_E}\Gamma(\varepsilon)(2\psi(1-\varepsilon) - \psi(\varepsilon) + i\pi + \gamma_E) \\ &= -\frac{1}{\varepsilon^2} - \frac{i\pi}{\varepsilon} + \frac{5\pi^2}{12} + \mathcal{O}(\varepsilon)\,, \end{aligned}} \tag{D.20}$$

which agrees with the results found in Eq. (18.59).

BIBLIOGRAPHY

[1] Georges Aad et al. “Observation of a new particle in the search for the Standard Model Higgs boson with the ATLAS detector at the LHC.” In: *Phys. Lett. B* 716 (2012), pp. 1–29. DOI: `10.1016/j.physletb.2012.08.020`. arXiv: `1207.7214 [hep-ex]`.

[2] G. Apollinari, O. Brüning, T. Nakamoto, and Lucio Rossi. “High Luminosity Large Hadron Collider HL-LHC.” In: *CERN Yellow Rep.* 5 (2015). Ed. by G Apollinari, I Béjar Alonso, O Brüning, M Lamont, and L Rossi, pp. 1–19. DOI: `10.5170/CERN-2015-005.1`. arXiv: `1705.08830 [physics.acc-ph]`.

[3] ATLAS collaboration. “Standard Model Summary Plots February 2022.” In: (2022).

[4] Ilaria Brivio, Florian Goertz, and Gino Isidori. “Probing the Charm Quark Yukawa Coupling in Higgs+Charm Production.” In: *Phys. Rev. Lett.* 115.21 (2015), p. 211801. DOI: `10.1103/PhysRevLett.115.211801`. arXiv: `1507.02916 [hep-ph]`.

[5] Mathias Brucherseifer, Fabrizio Caola, and Kirill Melnikov. “On the NNLO QCD corrections to single-top production at the LHC.” In: *Phys. Lett. B* 736 (2014), pp. 58–63. DOI: `10.1016/j.physletb.2014.06.075`. arXiv: `1404.7116 [hep-ph]`.

[6] John Campbell, Tobias Neumann, and Zack Sullivan. “Single-top-quark production in the t-channel at NNLO.” In: *JHEP* 02 (2021), p. 040. DOI: `10.1007/JHEP02(2021)040`. arXiv: `2012.01574 [hep-ph]`.

[7] Tao Liu, Kirill Melnikov, and Alexander A. Penin. “Nonfactorizable QCD Effects in Higgs Boson Production via Vector Boson Fusion.” In: *Phys. Rev. Lett.* 123.12 (2019), p. 122002. DOI: `10.1103/PhysRevLett.123.122002`. arXiv: `1906.10899 [hep-ph]`.

[8] Michelangelo Mangano. “Physics at the FCC-hh, a 100 TeV pp collider.” In: 3/2017 (June 2017). DOI: `10.23731/CYRM-2017-003`. arXiv: `1710.06353 [hep-ph]`.

[9] A. Abada et al. “FCC-hh: The Hadron Collider: Future Circular Collider Conceptual Design Report Volume 3.” In: *Eur. Phys. J. ST* 228.4 (2019), pp. 755–1107. DOI: `10.1140/epjst/e2019-900087-0`.

[10] H. Weyl. “Electron and Gravitation. 1. (In German).” In: *Z. Phys.* 56 (1929), pp. 330–352. DOI: `10.1007/BF01339504`.

[11] Chen-Ning Yang and Robert L. Mills. “Conservation of Isotopic Spin and Isotopic Gauge Invariance.” In: *Phys. Rev.* 96 (1954). Ed. by Jong-Ping Hsu and D. Fine, pp. 191–195. DOI: `10.1103/PhysRev.96.191`.

[12] G Zweig. *An SU3 model for strong interaction symmetry and its breaking*. en. 2002. DOI: `10.17181/CERN-TH-412`. URL: `http://cds.cern.ch/record/570209`.

[13] M. Gell-Mann. "A schematic model of baryons and mesons." In: *Physics Letters* 8.3 (Feb. 1964), pp. 214–215. DOI: `10.1016/s0031-9163(64)92001-3`. URL: `https://doi.org/10.1016/s0031-9163(64)92001-3`.

[14] M. Y. Han and Yoichiro Nambu. "Three Triplet Model with Double SU(3) Symmetry." In: *Phys. Rev.* 139 (1965). Ed. by T. Eguchi, B1006–B1010. DOI: `10.1103/PhysRev.139.B1006`.

[15] Richard P. Feynman. "Very High-Energy Collisions of Hadrons." In: *Phys. Rev. Lett.* 23 (24 1969), pp. 1415–1417. DOI: `10.1103/PhysRevLett.23.1415`. URL: `https://link.aps.org/doi/10.1103/PhysRevLett.23.1415`.

[16] S. L. Glashow, J. Iliopoulos, and L. Maiani. "Weak Interactions with Lepton-Hadron Symmetry." In: *Phys. Rev. D* 2 (7 1970), pp. 1285–1292. DOI: `10.1103/PhysRevD.2.1285`. URL: `https://link.aps.org/doi/10.1103/PhysRevD.2.1285`.

[17] Makoto Kobayashi and Toshihide Maskawa. "CP Violation in the Renormalizable Theory of Weak Interaction." In: *Prog. Theor. Phys.* 49 (1973), pp. 652–657. DOI: `10.1143/PTP.49.652`.

[18] H. Fritzsch, Murray Gell-Mann, and H. Leutwyler. "Advantages of the Color Octet Gluon Picture." In: *Phys. Lett. B* 47 (1973), pp. 365–368. DOI: `10.1016/0370-2693(73)90625-4`.

[19] Abdus Salam and John Clive Ward. "Electromagnetic and weak interactions." In: *Phys. Lett.* 13 (1964), pp. 168–171. DOI: `10.1016/0031-9163(64)90711-5`.

[20] Steven Weinberg. "A Model of Leptons." In: *Phys. Rev. Lett.* 19 (1967), pp. 1264–1266. DOI: `10.1103/PhysRevLett.19.1264`.

[21] Gerard 't Hooft and M. J. G. Veltman. "Regularization and Renormalization of Gauge Fields." In: *Nucl. Phys. B* 44 (1972), pp. 189–213. DOI: `10.1016/0550-3213(72)90279-9`.

[22] S. L. Glashow, J. Iliopoulos, and L. Maiani. "Weak Interactions with Lepton-Hadron Symmetry." In: *Phys. Rev. D* 2 (1970), pp. 1285–1292. DOI: `10.1103/PhysRevD.2.1285`.

[23] S. L. Glashow. "Partial Symmetries of Weak Interactions." In: *Nucl. Phys.* 22 (1961), pp. 579–588. DOI: `10.1016/0029-5582(61)90469-2`.

[24] Peter W. Higgs. "Broken Symmetries and the Masses of Gauge Bosons." In: *Phys. Rev. Lett.* 13 (16 1964), pp. 508–509. DOI: `10.1103/PhysRevLett.13.508`. URL: `https://link.aps.org/doi/10.1103/PhysRevLett.13.508`.

[25] F. Englert and R. Brout. "Broken Symmetry and the Mass of Gauge Vector Mesons." In: *Phys. Rev. Lett.* 13 (1964). Ed. by J. C. Taylor, pp. 321–323. DOI: `10.1103/PhysRevLett.13.321`.

[26] Charalampos Anastasiou, Claude Duhr, Falko Dulat, Elisabetta Furlan, Thomas Gehrmann, Franz Herzog, and Bernhard Mistlberger. "Higgs boson gluon–fusion production at threshold in N^{3}LO QCD." In: *Phys. Lett. B* 737 (2014), pp. 325–328. DOI: 10.1016/j.physletb.2014.08.067. arXiv: 1403.4616 [hep-ph].

[27] Julien Baglio, Claude Duhr, Bernhard Mistlberger, and Robert Szafron. "Inclusive production cross sections at N^{3}LO." In: *JHEP* 12 (2022), p. 066. DOI: 10.1007/JHEP12(2022)066. arXiv: 2209.06138 [hep-ph].

[28] Federico Buccioni, Fabrizio Caola, Herschel A. Chawdhry, Federica Devoto, Matthias Heller, Andreas von Manteuffel, Kirill Melnikov, Raoul Röntsch, and Chiara Signorile-Signorile. "Mixed QCD-electroweak corrections to dilepton production at the LHC in the high invariant mass region." In: *JHEP* 06 (2022), p. 022. DOI: 10.1007/JHEP06(2022)022. arXiv: 2203.11237 [hep-ph].

[29] John M. Campbell, R. Keith Ellis, and Francesco Tramontano. "Single top production and decay at next-to-leading order." In: *Phys. Rev. D* 70 (2004), p. 094012. DOI: 10.1103/PhysRevD.70.094012. arXiv: hep-ph/0408158.

[30] Edmond L. Berger, Jun Gao, C. P. Yuan, and Hua Xing Zhu. "NNLO QCD Corrections to t-channel Single Top-Quark Production and Decay." In: *Phys. Rev. D* 94.7 (2016), p. 071501. DOI: 10.1103/PhysRevD.94.071501. arXiv: 1606.08463 [hep-ph].

[31] Edmond L. Berger, Jun Gao, and Hua Xing Zhu. "Differential Distributions for t-channel Single Top-Quark Production and Decay at Next-to-Next-to-Leading Order in QCD." In: *JHEP* 11 (2017), p. 158. DOI: 10.1007/JHEP11(2017)158. arXiv: 1708.09405 [hep-ph].

[32] Matteo Cacciari, Frédéric A. Dreyer, Alexander Karlberg, Gavin P. Salam, and Giulia Zanderighi. "Fully Differential Vector-Boson-Fusion Higgs Production at Next-to-Next-to-Leading Order." In: *Phys. Rev. Lett.* 115.8 (2015). [Erratum: Phys.Rev.Lett. 120, 139901 (2018)], p. 082002. DOI: 10.1103/PhysRevLett.115.082002. arXiv: 1506.02660 [hep-ph].

[33] J. Cruz-Martinez, T. Gehrmann, E. W. N. Glover, and A. Huss. "Second-order QCD effects in Higgs boson production through vector boson fusion." In: *Phys. Lett. B* 781 (2018), pp. 672–677. DOI: 10.1016/j.physletb.2018.04.046. arXiv: 1802.02445 [hep-ph].

[34] Frédéric A. Dreyer and Alexander Karlberg. "Vector-Boson Fusion Higgs Production at Three Loops in QCD." In: *Phys. Rev. Lett.* 117.7 (2016), p. 072001. DOI: 10.1103/PhysRevLett.117.072001. arXiv: 1606.00840 [hep-ph].

[35] Wojciech Bizon, Kirill Melnikov, and Jérémie Quarroz. "On the interference of ggH and $\bar{c}c$H Higgs production mechanisms and the determination of charm Yukawa coupling at the LHC." In: *JHEP* 06 (2021), p. 107. DOI: 10.1007/JHEP06(2021)107. arXiv: 2102.04242 [hep-ph].

[36] G. Aad and al. "Combined measurements of Higgs boson production and decay using up to 80 fb^{-1} of proton-proton collision data at $\sqrt{s} = 13$ TeV collected with the ATLAS experiment." In: *Phys. Rev. D* 101 (1 2020), p. 012002. DOI: 10.1103/PhysRevD.101.012002. URL: https://link.aps.org/doi/10.1103/PhysRevD.101.012002.

[37] Georges Aad et al. "A search for the dimuon decay of the Standard Model Higgs boson with the ATLAS detector." In: *Phys. Lett. B* 812 (2021), p. 135980. DOI: 10.1016/j.physletb.2020.135980. arXiv: 2007.07830 [hep-ex].

[38] Morad Aaboud et al. "Observation of $H \to b\bar{b}$ decays and VH production with the ATLAS detector." In: *Phys. Lett. B* 786 (2018), pp. 59–86. DOI: 10.1016/j.physletb.2018.09.013. arXiv: 1808.08238 [hep-ex].

[39] A. M. Sirunyan et al. "Observation of Higgs boson decay to bottom quarks." In: *Phys. Rev. Lett.* 121.12 (2018), p. 121801. DOI: 10.1103/PhysRevLett.121.121801. arXiv: 1808.08242 [hep-ex].

[40] Morad Aaboud et al. "Cross-section measurements of the Higgs boson decaying into a pair of τ-leptons in proton-proton collisions at $\sqrt{s} = 13$ TeV with the ATLAS detector." In: *Phys. Rev. D* 99 (2019), p. 072001. DOI: 10.1103/PhysRevD.99.072001. arXiv: 1811.08856 [hep-ex].

[41] Albert M Sirunyan et al. "Search for the associated production of the Higgs boson and a vector boson in proton-proton collisions at $\sqrt{s} = 13$ TeV via Higgs boson decays to τ leptons." In: *JHEP* 06 (2019), p. 093. DOI: 10.1007/JHEP06(2019)093. arXiv: 1809.03590 [hep-ex].

[42] Albert M. Sirunyan et al. "Search for the Higgs boson decaying to two muons in proton-proton collisions at $\sqrt{s} = 13$ TeV." In: *Phys. Rev. Lett.* 122.2 (2019), p. 021801. DOI: 10.1103/PhysRevLett.122.021801. arXiv: 1807.06325 [hep-ex].

[43] Gilad Perez, Yotam Soreq, Emmanuel Stamou, and Kohsaku Tobioka. "Prospects for measuring the Higgs boson coupling to light quarks." In: *Phys. Rev. D* 93.1 (2016), p. 013001. DOI: 10.1103/PhysRevD.93.013001. arXiv: 1505.06689 [hep-ph].

[44] Joseph Walker and Frank Krauss. "Constraining the Charm-Yukawa coupling at the Large Hadron Collider." In: *Phys. Lett. B* 832 (2022), p. 137255. DOI: 10.1016/j.physletb.2022.137255. arXiv: 2202.13937 [hep-ph].

[45] Alexander L. Kagan, Gilad Perez, Frank Petriello, Yotam Soreq, Stoyan Stoynev, and Jure Zupan. "Exclusive Window onto Higgs Yukawa Couplings." In: *Phys. Rev. Lett.* 114.10 (2015), p. 101802. DOI: 10.1103/PhysRevLett.114.101802. arXiv: 1406.1722 [hep-ph].

[46] Tanmoy Modak and Rahul Srivastava. "Probing anomalous Higgs couplings in H → ZV decays." In: *Mod. Phys. Lett. A* 32.03 (2017), p. 1750004. DOI: 10.1142/S0217732317500043. arXiv: 1411.2210 [hep-ph].

[47] Matthias König and Matthias Neubert. "Exclusive Radiative Higgs Decays as Probes of Light-Quark Yukawa Couplings." In: *JHEP* 08 (2015), p. 012. DOI: `10.1007/JHEP08(2015)012`. arXiv: `1505.03870 [hep-ph]`.

[48] Geoffrey T. Bodwin. "Factorization of the Drell-Yan Cross-Section in Perturbation Theory." In: *Phys. Rev. D* 31 (1985). [Erratum: Phys.Rev.D 34, 3932 (1986)], p. 2616. DOI: `10.1103/PhysRevD.34.3932`.

[49] John C. Collins and Davison E. Soper. "The Theorems of Perturbative QCD." In: *Ann. Rev. Nucl. Part. Sci.* 37 (1987), pp. 383–409. DOI: `10.1146/annurev.ns.37.120187.002123`.

[50] John C. Collins, Davison E. Soper, and George F. Sterman. "Factorization of Hard Processes in QCD." In: *Adv. Ser. Direct. High Energy Phys.* 5 (1989), pp. 1–91. DOI: `10.1142/9789814503266_0001`. arXiv: `hep-ph/0409313`.

[51] John C Collins. *Cambridge monographs on particle physics, nuclear physics and cosmology: Foundations of perturbative QCD series number 32*. Cambridge, England: Cambridge University Press, Apr. 2011.

[52] R. Doria, J. Frenkel, and J. C. Taylor. "Counter Example to Nonabelian Bloch-Nordsieck Theorem." In: *Nucl. Phys. B* 168 (1980), pp. 93–110. DOI: `10.1016/0550-3213(80)90278-3`.

[53] C. Di'Lieto, S. Gendron, I. G. Halliday, and Christopher T. Sachrajda. "A Counter Example to the Bloch-Nordsieck Theorem in Nonabelian Gauge Theories." In: *Nucl. Phys. B* 183 (1981), pp. 223–250. DOI: `10.1016/0550-3213(81)90554-X`.

[54] J. Frenkel, J. G. M. Gatheral, and J. C. Taylor. "IS QUARK - ANTI-QUARK ANNIHILATION INFRARED SAFE AT HIGH-ENERGY?" In: *Nucl. Phys. B* 233 (1984), pp. 307–335. DOI: `10.1016/0550-3213(84)90418-8`.

[55] S. Catani, M. Ciafaloni, and G. Marchesini. "Noncancelling Infrared Divergences in QCD Coherent State." In: *Nucl. Phys. B* 264 (1986), pp. 588–620. DOI: `10.1016/0550-3213(86)90500-6`.

[56] Stefano Catani. "Violation of the Bloch-nordsieck Mechanism in General Non-abelian Theories and SUSY QCD." In: *Z. Phys. C* 37 (1988), p. 357. DOI: `10.1007/BF01578128`.

[57] A. Andrasi, M. Day, R. Doria, J. Frenkel, and J. C. Taylor. "Soft Divergences in Perturbative QCD." In: *Nucl. Phys. B* 182 (1981), pp. 104–124. DOI: `10.1016/0550-3213(81)90460-0`.

[58] C. A. Nelson. "Avoidance of Counter Example to Nonabelian Bloch-Nordsieck Conjecture by Using Coherent State Approach." In: *Nucl. Phys. B* 186 (1981), pp. 187–204. DOI: `10.1016/0550-3213(81)90099-7`.

[59] Ikuo Ito. "Cancellation of Infrared Divergence and Initial Degenerate State in QCD." In: *Prog. Theor. Phys.* 65 (1981), p. 1466. DOI: `10.1143/PTP.65.1466`.

[60] Nobuo Yoshida. “Diagrammatical Display of the Counter Example to Nonabelian Bloch-nordsieck Conjecture.” In: *Prog. Theor. Phys.* 66 (1981), p. 269. DOI: `10.1143/PTP.66.269`.

[61] Nobuo Yoshida. “Cancellation of the Infrared Singularity through the Unitarity Relation.” In: *Prog. Theor. Phys.* 66 (1981), p. 1803. DOI: `10.1143/PTP.66.1803`.

[62] T. Muta and Charles A. Nelson. “Role of Quark - Gluon Degenerate States in Perturbative QCD.” In: *Phys. Rev. D* 25 (1982), p. 2222. DOI: `10.1103/PhysRevD.25.2222`.

[63] B. F. L. Ward. “Quark masses and resummation in precision QCD theory.” In: *Phys. Rev. D* 78 (2008), p. 056001. DOI: `10.1103/PhysRevD.78.056001`. arXiv: `0707.2101 [hep-ph]`.

[64] Fabrizio Caola, Kirill Melnikov, Davide Napoletano, and Lorenzo Tancredi. “Noncancellation of infrared singularities in collisions of massive quarks.” In: *Phys. Rev. D* 103.5 (2021), p. 054013. DOI: `10.1103/PhysRevD.103.054013`. arXiv: `2011.04701 [hep-ph]`.

[65] Fabrizio Caola, Kirill Melnikov, and Raoul Röntsch. “Nested soft-collinear subtractions in NNLO QCD computations.” In: *Eur. Phys. J. C* 77.4 (2017), p. 248. DOI: `10.1140/epjc/s10052-017-4774-0`. arXiv: `1702.01352 [hep-ph]`.

[66] Stefano Catani. “The Singular behavior of QCD amplitudes at two loop order.” In: *Phys. Lett. B* 427 (1998), pp. 161–171. DOI: `10.1016/S0370-2693(98)00332-3`. arXiv: `hep-ph/9802439`.

[67] W. Bernreuther, R. Bonciani, T. Gehrmann, R. Heinesch, T. Leineweber, P. Mastrolia, and E. Remiddi. “Two-loop QCD corrections to the heavy quark form-factors: The Vector contributions.” In: *Nucl. Phys. B* 706 (2005), pp. 245–324. DOI: `10.1016/j.nuclphysb.2004.10.059`. arXiv: `hep-ph/0406046`.

[68] Stefano Frixione. “Initial conditions for electron and photon structure and fragmentation functions.” In: *JHEP* 11 (2019), p. 158. DOI: `10.1007/JHEP11(2019)158`. arXiv: `1909.03886 [hep-ph]`.

[69] Guido Altarelli and G. Parisi. “Asymptotic Freedom in Parton Language.” In: *Nucl. Phys. B* 126 (1977), pp. 298–318. DOI: `10.1016/0550-3213(77)90384-4`.

[70] Yuri L. Dokshitzer. “Calculation of the Structure Functions for Deep Inelastic Scattering and e+ e- Annihilation by Perturbation Theory in Quantum Chromodynamics.” In: *Sov. Phys. JETP* 46 (1977), pp. 641–653.

[71] V. N. Gribov and L. N. Lipatov. “Deep inelastic e p scattering in perturbation theory.” In: *Sov. J. Nucl. Phys.* 15 (1972), pp. 438–450.

[72] Johannes Reinking. “Infra-red Factorisation in Power Suppressed Contributions to $pp \to H + \text{jet}_c$ at the LHC.” MA thesis. KIT, 2022.

[73] J. A. M. Vermaseren. “New features of FORM.” In: (Oct. 2000). arXiv: math-ph/0010025.

[74] J. Kuipers, T. Ueda, J. A. M. Vermaseren, and J. Vollinga. “FORM version 4.0.” In: *Comput. Phys. Commun.* 184 (2013), pp. 1453–1467. DOI: 10.1016/j.cpc.2012.12.028. arXiv: 1203.6543 [cs.SC].

[75] J. Kuipers, T. Ueda, and J. A. M. Vermaseren. “Code Optimization in FORM.” In: *Comput. Phys. Commun.* 189 (2015), pp. 1–19. DOI: 10.1016/j.cpc.2014.08.008. arXiv: 1310.7007 [cs.SC].

[76] Ben Ruijl, Takahiro Ueda, and Jos Vermaseren. “FORM version 4.2.” In: (July 2017). arXiv: 1707.06453 [hep-ph].

[77] J. Alwall, R. Frederix, S. Frixione, V. Hirschi, F. Maltoni, O. Mattelaer, H. S. Shao, T. Stelzer, P. Torrielli, and M. Zaro. “The automated computation of tree-level and next-to-leading order differential cross sections, and their matching to parton shower simulations.” In: *JHEP* 07 (2014), p. 079. DOI: 10.1007/JHEP07(2014)079. arXiv: 1405.0301 [hep-ph].

[78] G Peter Lepage. “A new algorithm for adaptive multidimensional integration.” In: *Journal of Computational Physics* 27.2 (May 1978), pp. 192–203. DOI: 10.1016/0021-9991(78)90004-9. URL: https://doi.org/10.1016/0021-9991(78)90004-9.

[79] P. Nogueira. “Automatic Feynman Graph Generation.” In: *Journal of Computational Physics* 105.2 (1993), pp. 279–289. DOI: 10.1006/jcph.1993.1074. URL: https://doi.org/10.1006/jcph.1993.1074.

[80] G. Passarino and M. J. G. Veltman. “One Loop Corrections for e+ e- Annihilation Into mu+ mu- in the Weinberg Model.” In: *Nucl. Phys. B* 160 (1979), pp. 151–207. DOI: 10.1016/0550-3213(79)90234-7.

[81] Hiren H. Patel. “Package-X: A Mathematica package for the analytic calculation of one-loop integrals.” In: *Comput. Phys. Commun.* 197 (2015), pp. 276–290. DOI: 10.1016/j.cpc.2015.08.017. arXiv: 1503.01469 [hep-ph].

[82] Arnd Behring and Wojciech Bizoń. “Higgs decay into massive b-quarks at NNLO QCD in the nested soft-collinear subtraction scheme.” In: *JHEP* 01 (2020), p. 189. DOI: 10.1007/JHEP01(2020)189. arXiv: 1911.11524 [hep-ph].

[83] Roberto Mondini, Ulrich Schubert, and Ciaran Williams. “Top-induced contributions to $H \to b\bar{b}$ and $H \to c\bar{c}$ at $\mathcal{O}(\alpha_s^3)$.” In: *JHEP* 12 (2020), p. 058. DOI: 10.1007/JHEP12(2020)058. arXiv: 2006.03563 [hep-ph].

[84] Stefano Catani, Stefan Dittmaier, and Zoltan Trocsanyi. “One loop singular behavior of QCD and SUSY QCD amplitudes with massive partons.” In: *Phys. Lett. B* 500 (2001), pp. 149–160. DOI: 10.1016/S0370-2693(01)00065-X. arXiv: hep-ph/0011222.

[85] M. Czakon and D. Heymes. "Four-dimensional formulation of the sector-improved residue subtraction scheme." In: *Nucl. Phys. B* 890 (2014), pp. 152–227. DOI: 10.1016/j.nuclphysb.2014.11.006. arXiv: 1408.2500 [hep-ph].

[86] S. Mert Aybat, Lance J. Dixon, and George F. Sterman. "The Two-loop soft anomalous dimension matrix and resummation at next-to-next-to leading pole." In: *Phys. Rev. D* 74 (2006), p. 074004. DOI: 10.1103/PhysRevD.74.074004. arXiv: hep-ph/0607309.

[87] Thomas Becher and Matthias Neubert. "Infrared singularities of QCD amplitudes with massive partons." In: *Phys. Rev. D* 79 (2009), p. 125004. DOI: 10.1103/PhysRevD.79.125004. arXiv: 0904.1021 [hep-ph].

[88] Alexander Mitov, George F. Sterman, and Ilmo Sung. "The Massive Soft Anomalous Dimension Matrix at Two Loops." In: *Phys. Rev. D* 79 (2009), p. 094015. DOI: 10.1103/PhysRevD.79.094015. arXiv: 0903.3241 [hep-ph].

[89] Andrea Ferroglia, Matthias Neubert, Ben D. Pecjak, and Li Lin Yang. "Two-loop divergences of massive scattering amplitudes in non-abelian gauge theories." In: *JHEP* 11 (2009), p. 062. DOI: 10.1088/1126-6708/2009/11/062. arXiv: 0908.3676 [hep-ph].

[90] Alexander Mitov, George F. Sterman, and Ilmo Sung. "Computation of the Soft Anomalous Dimension Matrix in Coordinate Space." In: *Phys. Rev. D* 82 (2010), p. 034020. DOI: 10.1103/PhysRevD.82.034020. arXiv: 1005.4646 [hep-ph].

[91] Thomas Becher and Matthias Neubert. "Infrared singularities of scattering amplitudes in perturbative QCD." In: *Phys. Rev. Lett.* 102 (2009), p. 162001. DOI: 10.1103/PhysRevLett.102.162001. arXiv: 0901.0722 [hep-ph].

[92] V. V. Sudakov. "Vertex parts at very high-energies in quantum electrodynamics." In: *Sov. Phys. JETP* 3 (1956), pp. 65–71.

[93] Kirill Melnikov and Alexander Penin. "On the light quark mass effects in Higgs boson production in gluon fusion." In: *JHEP* 05 (2016), p. 172. DOI: 10.1007/JHEP05(2016)172. arXiv: 1602.09020 [hep-ph].

[94] Florian Herren and Matthias Steinhauser. "Version 3 of RunDec and CRunDec." In: *Comput. Phys. Commun.* 224 (2018), pp. 333–345. DOI: 10.1016/j.cpc.2017.11.014. arXiv: 1703.03751 [hep-ph].

[95] Andy Buckley, James Ferrando, Stephen Lloyd, Karl Nordström, Ben Page, Martin Rüfenacht, Marek Schönherr, and Graeme Watt. "LHAPDF6: parton density access in the LHC precision era." In: *Eur. Phys. J. C* 75 (2015), p. 132. DOI: 10.1140/epjc/s10052-015-3318-8. arXiv: 1412.7420 [hep-ph].

[96] Richard D. Ball et al. "Parton distributions from high-precision collider data." In: *Eur. Phys. J. C* 77.10 (2017), p. 663. DOI: 10.1140/epjc/s10052-017-5199-5. arXiv: 1706.00428 [hep-ph].

[97] Matteo Cacciari, Gavin P. Salam, and Gregory Soyez. "The anti-k_t jet clustering algorithm." In: *JHEP* 04 (2008), p. 063. DOI: `10.1088/1126-6708/2008/04/063`. arXiv: `0802.1189 [hep-ph]`.

[98] Christian Brønnum-Hansen, Kirill Melnikov, Jérémie Quarroz, and Chen-Yu Wang. "On non-factorisable contributions to t-channel single-top production." In: *JHEP* 11 (2021), p. 130. DOI: `10.1007/JHEP11(2021)130`. arXiv: `2108.09222 [hep-ph]`.

[99] Christian Brønnum-Hansen, Jeremie Quarroz, Chiara Signorile-Signorile, and Chen-Yu Wang. "Non-factorisable corrections to t- channel single-top production: comparing results for the LHC and FCC." In: *Strong interactions from QCD to new strong dynamics at LHC and Future Colliders*. 2022, pp. 67–72.

[100] Christian Brønnum-Hansen, Kirill Melnikov, Jérémie Quarroz, Chiara Signorile-Signorile, and Chen-Yu Wang. "Non-factorisable contribution to t-channel single-top production." In: *JHEP* 06 (2022), p. 061. DOI: `10.1007/JHEP06(2022)061`. arXiv: `2204.05770 [hep-ph]`.

[101] Christian Brønnum-Hansen, Jérémie Quarroz, and Chen-Yu Wang. "Non-factorisable two-loop contribution to t-channel single-top production." In: *14th International Workshop on Top Quark Physics*. Jan. 2022. arXiv: `2201.03480 [hep-ph]`.

[102] Christian Brønnum-Hansen, Jérémie Quarroz, Chiara Signorile-Signorile, and Chen-Yu Wang. "Non-factorisable contributions to t-channel single-top production at the LHC and FCC." In: *PoS* LL2022 (2022), p. 035. DOI: `10.22323/1.416.0035`. arXiv: `2207.10350 [hep-ph]`.

[103] P. Nason, S. Dawson, and R. Keith Ellis. "The Total Cross-Section for the Production of Heavy Quarks in Hadronic Collisions." In: *Nucl. Phys. B* 303 (1988), pp. 607–633. DOI: `10.1016/0550-3213(88)90422-1`.

[104] Johann H. Kuhn, A. Scharf, and P. Uwer. "Electroweak corrections to top-quark pair production in quark-antiquark annihilation." In: *Eur. Phys. J. C* 45 (2006), pp. 139–150. DOI: `10.1140/epjc/s2005-02423-6`. arXiv: `hep-ph/0508092`.

[105] Michal Czakon, David Heymes, Alexander Mitov, Davide Pagani, Ioannis Tsinikos, and Marco Zaro. "Top-pair production at the LHC through NNLO QCD and NLO EW." In: *JHEP* 10 (2017), p. 186. DOI: `10.1007/JHEP10(2017)186`. arXiv: `1705.04105 [hep-ph]`.

[106] Michal Czakon, Alexander Mitov, and George F. Sterman. "Threshold Resummation for Top-Pair Hadroproduction to Next-to-Next-to-Leading Log." In: *Phys. Rev. D* 80 (2009), p. 074017. DOI: `10.1103/PhysRevD.80.074017`. arXiv: `0907.1790 [hep-ph]`.

[107] Matteo Cacciari, Michal Czakon, Michelangelo Mangano, Alexander Mitov, and Paolo Nason. "Top-pair production at hadron colliders with next-to-next-to-leading logarithmic soft-gluon resummation." In: *Phys. Lett. B* 710 (2012), pp. 612–622. DOI: `10.1016/j.physletb.2012.03.013`. arXiv: `1111.5869 [hep-ph]`.

[108] Albert M Sirunyan et al. "Measurement of CKM matrix elements in single top quark t-channel production in proton-proton collisions at $\sqrt{s} = 13$ TeV." In: *Phys. Lett. B* 808 (2020), p. 135609. DOI: `10.1016/j.physletb.2020.135609`. arXiv: `2004.12181 [hep-ex]`.

[109] Morad Aaboud et al. "Combinations of single-top-quark production cross-section measurements and $|\mathrm{f}_{LV}\mathrm{V}_{tb}|$ determinations at $\sqrt{s}$ = 7 and 8 TeV with the ATLAS and CMS experiments." In: *JHEP* 05 (2019), p. 088. DOI: `10.1007/JHEP05(2019)088`. arXiv: `1902.07158 [hep-ex]`.

[110] Vardan Khachatryan et al. "Measurement of the t-channel single-top-quark production cross section and of the $\mid V_{tb} \mid$ CKM matrix element in pp collisions at $\sqrt{s}$= 8 TeV." In: *JHEP* 06 (2014), p. 090. DOI: `10.1007/JHEP06(2014)090`. arXiv: `1403.7366 [hep-ex]`.

[111] Timo Antero Aaltonen et al. "Tevatron Combination of Single-Top-Quark Cross Sections and Determination of the Magnitude of the Cabibbo-Kobayashi-Maskawa Matrix Element V_{tb}." In: *Phys. Rev. Lett.* 115.15 (2015), p. 152003. DOI: `10.1103/PhysRevLett.115.152003`. arXiv: `1503.05027 [hep-ex]`.

[112] Morad Aaboud et al. "Probing the W tb vertex structure in t-channel single-top-quark production and decay in pp collisions at $\sqrt{s} = 8$ TeV with the ATLAS detector." In: *JHEP* 04 (2017), p. 124. DOI: `10.1007/JHEP04(2017)124`. arXiv: `1702.08309 [hep-ex]`.

[113] Gabriel A. González-Sprinberg and Jordi Vidal. "The top quark right coupling in the tbW-vertex." In: *Eur. Phys. J. C* 75.12 (2015), p. 615. DOI: `10.1140/epjc/s10052-015-3844-4`. arXiv: `1510.02153 [hep-ph]`.

[114] Vardan Khachatryan et al. "Measurement of the ratio $\mathcal{B}(t \to Wb)/\mathcal{B}(t \to Wq)$ in pp collisions at $\sqrt{s}$ = 8 TeV." In: *Phys. Lett. B* 736 (2014), pp. 33–57. DOI: `10.1016/j.physletb.2014.06.076`. arXiv: `1404.2292 [hep-ex]`.

[115] Albert M Sirunyan et al. "Measurement of the top quark mass using single top quark events in proton-proton collisions at $\sqrt{s} = 8$ TeV." In: *Eur. Phys. J. C* 77.5 (2017), p. 354. DOI: `10.1140/epjc/s10052-017-4912-8`. arXiv: `1703.02530 [hep-ex]`.

[116] B. W. Harris, Eric Laenen, L. Phaf, Z. Sullivan, and S. Weinzierl. "The Fully Differential Single Top Quark Cross-Section in Next to Leading Order QCD." In: *Phys. Rev. D* 66 (2002), p. 054024. DOI: `10.1103/PhysRevD.66.054024`. arXiv: `hep-ph/0207055`.

[117] Qing-Hong Cao and C. P. Yuan. “Single top quark production and decay at next-to-leading order in hadron collision.” In: *Phys. Rev. D* 71 (2005), p. 054022. DOI: 10.1103/PhysRevD.71.054022. arXiv: hep-ph/0408180.

[118] Reinhard Schwienhorst, C. P. Yuan, Charles Mueller, and Qing-Hong Cao. “Single top quark production and decay in the t-channel at next-to-leading order at the LHC.” In: *Phys. Rev. D* 83 (2011), p. 034019. DOI: 10.1103/PhysRevD.83.034019. arXiv: 1012.5132 [hep-ph].

[119] G. Bordes and B. van Eijk. “Calculating QCD corrections to single top production in hadronic interactions.” In: *Nucl. Phys. B* 435 (1995), pp. 23–58. DOI: 10.1016/0550-3213(94)00460-V.

[120] Qing-Hong Cao, Reinhard Schwienhorst, Jorge A. Benitez, Raymond Brock, and C. P. Yuan. “Next-to-leading order corrections to single top quark production and decay at the Tevatron: 2. t^- channel process.” In: *Phys. Rev. D* 72 (2005), p. 094027. DOI: 10.1103/PhysRevD.72.094027. arXiv: hep-ph/0504230.

[121] R. J. Glauber. *Lectures in Theoretical Physics*. New York: Wiley-Interscience, 1959.

[122] Najam ul Basat, Zhao Li, and Yefan Wang. “Reduction of the planar double-box diagram for single-top production via auxiliary mass flow.” In: *Phys. Rev. D* 104.5 (2021), p. 056020. DOI: 10.1103/PhysRevD.104.056020. arXiv: 2102.08225 [hep-ph].

[123] M. Assadsolimani, P. Kant, B. Tausk, and P. Uwer. “Calculation of two-loop QCD corrections for hadronic single top-quark production in the t channel.” In: *Phys. Rev. D* 90.11 (2014), p. 114024. DOI: 10.1103/PhysRevD.90.114024. arXiv: 1409.3654 [hep-ph].

[124] Nikolaos Syrrakos. “Two-loop master integrals for a planar and a non-planar topology relevant for single top production.” In: (Mar. 2023). arXiv: 2303.07395 [hep-ph].

[125] Zihao Wu and Ming-Ming Long. “Evaluating master integrals in non-factorizable corrections to t-channel single-top production at NNLO QCD.” In: (Mar. 2023). arXiv: 2303.08814 [hep-ph].

[126] Xiao Liu and Yan-Qing Ma. “Multiloop corrections for collider processes using auxiliary mass flow.” In: (July 2021). arXiv: 2107.01864 [hep-ph].

[127] Xiao Liu, Yan-Qing Ma, Wei Tao, and Peng Zhang. “Calculation of Feynman loop integration and phase-space integration via auxiliary mass flow.” In: *Chin. Phys. C* 45.1 (2021), p. 013115. DOI: 10.1088/1674-1137/abc538. arXiv: 2009.07987 [hep-ph].

[128] Christian Brønnum-Hansen and Chen-Yu Wang. “Top quark contribution to two-loop helicity amplitudes for Z boson pair production in gluon fusion.” In: *JHEP* 05 (2021), p. 244. DOI: 10.1007/JHEP05(2021)244. arXiv: 2101.12095 [hep-ph].

[129] Christian Brønnum-Hansen and Chen-Yu Wang. "Contribution of third generation quarks to two-loop helicity amplitudes for W boson pair production in gluon fusion." In: *JHEP* 01 (2021), p. 170. DOI: `10.1007/JHEP01(2021)170`. arXiv: `2009.03742 [hep-ph]`.

[130] S. Catani and M. H. Seymour. "A General algorithm for calculating jet cross-sections in NLO QCD." In: *Nucl. Phys. B* 485 (1997). [Erratum: Nucl.Phys.B 510, 503–504 (1998)], pp. 291–419. DOI: `10.1016/S0550-3213(96)00589-5`. arXiv: `hep-ph/9605323`.

[131] Simone Alioli, Paolo Nason, Carlo Oleari, and Emanuele Re. "A general framework for implementing NLO calculations in shower Monte Carlo programs: the POWHEG BOX." In: *JHEP* 06 (2010), p. 043. DOI: `10.1007/JHEP06(2010)043`. arXiv: `1002.2581 [hep-ph]`.

[132] Erik Panzer. "Algorithms for the symbolic integration of hyperlogarithms with applications to Feynman integrals." In: *Comput. Phys. Commun.* 188 (2015), pp. 148–166. DOI: `10.1016/j.cpc.2014.10.019`. arXiv: `1403.3385 [hep-th]`.

[133] Claude Duhr and Falko Dulat. "PolyLogTools — polylogs for the masses." In: *JHEP* 08 (2019), p. 135. DOI: `10.1007/JHEP08(2019)135`. arXiv: `1904.07279 [hep-th]`.

[134] Christian Schubert. "On the gamma(5) problem of dimensional renormalization." In: (Dec. 1993).

[135] Michael S. Chanowitz, M. Furman, and I. Hinchliffe. "The Axial Current in Dimensional Regularization." In: *Nucl. Phys. B* 159 (1979), pp. 225–243. DOI: `10.1016/0550-3213(79)90333-X`.

[136] Lance J. Dixon. "Calculating scattering amplitudes efficiently." In: *Theoretical Advanced Study Institute in Elementary Particle Physics (TASI 95): QCD and Beyond*. Jan. 1996, pp. 539–584. arXiv: `hep-ph/9601359`.

[137] A. von Manteuffel and C. Studerus. "Reduze 2 - Distributed Feynman Integral Reduction." In: (Jan. 2012). arXiv: `1201.4330 [hep-ph]`.

[138] Jonas Klappert, Fabian Lange, Philipp Maierhöfer, and Johann Usovitsch. "Integral Reduction with Kira 2.0 and Finite Field Methods." In: (Aug. 2020). arXiv: `2008.06494 [hep-ph]`.

[139] S. Laporta. "High precision calculation of multiloop Feynman integrals by difference equations." In: *Int. J. Mod. Phys. A* 15 (2000), pp. 5087–5159. DOI: `10.1142/S0217751X00002159`. arXiv: `hep-ph/0102033`.

[140] Gerard 't Hooft and M. J. G. Veltman. "Scalar One Loop Integrals." In: *Nucl. Phys. B* 153 (1979), pp. 365–401. DOI: `10.1016/0550-3213(79)90605-9`.

[141] K. G. Chetyrkin, A. L. Kataev, and F. V. Tkachov. “New Approach to Evaluation of Multiloop Feynman Integrals: The Gegenbauer Polynomial x Space Technique.” In: *Nucl. Phys. B* 174 (1980), pp. 345–377. DOI: `10.1016/0550-3213(80)90289-8`.

[142] R. Scharf and J. B. Tausk. “Scalar two loop integrals for gauge boson selfenergy diagrams with a massless fermion loop.” In: *Nucl. Phys. B* 412 (1994), pp. 523–552. DOI: `10.1016/0550-3213(94)90391-3`.

[143] T. Gehrmann and E. Remiddi. “Differential equations for two loop four point functions.” In: *Nucl. Phys. B* 580 (2000), pp. 485–518. DOI: `10.1016/S0550-3213(00)00223-6`. arXiv: `hep-ph/9912329`.

[144] T. Gehrmann, T. Huber, and D. Maitre. “Two-loop quark and gluon form-factors in dimensional regularisation.” In: *Phys. Lett. B* 622 (2005), pp. 295–302. DOI: `10.1016/j.physletb.2005.07.019`. arXiv: `hep-ph/0507061`.

[145] Fabio Maltoni, Manoj K. Mandal, and Xiaoran Zhao. “Top-quark effects in diphoton production through gluon fusion at next-to-leading order in QCD.” In: *Phys. Rev. D* 100.7 (2019), p. 071501. DOI: `10.1103/PhysRevD.100.071501`. arXiv: `1812.08703 [hep-ph]`.

[146] Hjalte Frellesvig, Martijn Hidding, Leila Maestri, Francesco Moriello, and Giulio Salvatori. “The complete set of two-loop master integrals for Higgs + jet production in QCD.” In: *JHEP* 06 (2020), p. 093. DOI: `10.1007/JHEP06(2020)093`. arXiv: `1911.06308 [hep-ph]`.

[147] Samuel Abreu, Harald Ita, Francesco Moriello, Ben Page, Wladimir Tschernow, and Mao Zeng. “Two-Loop Integrals for Planar Five-Point One-Mass Processes.” In: *JHEP* 11 (2020), p. 117. DOI: `10.1007/JHEP11(2020)117`. arXiv: `2005.04195 [hep-ph]`.

[148] S. Borowka, G. Heinrich, S. Jahn, S. P. Jones, M. Kerner, J. Schlenk, and T. Zirke. “pySecDec: a toolbox for the numerical evaluation of multi-scale integrals.” In: *Comput. Phys. Commun.* 222 (2018), pp. 313–326. DOI: `10.1016/j.cpc.2017.09.015`. arXiv: `1703.09692 [hep-ph]`.

[149] S. Borowka, G. Heinrich, S. Jahn, S. P. Jones, M. Kerner, and J. Schlenk. “A GPU compatible quasi-Monte Carlo integrator interfaced to pySecDec.” In: *Comput. Phys. Commun.* 240 (2019), pp. 120–137. DOI: `10.1016/j.cpc.2019.02.015`. arXiv: `1811.11720 [physics.comp-ph]`.

[150] D. Maitre and P. Mastrolia. “S@M, a Mathematica Implementation of the Spinor-Helicity Formalism.” In: *Comput. Phys. Commun.* 179 (2008), pp. 501–574. DOI: `10.1016/j.cpc.2008.05.002`. arXiv: `0710.5559 [hep-ph]`.

[151] Tiziano Peraro and Lorenzo Tancredi. “Tensor decomposition for bosonic and fermionic scattering amplitudes.” In: *Phys. Rev. D* 103.5 (2021), p. 054042. DOI: `10.1103/PhysRevD.103.054042`. arXiv: `2012.00820 [hep-ph]`.

[152] W. L. van Neerven and J. A. M. Vermaseren. "LARGE LOOP INTEGRALS." In: *Phys. Lett. B* 137 (1984), pp. 241–244. DOI: `10.1016/0370-2693(84)90237-5`.

[153] R. Keith Ellis, Zoltan Kunszt, Kirill Melnikov, and Giulia Zanderighi. "One-loop calculations in quantum field theory: from Feynman diagrams to unitarity cuts." In: *Phys. Rept.* 518 (2012), pp. 141–250. DOI: `10.1016/j.physrep.2012.01.008`. arXiv: `1105.4319 [hep-ph]`.

[154] Zvi Bern, Lance J. Dixon, and David A. Kosower. "Dimensionally regulated one loop integrals." In: *Phys. Lett. B* 302 (1993), pp. 299–308. DOI: `10.1016/0370-2693(93)90400-C`. arXiv: `hep-ph/9212308`.

[155] Zvi Bern, Lance J. Dixon, and David A. Kosower. "Dimensionally regulated pentagon integrals." In: *Nucl. Phys. B* 412 (1994), pp. 751–816. DOI: `10.1016/0550-3213(94)90398-0`. arXiv: `hep-ph/9306240`.

[156] Simon Badger, Gustav Mogull, and Tiziano Peraro. "Local integrands for two-loop all-plus Yang-Mills amplitudes." In: *JHEP* 08 (2016), p. 063. DOI: `10.1007/JHEP08(2016)063`. arXiv: `1606.02244 [hep-ph]`.

[157] R. Keith Ellis and Giulia Zanderighi. "Scalar one-loop integrals for QCD." In: *JHEP* 02 (2008), p. 002. DOI: `10.1088/1126-6708/2008/02/002`. arXiv: `0712.1851 [hep-ph]`.

[158] Stefano Carrazza, R. Keith Ellis, and Giulia Zanderighi. "QCDLoop: a comprehensive framework for one-loop scalar integrals." In: *Comput. Phys. Commun.* 209 (2016), pp. 134–143. DOI: `10.1016/j.cpc.2016.07.033`. arXiv: `1605.03181 [hep-ph]`.

[159] Sayipjamal Dulat, Tie-Jiun Hou, Jun Gao, Marco Guzzi, Joey Huston, Pavel Nadolsky, Jon Pumplin, Carl Schmidt, Daniel Stump, and C. P. Yuan. "New parton distribution functions from a global analysis of quantum chromodynamics." In: *Phys. Rev. D* 93.3 (2016), p. 033006. DOI: `10.1103/PhysRevD.93.033006`. arXiv: `1506.07443 [hep-ph]`.

[160] Stephen D. Ellis and Davison E. Soper. "Successive combination jet algorithm for hadron collisions." In: *Phys. Rev. D* 48 (1993), pp. 3160–3166. DOI: `10.1103/PhysRevD.48.3160`. arXiv: `hep-ph/9305266`.

[161] Ming-Ming Long, Kirill Melnikov, and Jérémie Quarroz. "Non-factorizable virtual corrections to Higgs boson production in weak boson fusion beyond the eikonal approximation." In: *JHEP* 07 (2023), p. 035. DOI: `10.1007/JHEP07(2023)035`. arXiv: `2305.12937 [hep-ph]`.

[162] Gudrun Heinrich. "Collider Physics at the Precision Frontier." In: *Phys. Rept.* 922 (2021), pp. 1–69. DOI: `10.1016/j.physrep.2021.03.006`. arXiv: `2009.00516 [hep-ph]`.

[163] Morad Aaboud et al. “Search for Higgs bosons produced via vector-boson fusion and decaying into bottom quark pairs in $\sqrt{s} = 13$ TeV pp collisions with the ATLAS detector.” In: *Phys. Rev. D* 98.5 (2018), p. 052003. DOI: 10.1103/PhysRevD.98.052003. arXiv: 1807.08639 [hep-ex].

[164] Georges Aad et al. “Combined measurements of Higgs boson production and decay using up to 80 fb^{-1} of proton-proton collision data at $\sqrt{s} = 13$ TeV collected with the ATLAS experiment.” In: *Phys. Rev. D* 101.1 (2020), p. 012002. DOI: 10.1103/PhysRevD.101.012002. arXiv: 1909.02845 [hep-ex].

[165] Vardan Khachatryan et al. “Search for the standard model Higgs boson produced through vector boson fusion and decaying to $b\bar{b}$.” In: *Phys. Rev. D* 92.3 (2015), p. 032008. DOI: 10.1103/PhysRevD.92.032008. arXiv: 1506.01010 [hep-ex].

[166] Albert M Sirunyan et al. “Combined measurements of Higgs boson couplings in proton–proton collisions at $\sqrt{s} = 13\,\text{TeV}$.” In: *Eur. Phys. J. C* 79.5 (2019), p. 421. DOI: 10.1140/epjc/s10052-019-6909-y. arXiv: 1809.10733 [hep-ex].

[167] T. Figy, C. Oleari, and D. Zeppenfeld. “Next-to-leading order jet distributions for Higgs boson production via weak boson fusion.” In: *Phys. Rev. D* 68 (2003), p. 073005. DOI: 10.1103/PhysRevD.68.073005. arXiv: hep-ph/0306109.

[168] Edmond L. Berger and John M. Campbell. “Higgs boson production in weak boson fusion at next-to-leading order.” In: *Phys. Rev. D* 70 (2004), p. 073011. DOI: 10.1103/PhysRevD.70.073011. arXiv: hep-ph/0403194.

[169] Mariano Ciccolini, Ansgar Denner, and Stefan Dittmaier. “Electroweak and QCD corrections to Higgs production via vector-boson fusion at the LHC.” In: *Phys. Rev. D* 77 (2008), p. 013002. DOI: 10.1103/PhysRevD.77.013002. arXiv: 0710.4749 [hep-ph].

[170] Tao Han, G. Valencia, and S. Willenbrock. “Structure function approach to vector boson scattering in p p collisions.” In: *Phys. Rev. Lett.* 69 (1992), pp. 3274–3277. DOI: 10.1103/PhysRevLett.69.3274. arXiv: hep-ph/9206246.

[171] Frédéric A. Dreyer, Alexander Karlberg, and Lorenzo Tancredi. “On the impact of non-factorisable corrections in VBF single and double Higgs production.” In: *JHEP* 10 (2020), p. 131. DOI: 10.1007/JHEP10(2020)131. arXiv: 2005.11334 [hep-ph].

[172] M. Beneke and Vladimir A. Smirnov. “Asymptotic expansion of Feynman integrals near threshold.” In: *Nucl. Phys. B* 522 (1998), pp. 321–344. DOI: 10.1016/S0550-3213(98)00138-2. arXiv: hep-ph/9711391.

[173] Vladimir A Smirnov. *Applied asymptotic expansions in momenta and masses*. en. 2002nd ed. Springer Tracts in Modern Physics. Ergebnisse der exakten Naturwissenschaften. Berlin, Germany: Springer, July 2003.

[174] Bernd Jantzen, Alexander V. Smirnov, and Vladimir A. Smirnov. “Expansion by regions: revealing potential and Glauber regions automatically.” In: *Eur. Phys. J. C* 72 (2012), p. 2139. DOI: `10.1140/epjc/s10052-012-2139-2`. arXiv: `1206.0546 [hep-ph]`.

[175] A. Pak and A. Smirnov. “Geometric approach to asymptotic expansion of Feynman integrals.” In: *Eur. Phys. J. C* 71 (2011), p. 1626. DOI: `10.1140/epjc/s10052-011-1626-1`. arXiv: `1011.4863 [hep-ph]`.

[176] Vladimir Alexandrovich Smirnov. *Feynman Integral Calculus*. en. 2006th ed. Berlin, Germany: Springer, Aug. 2006.

[177] Michael E. Peskin. *An Introduction To Quantum Field Theory*. CRC Press, May 2018. DOI: `10.1201/9780429503559`. URL: `https://doi.org/10.1201/9780429503559`.

[178] Philipp Maierhöfer, Johann Usovitsch, and Peter Uwer. “Kira—A Feynman integral reduction program.” In: *Comput. Phys. Commun.* 230 (2018), pp. 99–112. DOI: `10.1016/j.cpc.2018.04.012`. arXiv: `1705.05610 [hep-ph]`.

[179] R. N. Lee. “Presenting LiteRed: a tool for the Loop InTEgrals REDuction.” In: (Dec. 2012). arXiv: `1212.2685 [hep-ph]`.

[180] M. Czakon. “Automatized analytic continuation of Mellin-Barnes integrals.” In: *Comput. Phys. Commun.* 175 (2006), pp. 559–571. DOI: `10.1016/j.cpc.2006.07.002`. arXiv: `hep-ph/0511200`.

[181] J. Gluza, K. Kajda, and T. Riemann. “AMBRE: A Mathematica package for the construction of Mellin-Barnes representations for Feynman integrals.” In: *Comput. Phys. Commun.* 177 (2007), pp. 879–893. DOI: `10.1016/j.cpc.2007.07.001`. arXiv: `0704.2423 [hep-ph]`.

[182] A. V. Smirnov and V. A. Smirnov. “On the Resolution of Singularities of Multiple Mellin-Barnes Integrals.” In: *Eur. Phys. J. C* 62 (2009), pp. 445–449. DOI: `10.1140/epjc/s10052-009-1039-6`. arXiv: `0901.0386 [hep-ph]`.

[183] Logan Gates. “On Evaluation of Nonfactorizable Corrections to Higgs Boson Production via Vector Boson Fusion.” In: (May 2023). arXiv: `2305.04407 [hep-ph]`.

[184] R.J. Glauber. *Lectures in Theoretical Physics*. New York: W. E. Brittin and L. C. Dunham, Eds., 1959.

[185] T. Hahn and M. Perez-Victoria. “Automatized one loop calculations in four-dimensions and D-dimensions.” In: *Comput. Phys. Commun.* 118 (1999), pp. 153–165. DOI: `10.1016/S0010-4655(98)00173-8`. arXiv: `hep-ph/9807565`.

[186] Konstantin Asteriadis, Fabrizio Caola, Kirill Melnikov, and Raoul Röntsch. “NNLO QCD corrections to weak boson fusion Higgs boson production in the $H \to b\bar{b}$ and $H \to WW^* \to 4l$ decay channels.” In: *JHEP* 02 (2022), p. 046. DOI: `10.1007/JHEP02(2022)046`. arXiv: `2110.02818 [hep-ph]`.

[187] Konstantin Asteriadis, Christian Brønnum-Hansen, and Kirill Melnikov. "On the non-factorizable corrections to Higgs boson production in weak boson fusion." In: (May 2023). arXiv: 2305.08016 [hep-ph].

[188] Matthew D. Schwartz. *Quantum Field Theory and the Standard Model*. Cambridge University Press, Dec. 2013. DOI: 10.1017/9781139540940. URL: https://doi.org/10.1017/9781139540940.

[189] Steven Weinberg. *The Quantum Theory of Fields*. Cambridge University Press, June 1995. DOI: 10.1017/cbo9781139644167. URL: https://doi.org/10.1017/cbo9781139644167.

[190] Murray Gell-Mann. "Symmetries of baryons and mesons." In: *Phys. Rev.* 125 (1962), pp. 1067–1084. DOI: 10.1103/PhysRev.125.1067.

[191] David J. Gross and Frank Wilczek. "Ultraviolet Behavior of Non-Abelian Gauge Theories." In: *Phys. Rev. Lett.* 30 (26 1973), pp. 1343–1346. DOI: 10.1103/PhysRevLett.30.1343. URL: https://link.aps.org/doi/10.1103/PhysRevLett.30.1343.

[192] H. David Politzer. "Reliable Perturbative Results for Strong Interactions?" In: *Phys. Rev. Lett.* 30 (26 1973), pp. 1346–1349. DOI: 10.1103/PhysRevLett.30.1346. URL: https://link.aps.org/doi/10.1103/PhysRevLett.30.1346.

[193] Toichiro Kinoshita. "Mass Singularities of Feynman Amplitudes." In: *Journal of Mathematical Physics* 3.4 (July 1962), pp. 650–677. DOI: 10.1063/1.1724268. URL: https://doi.org/10.1063/1.1724268.

[194] T. D. Lee and M. Nauenberg. "Degenerate Systems and Mass Singularities." In: *Physical Review* 133.6B (Mar. 1964), B1549–B1562. DOI: 10.1103/physrev.133.b1549. URL: https://doi.org/10.1103/physrev.133.b1549.

[195] A. Gehrmann-De Ridder, T. Gehrmann, and E. W. Nigel Glover. "Antenna subtraction at NNLO." In: *JHEP* 09 (2005), p. 056. DOI: 10.1088/1126-6708/2005/09/056. arXiv: hep-ph/0505111.

[196] Michael Czakon. "The NNLO subtraction scheme STRIPPER: Implementation and application." In: *PoS* RADCOR2015 (2016), p. 004. DOI: 10.22323/1.235.0004.

[197] Gloria Bertolotti, Lorenzo Magnea, Giovanni Pelliccioli, Alessandro Ratti, Chiara Signorile-Signorile, Paolo Torrielli, and Sandro Uccirati. "Towards the automation of the Local Analytic Sector Subtraction." In: *PoS* LL2022 (2022), p. 056. DOI: 10.22323/1.416.0056.

[198] Johannes M. Henn. "Multiloop integrals in dimensional regularization made simple." In: *Phys. Rev. Lett.* 110 (2013), p. 251601. DOI: 10.1103/PhysRevLett.110.251601. arXiv: 1304.1806 [hep-th].

[199] Roman N. Lee. "LiteRed 1.4: a powerful tool for reduction of multiloop integrals." In: *J. Phys. Conf. Ser.* 523 (2014). Ed. by Jianxiong Wang, p. 012059. DOI: 10.1088/1742-6596/523/1/012059. arXiv: 1310.1145 [hep-ph].

[200] Christoph Meyer. “Algorithmic transformation of multi-loop master integrals to a canonical basis with CANONICA.” In: *Comput. Phys. Commun.* 222 (2018), pp. 295–312. DOI: `10.1016/j.cpc.2017.09.014`. arXiv: `1705.06252 [hep-ph]`.

[201] E. Remiddi and J. A. M. Vermaseren. “Harmonic polylogarithms.” In: *Int. J. Mod. Phys. A* 15 (2000), pp. 725–754. DOI: `10.1142/S0217751X00000367`. arXiv: `hep-ph/9905237`.

[202] Alexander B. Goncharov. “Multiple polylogarithms, cyclotomy and modular complexes.” In: *Math. Res. Lett.* 5 (1998), pp. 497–516. DOI: `10.4310/MRL.1998.v5.n4.a7`. arXiv: `1105.2076 [math.AG]`.

[203] D Maitre. “HPL, a mathematica implementation of the harmonic polylogarithms.” In: *Comput. Phys. Commun.* 174 (2006), pp. 222–240. DOI: `10.1016/j.cpc.2005.10.008`. arXiv: `hep-ph/0507152`.

[204] B. A. Kniehl. “Dispersion Relations in Loop Calculations.” In: (1996). eprint: `arXiv:hep-ph/9607255`.

[205] V. A. Smirnov. *Feynman integral calculus.* 2006.

[206] R. E. Cutkosky. “Singularities and Discontinuities of Feynman Amplitudes.” In: *Journal of Mathematical Physics* 1.5 (1960), pp. 429–433.

[207] T. Huber and Daniel Maitre. “HypExp: A Mathematica package for expanding hypergeometric functions around integer-valued parameters.” In: *Comput. Phys. Commun.* 175 (2006), pp. 122–144. DOI: `10.1016/j.cpc.2006.01.007`. arXiv: `hep-ph/0507094`.

[208] D. Binosi and L. Theussl. “JaxoDraw: A Graphical user interface for drawing Feynman diagrams.” In: *Comput. Phys. Commun.* 161 (2004), pp. 76–86. DOI: `10.1016/j.cpc.2004.05.001`. arXiv: `hep-ph/0309015`.

[209] Joshua Ellis. “TikZ-Feynman: Feynman diagrams with TikZ.” In: *Comput. Phys. Commun.* 210 (2017), pp. 103–123. DOI: `10.1016/j.cpc.2016.08.019`. arXiv: `1601.05437 [hep-ph]`.

ACKNOWLEDGEMENT

First and foremost, I would like to express my gratitude to Kirill for granting me the opportunity to work within his research group and for providing invaluable guidance throughout my doctoral journey. I would also like to thank you for the meticulous review of this manuscript and the numerous insightful suggestions and corrections you have shared.

I wish to convey my profound appreciation to Gudrun for accepting to review and provide feedback on my work.

I am sincerely thankful to Wojciech, Chiara, Christian, Chen, and Ming-Ming, with whom I have had the pleasure of collaborating on the diverse problems addressed in this thesis. The results presented in this thesis also encompass the valuable contributions made by each of you.

I would like to express my utmost appreciation to Christian, whose company has made every cup of coffee in 12/02 more enjoyable. Additionally, I am grateful for the insightful remarks you provided to enhance the quality of this manuscript.

Lastly, I am eternally grateful to my beloved spouse, Fanny, whose unwavering support throughout our three years in Karlsruhe has been the foundation of everything I have accomplished. I cannot thank you enough for the constant encouragement and assistance you have provided me. I am truly fortunate to have you by my side.

This research is supported by the Deutsche Forschungsgemeinschaft (DFG, German Research Foundation) under the grant 396021762 - TRR 257.

COLOPHON

All Feynman diagrams were drawn using `Jaxodraw` [208] and `TikZ-Feynman` [209].

This document was typeset using the typographical look-and-feel `classicthesis` developed by André Miede and Ivo Pletikosić. The style was inspired by Robert Bringhurst's seminal book on typography "*The Elements of Typographic Style*". `classicthesis` is available for both LaTeX and LyX:

`https://bitbucket.org/amiede/classicthesis/`

Happy users of `classicthesis` usually send a real postcard to the author, a collection of postcards received so far is featured here:

`http://postcards.miede.de/`

Thank you very much for your feedback and contribution.

Final Version as of July 20, 2023 (classicthesis v4.6).